UNIVERSITY OF SOUTHAMPTON

FACULTY OF ENGINEERING AND APPLIED SCIENCE

CIVIL ENGINEERING

A TIME-STEPPING TECHNIQUE TO SOLVE WAVE PROPAGATION PROBLEMS USING THE BOUNDARY ELEMENT METHOD

by

Webe João Mansur

Thesis submitted for the degree of

Doctor of Philosophy

September 1983.

TABLE OF CONTENTS

UNIVERSITY OF SOUTHAMPTON

ABSTRACT

FACULTY OF ENGINEERING AND APPLIED SCIENCE
CIVIL ENGINEERING

Doctor of Philosophy

A TIME-STEPPING TECHNIQUE TO SOLVE WAVE PROPAGATION PROBLEMS USING THE BOUNDARY ELEMENT METHOD

by Webe João Mansur

In this work the direct boundary element method is applied to solve transient wave propagation problems.

At first, the scalar wave equation is considered and the discussion initially carried out illustrates the mathematical operations that are required in order to obtain two- and three-dimensional boundary integral equations which are amenable to numerical solutions.

Linear discretization is adopted to represent the boundary geometry with linear and constant time and space interpolation functions being employed to approximate the boundary unknowns. Consequently the two-dimensional boundary integral equation is transformed into a system of algebraic equations, which is solved by implementing a time-stepping scheme in which time integrations are carried out analytically. One-dimensional Gauss quadrature is used to perform all boundary integrals except those in the Cauchy principal value sense which are calculated analytically. Linear triangular cells are used to compute contributions due to initial conditions.

An investigation concerning elastodynamics, where two- and three-dimensional formulations are considered is also included. The numerical procedure which is employed in solving two-dimensional elastodynamic problems is very similar to that concerning the scalar wave equation, for this reason the discussion concerning this subject is only cursory. Initial conditions are not included, but cells are also used in the elastodynamic analysis, to compute internal stresses.

A number of examples which relate to the two wave propagation problems previously mentioned are analysed and numerical results together with discussions regarding their accuracy are included. Certain other topics are also considered like the number of integration points that should be used, the relation between the element length and time interval size that should be chosen, etc.

ACKNOWLEDGEMENTS

The author is indebted to his supervisor Dr. C.A. Brebbia for his keen guidance and helpful advice. Warm appreciation is also extended to J.C.F. Telles, L.C. Wrobel, W.S. Venturini, J. Waters and M. Kavanagh for many invaluable discussions.

Mr. A.G. Day kindly reviewed this thesis and made many useful suggestions, whilst Mrs. G.J. Cooper successfully completed the typing of this rather difficult manuscript.

Finally, the author wishes to acknowledge the financial support provided by the National Council for Scientifical and Technological Development (C.N.Pq.), and also from the Federal University of Rio de Janeiro, without whose help this research work could not have been undertaken.

NOTATION

x_1, x_2, x_3	Cartesian coordinates
$\underline{x}$	position vector of a point with the Cartesian coordinates x_1, x_2 and x_3
$\underline{i}$, $\underline{j}$, $\underline{k}$	unit vectors in the direction of the x_1, x_2 and x_3 coordinate axes
δ_{ij}	Kronecker delta symbol
e_{ijk}	permutation symbol
(r,θ,ψ)	spherical coordinates
(r,θ,z)	cylindrical polar coordinates
(r,θ)	polar coordinates
Ω	domain of the body
Γ	boundary of the body
π	propagating singular wave surface
$\left[\!\left[f \right]\!\right]$	$= f^+ - f^-$
q,Q	field points
s,S	source points
$\underline{q}$,$\underline{Q}$	position vectors of the points q and Q
$\underline{s}$,$\underline{S}$	position vectors of the points s and S
r(q,s)	$= \lvert\underline{q}-\underline{s}\rvert$ is the distance between q and s
t	time
τ	time in which an impulse is applied
t_o,0	initial time
t_r	retarded time
Δt	time interval
ξ	intrinsic one-dimensional coordinate
μ_k	homogeneous coordinates regarding the two-dimensional triangular cells

$\underline{n}$	unit outward vector normal to Γ
n	coordinate in the direction parallel to $\underline{n}$
n_j	Cartesian components of $\underline{n}$
$\underline{t}$	unit vector tangent to Γ
$\underline{\nu}$	unit vector parallel to $\underline{r}(s,Q) = \underline{Q}-\underline{s}$
$\delta(q-s)$	Dirac delta function
$\delta^{(k)}(r-ct)$	$= \frac{\partial^k}{\partial r^k}\left[\delta(r-ct)\right]$
$\dot{\delta}(t'-r/c)$	time derivative of the Dirac delta function
$H(x-a)$	Heaviside function
u	scalar potential
v	scalar velocity equal to the time derivative of u
p	derivative of u with respect to n
u_o	initial potential equal to u at $t=t_o$
v_o	initial velocity equal to v at $t=t_o$
γ	source density
u*	fundamental solution to the scalar wave equation
v*	derivative of u* with respect to τ
p*	derivative of u* with respect to n
u_o^*	u* at $\tau=0$
v_o^*	v* at $\tau=0$
u_i	displacement components
v_i	velocity components
p_i	traction components
ε_{ij}	strain components

ω_{ij}	rotation components
σ_{ij}	stress components
u_{oi}	initial displacement components
v_{oi}	initial velocity components
b_k	body force components
e	dilatation
u^*_{ik}	fundamental displacement components
v^*_{ik}	fundamental velocity components
p^*_{ik}	fundamental traction components
ε^*_{ijk}	fundamental strain components
σ^*_{ijk}	fundamental stress components
u^*_{oik}	u^*_{ik} at $\tau=0$
v^*_{oik}	v^*_{ik} at $\tau=0$
ρ	density
λ, G	Lamé constants
ν	Poisson's ratio
E	Young's modulus
c	wave propagation speed for problems concerning the scalar wave equation
c_s	speed of propagation of equivoluminal waves
c_d	speed of propagation of dilatational waves
ϕ^m, θ^m	time interpolation functions
η_j, ν_j	space interpolation functions
∇^2	Laplacian
J	Jacobian

CHAPTER 1

INTRODUCTION

1.1 Preliminary Remarks

The discovery by Fresnel (1816) and Young (1817) concerning the properties of light stimulated scientists to study the rather complicated phenomena of the propagation of waves in elastic bodies. The conceptual problem of interpreting the physical features of waves in elastic bodies was as difficult as the mathematical formulation. Apparently Poisson {1} was the first to recognize that an elastic disturbance is in general composed of the dilational (irrotational, longitudinal, primary) and equivoluminal (shear, transverse, distortional, secondary) waves. Nearly sixty years elapsed before Lord Rayleigh {2} discovered the now well known surface waves (Rayleigh waves). Such waves are confined to the region close to the surface of the half-space and propagate with a speed which is less than that of the equivoluminal body wave. Surface waves were also studied by Lamb {3} and Love {4,5} who contributed considerably to the understanding of the subject. A complete historical review of the early investigations carried out by Poisson, Cauchy, Ostrogradsky, Green, Lamé, Stokes, Clebsh and Christoffel, together with works published later on surface waves can be found in the book by Love {5}.

Due to its inumerable applications the theory of wave propagation has been studied by an increasing number of researchers, but despite the progress achieved in recent years quite a lot more investigations are required. There

are now many books on wave propagation and a modern approach to the subject can be found in references {6,7,8,9,10}.

The need to find solutions to engineering problems involving non-homogeneous, non-isotropic solids with complex geometries and sometimes having non-linear behaviour stimulated the development of numerical techniques; finite differences being the first one to be commonly adopted by engineers. A review of its applications to wave propagation can be found in reference {11}.

Presently the finite element method {12-16} is by far the most popular numerical technique. It is undoubtedly more efficient than the finite difference technique in most engineering applications. Since the sixties the finite element method has been used to solve elastodynamic problems {12} and due to the large number of researchers working in the field, as soon as the year of 1974 general computer programs of the type described in references {17-19} became available. One of the drawbacks of finite elements and finite differences when used to solve wave propagation problems is the need to terminate the mesh when the domain being analysed is not bounded. In this situation artificial boundaries reflect unwanted waves that can interfere and sometimes completely invalidate the results. In order to avoid this problem researchers developed transmitting (non-reflecting) boundaries; their application can increase the cost of the analysis. Besides, the number of finite elements required can still be large, as such boundaries are usually capable of transmitting plane or cylindrical waves only {11}, and therefore they must be placed far from the

initially disturbed region. Consequently a method such as the boundary element method {20-22} that performs well for both bounded and unbounded domains and does not necessarily require domain discretization can be an advantage in many practical applications.

A great deal of the work carried out using integral representations is concerned with the use of this useful mathematical tool to prove uniqueness and existence of solutions of differential equations {6,8,9,23,24}. Its use to obtain solutions of problems was restricted to some simple applications, sometimes numerical {7,25}; but no general algorithm of solution was derived until researchers started developing boundary element methods. Boundary integral equation method {26,27} is also a common equivalent name found in the literature. These methods are called direct when physical parameters such as displacements and tractions in elasticity, are directly obtained from the solution of an integral equation {20-22, 28-37} and indirect if this is not the case {27,38,39}. References to most of the investigations carried out so far on boundary elements can be found in many textbooks that have now been published on the subject {20-22, 27, 40-49}.

Different procedures have been adopted to formulate the boundary element method, all of them dependent on the previous knowledge of a singular solution (fundamental solution). In considering the elasticity case, Rizzo {28} and later on Cruse {29,30} employed Betti's reciprocal theorem {51} and the fundamental solution developed by Lord Kelvin {52} to obtain Somigliana's identity {53}.

Through a limiting process an integral equation relating boundary displacements and tractions was subsequently obtained and transformed into an algebraic system of equations by using interpolation functions. An alternative approach which leads to the same equations obtained by Rizzo is the one used by Brebbia {20} who formulates the problem through weighted residual considerations. One of the main advantages of this approach is to make it easier to relate and combine the boundary element method with other numerical techniques. Alternative fundamental solutions that satisfy certain boundary conditions have also been used {34,36,54} and can be of great advantage in many applications.

The purpose of this work is to solve transient two-dimensional elastodynamic and scalar wave equation problems using the boundary element method. The fundamental solutions adopted here are time-dependent. The integral equations obtained are solved numerically using a time-stepping scheme.

Two- and three-dimensional integral representations for the two previously stated problems can be found in many works {6,8,9,55}; but need to undergo further transformations in order to be used as a basis for numerical analysis. This fact becomes evident in that the integral representation for the scalar wave equation in three dimensions involves Dirac delta functions which must be eliminated before a numerical scheme of solution can be implemented. This transformation was primarily completed by Kirchhoff {57} who obtained an expression from which the potential at internal points can be computed. Later on, integral equations relating only

boundary unknowns were derived and successfully used to obtain boundary element solutions {58-60}.

Most of the research carried out so far on boundary elements are concerned with solutions of elliptic and parabolic type differential equations. Quite a lot of investigations have already been carried out showing that the boundary element method is an efficient technique for these types of problem. However the same amount of effort has not been directed towards solving hyperbolic differential equations. Therefore, this a developing research area with a great deal to be accomplished in both the analytical formulation and implementation of general numerical procedures.

1.2 Literature Survey - Transient Applications

Cruse {61}and Cruse and Rizzo {62 and 63} were the first researchers in the field of boundary elements to implement a general numerical procedure to solve two-dimensional elastodynamic transient problems. In their approach, boundary elements are used to solve elliptic differential equations in the Laplace transform domain and a numerical algorithm due to Papoulis {64} is used to obtain time domain solutions. The two numerical applications carried out by Cruse and Rizzo were concerned with half-plane problems and showed that their approach gives very accurate results for early times.

As an extension of Cruse's work, Manolis {65} and later Manolis and Beskos {66} compared Papoulis' and Durbin {67} algorithms to obtain time domain solutions. These researchers studied stress concentration in underground

structures and found that Durbin's algorithm, although more time consuming than Papoulis', had a high accuracy even for late times. They carried out a finite element analysis as well and concluded that due to the low accuracy of some of the results finite elements were not efficient for this type of problem.

Manolis {65} also formulated the steady state elastodynamic problem and pointed out that the integral equations for this case can be obtained from those employed by Cruse, by replacing the Laplace parameter 's' by 'iω' where 'ω' is the exciting frequency. Alarcon et al. {68} used the same idea subsequently to find the dynamic stiffness of foundations.

Direct solution of hyperbolic differential equations using time-stepping techniques was first carried out by Friedman and Shaw {58} and later on by Shaw et al. {69-76}.

The initial investigations carried out by these authors appear to have marked the shift to computer solutions of wave propagation problems using integral equations. Their boundary equations are basically modifications of Kirchhoff's integral representation, which is taken to the boundary of the domain using standard results of potential theory {77}, and then adapted to the problems they wanted to solve. However, their applications were mainly concerned with particular geometries and boundary conditions and no general numerical formulation was attempted. They solved two-dimensional problems by considering them as three-dimensional cylindrical ones with arbitrary axes length. In this way the three-dimensional formulation can be used, with the artificially introduced

third spatial coordinate playing the role of a time like variable. With this procedure the time integration which is required in two-dimensional formulations is avoided at the expense of introducing an additional spatial dimension.

Further investigations related to Kirchhoff's integral equation were carried out by Mitzener {59}. He presented a general numerical procedure to analyse transient scattering from a hard surface but only considered in his formulation particular boundary conditions related to the problem he studied.

Recently Groenenboon {60} using an approach similar to Mitzener's presented a general boundary element retarded potential technique to solve unsteady potential fluid flow problems in three dimensions. He applied the boundary element method to study the flow of liquid sodium in cooling components of liquid metal fast breeder reactors. Radiation condition was introduced to simulate openings that give an entrance to other parts of the steam generators and interconnecting piping system. A concentrated source term was included in the formulation to simulate the expanding reaction bubble originating from the sodium-water reaction. The numerical applications which he carried out produced encouraging results.

Further contributions to the subject were given by Neilson et al. {78} and Herman {79}. The former extended Shaw's formulation to a wider range of problems and the latter presented an iteractive method which eliminated spurious oscillations that can appear at late stages in a time-stepping analysis.

Three-dimensional fundamental solutions were also used by Niwa et al. {80} and Manolis {81}. These authors analysed two-dimensional transient elastodynamic problems using a scheme identical to Shaw's, i.e., they considered two-dimensional bodies as cylinders with axes of arbitrary length.

So far, very few numerical schemes have been implemented to solve wave propagation problems using two-dimensional time dependent fundamental solutions. Das {82} and Das and Aki {83} studied the propagation of a two-dimensiona shear crack in an infinite homogeneous elastic medium using a time-stepping approach. However, their formulation was not a general one.

Cole et al. {84} applied the well known two-dimensional time domain integral equation for the scalar wave equation {6} to solve transient elastodynamic antiplane motions. In that work a time-stepping scheme was used to obtain numerical solutions for the problem of two welded half-planes excited by a concentrated source. Very accurate displacements at the common surface were obtained. Their formulation was however restricted to problems in which the boundary integral involving the potential (displacement) disappears, which implies that internal displacements could not be computed with their procedure. In spite of this their paper represents the first contribution towards finding a general formulation using a two-dimensional time-dependent fundamental solution.

Mansur and Brebbia {85,86} have also applied the boundary element method to analyse transient problems governed by the two-dimensional scalar wave equation. Commencing with weighted residual considerations they initially derived the same integral equation obtained by Morse and Feshbach {6} using Green's theorem. Further transformations were then carried out to eliminate derivatives of Heaviside functions that appeared in the integral equation and a general approach amenable to numerical solutions was derived. Contributions due to initial conditions and source terms were also included. A time-stepping scheme similar to that proposed by Cole et al. was used to obtain time domain solutions. The numerical features of this approach were illustrated by three examples for all of which highly accurate results were obtained.

1.3 Contents of the Present Work

In Chapter 2 a short review of the basic theory of elastodynamics is presented, but those not familiar with this topic may find it necessary to read further on the subject before continuing with subsequent chapters. If this is the case suitable explanation can be obtained from consulting any of the selected references on elastodynamics previously mentioned in this section. The objective of chapter two is to introduce some simple but useful concepts as well as to describe simultaneously some of the notation and terminology used in this thesis.

Initially a review of the small strain theory of elastostatics is carried out. The main topics presented in this preliminary discussion are concerned with stress

equilibrium equations of motion, strain displacement relationships, definition of rotation and Hookes' law for homogeneous isotropic elastic bodies. Following this some basic concepts of elastodynamics are introduced. This is carried out by describing the boundary initial value problem of elastodynamics, conditions at wave fronts and equivoluminal and dilatational body waves. Lamé potentials, regularity and radiation conditions for infinite bodies are then analysed. In order to clarify further concepts a discussion on one dimensional, plane, spherical and cylindrical waves follows. The last part of chapter 2 concentrates on plane motions, i.e., antiplane, plane strain and plane stress motions.

Chapter 3 is concerned with time domain integral representations related to the scalar wave equation. The discussion carried out within that chapter uses many properties of the Dirac delta and Heaviside functions. For this reason after an initial description of the boundary initial value problem, definition and some properties of these special functions are presented. Next the Green's function for three dimensions, together with an weighted residual statement are used to obtain an integral representation for the problem. Further operations to eliminate derivatives of the Dirac delta function are then performed leading to the Kirchhoff integral representation.

The two-dimensional integral representation due to Volterra is next obtained using the method of descent. Volterra's formula is then modified following the procedure described in references {85 and 86}. An integral equation is obtained suitable for applying in a general numerical analysis.

Chapter 4 presents a discussion on the numerical implementation of the two-dimensional integral equation obtained in the previous chapter. The interpolation functions used to approximate boundary displacements and their normal derivatives, together with the procedure used to perform the boundary integrations are the topics initially discussed. Next, domain integrations are considered, and the chapter concludes with an investigation of three illustrative numerical examples.

In Chapter 5 the discussion presented in Chapter 3 concerning the scalar wave equation is extended to elastodynamics. The chapter opens with a summarized description of the boundary initial value problem of elastodynamics. This is followed by two- and three-dimensional fundamental solutions being employed together with the reciprocal theorem of elastodynamics to work out the integral representations for the problem.

The last part of Chapter five is concerned with additional transformations which must be carried out in order to obtain a two-dimensional boundary integral equation for elastodynamics,suitable to be used in a general numerical time-stepping analysis.

Chapter 6 is concerned with the numerical implementation of a time-stepping scheme to solve the two-dimensional boundary integral equation obtained in Chapter 5. The numerical procedure used to solve elastodynamic problems with boundary elements is similar to the one described in Chapter 4. For this reason the initial discussion presented in Chapter 6 referring to interpolation functions and to the

implementation of the time-stepping technique is only cursory. Next the numerical scheme used to compute stresses at internal points is presented, the chapter ending with a study of five illustrative examples.

Chapter 7 presents a general discussion of the matters investigated in the previous chapters with conclusions developed from the present work and recommendations for future research.

CHAPTER 2

LINEAR ELASTODYNAMICS

2.1 Introduction

This chapter is concerned with a short description of the linear elastodynamic problem. The intention here is to provide an account of the basic theory and concepts employed in subsequent chapters. A more comprehensive investigation can be found in any of the many standard textbooks cited on the subject {5,7-10,87}.

Because of the complex nature of the Navier's equilibrium equations, alternative differential operators have been used to represent motions of isotropic elastic bodies. A very convenient approach is that which adopts Lamé potentials, in which the displacement components are expressed in terms of derivatives of potentials that satisfy wave equations. The comprehensive information available on the wave equation, in conjunction with its simplicity can be of great advantage in quite a number of applications. However, particularly in numerical analysis, the adoption of Navier's equations of motion is preferred. One of the arguments for this is that it is possible to work directly with variables of physical interest rather than with elastic potentials.

In section 2.2 the aforementioned approaches and also other basic topics are considered.

The following section is concerned with one-dimensional motions and plane, cylindrical and spherical waves. The objective of this investigation is to introduce

more of the descriptive terminology used as well as to clarify some concepts.

The chapter concludes with a section concerned with plane motions.

2.2 Basic Theory

Throughout this work the Cartesian tensor notation is used. This notation permits expressions to be written in a compact form and it is very useful when considering equations related to mathematical physics. Such notation makes use of subscript indices (1,2,3) to represent (x,y,z). In this work the summation convention will be employed, i.e., a repeated index (subscript or superscript) in a term implies summation with respect to that index over its range. Hence in three dimensions,

$$a_{ij}x_j = a_{i1}x_1+a_{i2}x_2+a_{i3}x_3 \quad . \tag{2.2.1}$$

In addition, the Kronecker delta symbol δ_{ij} and the permutation symbol e_{ijk}, as defined by expression (2.2.2), will be used.

$$\delta_{ij} = \begin{cases} 1 \text{ when } i = j \\ 0 \text{ when } i \neq j \end{cases}$$

$$e_{ijk} = \begin{cases} 0 \text{ when any two indices are equal,} \\ 1 \text{ when } i,j,k \text{ are an even permutation} \\ \text{of } 1,2,3, \\ -1 \text{ when } i,j,k \text{ are an odd permutation} \\ \text{of } 1,2,3 \quad . \end{cases} \tag{2.2.2}$$

Another useful convention refers to partial differentiation of functions. The following representation is used,

$$\frac{\partial f_{ij}}{\partial x_l} = f_{ij,l} \quad . \tag{2.2.3}$$

Within this work unless otherwise stated indices are assumed to have respectively a range of three or two for three- or two-dimensional analysis.

Consider an infinitesimal parallelepiped surrounding a point within a body. If one isolates such a parallelepiped the remainder of the body can be replaced by the components of the stress tensor σ_{ij} (force per unit area) as depicted in figure 2.2.1. The sign convention for stresses is such that if σ_{ij} is positive the vector representing σ_{ij} (stress vector) points in the positive or negative x_j-direction if the outer normal to the surface element under consideration points respectively in the positive or negative x_i-direction. Therefore, the components of the stress tensor illustrated in figure 2.2.1 are positive.

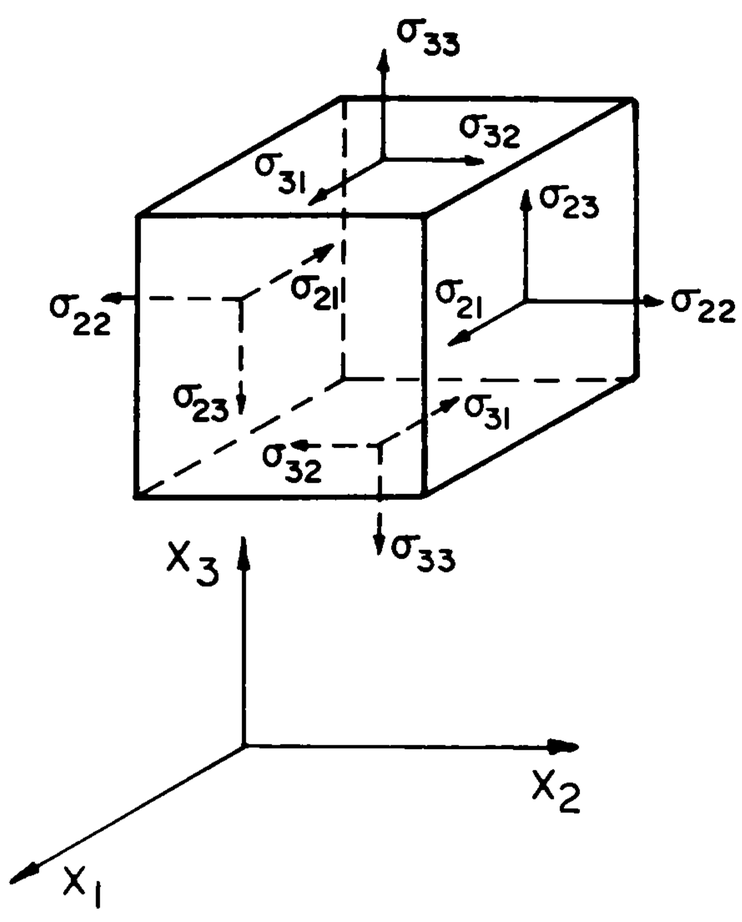

Figure 2.2.1 Sense of positive stresses.

Once the components of the stress tensor are known, surface forces p_i (force per unit area) acting across any surface in the body, including its boundary, can be computed from

$$p_i = \sigma_{ji} n_j \tag{2.2.4}$$

where n_j stands for the components of the unit vector $\underline{n}$ normal to the surface at the point under consideration. p_i must be interpreted according to the sense of the vector $\underline{n}$. It is apparent that the surface over which p_i is being computed can be considered to divide the body into two others. p_i stands for the forces exerted by the body for which $\underline{n}$ is inwards over the body for which $\underline{n}$ is outwards.

Dynamic equilibrium of forces acting on the parallelepiped shown in figure 2.2.1 requires that

$$\sigma_{ij,i} + b_j = \rho \ddot{u}_j \tag{2.2.5}$$

where b_j stands for the components of the body forces (force per unit volume) and ρ is the density of the body (mass per unit volume). Time derivatives are indicated by dots, i.e., $\partial^2 u_i / \partial t^2 = \ddot{u}_i$. Equations (2.2.5) will be referred to hereafter as the stress equations of motion.

Furthermore, if there are no body moments present, dynamic equilibrium of moments requires that

$$\sigma_{ij} = \sigma_{ji} \quad . \tag{2.2.6}$$

Let $\underline{x}$ represent the position vector of a point within a body in its undeformed configuration. Under the action of loads this point moves into a new position described by the coordinates x_i'. The displacement components

u_i are given by

$$u_i(\underline{x},t) = x_i'(\underline{x},t) - x_i \quad . \tag{2.2.7}$$

If the u_i displacement components are such that their first derivatives are so small that the squares and products of the partial derivatives of u_i are negligible, then strains can be computed using Cauchy's infinitesimal strain tensor,

$$\varepsilon_{ij} = \frac{1}{2}(u_{i,j} + u_{j,i}) \quad . \tag{2.2.8}$$

Consider a point P' in the neighbourhood of a point P within a body. Let the coordinates of P and P' be represented by x_i and x_i+dx_i respectively. The relative displacement of P' with respect to P is given by

$$du_i = u_{i,j}dx_j \quad . \tag{2.2.9}$$

In the above expression the time variation of the displacement field has not been included, therefore it is valid for the static case. However the discussion now under consideration also applies to elastodynamics if one considers the displacement field corresponding to a fixed instant. Equation (2.2.9) can also be written as {87}

$$du_i = \frac{1}{2}(u_{i,j}+u_{j,i})dx_j + \frac{1}{2}(u_{i,j}-u_{j,i})dx_j \tag{2.2.10}$$

or

$$du_i = \frac{1}{2}\varepsilon_{ij}dx_j - \frac{1}{2}\omega_{ij}dx_j \tag{2.2.11}$$

where

$$\omega_{ij} = \frac{1}{2}(u_{j,i}-u_{i,j}) \quad . \tag{2.2.12}$$

The tensor ω_{ij} is called the infinitesimal rotation tensor. From expressions (2.2.8) and (2.2.12) it is easy to see that the tensors ε_{ij} and ω_{ij} are respectively symmetric and antisymmetric, i.e.

$$\varepsilon_{ij} = \varepsilon_{ji}$$
$$\omega_{ij} = -\omega_{ji} \quad . \tag{2.2.13}$$

The components of the strain tensor are not independent from each other. If arbitrary values are assigned to ε_{ij}, from expression (2.2.8) it is possible to obtain a system of six equations from which only three unknown functions, u_i are to be computed. Therefore one must not expect this system to have a solution, unless some additional constraints are satisfied. This problem was solved by St. Venant in 1860 who demonstrated that the strain tensor must obey the following compatibility equation

$$\varepsilon_{ij,kl}+\varepsilon_{kl,ij}-\varepsilon_{ik,jl}-\varepsilon_{jl,ik} = 0 \quad . \tag{2.2.14}$$

Equation (2.2.14) is a necessary and sufficient condition that strain components give single-valued displacements for simply connected regions. For multiply connected regions, however, this condition is necessary but usually not sufficient.

It should be recognized that a displacement field obtained from equation (2.2.8) does not include rigid body motions. Therefore, the complete displacement field can only be obtained if together with the components of strain one also has knowledge of the rigid body motion (i.e. displacement and rotation) at some point within the body.

In addition to the stress equations of motion, Hooke's Law relating strain and stress must also be considered when formulating the elastodynamic problem. For isotropic elastic materials in which there is no change in temperature, Hooke's law can be stated in the form

$$\sigma_{ij} = \lambda \varepsilon_{mm} \delta_{ij} + 2G\varepsilon_{ij} \qquad (2.2.15)$$

or inversely

$$\varepsilon_{ij} = \frac{1}{2G}\left(\sigma_{ij} - \frac{\nu}{1+\nu}\, \sigma_{kk}\delta_{ij}\right) \qquad (2.2.16)$$

where λ and G are the Lamé's constants and ν is the Poisson ratio. λ and G can be computed from ν and the elasticity (Young's) modulus E as follows

$$\lambda = \frac{E\nu}{(1-2\nu)(1+\nu)}$$

$$G = \frac{E}{2(1+\nu)} \quad . \qquad (2.2.17)$$

Equations (2.2.5), (2.2.8) and (2.2.15) represent a set of 15 equations for the 15 unknowns σ_{ij}, ε_{ij} and u_i. σ_{ij} can be eliminated by substituting equation (2.2.15) into (2.2.5). Then, using equation (2.2.8) one obtains Navier's equations which are outlined below

$$Gu_{j,kk} + (\lambda+G)u_{k,kj} + b_j = \rho\ddot{u}_j \quad . \qquad (2.2.18)$$

Equations (2.2.18) are also referred to as the displacement equations of motion and constitute a linear system of hyperbolic differential equations for the dependent variable u_i.

When solving an isotropic elastodynamic problem, it is necessary to determine components $u_i(\underline{x},t)$ that satisfy:

(a) equation (2.2.18) for $t \geq t_o$ at all points inside a domain Ω,

(b) initial conditions

$$u_i(\underline{x},t_o) = u_{oi}(\underline{x}) \quad ,$$

$$\dot{u}_i(\underline{x},t_o) = \left|\frac{\partial}{\partial t} u_i(\underline{x},t)\right|_{t=t_o} = v_{oi}(\underline{x}) \qquad (2.2.19)$$

prescribed all over Ω including its boundary Γ,

(c) boundary conditions

$$u_i(\underline{x},t) = \bar{u}_i(\underline{x},t), \underline{x} \in \Gamma_1$$
$$p_i(\underline{x},t) = \sigma_{ij}n_j = \bar{p}_i(\underline{x},t), \underline{x} \in \Gamma_2 \qquad (2.2.20)$$

specified over the boundary $\Gamma(\Gamma=\Gamma_1+\Gamma_2)$. Γ may be the union of several closed surfaces with a piecewise continuous exterior unit normal.

From equations (2.2.8) and (2.2.15) stresses can also be written as,

$$\sigma_{ij} = \lambda u_{k,k}\delta_{ij} + G(u_{i,j}+u_{j,i}) \quad . \qquad (2.2.21)$$

Hence, using equation (2.2.4), the second of the conditions given by equation (2.2.20) can be described in terms of displacement components as

$$\lambda u_{k,k}n_i + G(u_{i,j}+u_{j,i})n_j = \bar{p}_i \quad . \qquad (2.2.22)$$

Consider that a body initially at rest has part of its domain (or boundary) disturbed. As time elapses this disturbance propagates setting in motion points of the body that initially were at rest. The moving surface which separates the disturbed from the undisturbed part of the

body is called the wavefront. Wavefronts are also referred to as surfaces of discontinuity because stresses, strains and velocities $\left(\frac{\partial u_i}{\partial t}\right)$ can be discontinuous there. It should however be realized that discontinuities do not in reality exist in the physical problem, but are mathematical idealizations of physical quantities that vary rapidly in a small interval of space and time. Wavefronts do not need necessarily to be considered as moving into an undisturbed region of a body. It is quite common to find situations in which a region is already disturbed before the wavefront of an additional disturbance arrives.

Consider a surface of discontinuity π moving through Ω; π moves normal to itself with a speed c, from the region Ω_1 to the region Ω_2 as shown in figure 2.2.2. Let l_i be the components of the unit vector normal to π pointing out from the region 1 to the region 2. The jump conditions for displacements in Ω are given by

$$\left[u_i\right] = (u_i)_2 - (u_i)_1 = 0 \quad . \tag{2.2.23}$$

Displacements are continuous functions of space and time, however stresses and velocities can be discontinuous. In the neighbourhood of π the kinematical condition

$$\left[\dot{u}_i\right] = -c l_j \left[u_{i,j}\right] \tag{2.2.24}$$

as well as the dynamical condition

$$\left[\sigma_{ij} l_j\right] = -\rho c \left[\dot{u}_i\right] \tag{2.2.25}$$

must be satisfied.

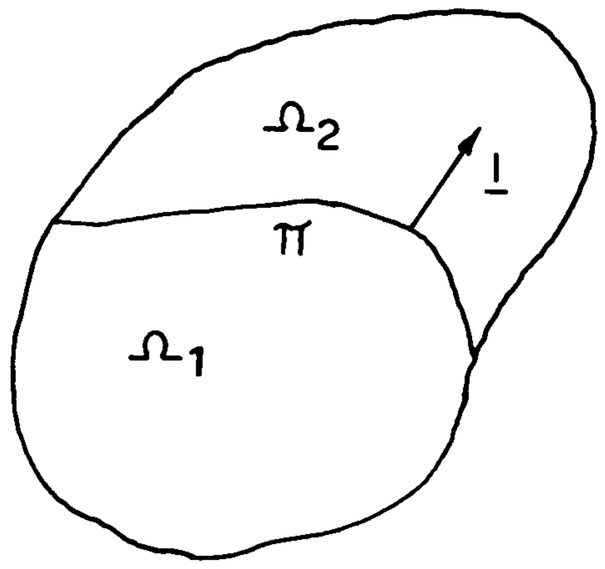

Figure 2.2.2 Surface of discontinuity.

A very important topic in elastodynamic theory (and other branches of mathematical physics) relates to the existence and uniqueness of solutions. Discussions that can be found in modern texts {7-10} reveal that further studies on this subject are still needed. The first proof of uniqueness, provided by Neumann {88}, is based on strain energy considerations and applies only for bounded domains. It also requires displacements and its first and second order time and space derivatives (hence stresses and strains) to be continuous functions of x_i and t. There exists however a great variety of elastodynamic problems which do not obey the restrictions imposed by Neumann's uniqueness theorem. Solutions to these problems have been assumed to be unique except in some situations for which uniqueness have recently been proved {89-91}.

Studies concerning existence of elastodynamics solutions have shown that this is a more complex subject. In this regard reference {9} recommends the article by Fishera {92} where a relevant historical bibliography on the subject is also presented.

The increase in volume per unit volume that occurs when a body is deformed is called dilatation and is given by

$$e = u_{k,k} \quad . \tag{2.2.26}$$

Consider a displacement field for which e=0. In this situation, no change in volume occurs and deformation consists of shear and rotation only. Assuming that the body forces are zero (b_i=0) equation (2.2.18) reduces to {10}

$$\nabla^2 u_j = \ddot{u}_j / c_s^2 \tag{2.2.27}$$

where c_s is given by

$$c_s = \sqrt{G/\rho} \tag{2.2.28}$$

and ∇^2 is the Laplacian operator, i.e.,

$$\nabla^2 u_j = u_{j,kk} \quad . \tag{2.2.29}$$

Equation (2.2.27) is a wave equation for the displacement u_j, governing equivoluminal waves; c_s is the speed of propagation of these waves.

Assign now the value of zero to the rotation ω_{ij}. Considering again that b_i=0, Navier's equations reduces to {10}

$$\nabla^2 u_j = \ddot{u}_j / c_d^2 \tag{2.2.30}$$

where c_d is given by

$$c_d = \sqrt{(\lambda+2G)/\rho} \quad . \tag{2.2.31}$$

Equation (2.2.30) is a wave equation for the displacements u_j governing dilatational waves; c_d is the speed of propagation of these waves.

Each of the displacement body waves governed by equations (2.2.27) and (2.2.30) can be identified by numerous distinct physical characteristics. For this reason , dilatational waves are also known as primary, irrotational, compressional or longitudinal waves. The corresponding names for equivoluminal waves are secondary, shear, rotational, transverse and distortional waves.

The displacement equations of motion can be replaced by two scalar wave equations by employing Lamé potentials. This procedure, first introduced by Lamé, can be described by the following completeness theorem {9}: Let $u_i(\underline{x},t)$ represent the components of a twice-differentiable particular solution of Navier's equations in a region of space Ω, for $t_1<t<t_2$. There then exists a scalar function $\psi(\underline{x},t)$ and a vector function $\underline{\Psi}(\underline{x},t)$, such that $u_i(\underline{x},t)$ is represented by

$$u_i = \psi_{,i} + e_{ijk}\Psi_{k,j} \tag{2.2.32}$$

and ψ and Ψ_k satisfy wave equations

$$c_d^2\left(\nabla^2\psi - \frac{1}{c_d^2}\ddot{\psi}\right) + \alpha = 0, \; c_s^2\left(\nabla^2\Psi_k - \frac{1}{c_s^2}\ddot{\Psi}_k\right) + \beta_k = 0 \tag{2.2.33}$$

where α and β_k are such that

$$b_i = \rho(\alpha_{,i} + e_{ijk}\beta_{k,j}) \quad . \tag{2.2.34}$$

It is important to point out that Stokes-Helmholtz resolution theorem {8-10} ensures that any sufficiently smooth vector may be decomposed into irrotational and solenoidal parts as shown by equations (2.2.32) and (2.2.34).

In equation (2.2.32) the three components of the displacement vector u_i are given in terms of four scalar functions, as a result ψ and Ψ_i can not be completely independent from each other. An additional constraint very commonly found implies that the vector Ψ_i is divergent free, i.e.,

$$\Psi_{i,i} = 0 \quad . \tag{2.2.35}$$

Although equation (2.2.35) is very useful, other types of conditions are also found in the literature, information on this subject can be found in references {7-10} .

In an unbounded body there exists some restrictions concerning the behaviour of fields at infinity which are important to recognize. If an unbounded body is subjected to a disturbance which is confined in a finite region within it, physical considerations require that there exist no waves propagating back from infinity towards the interior of the body.

In order to exemplify this fact the wave equation (equations (2.2.27), (2.2.30) or (2.2.33)) in three dimensions will be initially considered. The behaviour of fields at infinity {9} can be studied by considering a

large sphere Σ_r of radius r, centered at a point ξ, which contains the boundary Γ of the region under consideration (see figure 2.2.3). Let r approach infinity and impose the condition that the field at ξ will not receive any contribution from Σ_r, i.e., waves do not propagate back from infinity. Then from Kirchhoff's integral representation (equation 3.5.16) one obtains the Summerfield radiation condition,

$$\lim_{r\to\infty} r\left(\frac{\partial u_j}{\partial r} + \frac{1}{c}\,\dot{u}_j\right) = 0 \qquad (2.2.36)$$

and the regularity condition

$$\lim_{r\to\infty} u_j = 0 \quad . \qquad (2.2.37)$$

c in expression (2.2.36) is the wave propagation speed.

In two dimensions radiation and regularity conditions read

$$\lim_{r\to\infty} r^{1/2}\left(\frac{\partial u_j}{\partial r} + \frac{1}{c}\,\dot{u}_j\right) = 0, \quad \lim_{r\to\infty} r^{-1/2}\,u_j = 0 \quad . \qquad (2.2.38)$$

Σ_r in this case, is a circle of radius r, rather than a sphere.

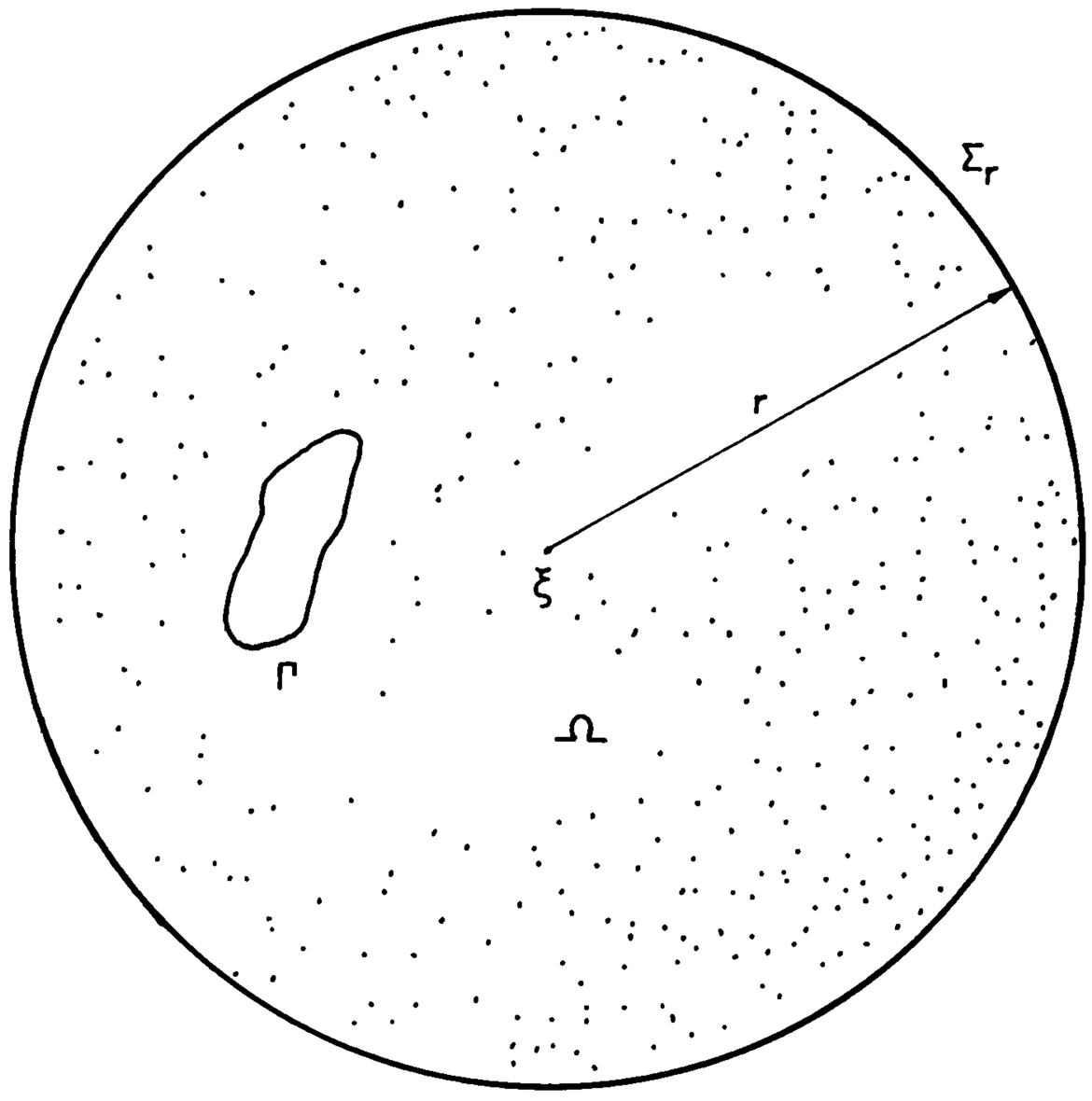

Figure 2.2.3 Simulation of an infinite domain by an infinite sphere.

Radiation and regularity conditions for elastodynamics can be worked out following procedures similar to those just described for the scalar wave equation {9}.

2.3 Some Simple Waves

If the displacement is a function of one space variable only,

$$u_i = u_i(x_1,t) \qquad (2.3.1)$$

and body forces are null ($b_i=0$) equation (2.2.18) reduces to the three uncoupled one-dimensional wave equations {9},

$$\frac{\partial^2 u_1}{\partial x_1^2} = \frac{1}{c_d^2}\ddot{u}_1 \quad , \quad \frac{\partial^2 u_\alpha}{\partial^2 x_1} = \frac{1}{c_s^2}\ddot{u}_\alpha \quad (\alpha=2,3) \quad . \qquad (2.3.2)$$

u_1, u_2 and u_3 represent displacement waves travelling in the

infinite strip shown in figure 2.3.1. Solutions of equations (2.3.2) can also be regarded as representing waves in one-dimensional bodies like strings, rods, etc. The dilatational component of the displacement, u_1, is directed along the direction of propagation x_1, whereas the equivoluminal components of the displacements, u_2 and u_3, are directed along directions perpendicular to x_1. As $c_d > c_s$ the dilatational disturbance travels faster than the equivoluminal one. If the plane that contains x_1 and x_2 in figure 2.3.1 is the horizontal one u_1, u_2 and u_3 can be identified respectively with P, SH and SV waves of seismology.

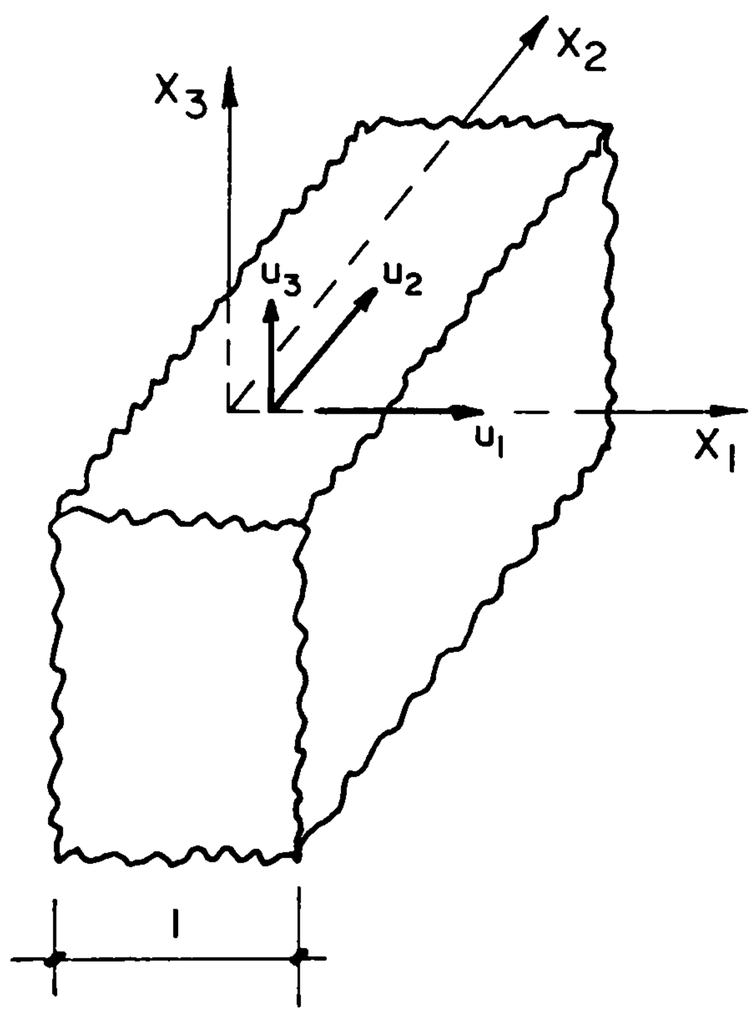

Figure 2.3.1 Infinite strip of width l.

Boundary conditions must be specified on two planes parallel to each other. If the planes $x_1=0$ and $x_1=l$ are chosen the boundary conditions can be of type (a), (b) or (c) described below.

(a) displacement boundary conditions

$$u_i(0,t) = \bar{u}_i^1(t)$$
$$u_i(1,t) = \bar{u}_i^2(t) \qquad (2.3.3)$$

(b) traction boundary conditions

$$p_i(0,t) = \bar{p}_i^1(t)$$
$$p_i(1,t) = \bar{p}_i^2(t) \qquad (2.3.4)$$

(c) mixed boundary conditions

$$u_i(0,t) = \bar{u}_i(t)$$
$$p_i(1,t) = \bar{p}_i(t) \quad . \qquad (2.3.5)$$

In addition, initial conditions

$$u_i(x_1,0) = u_{oi}(x_1) \quad , \quad \dot{u}_i(x_1,0) = v_{oi}(x_1) \qquad (2.3.6)$$

must also be prescribed.

Analytical solutions for the one-dimensional wave equation are not difficult to find. The general solution of an equation such as the first of those given by expression (2.3.2) was first derived by D'Alembert, and reads

$$u_1 = f(x_1 - c_d t) + g(x_1 + c_d t) \quad . \qquad (2.3.7)$$

Equation (2.3.7) has a very simple physical interpretation; it can be regarded as being composed of two one-dimensional waves $f(x_1-c_dt)$ and $g(x_1+c_dt)$ propagating in the positive and negative x_1-direction respectively. A consideration for instance of contributions due to $f(x_1-c_dt)$ only, result in a conclusion that at $t=0$ $u_1=f(x_1)$. At a time instant $t=t_1$ the shape of the wave given by $u_1=f(x_1-c_dt)$ is that which is obtained by displacing the initial shape by a distance

$c_d t_1$ in the positive x_1 direction as illustrated in figure 2.3.2.

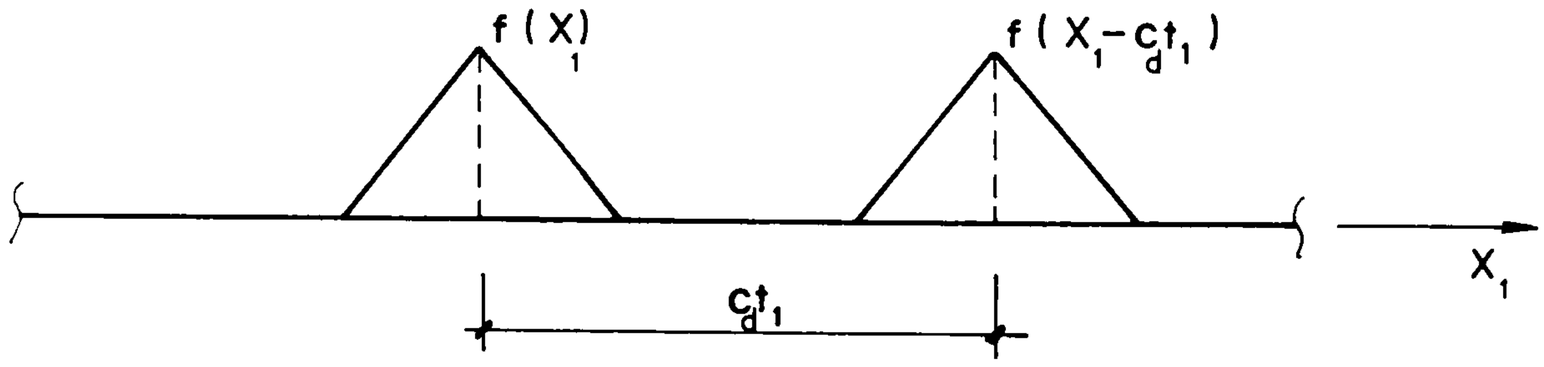

Figure 2.3.2 Propagation of one-dimensional waves.

A plane displacement wave propagating in the direction of an unit vector l can be represented by

$$u_i(\underline{x},t) = u_i(x_i l_i - ct) \qquad (2.3.8)$$

where $x_i l_i = d+ct$ defines planes normal to $\underline{l}$ over which u_i is constant. The argument of u_i, $x_i l_i - ct = d$ is called the phase of the wave. Figure 2.3.3 shows two planes of constant phase, L_0 and L_1, that correspond respectively to $t=0$ and $t=t_1$. It should be noticed that u_i over L_0 is equal to u_i over L_1, therefore, plane waves have the same characteristics of propagation exhibited by D'Alembert solution for the one-dimensional case.

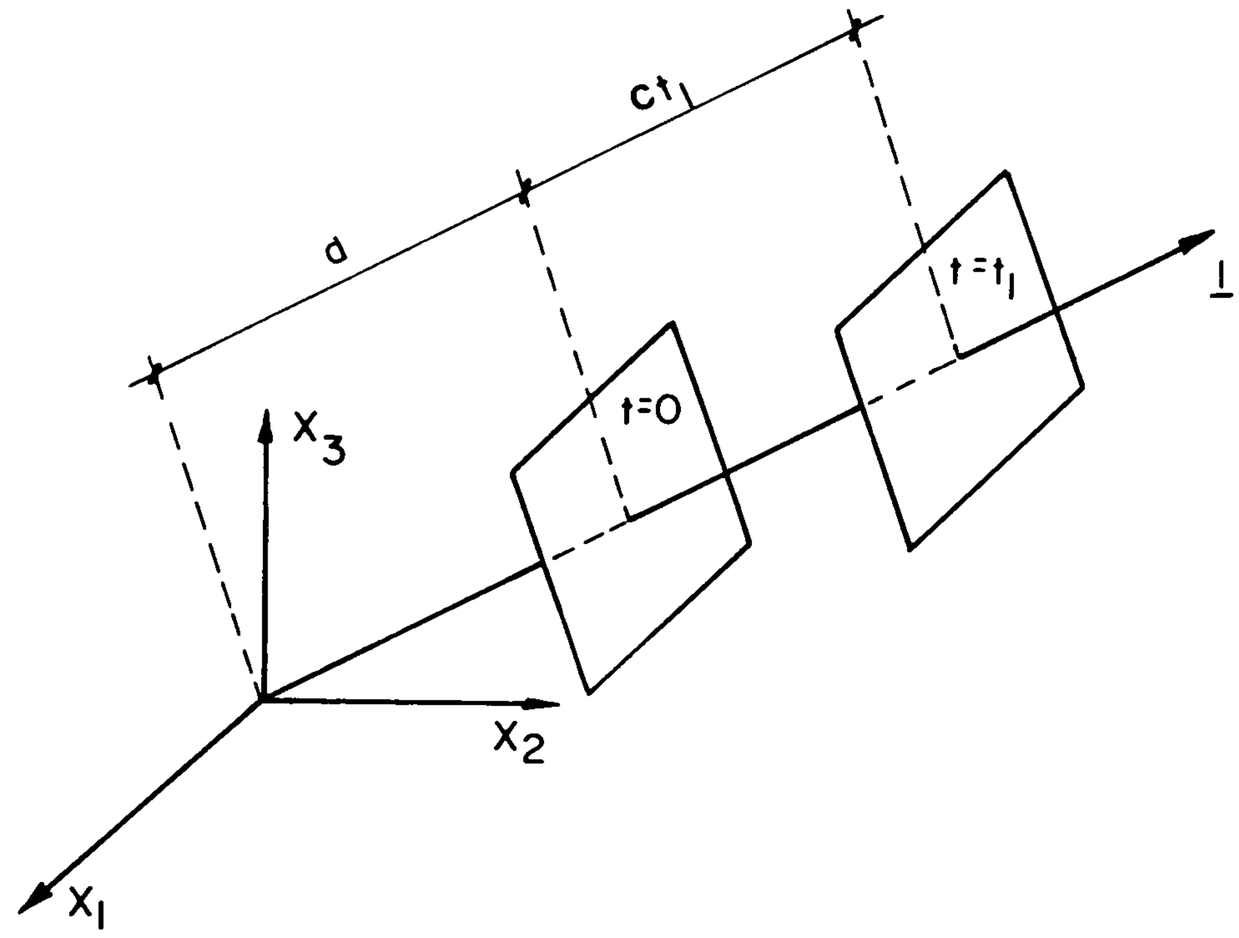

Figure 2.3.3 Propagation of plane waves.

Waves like those represented by equation (2.3.8) only obey Navier's equations if

$$\begin{aligned} &(1)\quad l_i u_i = \pm\sqrt{u_i u_i} \qquad \text{and } c=c_d \\ &(2)\quad l_i u_i = 0 \qquad\qquad\quad \text{and } c=c_s \quad . \end{aligned} \tag{2.3.9}$$

It can be demonstrated {7,8,9,10} that waves defined by equation (2.3.8) and which consequently obey (1) and (2) in expression (2.3.9) are in fact equivoluminal and dilatational displacement waves respectively. Hence, a complete analogy with the one-dimensional case previously studied can be forthcoming if one considers that the coordinate axis x_1 is parallel to the direction of propagation defined by the unit vector $\underline{l}$.

When a displacement field has radial symmetry with regard to a point ξ, a system of spherical coordinates

(r,θ,ψ), centered at ξ, is the most convenient to be employed. Due to the radial symmetry of this problem, the components of the displacement in the direction θ and ψ are null. Hence the displacement vector reads,

$$\underline{u}(\underline{x},t) = u_r(r,t)\underline{e}_r \qquad (2.3.10)$$

where $\underline{e}_r$ is the unit vector in the direction of the coordinate r. Navier's equations ($b_i=0$) then reduce to

$$\frac{\partial^2 u_r}{\partial r^2} + \frac{2}{r}\frac{\partial u_r}{\partial r} - \frac{2}{r^2}u_r = \frac{1}{c_d^2}\ddot{u}_r \quad . \qquad (2.3.11)$$

Introducing a variable ϕ such that $u_r = \frac{\partial \phi}{\partial r}$ equation (2.3.11) gives

$$\frac{\partial^2 (r\phi)}{\partial r^2} = \frac{1}{c_d^2}\frac{\partial^2 (r\phi)}{\partial t^2} \qquad (2.3.12)$$

which is the well known one-dimensional wave equation whose solution (D'Alembert solution) results in

$$\phi = \frac{1}{r}\left[f(r-c_d t)+g(r+c_d t)\right] \quad . \qquad (2.3.13)$$

The waves just described are known as spherical waves with radial symmetry shortened in common use to spherical waves.

When the displacement field has symmetry with regard to a line one has disturbances which are usually termed cylindrical waves. This problem can be best studied by using a system of cylindrical coordinates (r,θ,z) where z coincides with the line of radial symmetry. In this case the only variable not equal to null is u_r and the Navier's equations ($b_i=0$) reduce to

$$\frac{\partial^2 u_r}{\partial r^2} + \frac{1}{r}\frac{\partial u_r}{\partial r} - \frac{u_r}{r^2} = \frac{1}{c_d^2}\ddot{u}_r \quad . \qquad (2.3.14)$$

As for the case of spherical waves, when a variable ϕ such that $u_r = \frac{\partial \phi}{\partial r}$ is introduced, equation (2.3.14) can be written as

$$\frac{\partial^2 \phi}{\partial r^2} + \frac{1}{r} \frac{\partial \phi}{\partial r} = \frac{1}{c_d^2} \frac{\partial^2 \phi}{\partial t^2} \quad . \tag{2.3.15}$$

The general solution of equation (2.3.15) was first derived by Lamb, and is discussed in reference {93}.

Equations (2.3.11) and (2.3.14) are particular versions of Navier's equations, and the complete differential operators in cylindrical and spherical coordinates can be found in textbooks concerned with the subject.

The body waves discussed in this section are very often the subject of discussion because as a result of their simplicity they make clear many concepts involved with the phenomena of wave propagation.

2.4 Plane Motions

If the displacement is a function of two rectangular coordinates only, i.e.

$$u_i(\underline{x},t) = u_i(x_1,x_2,t) \tag{2.4.1}$$

the problem is termed elastodynamic in the plane {9} or complete plane strain {37}. In view of equation (2.4.1), $u_{3,3} = 0$ and all other derivatives of the displacement components are functions of x_1 and x_2 only. Therefore the Navier's equations take the following form,

$$Gu_{j,kk} + (\lambda+G)u_{k,kj} + b_j = \rho\ddot{u}_j \tag{2.4.2}$$

$$Gu_{3,kk} + b_3 = \rho\ddot{u}_3 \tag{2.4.3}$$

where j and k can be 1 or 2.

The domains in which complete plane strain problems are studied are infinite cylinders whose axes are parallel to the x_3-direction. The mathematical problem of solving the differential equations (2.4.2) and (2.4.3) can then be considered as two-dimensional. The domain Ω and the boundary Γ in this case are defined by the intersection of the infinite cylinder with the (x_1,x_2) plane. Of course the physical problem is three-dimensional because displacements and stresses in the x_3-direction do not equal null. Equation (2.2.21) in this case is written as

$$\sigma_{ij} = \lambda u_{k,k}\delta_{ij} + G(u_{i,j}+u_{j,i})$$

$$\sigma_{33} = \lambda u_{k,k} \qquad (2.4.4)$$

$$\sigma_{i3} = Gu_{3,i} \quad .$$

Equations (2.4.2), (2,4.3) and (2.4.4) show that equations (2.4.2) and (2.4.3) can be solved independently. For this reason, complete plane strain can also be seen as resulting from the superposition of the plane strain and antiplane motions governed respecitvely by equations (2.4.2) and (2.4.3). These motions are described in (a) and (b) below.

(a) Antiplane motion:

This motion is governed by the scalar wave equation [equation (2.4.3)] which is of the same type as equations (2.2.27) and (2.2.30) previously described in section 2.2. The boundary conditions in this case are given by,

$$u_3 = \bar{u}_3(x_1,x_2,t) \qquad \text{on } \Gamma_1'$$
$$p_3 = \sigma_{i3}n_i = Gu_{3,i}n_i = \bar{p}_3(x_1,x_2,t) \qquad \text{on } \Gamma_2' \tag{2.4.5}$$

where $\Gamma_1'+\Gamma_2' = \Gamma$. The initial conditions for the antiplane motion are written as

$$u_3(x_1,x_2,0) = u_{o3}(x_1,x_2)$$
$$\text{in } \Omega. \tag{2.4.6}$$
$$\dot{u}_3(x_1,x_2,0) = v_{o3}(x_1,x_2)$$

In this problem the normal stress σ_{33} is null, therefore only the shear stresses $\sigma_{13} = \sigma_{31}$ and $\sigma_{23} = \sigma_{32}$ are present in the analysis. In addition the vector representing the displacement u_3 is perpendicular to the direction of propagation of the displacement waves. For these reasons this motion is also called shear antiplane or horizontally polarized shear motion {8}.

(b) Plane strain motion:

Plane strain motions are governed by equation (2.4.2), which is of the same form as Navier's equations for three dimensions. The only difference is that in the present situation the indices range from 1 to 2, rather than from 1 to 3. The boundary conditions for this problem are given by

$$u_i = \bar{u}_i(x_1,x_2,t) \qquad \text{on } \Gamma_1$$
$$p_i = \sigma_{ij}n_j = \bar{p}_i(x_1,x_2,t) \qquad \text{on } \Gamma_2 \tag{2.4.7}$$

where $\Gamma = \Gamma_1+\Gamma_2$. The initial conditions for plane strain read

$$u_i(x_1,x_2,0) = u_{oi}(x_1,x_2) \qquad \text{in } \Omega \ . \qquad (2.4.8)$$
$$v_i(x_1,x_2,0) = v_{oi}(x_1,x_2)$$

In a plane strain problem

$$u_3 = \varepsilon_{13} = \varepsilon_{31} = \varepsilon_{23} = \varepsilon_{32} = 0 \quad . \qquad (2.4.9)$$

However, the stress σ_{33} is not null and can be computed from the second of equations (2.4.4).

When the domain of the problem being analysed does not extend to infinity in the x_3-direction a plane strain condition can not be assumed to exist. In this case a three-dimensional analysis must be carried out, however when the dimensions of the body in the x_3-direction are small, a condition known as plane stress can be assumed. This situation occurs when analysing thin plates acted on by forces parallel to its midplane. The plane stress hypothesis assumes that

$$\sigma_{33} = \sigma_{31} = \sigma_{13} = \sigma_{32} = \sigma_{23} = 0 \quad . \qquad (2.4.10)$$

In this case the same equations of plane strain can be used provided that the constants ν and E are replaced by fictitious ones, $\bar{\nu}$ and $\bar{E}$, given by

$$\bar{\nu} = \nu/(1+\nu) \qquad (2.4.11)$$

$$\bar{E} = E(1+2\nu)/(1+\nu^2)$$

which implies that

$$\bar{G} = G \qquad (2.4.12)$$

$$\bar{\lambda} = 2\lambda G/(\lambda+2G) \quad .$$

It is important to state that since ε_{33} is not necessarily null, u_i depends on x_3 and the problem is not really two-dimensional. However, plane stress can be considered a good assumption when the plate being studied is sufficiently thin {87}.

CHAPTER 3

BOUNDARY INTEGRAL EQUATIONS FOR TRANSIENT PROBLEMS GOVERNED BY THE SCALAR WAVE EQUATION

3.1 Introduction

The scalar wave equation governs many physical phenomena such as transverse motions of strings and membranes, longitudinal motions of rods, elastodynamic antiplane motions etc. Its application however is not only restricted to the simple problems just mentioned. The discussion on Lamé potential outlined in section 2.2 illustrated that even rather complicated differential equations can sometimes be reduced to a set of wave equations. In addition, there is another very important reason for studying the scalar wave equation; namely its great simplicity. Through the study of this equation it is easier to understand basic concepts and to derive techniques of analysis that can be extended to more complicated problems. This can be clearly seen in this work by a comparison of chapters 3 and 4, which deals with the scalar wave equation, with chapters 5 and 6, concerned with elastodynamics.

This chapter is concerned with the reduction of the scalar wave equation (differential equation) to an integral equation. For this purpose Green's functions (fundamental solutions) for infinite domains together with a weighted residual statement are employed. Kirchhoff's integral representation is obtained and then the two-dimensional problem is formulated using the method of descent. Volterra's integral equation {94} is then

modified following the procedure described by Mansur and Brebbia {85}.

3.2 The Boundary-Initial Value Problem - Transient Scalar Wave Equation

The boundary-initial value problem for the scalar wave equation has already been discussed in section 2.4. However the notation used there referred to elastodynamics. For this reason a description of the problem will be presented again together with a more convenient notation and terminology.

The wave equation can be written in terms of a potential u as

$$\nabla^2 u - \ddot{u}/c^2 = -\gamma \qquad (3.2.1)$$

where c is the speed of wave propagation, γ describes space and time dependence of source density and $\ddot{u} = \partial^2 u/\partial t^2$. The region Ω in which two-dimensional solutions of equation (3.2.1) are sought will be considered to be regular in the sense defined by Kellog {77}, i.e. the Γ boundary of Ω can be composed of several closed regular surfaces which may have corners or edges provided they are not too sharp {27}.

In order to find the particular solution to equation (3.2.1) corresponding to the specific problem which needs to be solved it is necessary to specify the initial conditions

$$\begin{aligned} u(\underline{x},o) &= u_o(\underline{x}) \\ v(\underline{x},o) &= v_o(\underline{x}) \end{aligned} \qquad \text{in } \Omega \text{ at } t=0, \qquad (3.2.2)$$

and the boundary conditions

$$u = \bar{u} \qquad \text{on } \Gamma_1$$
$$p = u_{,i}n_i = \frac{\partial u}{\partial n} = \bar{p} \qquad \text{on } \Gamma_2, \tag{3.2.3}$$

where $\Gamma = \Gamma_1+\Gamma_2$ and n is the coordinate in the direction parallel to the unit outward vector $\underline{n}$, normal to Γ.

3.3 Dirac Delta and Heaviside Functions

When studying Green's functions it is convenient to employ the Dirac delta function {56}. In one dimension the Dirac delta is defined by

$$\begin{cases} \delta(x-a) = 0 \quad \text{when} \quad x \neq a \quad \text{and} \\ \\ \int_{-\infty}^{+\infty} \delta(x-a)f(x)dx = f(a) \quad . \end{cases} \tag{3.3.1}$$

The derivatives of the Dirac delta are functions such that,

$$\begin{cases} \delta^{(k)}(x-a) = 0 \quad \text{when} \quad x \neq a \quad \text{and} \\ \\ \int_{-\infty}^{+\infty} \delta^{(k)}(x-a)f(x)dx = (-1)^k f^{(k)}(a) \quad , \end{cases} \tag{3.3.2}$$

where $\delta^{(k)}(x-a)$ and $f^{(k)}(a)$ stand for $\frac{\partial^k}{\partial x^k}\delta(x-a)$ and $\frac{\partial^k}{\partial x^k}f(x)\Big/_{x=a}$ respectively.

The definition of the Dirac delta function can be easily extended to domains which are not one-dimensional. When a two- or three-dimensional domain Ω is considered the Dirac delta can be defined as follows,

$$\begin{cases} \delta(q-s) = 0 \quad \text{when} \quad s \neq q \ , \text{ and} \\ \\ \int_{\Omega} \delta(q-s) f(q) d\Omega(q) = f(s) \ , \end{cases} \tag{3.3.3}$$

where s and q represent two points within Ω.

Two-dimensional Green's functions corresponding to equations (2.2.18) and (3.2.1) can be conveniently represented using the Heaviside function (see figure 3.3.1) given by,

$$H(x-a) = \begin{cases} 1 \quad \text{if } x>a \ , \\ \\ 0 \quad \text{if } x<a \ . \end{cases} \tag{3.3.4}$$

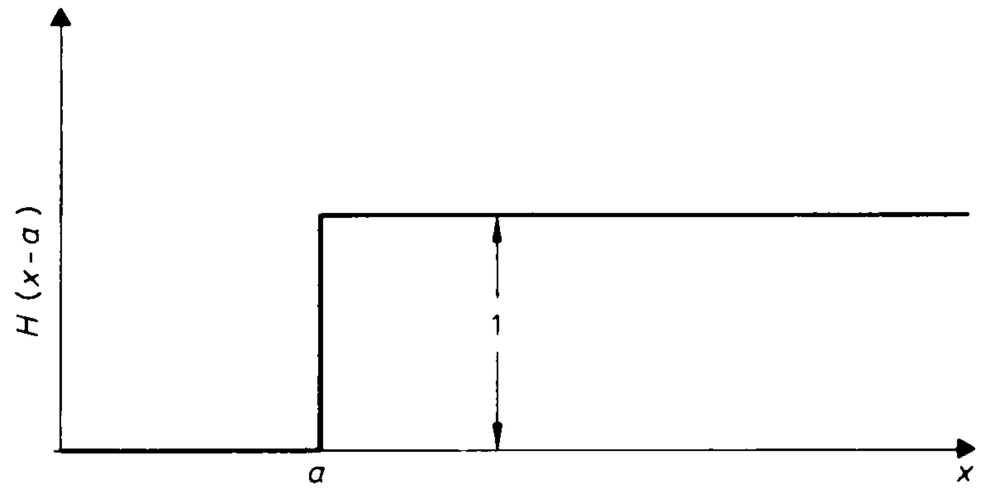

Figure 3.3.1 The Heaviside function.

The Dirac delta and Heaviside functions can be related to each other as follows

$$\frac{d}{dx} H(x-a) = \delta(x-a) \ . \tag{3.3.5}$$

In the discussion just carried out, definitions and also certain basic properties of the Dirac delta and the Heaviside functions were presented. Additional properties

to the ones previously described will be introduced where required. For a rigorous and detailed discussion on this subject attention should be directed to references {95 and 96}.

3.4 Fundamental Solution in Three Dimensions - Transient Scalar Wave Equation

The Green's function (fundamental solution) for the scalar wave equation is the solution of equation (3.2.1) for an unbounded domain {6,9} and a particular concentrated source, i.e.

$$\gamma = 4\pi\delta(q-s)\delta(t-\tau) \quad . \tag{3.4.1}$$

Equation (3.2.1), in this case, can then be written as

$$\nabla^2 u^* - \ddot{u}^*/c^2 = -4\pi\delta(q-s)\delta(t-\tau) \quad . \tag{3.4.2}$$

Thus u* is the effect of a source represented by an impulse at $t=\tau$ located at $q=s$, whilst q and s are referred to in the literature as observation (field) and source points respectively.

The fundamental solution represented by equation (3.4.2) has the following properties {6,9}:

(i) causality

$$u^*(q,t;s,\tau) = 0 \text{ whenever } c(t-\tau) < |\underline{q}-\underline{s}| \tag{3.4.3}$$

(ii) reciprocity

$$u^*(q,t;s,\tau) = u^*(s,-\tau;q,-t) \tag{3.4.4}$$

(iii) time translation

$$u^*(q,t+t_1;s,\tau+t_1) = u^*(q,t;s,\tau) \tag{3.4.5}$$

In three dimensions the solution of equation (3.4.2) is given by {6,9}

$$u^*(q,t;s,\tau) = \frac{\delta\left[(r/c)-(t-\tau)\right]}{r} = \frac{c}{r}\delta\left[r-c(t-\tau)\right] \quad (3.4.6)$$

where $r = r(q,s) = |\underline{q}-\underline{s}|$, as shown in figure 3.4.1. In reference {9} substitution of u^* given by equation (3.4.6) into equation (3.2.1) is carried out in order to illustrate that the first is a solution of the second. A rigorous derivation of expression (3.4.6) can be found in reference {6}.

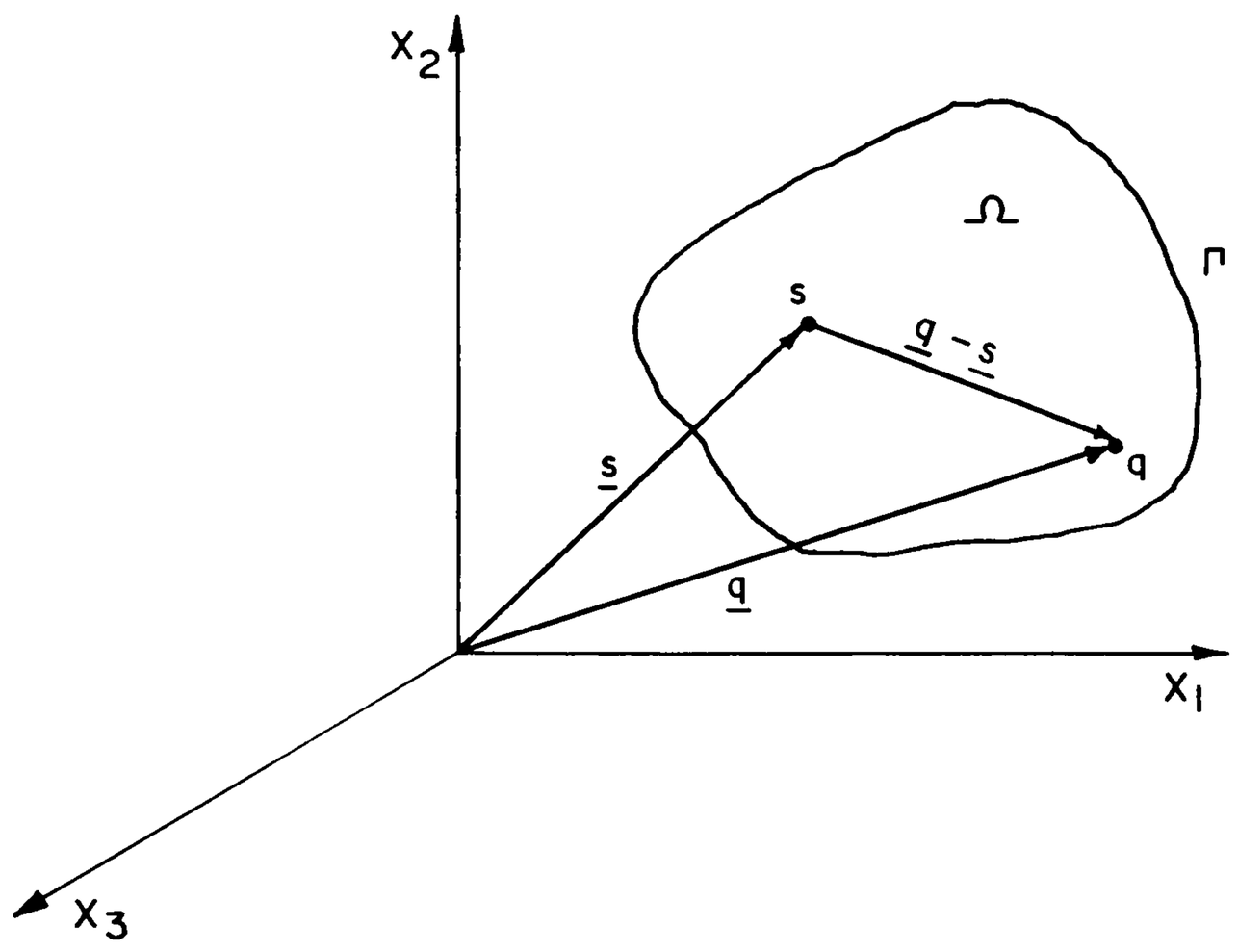

Figure 3.4.1 Definition of the vector $\underline{q}-\underline{s}$.

3.5 Kirchhoff Integral Representation

When t is replaced by τ, equation (3.2.1) is written as

$$\nabla^2 u(q,\tau) - \frac{1}{c^2}\frac{\partial^2 u(q,\tau)}{\partial \tau^2} = -\gamma(q,\tau) \quad . \quad (3.5.1)$$

From the reciprocity property equation (3.4.2) can be written as {6}

$$\nabla^2 u^*(q,t;s,\tau) - \frac{1}{c^2}\frac{\partial^2 u^*(q,t;s,\tau)}{\partial \tau^2} = -4\pi\delta(q-s)\delta(t-\tau) \quad . \tag{3.5.2}$$

It is now convenient to introduce a notation which will be employed later. In future source and field points when over the Γ boundary will be denoted respectively by S and Q.

In order to deduce a singular boundary integral equation for the problem it is necessary to consider two distribution of potentials u* and u that satisfy respectively equations (3.4.2) and (3.5.1). In addition, u* and u are assumed to be distributed respectively over the regions $\Omega+\Gamma$ and $\Omega^*+\Gamma^*$ (see figures 3.5.1 and 3.5.2) which have the same physical properties and are such that Ω^* contains $\Omega+\Gamma$. Only fundamental solutions concerning the infinite space are used in this work, therefore Γ^* must be placed at infinity and u* must obey the radiation and regularity conditions given respectively by equations (2.2.36) and (2.2.37). It is important to recognize that a procedure similar to the one described in this chapter can also be used when the fundamental solutions employed do not relate to the infinite space {34,36,54}.

A weighted residual statement for the problem under consideration can be written as {20-22}

$$\int_0^{t^+}\int_\Omega \left(\nabla^2 u - \frac{1}{c^2}\frac{\partial^2 u}{\partial \tau^2} + \gamma\right) u^* d\Omega d\tau$$

$$= \int_0^{t^+}\int_{\Gamma_2} (p-\bar{p})u^* d\Gamma d\tau - \int_0^{t^+}\int_{\Gamma_1} (u-\bar{u})p^* d\Gamma d\tau \tag{3.5.3}$$

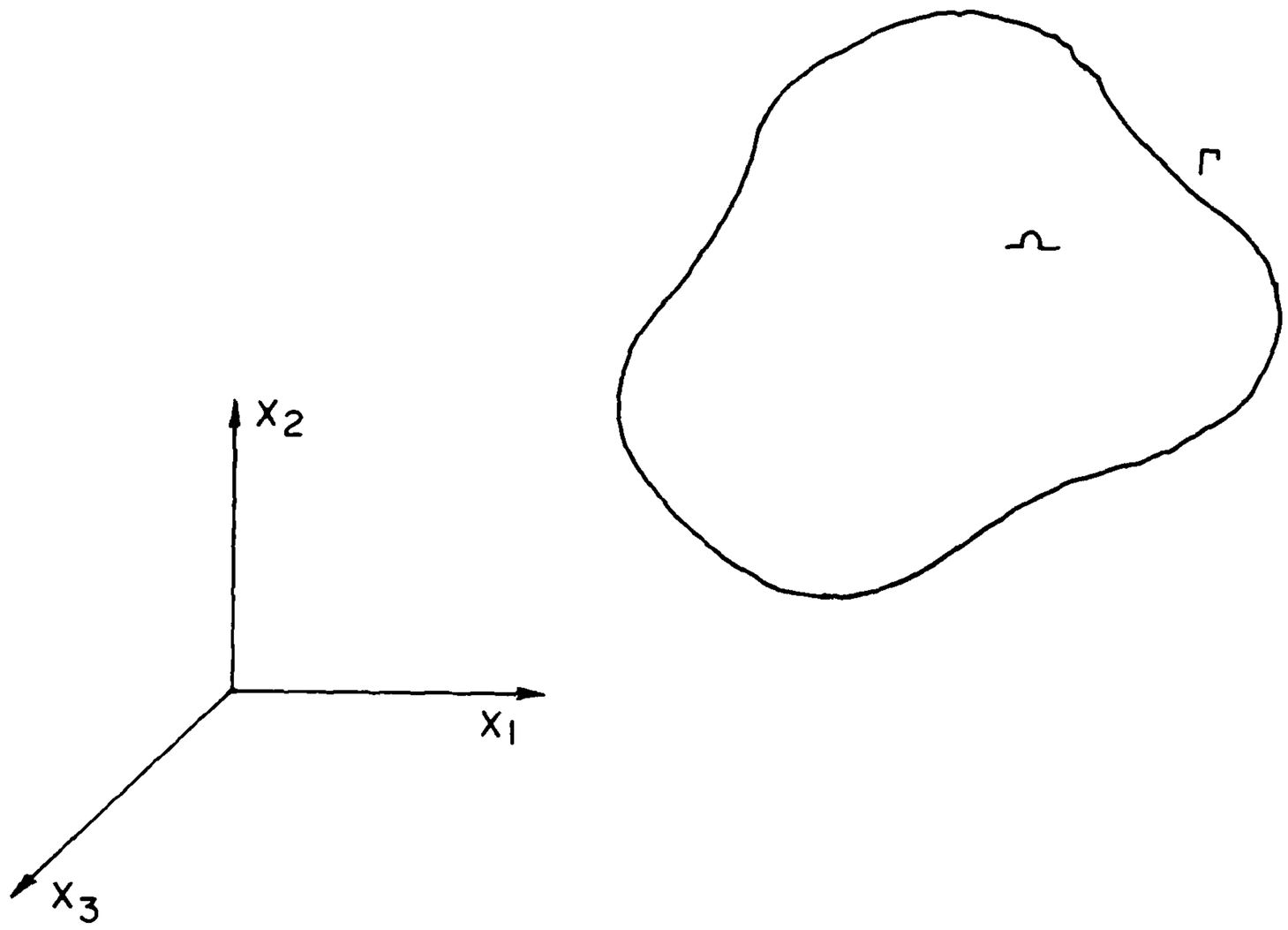

Figure 3.5.1 Three-dimensional region $\Omega+\Gamma$.

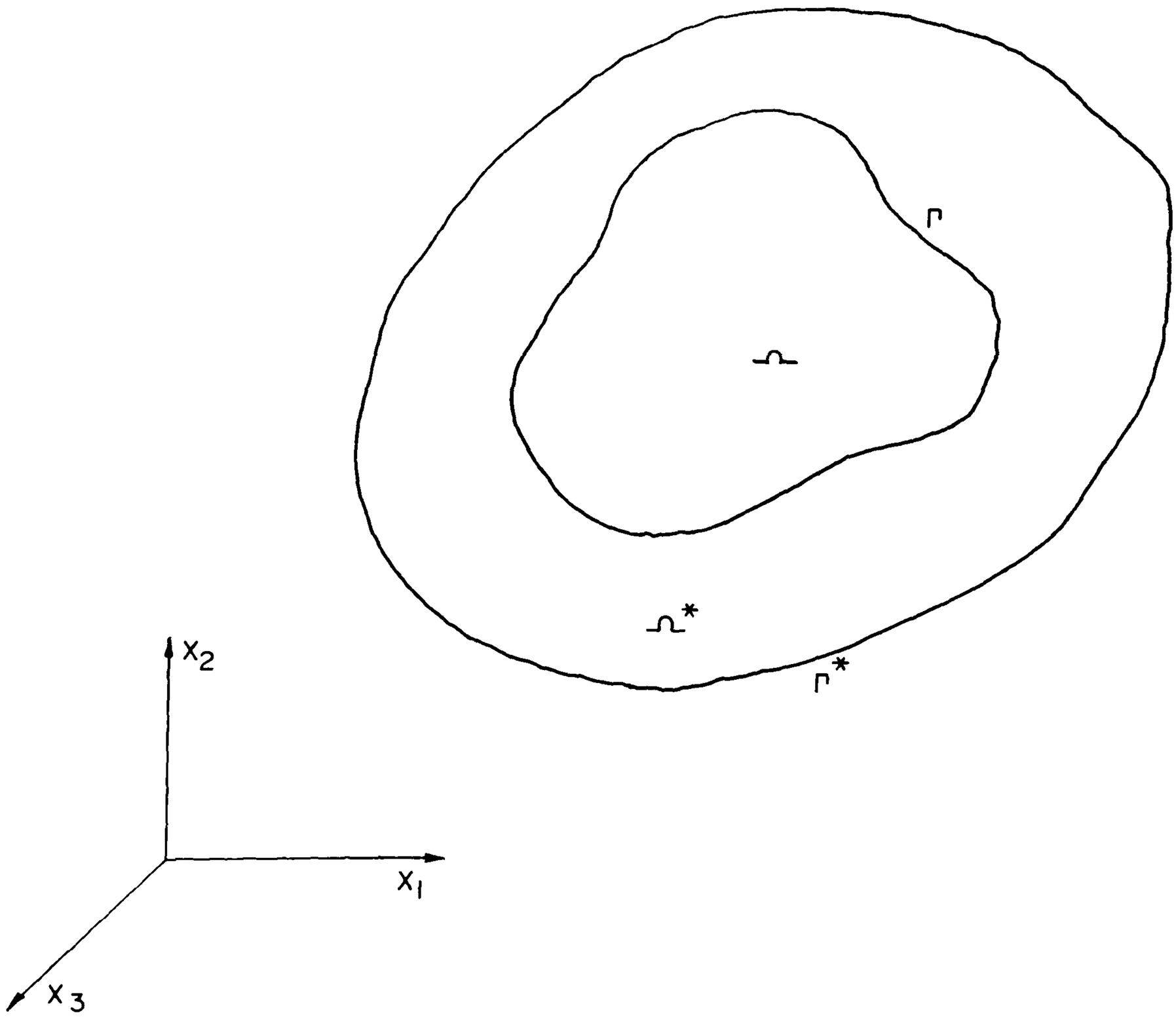

Figure 3.5.2 Region $\Omega^*+\Gamma^*$ containing $\Omega+\Gamma$.

where $p^* = \frac{\partial u^*}{\partial n}$. t^+ in equation (3.5.3) represents $t+\varepsilon$, ε being arbitrarily small. Applying this procedure avoids terminating the integration exactly at the peak of a Dirac delta function. In equation (3.5.3) space integration and derivatives refer to the coordinates of the field points q or Q. Applying the divergence theorem twice to the term of equation (3.5.3) that contains the Laplacian operator ($\nabla^2 u$) and integrating by parts twice with respect to τ the term that contains the time derivative $\frac{\partial^2 u}{\partial \tau^2}$, the following expression is obtained (see appendix A)

$$\int_0^{t^+}\int_\Gamma (u^*p-up^*)d\Gamma d\tau + \int_0^{t^+}\int_\Omega \left(\nabla^2 u^* - \frac{1}{c^2}\frac{\partial^2 u^*}{\partial \tau^2}\right) u d\Omega d\tau$$

$$+ \int_0^{t^+}\int_\Omega u^*\gamma d\Omega d\tau + \frac{1}{c^2}\int_\Omega \left[\frac{\partial u^*}{\partial \tau}u - \frac{\partial u}{\partial \tau}u^*\right]_0^{t^+} d\Omega = 0 \quad . \qquad (3.5.4)$$

Bearing in mind equation (3.5.2) and that due to the causality property

$$\left|\frac{\partial u^*}{\partial \tau}u\right|^{\tau=t^+} = \left|\frac{\partial u}{\partial \tau}u^*\right|^{\tau=t^+} = 0 \qquad (3.5.5)$$

equation (3.5.4) can be written as

$$\int_0^{t^+}\int_\Gamma (u^*p-up^*)d\Gamma d\tau - \int_0^{t^+}\int_\Omega 4\pi\delta(q-s)\delta(t-\tau)u d\Omega d\tau$$

$$+ \int_0^{t^+}\int_\Omega u^*\gamma d\Omega d\tau - \frac{1}{c^2}\int_\Omega (v_o^*u_o - v_o u_o^*)d\Omega = 0 \quad , \qquad (3.5.6)$$

where

$$v_o^* = \left|\frac{\partial u^*}{\partial \tau}\right|_{\tau=0}$$

$$u_o^* = \left|u^*\right|_{\tau=0} \quad . \tag{3.5.7}$$

When the Dirac delta properties are applied to the second term on the left-hand side of equation (3.5.6) the following integral equation is obtained,

$$\begin{aligned} u(s,t) = \frac{1}{4\pi}\Bigg[& \int_0^{t^+}\int_\Gamma u^*(Q,t;s,\tau)p(Q,\tau)d\Gamma(Q)d\tau \\ & - \int_0^{t^+}\int_\Gamma p^*(Q,t;s,\tau)u(Q,\tau)d\Gamma(Q)d\tau \\ & - \frac{1}{c^2}\int_\Omega v_o^*(q,t;s)u_o(q)d\Omega(q) \\ & + \frac{1}{c^2}\int_\Omega u_o^*(q,t;s)v_o(q)d\Omega(q) \\ & + \int_0^{t^+}\int_\Omega u^*(q,t;s,\tau)\gamma(q,\tau)d\Omega(q)d\tau\Bigg] \quad . \end{aligned} \tag{3.5.8}$$

In the operations carried out to obtain equation (3.5.8), u was assumed to be twice differentiable with respect to time and space coordinates. However, this may not be the case in many wave propagation problems. Therefore further studies concerning this situation are still required.

The properties of the Dirac delta function can be used to eliminate the time integrations in equation (3.5.8) {5,6,9,60}. Taking into consideration u* given by equation

(3.4.6) the following operations can be carried out for the first term on the right-hand side of equation (3.5.8),

$$\int_0^{t^+}\int_\Gamma u^*p\,d\Gamma d\tau = \int_\Gamma \frac{1}{r}\int_0^{t^+} \delta\left[(r/c)-(t-\tau)\right]p(Q,\tau)\,d\tau d\Gamma$$

$$= \int_\Gamma \frac{1}{r}\int_0^{t^+} \delta(\tau-t_r)p(Q,\tau)\,d\tau d\Gamma = \int_\Gamma \frac{1}{r}p(Q,t_r)\,d\Gamma \qquad (3.5.9)$$

where t_r stands for 'retarded time', equal to $\left[t-r/c\right]$.

The fundamental traction can be computed from

$$p^*(Q,t;s,\tau) = \frac{\partial}{\partial n}\left[u^*(Q,t;s,\tau)\right] = \frac{\partial r}{\partial n}\,\frac{\partial u^*}{\partial r} \quad . \qquad (3.5.10)$$

The derivatives indicated in equation (3.5.10) refers to boundary points Q. Using formula (3.4.6), p* can be written as

$$p^* = \frac{\partial r}{\partial n}\left(-\frac{1}{r^2}\delta\left[(r/c)-(t-\tau)\right] + \frac{1}{r}\,\frac{\partial}{\partial r}\delta\left[(r/c)-(t-\tau)\right]\right) . \qquad (3.5.11)$$

Equation (3.5.11) can also be written as

$$p^* = \frac{\partial r}{\partial n}\left(-\frac{1}{r^2}\delta(\tau-t_r) + \frac{1}{cr}\,\frac{\partial}{\partial \tau}\left[\delta(\tau-t_r)\right]\right) \quad . \qquad (3.5.12)$$

In view of expression (3.5.12) the second term on the right-hand side of equation (3.5.8) can be written in the following way

$$\int_0^{t^+}\int_\Gamma p^*u\,d\Gamma d\tau = \int_\Gamma \frac{\partial r}{\partial n}\int_0^{t^+}\left(-\frac{1}{r^2}\delta(\tau-t_r) + \frac{1}{cr}\,\frac{\partial}{\partial\tau}\left[\delta(\tau-t_r)\right]\right)u\,d\tau d\Gamma . \qquad (3.5.13)$$

Taking expression (3.3.2) into consideration the following equation is then obtained

$$\int_0^{t^+}\int_\Gamma p^*u\,d\Gamma d\tau = -\int_\Gamma \frac{\partial r}{\partial n}\left(\frac{1}{r^2}\,u(Q,t_r) + \frac{1}{cr}\left[\frac{\partial u(Q,\tau)}{\partial \tau}\right]_{\tau=t_r}\right)d\Gamma \quad . \qquad (3.5.14)$$

The integral involving source density in equation (3.5.8) can be operated as follows,

$$\int_0^{t^+}\int_\Omega u^*\gamma\,d\Omega d\tau = \int_\Omega \frac{1}{r}\int_0^{t^+} \gamma(q,\tau)\,\delta(\tau-t_r)\,d\tau d\Omega$$

$$= \int_\Omega \frac{1}{r}\gamma(q,t_r)\,d\Omega \quad . \qquad (3.5.15)$$

Dirac delta properties can also be applied to the terms that involve initial conditions {9} in equation (3.5.8). The final integral equation then obtained has the following form

$$u(s,t) = \frac{1}{4\pi}\int_\Gamma \frac{1}{r(s,Q)}\,p(Q,t_r)\,d\Gamma(Q)$$

$$+ \frac{1}{4\pi}\int_\Gamma \frac{\partial r(s,Q)}{\partial n(Q)}\left(\frac{1}{r^2(s,Q)}\,u(Q,t_r) + \frac{1}{cr(s,Q)}\left[\frac{\partial u(Q,\tau)}{\partial \tau}\right]_{\tau=t_r}\right)d\Gamma(Q)$$

$$+ tN_o + \frac{\partial}{\partial t}(tM_o) + \frac{1}{4\pi}\int_\Omega \frac{1}{r(s,q)}\gamma(q,t_r)\,d\Omega(q) \qquad (3.5.16)$$

where M_o and N_o are respectively the mean value of u_o and v_o over a spherical surface with centre at s and with a variable radius ct. It should be noticed that as a result of the causality property, when $t_r \leq 0$ the terms on the right-hand side of expression (3.5.16) give no contribution to u(s,t).

Equation (3.5.16) is known as the Kirchhoff's integral representation and can be considered as the mathematical representation of Huygens' principle {6,97}.

The singular integrands of the integrals referring to initial conditions in equation (3.5.8) have been eliminated. However computation of source density contributions requires integrations of a singular function $(\frac{1}{r}\gamma)$ to be performed. This is not much of a problem and can easily be done numerically using the ordinary concept of integration.

Kirchhoff's integral representation can be used to compute u at internal points in terms of u, $\frac{\partial u}{\partial n}$ and $\frac{\partial u}{\partial \tau}$ on the Γ boundary and in terms of source density and initial conditions. However, in a well-posed problem u and p are not known over the entire Γ boundary. As a result equation (3.5.16) alone does not represent the complete solution of the boundary-initial value problem described in section 3.2. A boundary integral equation from which boundary unknowns can be computed, can be derived by taking equation (3.5.16) to the Γ boundary. The integral equation obtained, unlike Kirchhoff's representation, has boundary integrals of singular functions which must be computed in the Cauchy principal value sense. The analytical manipulations required will be described next.

When the Γ boundary is assumed to satisfy the Liapunov smoothness condition {27}, the domain Ω can be augmented by a small hemisphere of radius ε, whose centre is at a boundary point S as depicted in figure 3.5.3;

Γ_ε displayed in this figure is the boundary of the hemisphere. In this situation, when initial conditions and source density are not considered, equation (3.5.16) can be written as

$$u(S,t) = \frac{1}{4\pi}\int_{\Gamma-\Gamma_\varepsilon} \frac{1}{r(S,Q)}\, p(Q,t_r)\,d\Gamma(Q)$$

$$+ \frac{1}{4\pi}\int_{\Gamma-\Gamma_\varepsilon} \frac{\partial r(S,Q)}{\partial n(Q)}\left(\frac{1}{r^2(S,Q)}u(Q,t_r) + \frac{1}{cr(S,Q)}\left[\frac{\partial u(Q,\tau)}{\partial \tau}\right]_{\tau=t_r}\right)d\Gamma(Q)$$

$$+ \frac{1}{4\pi}(S_p+S_u+S_v) \qquad (3.5.17)$$

where

$$S_p = \int_{\Gamma_\varepsilon} \frac{1}{r(S,Q)}\, p(Q,t_r)\,d\Gamma_\varepsilon(Q) \qquad (3.5.18)$$

$$S_u = \int_{\Gamma_\varepsilon} \frac{\partial r(S,Q)}{\partial n(Q)}\,\frac{1}{r^2(S,Q)}\, u(Q,t_r)\,d\Gamma_\varepsilon(Q) \qquad (3.5.19)$$

$$S_v = \int_{\Gamma_\varepsilon} \frac{\partial r(S,Q)}{\partial n(Q)}\,\frac{1}{cr(S,Q)}\left[\frac{\partial u(Q,\tau)}{\partial \tau}\right]_{\tau=t_r} d\Gamma_\varepsilon(Q)\ . \qquad (3.5.20)$$

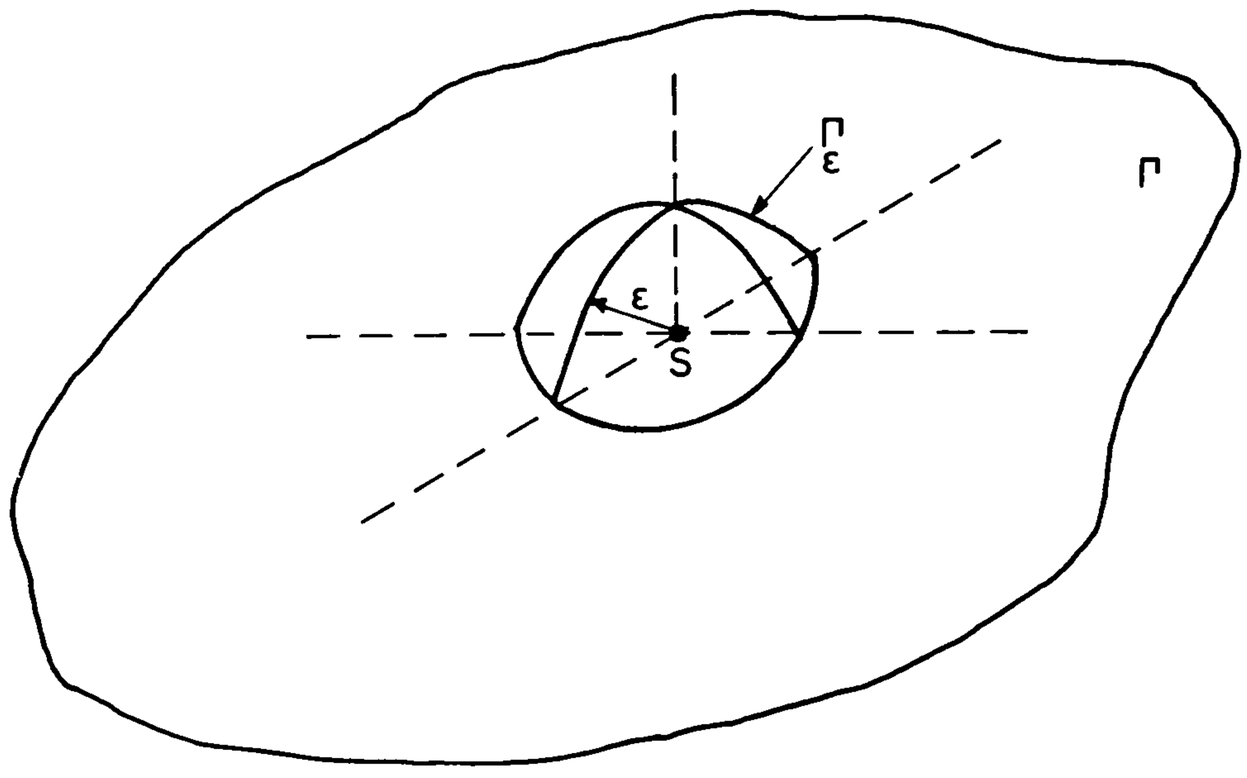

Figure 3.5.3 Domain augmented by a hemisphere of radius ε whose centre is at a boundary point S.

When $\varepsilon \to 0$; $\Gamma - \Gamma_\varepsilon \to \Gamma$, and as shown in appendix B

$$S_p = 0$$

$$\frac{1}{4\pi} S_u = \frac{1}{2} u(S,t) \qquad (3.5.21)$$

$$S_v = 0 \quad .$$

Therefore for boundary points located on smooth parts of the Γ boundary the following boundary integral equation can be written,

$$\frac{1}{2}u(S,t) = \frac{1}{4\pi}\int_\Gamma \frac{1}{r(S,Q)}\, p(Q,t_r)\, d\Gamma(Q)$$

$$+ \frac{1}{4\pi}\int_\Gamma \frac{\partial r(S,Q)}{\partial n(Q)}\left(\frac{1}{r^2(S,Q)}u(Q,t_r) + \frac{1}{cr(S,Q)}\left[\frac{\partial u(Q,\tau)}{\partial \tau}\right]_{\tau=t_r}\right) d\Gamma(Q)$$

$$+ tN_o + \frac{\partial}{\partial t}(tM_o) + \frac{1}{4\pi}\int_\Omega \frac{1}{r(S,q)}\gamma(q,t_r)\, d\Omega(q) \quad . \qquad (3.5.22)$$

It should be noticed that the integrals outlined in equation (3.5.22) are to be computed in the Cauchy principal value sense.

It is important to point out that at points s located outside $\Omega+\Gamma$ the potential is equal to zero. The integral equation corresponding to this situation can be obtained by making the left-hand side of equation (3.5.16) equal to zero, i.e., u(s,t) = 0.

Occasionally a physical phenomenon can be best represented by a concentrated source given as

$$\gamma(q,t) = f(t)\,\delta(q-q_c) \qquad (3.5.23)$$

where q_c gives the position of the source. The last integral on the right-hand side of equation (3.5.22) then

becomes

$$\frac{1}{r_c} f(t_c) \qquad (3.5.24)$$

where $r_c = |\underline{S} - \underline{q}_c|$ and $t_c = t - r_c/c$.

The numerical implementation of equation (3.5.22) is discussed in reference {60}. A special feature of the three-dimensional analysis is that no time integration is required. The same does not apply for the two-dimensional case as will be shown in the next section.

3.6 Two-Dimensional Boundary Integral Equation - Transient Scalar Wave Equation

As previously described in section 2.4 a two-dimensional problem can be seen as a three-dimensional one in which u is a function of two rectangular coordinates only, i.e.

$$u(\underline{x},t) = u(x_1,x_2,t) \quad . \qquad (3.6.1)$$

Expression (3.6.1) implies that tractions, source density and initial conditions are also independent of x_3. In this case the domain in which the problem is studied can be considered to be a cylinder whose axis has infinite length and is parallel to the x_3-direction. Then, the two-dimensional domain Ω and the Γ boundary are defined by the intersection of the cylinder with the (x_1,x_2) plane as depicted in figure 3.6.1. Therefore, for this particular three-dimensional situation the first term on the right-hand side of equation (3.5.8) can be operated as outlined below

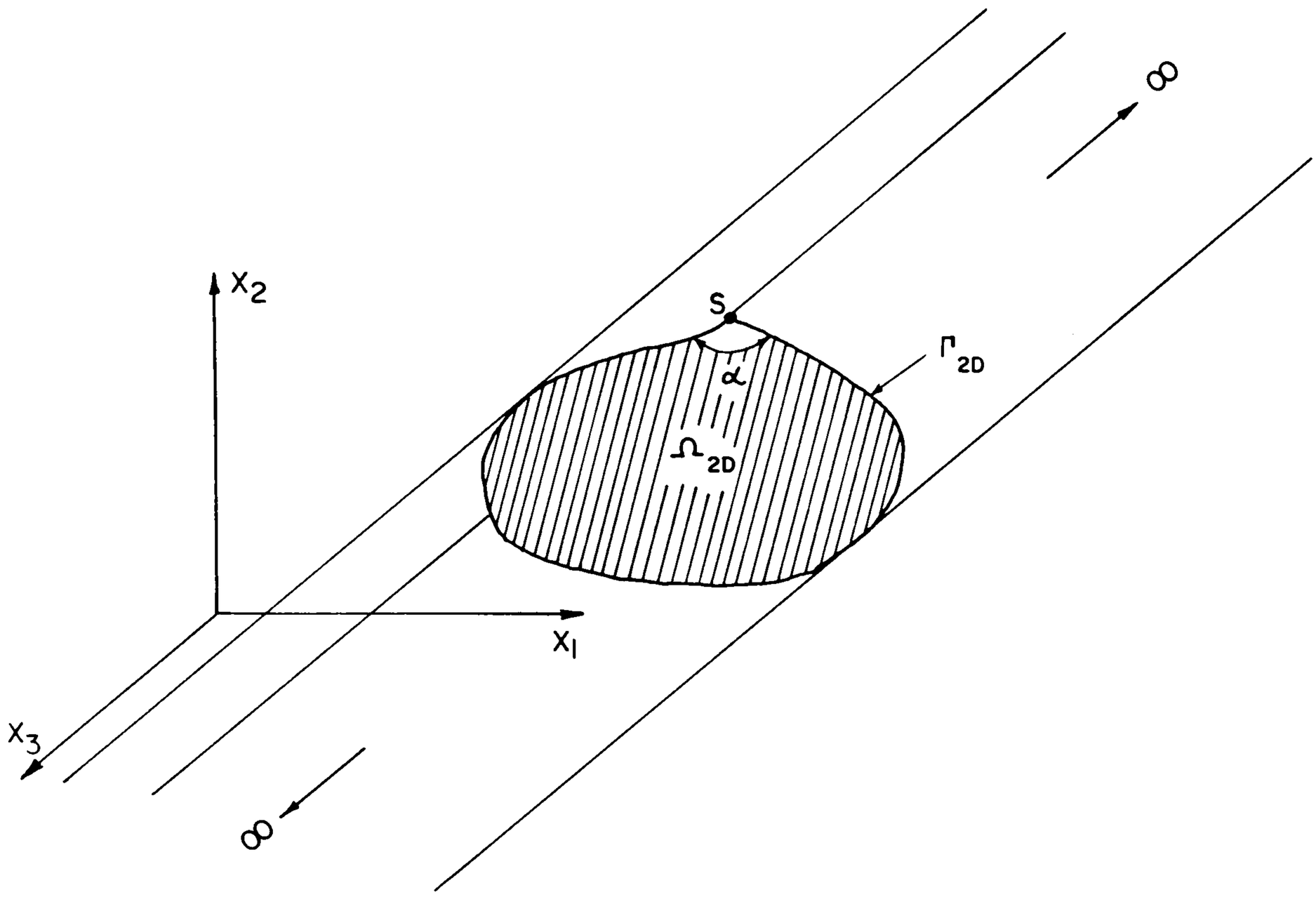

Figure 3.6.1 Two-dimensional domain with a Kellog type Γ boundary.

$$\int_0^{t^+}\int_{\Gamma_{3D}} u^*_{3D} p\, d\Gamma d\tau = \int_0^{t^+}\int_{\Gamma_{2D}} p \int_{-\infty}^{+\infty} u^*_{3D}\, dx_3\, d\Gamma_{2D}\, d\tau$$

$$= \int_0^{t^+}\int_{\Gamma_{2D}} p u^*_{2D}\, d\Gamma_{2D}\, d\tau \qquad (3.6.2)$$

where u^*_{2D} is the two-dimensional fundamental solution given by

$$u^*_{2D} = \int_{-\infty}^{+\infty} u^*_{3D}\, dx_3 \quad . \qquad (3.6.3)$$

The subscripts symbols 2D and 3D used in equations (3.6.2) and (3.6.3) indicate respectively two- and three-dimensions and will be used hereafter only when confusion is a possibility.

Transformations similar to the ones shown in expression (3.6.2) can be carried out on the other integrals in equation (3.5.8). When the resulting expression is taken to the Γ boundary the following integral equation is obtained

$$
\begin{aligned}
c(S)u(S,t) = \frac{1}{4\pi}\Bigg[& \int_0^{t^+}\int_\Gamma u^*(Q,t;S,\tau)p(Q,\tau)d\Gamma(Q)d\tau \\
& - \int_0^{t^+}\int_\Gamma p^*(Q,t;S,\tau)u(Q,\tau)d\Gamma(Q)d\tau \\
& - \frac{1}{c^2}\int_\Omega v_o^*(q,t;S)\ u_o(q)\ d\Omega(q) \\
& + \frac{1}{c^2}\int_\Omega u_o^*(q,t;S)\ v_o(q)\ d\Omega(q) \\
& + \int_0^{t^+}\int_\Omega u^*(q,t;S,\tau)\gamma(q,\tau)d\Omega(q)d\tau\Bigg]
\end{aligned}
\tag{3.6.4}
$$

where $u^* = u^*_{2D}$ is given by expression (3.6.3) and

$$
p^* = p^*_{2D} = \int_{-\infty}^{+\infty} p^*_{3D}dx_3 = \frac{\partial}{\partial n}(u^*_{2D}) \tag{3.6.5}
$$

$$
v^*_o = v^*_{o2D} = \left|\frac{\partial u^*_{2D}}{\partial \tau}\right|_{\tau=0} \tag{3.6.6}
$$

$$
u^*_o = u^*_{o2D} = \left|u^*_{2D}\right|_{\tau=0} . \tag{3.6.7}
$$

It should be understood that as it is clear that equation (3.6.4) refers to two-dimensions, the subscript symbol 2D was not used in that case.

In the three-dimensional analysis,only Liapunov boundaries were considered, hence c(S) in that situation was equal to 1/2. However, in the two-dimensional formulation a generalization was introduced, namely that the Γ boundary can be of Kellog type. The parameter c(S) in this case, as shown in appendix B, is represented by

$$c(S) = \frac{\alpha}{2\pi} \tag{3.6.8}$$

where α is the internal angle depicted in figure 3.6.1. In a similar manner to the three-dimensional case, two-dimensional integral equations that apply to points located inside and outside $\Omega+\Gamma$ can be obtained by considering c(S) in equation (3.6.4) to be respectively equal to one and zero.

The methodology used here to obtain a two-dimensional boundary integral equation for the scalar wave equation is called the method of descent {6 and 9}. Descending from the three space dimensions is not the only choice in formulating the two-dimensional problem. If the same procedure described in section 3.5 had been applied for the two-dimensional case, the result would be that equation (3.6.4) would have been obtained again.

The two-dimensional fundamental solution evolved from carrying out the integration indicated in expression (3.6.3) (for further details see appendix C) is

$$u^*(q,t;s,\tau) = \frac{2c}{\sqrt{c^2(t-\tau)^2 - r^2}} H\left[c(t-\tau)-r\right] . \qquad (3.6.9)$$

The integral equation for the two-dimensional scalar wave equation was first obtained by Volterra {94}. A comparison between Volterra's and Kirchhoff's formulas displays a significant difference between two- and three-dimensional waves. Kirchhoff's formula demonstrates that at a time t, only the signal emitted at a point s at a time $(t - |q-s|/c)$ affects a point q. Volterra's formula, however, implies that in two dimensions a point q is affected at an instant t, by signals emitted at a point s, at all times previous to $(t - |q-s|/c)$. A more comprehensive discussion of this interesting discrepancy of behaviour of two- and three-dimensional waves can be found in references {6 and 9}.

In addition to being of great benefit to the more complete understanding of wave propagation phenomena, Volterra's formula can also be used to obtain analytical solutions. However it has to undergo further transformations before it can be used in a numerical analysis.

3.7 Additional Transformations to Volterra's Integral Representation

The objective of the operations carried out in (i) and (ii) that follow is to remove the time and space derivatives of the Heaviside function that appear in Volterra's integral equation.

(i) The second term on the right-hand side of equation (3.6.4) can be operated as follows,

$$\int_0^{t^+}\int_\Gamma p^*u\,d\Gamma d\tau = \int_0^{t^+}\int_\Gamma u\,\frac{\partial u^*}{\partial n}\,d\Gamma d\tau = \int_0^{t^+}\int_\Gamma \frac{\partial r}{\partial n}\,u\,\frac{\partial u^*}{\partial r}\,d\Gamma d\tau. \tag{3.7.1}$$

Substituting formula (3.6.9) into expression (3.7.1), the following expression is obtained

$$\int_\Gamma\int_0^{t^+} \frac{\partial r}{\partial n}\,u\,\frac{\partial u^*}{\partial r}\,d\tau d\Gamma$$

$$= \int_\Gamma\int_0^{t^+} \frac{\partial r}{\partial n}\,u\,\frac{2cr}{\sqrt{\left[c^2(t-\tau)^2-r^2\right]^3}}\,H\left[c(t-\tau)-r\right]d\tau d\Gamma$$

$$+ \int_\Gamma \frac{\partial r}{\partial n}\int_0^{t^+} u\,\frac{2c}{\sqrt{c^2(t-\tau)^2-r^2}}\,\frac{\partial}{\partial r}\left(H\left[c(t-\tau)-r\right]\right)d\tau d\Gamma \quad . \tag{3.7.2}$$

Further operations must now be performed on the second term on the right-hand side of equation (3.7.2). The following relationship will be used

$$\frac{\partial}{\partial r}\left(H\left[c(t-\tau)-r\right]\right) = \frac{\partial}{\partial(c\tau)}\left(H\left[c(t-\tau)-r\right]\right)$$

$$= \frac{\partial}{\partial r}\left(1 - H\left[r-c(t-\tau)\right]\right) = -\delta\left[r-c(t-\tau)\right] \quad . \tag{3.7.3}$$

Therefore, using the notation,

$$L = L(r,t,\tau) = 2\left[c^2(t-\tau)^2-r^2\right]^{-1/2} \tag{3.7.4}$$

$$L_o = L_o(r,t,0) = 2(c^2t^2-r^2)^{-1/2} \tag{3.7.5}$$

and bearing in mind expressions (3.3.1) and (3.7.3) the following transformations can be carried out

$$\int_\Gamma \frac{\partial r}{\partial n} \int_0^{t^+} u \frac{2c}{\sqrt{c^2(t-\tau)^2-r^2}} \frac{\partial}{\partial r}\left(H\left[c(t-\tau)-r\right]\right) d\tau d\Gamma$$

$$= \int_\Gamma \frac{\partial r}{\partial n} \int_0^{t^+} ucL \frac{\partial}{\partial r}\left(H\left[c(t-\tau)-r\right]\right) d\tau d\Gamma$$

$$= -\int_\Gamma \frac{\partial r}{\partial n} \int_0^{ct^+} uL\,\delta\left[c\tau-(ct-r)\right] d(c\tau) d\Gamma$$

$$= -\int_\Gamma \frac{\partial r}{\partial n} \left[uL\right]_{c\tau=ct-r} d\Gamma$$

$$= -\int_\Gamma \frac{\partial r}{\partial n} \int_0^{ct-r} \frac{\partial}{\partial(c\tau)} (uL) d(c\tau) d\Gamma - \int_\Gamma \frac{\partial r}{\partial n} u_o L_o H\left[ct-r\right] d\Gamma$$

$$= -\int_0^{t^+} \int_\Gamma \frac{\partial r}{\partial n}\left[c^2(t-\tau)\, u \frac{L^3}{4} + (\partial u/\partial\tau) L\right] H\left[c(t-\tau)-r\right] d\Gamma d\tau$$

$$-\int_\Gamma \frac{\partial r}{\partial n} u_o L_o H\left[ct-r\right] d\Gamma \quad . \qquad (3.7.6)$$

Taking expressions (3.7.1), (3.7.2), (3.7.4), (3.7.5) and (3.7.6) into consideration the following expression can be derived

$$\int_0^{t^+} \int_\Gamma p^* u \, d\Gamma d\tau$$

$$= -\int_0^{t^+} \int_\Gamma \frac{\partial r}{\partial n}\left[u \frac{2c\left[c(t-\tau)-r\right]}{\sqrt{\left[c^2(t-\tau)^2-r^2\right]^3}} + \frac{2(\partial u/\partial\tau)}{\sqrt{c^2(t-\tau)^2-r^2}}\right] H\left[c(t-\tau)-r\right] d\Gamma d\tau$$

$$-\int_\Gamma \frac{\partial r}{\partial n} \frac{2u_o}{\sqrt{c^2t^2-r^2}} H\left[ct-r\right] d\Gamma \quad . \qquad (3.7.7)$$

(ii) The following property of the Heaviside function

$$\frac{\partial}{\partial \tau} H\left[c(t-\tau)-r\right] = c \frac{\partial}{\partial r} H\left[c(t-\tau)-r\right] \qquad (3.7.8)$$

is required in the transformations regarding the third term of the right-hand side of equation (3.6.4), given by

$$\int_{\Omega} v_o^* u_o \, d\Omega \quad . \qquad (3.7.9)$$

Taking account of expression (3.6.9) it is possible to write

$$\int_{\Omega} v_o^* u_o \, d\Omega = \int_{\Omega} \left[\frac{\partial u^*}{\partial \tau}\right]_{\tau=0} u_o d\Omega$$

$$= \int_{\Omega} u_o \frac{2c^3 t}{\sqrt{\left[c^2t^2-r^2\right]^3}} H\left[ct-r\right] d\Omega$$

$$+ \int_{\Omega} u_o \frac{2c^2}{\sqrt{c^2t^2-r^2}} \frac{\partial}{\partial r}\left(H\left[ct-r\right]\right) d\Omega \quad . \qquad (3.7.10)$$

A further investigation concerning the second term on the right-hand side of expression (3.7.10) is now required. If this term is called I_2, and a system of polar coordinates is adopted (see figure 3.7.1) whose origin is at the source point s, I_2 can be written as

$$I_2 = \int_{\theta_1}^{\theta_2} \int_{r=0}^{r=r_\Gamma(\theta)} r u_o \frac{2c^2}{\sqrt{c^2t^2-r^2}} \frac{\partial}{\partial r}\left(H\left[ct-r\right]\right) dr d\theta \qquad (3.7.11)$$

where $\theta_1 = 0$, $\theta_2 = 2\pi$ and

$$r_\Gamma(\theta) = r(s,Q) = |\underline{Q}-\underline{s}| \qquad (3.7.12)$$

defines the Γ boundary in polar coordinates (see figure 3.7.1).

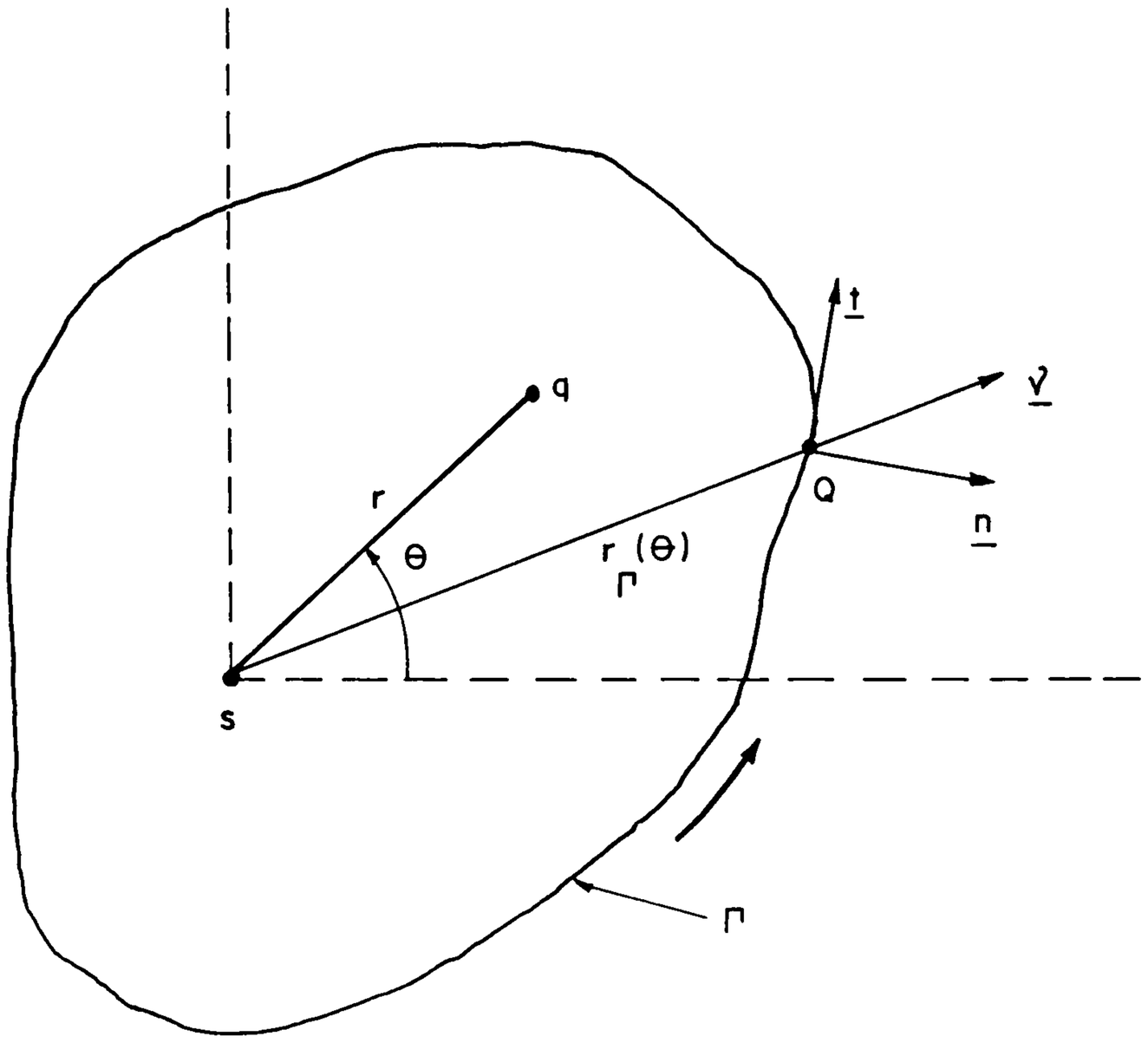

Figure 3.7.1 System of polar coordinates.

If expression (3.7.11) is integrated by parts with respect to r, the following expression is obtained,

$$I_2 = \int_{\theta_1}^{\theta_2} \left[r u_o \frac{2c^2}{\sqrt{c^2t^2-r^2}} H\left[ct-r\right] \right]_0^{r_\Gamma(\theta)} d\theta$$

$$- \int_{\theta_1}^{\theta_2} \int_{r=0}^{r=r_\Gamma(\theta)} \frac{\partial}{\partial r} \left(r u_o c^2 L_o \right) H\left[ct-r\right] dr d\theta \quad . \qquad (3.7.13)$$

Further manipulations give

$$I_2 = \int_{\theta_1}^{\theta_2} u_o\left[\bar{r}_\Gamma(\theta)\right] \frac{2c^2}{\sqrt{c^2t^2-r_\Gamma^2(\theta)}} H\left[ct-r_\Gamma(\theta)\right] r_\Gamma(\theta)\,d\theta$$

$$- \int_\Omega \frac{1}{r} u_o c^2 L_o H\left[ct-r\right] d\Omega - \int_\Omega \frac{\partial u_o}{\partial r} c^2 L_o H\left[ct-r\right] d\Omega$$

$$- \int_\Omega u_o c^2 r \frac{L_o^3}{4} H\left[ct-r\right] d\Omega \quad . \qquad (3.7.14)$$

The first integral on the right-hand side of expression (3.7.14) can be transformed by applying the following formula (see appendix D)

$$\int_{\theta_1}^{\theta_2} f\left[\bar{r}_\Gamma(\theta)\right] r_\Gamma(\theta)\,d\theta = \int_\Gamma f\left[\bar{r}(s,Q)\right] \frac{\partial r(s,Q)}{\partial n(Q)}\, d\Gamma(Q) \qquad (3.7.15)$$

and so it is possible to write

$$\int_{\theta_1}^{\theta_2} u_o\left[\bar{r}_\Gamma(\theta)\right] \frac{2c^2}{\sqrt{c^2t^2-r_\Gamma^2(\theta)}} H\left[ct-r_\Gamma(\theta)\right] r_\Gamma(\theta)\,d\theta$$

$$= \int_\Gamma \frac{\partial r(s,Q)}{\partial n(Q)} \frac{2c^2 u_o(Q)}{\sqrt{c^2t^2-r^2(s,Q)}} H\left[ct-r(s,Q)\right] d\Gamma(Q) \quad . \qquad (3.7.16)$$

Taking expressions (3.7.5), (3.7.10), (3.7.14) and (3.7.16) into consideration, the following relationship can be stated

$$\int_\Omega v_o^* u_o\, d\Omega$$

$$= -\int_\Omega \left\{ u_o \left[\frac{2c^2(r-ct)}{\sqrt{\left[c^2t^2-r^2\right]^3}} + \frac{2c^2}{r\sqrt{c^2t^2-r^2}} \right] \right.$$

$$+ \frac{\partial u_o}{\partial r} \frac{2c^2}{\sqrt{c^2t^2-r^2}} \Bigg) H\left[ct-r\right] d\Omega$$

$$+ \int_\Gamma \frac{\partial r}{\partial n} u_o \frac{2c^2}{\sqrt{c^2t^2-r^2}} H\left[ct-r\right] d\Gamma \quad . \tag{3.7.17}$$

The last terms on the right-hand side of expressions (3.7.7) and (3.7.17) will cancel out within equation (3.6.4) to produce the final integral statement which for points located on the Γ boundary is written as

$$4\pi c(S)u(S,t) = \int_0^{t^+}\int_\Gamma u^* p \, d\Gamma d\tau + \int_0^{t^+}\int_\Gamma \frac{\partial r}{\partial n} (B^* u + u^* \frac{v}{c}) d\Gamma d\tau$$

$$+ \frac{1}{c^2} \int_\Omega u_o^* v_o d\Omega + \frac{1}{c} \int_\Omega (-B_o^* u_o + u_o^* \frac{\partial u_o}{\partial r} + u_o^* \frac{u_o}{r}) d\Omega$$

$$+ \int_0^{t^+}\int_\Omega \gamma u^* d\Omega d\tau \tag{3.7.18}$$

where u^* and u_o^* are given respectively by expressions (3.6.9) and (3.5.7),

$$B^* = B^*(Q,t;S,\tau) = \frac{2c\left[c(t-\tau)-r\right]}{\sqrt{\left[c^2(t-\tau)^2-r^2\right]^3}} H\left[c(t-\tau)-r\right] \quad , \tag{3.7.19}$$

$$B_o^* = B_o^*(Q,t;S) = B^*(Q,t;S,0) \tag{3.7.20}$$

and v indicates velocity as given by

$$v = \frac{\partial u}{\partial \tau} \quad . \tag{3.7.21}$$

It should be recognized that equation (3.7.18) can also be used for points inside the domain Ω. As stated previously, c(s) must be regarded as equal to 1 in this situation.

Two distinct types of singularities can occur in the integrands of equation (3.7.18). The first type of singularity occurs in the integral of the initial conditions when $r=0$ and in the boundary integrals when r and $c(t-\tau)$ are simultaneously null. The second type of singularity occurs at points located at the front of the wave represented by the Green's function, that is, in the boundary and source density integrals when $r=c(t-\tau)$, and in the integrals of the initial conditions when $r=ct$. Nevertheless numerical integration of equation (3.7.18) does not present any notable difficulty as it will be discussed in the next chapter.

CHAPTER 4

BOUNDARY ELEMENT METHOD FOR TWO-DIMENSIONAL TRANSIENT PROBLEMS GOVERNED BY THE SCALAR WAVE EQUATION

4.1 Introduction

Time and space interpolation functions, similar to the ones used in finite elements, can be employed to transform the integral equation (3.7.18) into a system of algebraic equations whose solution supplies the boundary unknowns u and p. The potential u(s,t) at internal points can then be calculated by using equation (3.7.18) with c(S) = 1. This procedure is standard in boundary element formulations {20 and 21}; but a discussion about this subject is necessary in order to clarify certain factors which only appear in the problem under consideration.

The usual time marching schemes consider each time step as a new problem and consequently at the end of each time interval, values of displacements and velocities are calculated for a sufficient number of internal points; this is in order to use them as pseudo-initial conditions for the next step, i.e. the integral equation (3.7.18) is applied from 0 to Δt, Δt to $2\Delta t$ etc. In this thesis however the time integration process is always considered to start at the time '0' and so values of displacements and velocities do not need to be calculated at intermediate steps. With this procedure the domain discretization is restricted to regions where source density and initial conditions do not disappear. Domain integrations at a time step 'j' are then avoided at the cost of having to

compute time integrations for all time steps previous to 'j'. This technique is especially suitable for infinite and semi-infinite domains. A comparison of the performance of both techniques for transient heat transfer problems can be found in reference {35}.

The examples presented in this chapter illustrate the numerical procedure of solution implemented in this thesis and also show the degree of accuracy that can be expected from this scheme. The examples also elucidate other important factors such as the number of integration points, and also the relation between boundary elements length and time step size that are suitable in the numerical analysis.

4.2 Numerical Implementation

In this section the numerical implementation of equation (3.7.18) is discussed. Occasionally the summation symbol is used instead of the summation convention defined by equation (2.2.1). This is done to simplify the comprehension of certain equations, and in this case summation symbols invalidate summation convention over repeated indices.

4.2.1 Boundary Integrals - In order to implement a numerical scheme to solve equation (3.7.18), it is necessary to consider a set of discrete points (nodes) Q_j, j=1,...,J on the Γ boundary, and also a set of values of time t_n, n=1,...,N. u(Q,t), v(Q,t) and p(Q,t) can be approximated using a set of interpolation functions as indicated below

$$u(Q,t) = \sum_{j=1}^{J} \sum_{m=1}^{N} \phi^m(t)\,\eta_j(Q)\,u_j^m$$

$$v(Q,t) = \sum_{j=1}^{J} \sum_{m=1}^{N} \frac{d\phi^m(t)}{dt}\,\eta_j(Q)\,u_j^m \qquad (4.2.1)$$

$$p(Q,t) = \sum_{j=1}^{J} \sum_{m=1}^{N} \theta^m(t)\,\nu_j(Q)\,p_j^m$$

where m and j refer to time and space respectively. $\phi^m(t)$, $\eta_j(Q)$, $\theta^m(t)$ and $\nu_j(Q)$ are chosen such that

$$\eta_j(Q_i) = \delta_{ij}$$

$$\nu_j(Q_i) = \delta_{ij} \qquad (4.2.2)$$

$$\phi^m(t_n) = \delta_{mn}$$

$$\theta^m(t_n) = \delta_{mn}$$

where δ_{ij} is the Kronecker delta defined by expression (2.2.2). Therefore

$$u_j^m = u(Q_j,t_m) \qquad (4.2.3)$$

$$p_j^m = p(Q_j,t_m) \quad .$$

If equation (3.7.18) is written for every node i and for every value of time t_n, and u, v and p are replaced by their approximations given by expression (4.2.1), the following system of algebraic equations is then obtained

$$c(S_i)u_i^n + \frac{1}{4\pi}\sum_{m=1}^{N}\sum_{j=1}^{J} H_{ij}^{nm}u_j^m = \frac{1}{4\pi}\left(\sum_{m=1}^{N}\sum_{j=1}^{J} G_{ij}^{nm}p_j^m + F_i^n + S_i^n\right) \tag{4.2.4}$$

where

$$H_{ij}^{nm} = -\int_\Gamma \frac{\partial r(S_i,Q)}{\partial n(Q)}\,\eta_j(Q)\int_0^{t_n}\Big[\phi^m(\tau)B^*(Q,t_n;S_i,\tau)$$

$$+ \frac{1}{c}\frac{d\phi^m(\tau)}{d\tau}\,u^*(Q,t_n;S_i,\tau)\Big]d\tau d\Gamma(Q) \tag{4.2.5}$$

$$G_{ij}^{nm} = \int_\Gamma \nu_j(Q)\int_0^{t_n}\theta^m(\tau)u^*(Q,t_n;S_i,\tau)d\tau d\Gamma(Q) \tag{4.2.6}$$

$$F_i^n = \frac{1}{c^2}\int_\Omega u_o^*(q,t_n;S_i)v_o(q)d\Omega(q)$$

$$+ \frac{1}{c}\int_\Omega u_o^*(q,t_n;S_i)\,\frac{\partial u_o(q)}{\partial r(S_i,q)}\,d\Omega(q) \tag{4.2.7}$$

$$+ t_n\int_\Omega \frac{1}{r(S_i,q)}\,B_o^*(q,t_n;S_i)\,u_o(q)\,d\Omega(q)$$

$$S_i^n = \int_0^{t_n}\int_\Omega u^*(q,t_n;S_i,\tau)\gamma(q,\tau)d\Omega(q)d\tau \quad . \tag{4.2.8}$$

It should be recognized that the third term on the right-hand side of equation (4.2.7) is the sum of the first and third terms of the integrand of the fourth integral on the right-hand side of equation (3.7.18).

Let Δt_m be such that $\phi^m(\tau) = 0$ whenever $\tau < t_m - \Delta t_m$ (see figure 4.2.1.a) and allow c_i^{nm} to be a domain

bounded by a circle of radius $c(t_n-t_m+\Delta t_m)$ with centre at the node i (see figure 4.2.1.b).

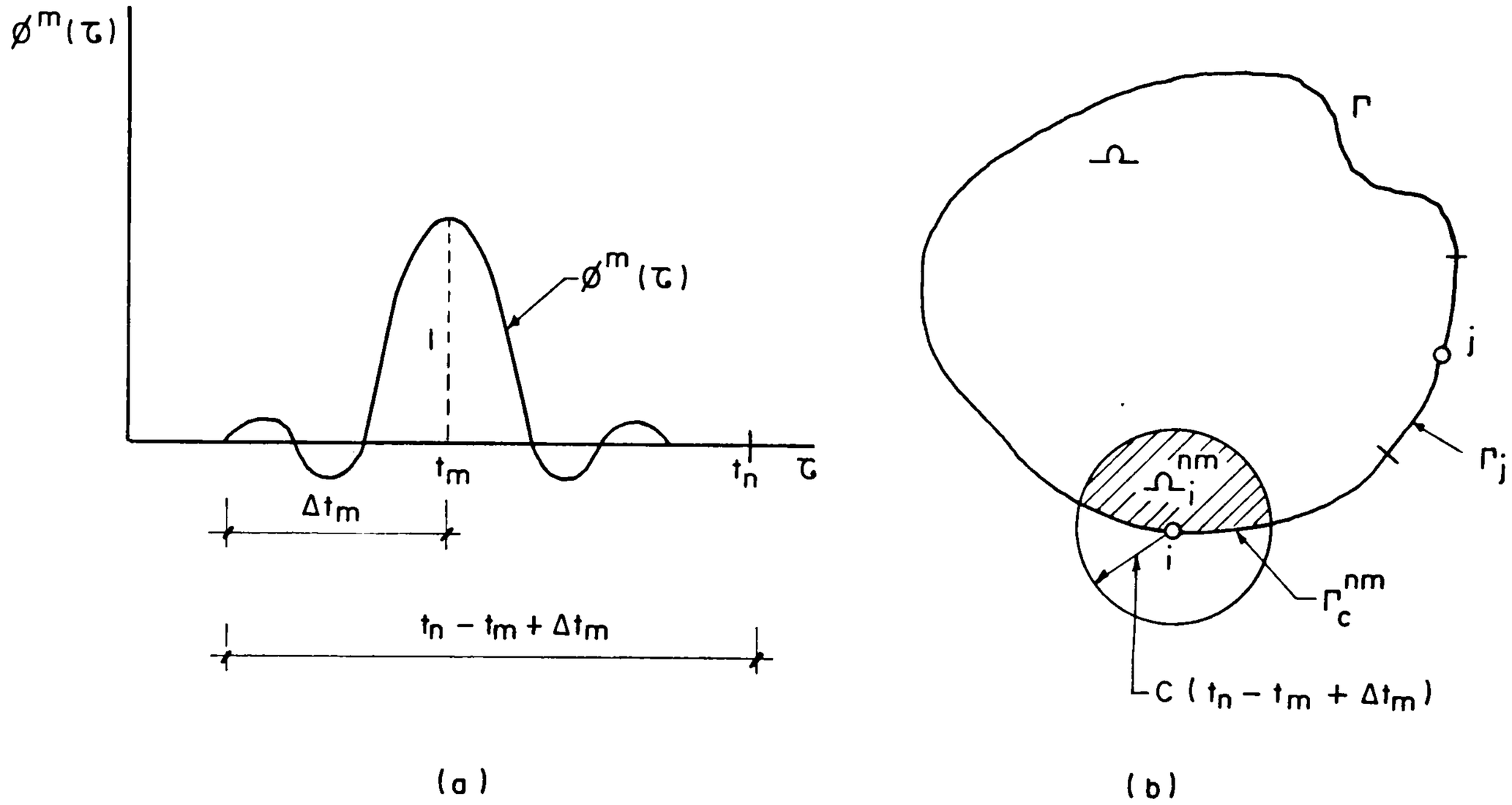

Figure 4.2.1 Interpolation function $\phi^m(\tau)$, domain Ω_i^{nm} and boundary segments Γ_c^{nm} and Γ_j.

A coefficient H_{ij}^{nm} given by equation (4.2.5) is null whenever $\Gamma_j \cap \Gamma_c^{nm} = \mathbf{o}$; $\mathbf{o}$ is the null space, Γ_c^{nm} is $\Gamma \cap c_i^{nm}$ and Γ_j is such that $\phi_j(Q) = 0$ whenever $Q \notin \Gamma_j$. It should be noted that a similar discussion leads to similar conclusions for the coefficients G_{ij}^{nm} given by expression (4.2.6).

If Ω_i^{nm} is $c_i^{nm} \cap \Omega$, then due to the causality property, F_i^n and S_i^n given respectively by expressions (4.2.7) and (4.2.8), can be obtained by carrying out domain

integrations over Ω_i^{no} only, where Ω_i^{no} is equivalent to Ω_i^{nm} for $t_m = \Delta t_m = 0$.

If the discussion just carried out is taken into consideration computer time can be saved.

Due to the difficulty to visualize how boundary unknowns vary with time it is usual to adopt

$$t_{m+1} - t_m = \Delta t = \text{constant} \quad . \tag{4.2.9}$$

In this case $\phi^m(t)$ can be assigned the time translation property, i.e.

$$\phi^m(t) = \phi^{m+l}(t+l\Delta t) \quad . \tag{4.2.10}$$

Hence

$$H_{ij}^{nm} = H_{ij}^{(n+l)(m+l)}$$

$$G_{ij}^{nm} = G_{ij}^{(n+l)(m+l)} \quad . \tag{4.2.11}$$

If expression (4.2.11) is taken into consideration, a large number of redundant operations can be avoided in the numerical analysis.

A time-stepping scheme in which equation (4.2.4) is successively solved for n=1,...,N can be used to calculate unknowns u_j^N and q_j^N at the time t_N. The actual numerical implementation of such a scheme requires, of course, the specification of the type of interpolation function to be used; this will be considered next.

Initially linear time interpolation functions $\phi^m(\tau)$ and $\theta^m(\tau)$ (see figure 4.2.2) will be considered, i.e.

$$\phi^m(\tau) = \theta^m(\tau) = \begin{cases} \frac{1}{\Delta t}(\tau - t_{m-1}) & \text{if } t_{m-1} < \tau < t_m, \\ \frac{1}{\Delta t}(t_{m+1} - \tau) & \text{if } t_m < \tau < t_{m+1}, \\ 0 \quad \text{otherwise} & . \end{cases} \tag{4.2.12}$$

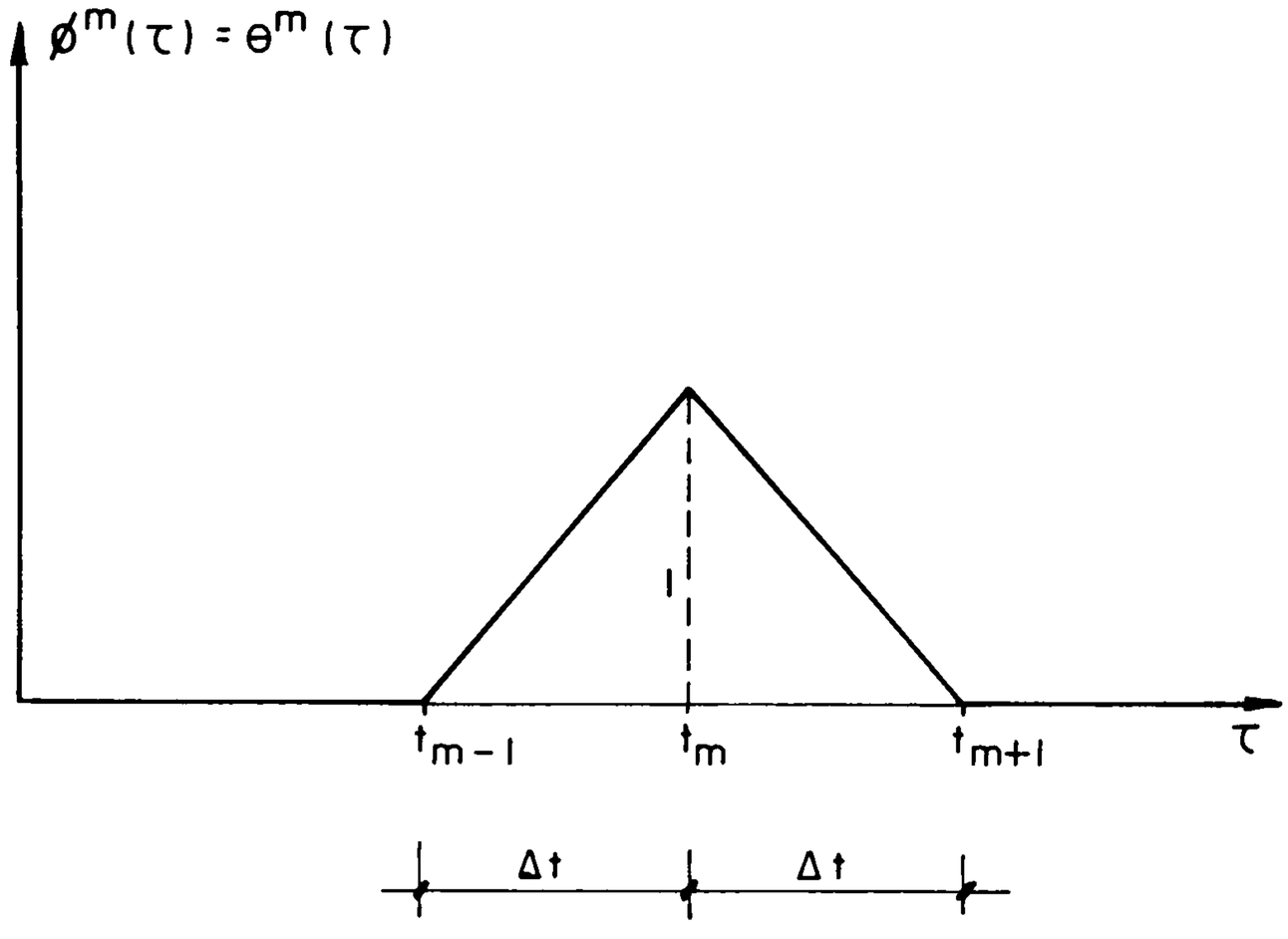

Figure 4.2.2 Linear time interpolation functions for u and p on the Γ boundary.

The substitution of expression (4.2.12) into formulas (4.2.5) and (4.2.6) gives

$$H_{ij}^{nm} = (H_{ij}^{nm})_I + (H_{ij}^{nm})_F$$

$$G_{ij}^{nm} = (G_{ij}^{nm})_I + (G_{ij}^{nm})_F \tag{4.2.13}$$

where

$$(H_{ij}^{nm})_I = -\frac{1}{\Delta t}\int_\Gamma \frac{\partial r}{\partial n}\,\eta_j(Q)\int_{t_{m-1}}^{t_m}\left[(\tau - t_{m-1})B_i^{*n} + \frac{1}{c}\,u_i^{*n}\right]d\tau d\Gamma$$

$$(H_{ij}^{nm})_F = -\frac{1}{\Delta t}\int_\Gamma \frac{\partial r}{\partial n}\,\eta_j(Q)\int_{t_m}^{t_{m+1}}\left[(t_{m+1} - \tau)B_i^{*n} - \frac{1}{c}\,u_i^{*n}\right]d\tau d\Gamma$$

$$(G_{ij}^{nm})_I = \frac{1}{\Delta t}\int_\Gamma \nu_j(Q)\int_{t_{m-1}}^{t_m}(\tau - t_{m-1})u_i^{*n}\,d\tau d\Gamma$$

$$(G_{ij}^{nm})_F = \frac{1}{\Delta t}\int_\Gamma \nu_j(Q)\int_{t_m}^{t_{m+1}}(t_{m+1}-\tau)u_i^{*n}\,d\tau d\Gamma \quad . \qquad (4.2.14)$$

In expression (4.2.14)

$$u_i^{*n} = u^*(Q,t_n;S_i,\tau)$$

$$B_i^{*n} = B^*(Q,t_n;S_i,\tau) \quad . \qquad (4.2.15)$$

When $\phi^m(\tau)$ and $\theta^m(\tau)$ are linear, H_{ij}^{nm} and G_{ij}^{nm} are null whenever m>n because in this situation

$$H\left[c(t_n-\tau)-r\right]\phi^m(\tau) = 0 \qquad (4.2.16)$$

$$H\left[c(t_n-\tau)-r\right]\theta^m(\tau) = 0$$

as illustrated in figure 4.2.3.

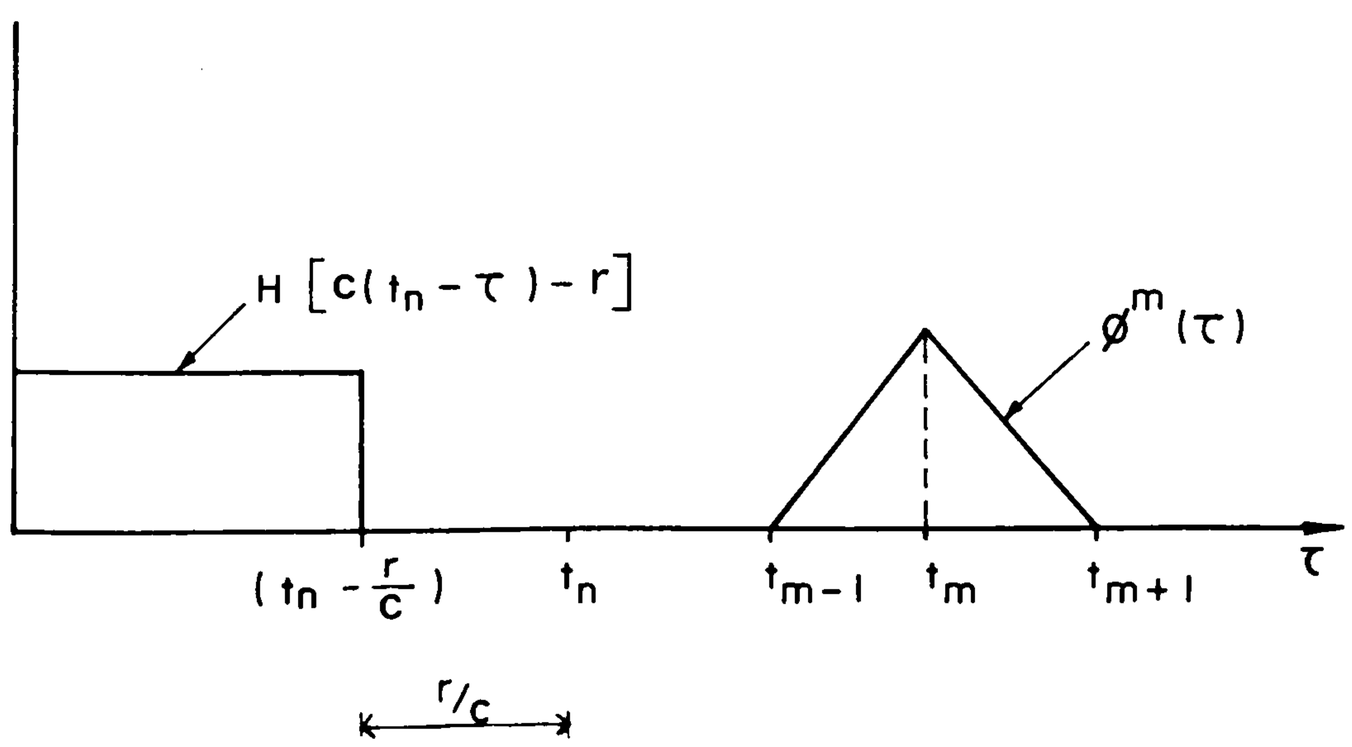

Figure 4.2.3 Illustration of a situation in which $H_{ij}^{nm} = G_{ij}^{nm} = 0$.

The time integration indicated in equation (4.2.14) can be carried out analytically giving

$$(H_{ij}^{nm})_I = \frac{2}{c\Delta t} \int_\Gamma \frac{\partial r}{\partial n}\, \eta_j(Q)\ \ (D_i^{nm})_I\, d\Gamma$$

$$(H_{ij}^{nm})_F = \frac{2}{c\Delta t} \int_\Gamma \frac{\partial r}{\partial n}\, \eta_j(Q)\ \ (D_i^{nm})_F\, d\Gamma$$

$$(G_{ij}^{nm})_I = \frac{2}{c\Delta t} \int_\Gamma \nu_j(Q)\ \ (E_i^{nm})_I\, d\Gamma$$

$$(G_{ij}^{nm})_F = \frac{2}{c\Delta t} \int_\Gamma \nu_j(Q)\ \ (E_i^{nm})_F\, d\Gamma \qquad (4.2.17)$$

where $(D_i^{nm})_I$, $(D_i^{nm})_F$, $(E_i^{nm})_I$ and $(E_i^{nm})_F$ are given in appendix E.

When $\theta^m(\tau)$ is constant (see figure 4.2.4), $\theta^m(\tau)$ can be represented in the following way

$$\theta^m(\tau) = \begin{cases} 1 & \text{if } t_{m-1} < \tau < t_m \\ 0 & \text{otherwise} \end{cases} \qquad (4.2.18)$$

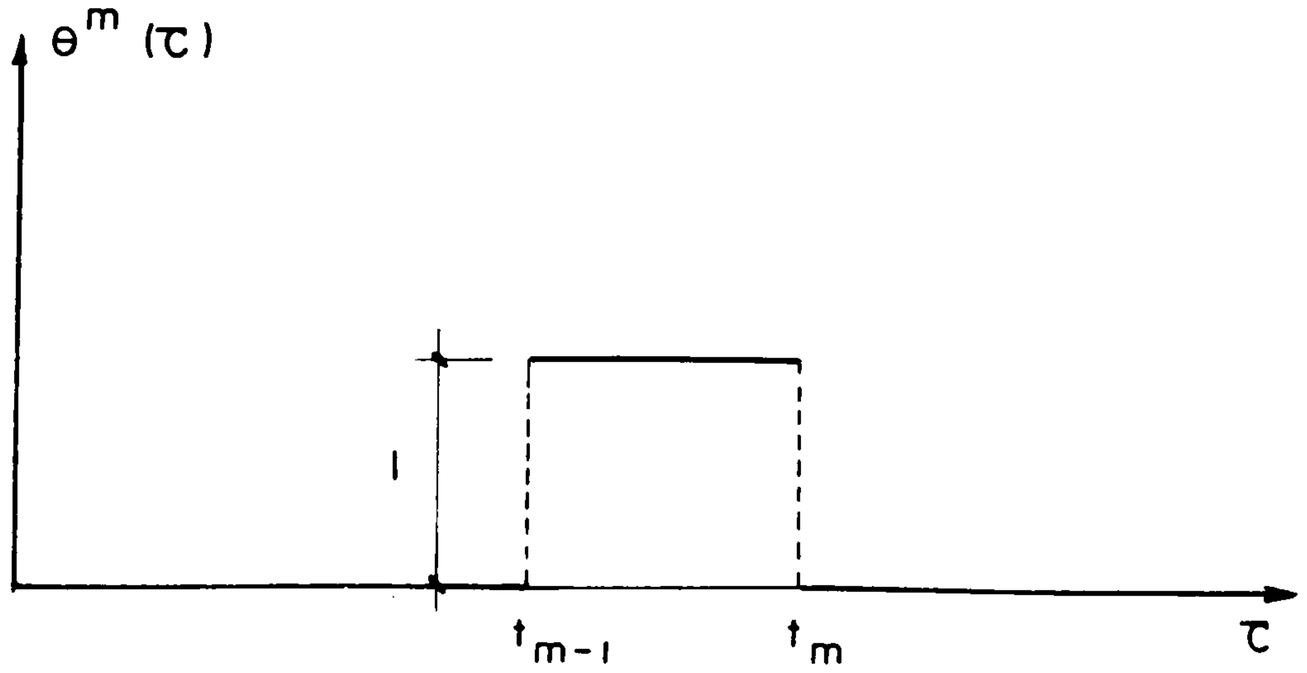

Figure 4.2.4 Constant time interpolation for p.

The substitution of formula (4.2.18) into expression (4.2.6) gives

$$G_{ij}^{nm} = \int_{\Gamma} \nu_j(Q) \int_{t_{m-1}}^{t_m} u_i^{*n} \, d\tau d\Gamma \quad . \tag{4.2.19}$$

Analytical time integration can now be carried out giving

$$G_{ij}^{nm} = \frac{2}{c\Delta t} \int_{\Gamma} \nu_j(Q) \; F_i^{nm} \, d\Gamma \quad , \tag{4.2.20}$$

where F_i^{nm} can be computed as shown in appendix E.

In order to perform numerically the integrations indicated in expressions (4.2.17) and (4.2.20) the Γ boundary must be replaced by an approximated one. Linear discretization is used in this work, that is, Γ is represented by a series of straight line segments, e_k (elements), each one joining two consecutives nodes of Γ. l_k and $\underline{n}_k$ are the length of e_k and the unit outward vector normal to e_k respectively (see figure 4.2.5).

When two elements e_p and e_q with a common node j are considered, and the interpolation functions $\eta_j(Q)$ and $\nu_j(Q)$ are linear, the use of natural coordinates gives (see figure 4.2.6)

$$\eta_j(\xi) = \nu_j(\xi) = \begin{cases} \frac{1}{2}\,(\xi_p+1) & Q \in e_p \\ \\ -\frac{1}{2}\,(\xi_q-1) & Q \in e_q \\ \\ 0 \text{ otherwise} & . \end{cases} \tag{4.2.21}$$

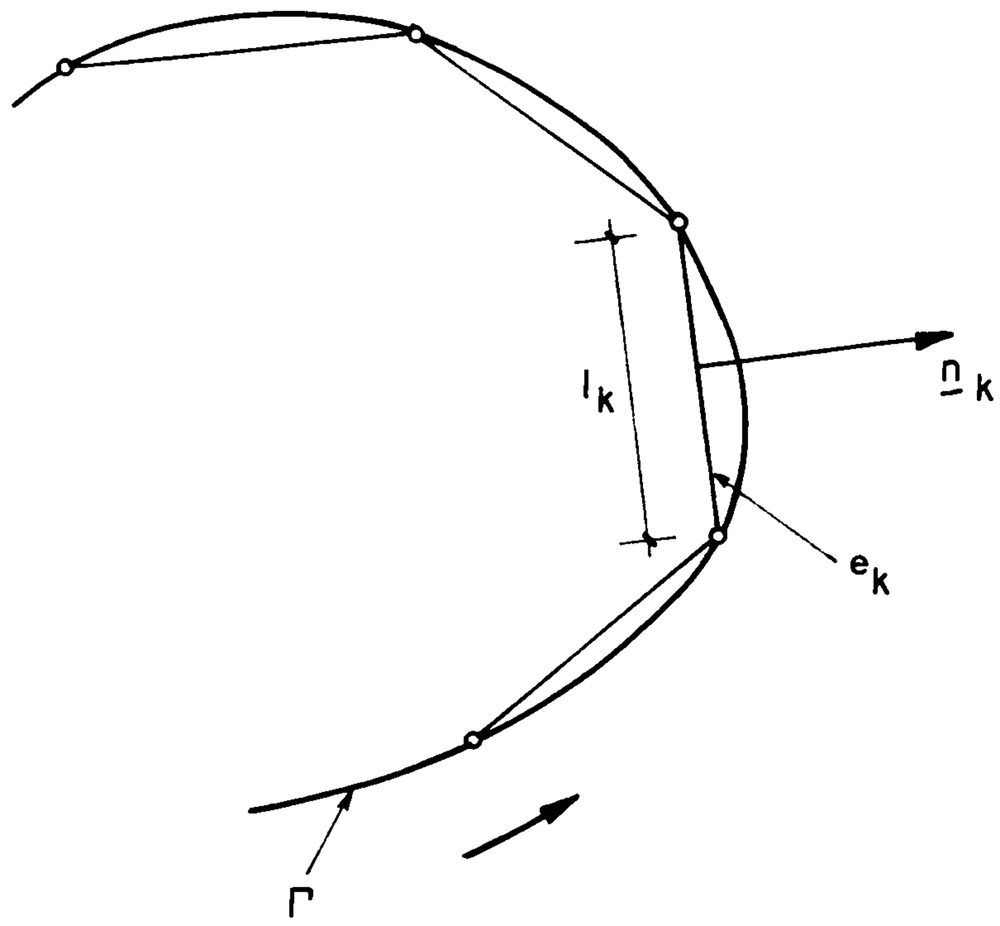

Figure 4.2.5 Linear discretization of the Γ boundary.

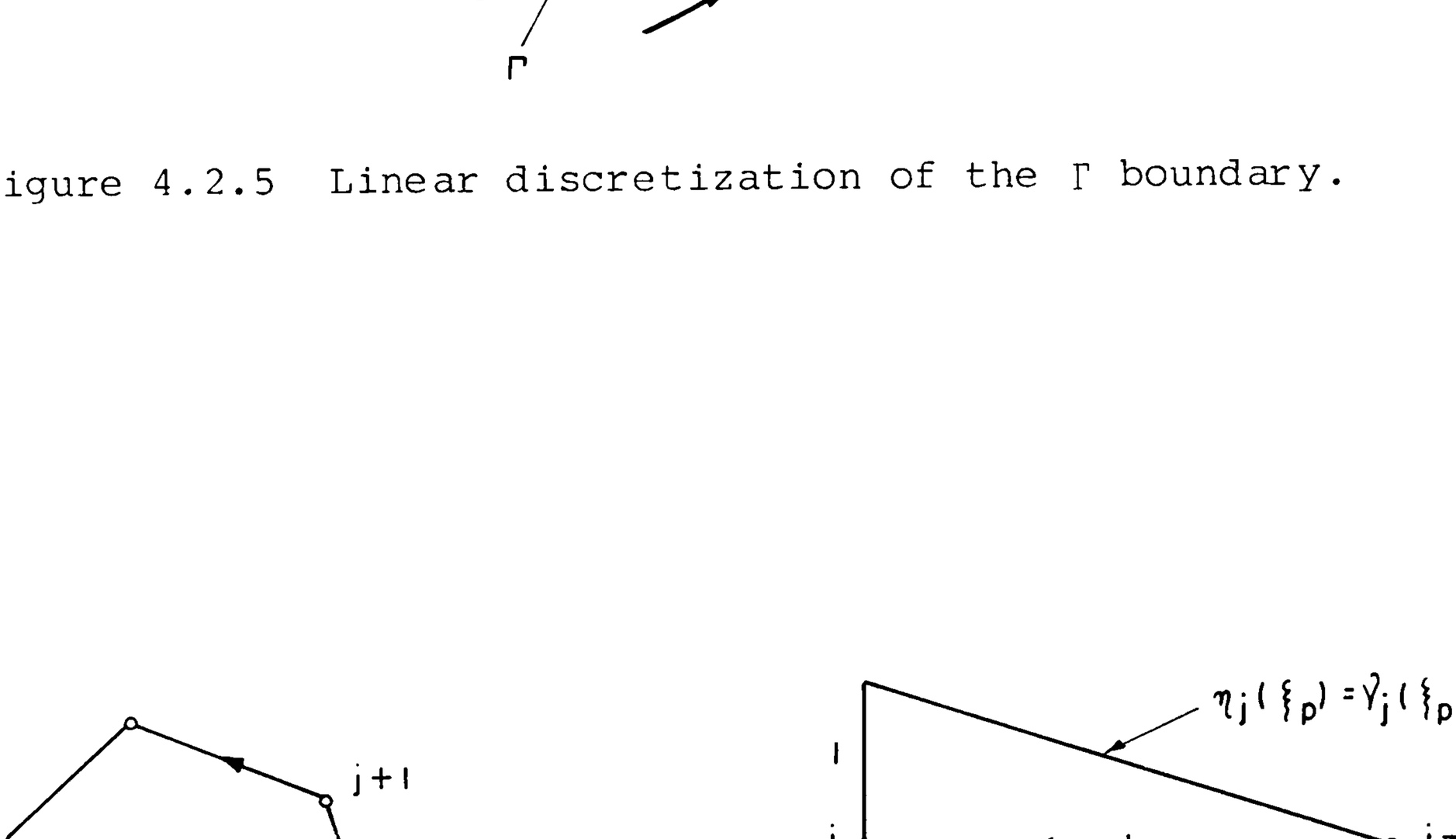

Figure 4.2.6 Linear space interpolation functions for u and p on the Γ boundary.

When formula (4.2.21) is considered, expression (4.2.17) is given as follows

$$(H_{ij}^{nm})_I = \frac{2}{c\Delta t}\left[\int_{e_p} \frac{\partial r}{\partial n}\, \eta_j (D_i^{nm})_I d\Gamma_p + \int_{e_q} \frac{\partial r}{\partial n}\, \eta_j (D_i^{nm})_I d\Gamma_q\right]$$

$$(H_{ij}^{nm})_F = \frac{2}{c\Delta t}\left[\int_{e_p} \frac{\partial r}{\partial n}\, \eta_j (D_i^{nm})_F d\Gamma_p + \int_{e_q} \frac{\partial r}{\partial n}\, \eta_j (D_i^{nm})_F d\Gamma_q\right]$$

$$(G_{ij}^{nm})_I = \frac{2}{c\Delta t}\left[\int_{e_p} \nu_j (E_i^{nm})_I d\Gamma_p + \int_{e_q} \nu_j (E_i^{nm})_I d\Gamma_q\right]$$

$$(G_{ij}^{nm})_F = \frac{2}{c\Delta t}\left[\int_{e_p} \nu_j (E_i^{nm})_F d\Gamma_p + \int_{e_q} \nu_j (E_i^{nm})_F d\Gamma_q\right] \quad . \qquad (4.2.22)$$

Since the interpolation functions are expressed in terms of the homogeneous coordinates ξ, a change of coordinates has to be carried out before performing the integrations indicated in expression (4.2.22); this problem is considered in appendix F.

When $\theta^m(\tau)$ is constant and formula (4.2.21) is taken into consideration, expression (4.2.20) can be written as

$$(G_{ij}^{nm})_I = G_{ij}^{nm} = \frac{2}{c\Delta t}\left[\int_{e_p} \nu_j\, F_i^{nm}\, d\Gamma_p + \int_{e_q} \nu_j\, F_i^{nm}\, d\Gamma_q\right]$$

$$(G_{ij}^{nm})_F = 0 \quad . \qquad (4.2.23)$$

When n = m, the coefficient $(H_{ii}^{nm})_I$ in expression (4.2.22) contains integrals which must be evaluated in the

Cauchy principal value sense. The function being integrated has a singularity of the type 1/r, as shown in expression (E.4). However when linear discretization is used these integrals disappear due to the orthogonality of Γ_k and $\underline{n}_k$ (see figure 4.2.5) which makes $\frac{\partial r}{\partial n} = 0$. This problem deserves special attention when interpolation functions of order higher than linear are used to approximate the geometry of the Γ boundary.

When n = m the coefficient $(G_{ii}^{nm})_I$ in expressions (4.2.22) and (4.2.23) contains integrals which have a singularity of the type $\ln r$. These integrals can be computed in the ordinary sense using Gaussian quadrature. However, a greater precision can be obtained if these integrals are carried out analytically rather than numerically as shown in appendix F.

The rest of the coefficients in expressions (4.2.22) and (4.2.23) can be calculated using standard Gauss quadrature formulae.

Another situation to be examined is that in which $\eta_j(Q)$ and $\nu_j(Q)$ are constant, i.e.

$$\eta_j(Q) = \nu_j(Q) = \begin{cases} 1 & \text{when } Q \in e_j \\ 0 & \text{otherwise .} \end{cases} \qquad (4.2.24)$$

In this case a node j can be considered as belonging to a set of discrete points Q_j on the Γ boundary, j=1,...,J where each Q_j is placed at the middle of an element e_j as shown in figure 4.2.7.

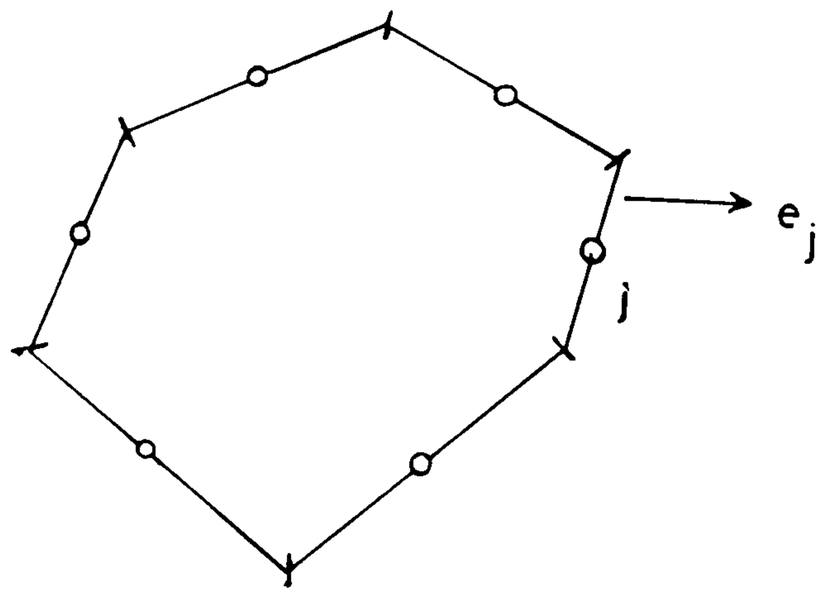

Figure 4.2.7 Position of nodes when constant interpolation functions η_j and ν_j are used.

When $\phi^m(\tau)$ and $\theta^m(\tau)$ are linear the following expression can be written

$$(H_{ij}^{nm})_I = \frac{2}{c\Delta t}\int_{e_j}\frac{\partial r}{\partial n}(D_i^{nm})_I d\Gamma_j$$

$$(H_{ij}^{nm})_F = \frac{2}{c\Delta t}\int_{e_j}\frac{\partial r}{\partial n}(D_i^{nm})_F d\Gamma_j$$

$$(G_{ij}^{nm})_I = \frac{2}{c\Delta t}\int_{e_j}(E_i^{nm})_I d\Gamma_j$$

$$(G_{ij}^{nm})_F = \frac{2}{c\Delta t}\int_{e_j}(E_i^{nm})_F d\Gamma_j \quad . \qquad (4.2.25)$$

It should be recognized that in this case $c(S_i)$ is always 1/2. When $\theta^m(\tau)$ is constant, $(G_{ij}^{nm})_I$ and $(G_{ij}^{nm})_F$ can be calculated from

$$(G_{ij}^{nm})_I = \frac{2}{c\Delta t} \int_{e_j} F_i^{nm} \, d\Gamma_j$$

$$(G_{ij}^{nm})_F = 0 \qquad . \tag{4.2.26}$$

Because of the causality property a situation exists, in which it is necessary to carry out numerical integrations of functions which are null over part of an element. In this case it became obvious that greater precision could be obtained if such integrations were performed from j to k' instead of from j to k as depicted in figure 4.2.8.

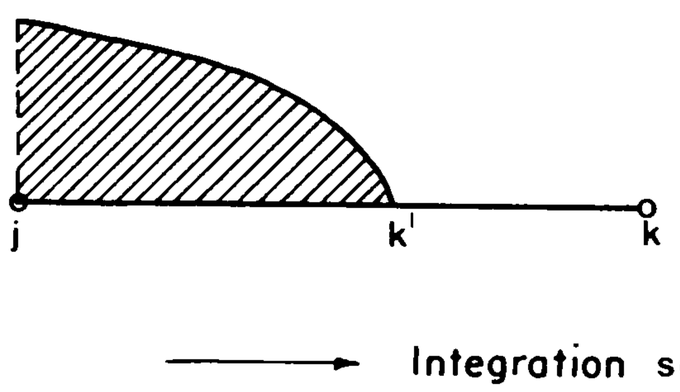

Figure 4.2.8 Integration over part of an element.

The fundamental solution of the problem under consideration (see equation (3.6.9)) suggests that the number of Gauss points can be gradually reduced as $(t-\tau)$ gets bigger. This procedure was used in the numerical analysis carried out in this research, in order to save computer time.

4.2.2 Domain Integrals - The domain contributions due to initial conditions can be calculated from expression (4.2.7) which can be written as

$$F_i^n = \frac{1}{c^2} \int_\Omega u_{oi}^{*n} \, v_o \, d\Omega(q) + \frac{1}{c} \int_\Omega u_{oi}^{*n} \, \frac{\partial u_o}{\partial r} \, d\Omega(q) +$$

$$+ t_n \int_\Omega \frac{1}{r} \, B_{oi}^{*n} \, u_o \, d\Omega(q) \qquad (4.2.27)$$

where $u_{oi}^{*n} = u_o(q,t_n;S_i)$ and $B_{oi}^{*n} = B_o(q,t_n;S_i)$.

In order to carry out the integrations indicated in expression (4.2.27) the domain Ω is divided into L triangular subdomains, O_l (cells), as shown in figure 4.2.9. Then the expression (4.2.27) can be written as

$$F_i^n = \sum_{l=1}^{L} \left(\frac{1}{c^2} \int_{O_l} u_{oi}^{*n} \, v_o \, d\Omega(q) + \frac{1}{c} \int_{O_l} u_{oi}^{*n} \, \frac{\partial u_o}{\partial r} \, d\Omega(q) \right.$$

$$\left. + t_n \int_{O_l} \frac{1}{r} \, B_{oi}^{*n} \, u_o \, d\Omega(q) \right) \quad . \qquad (4.2.28)$$

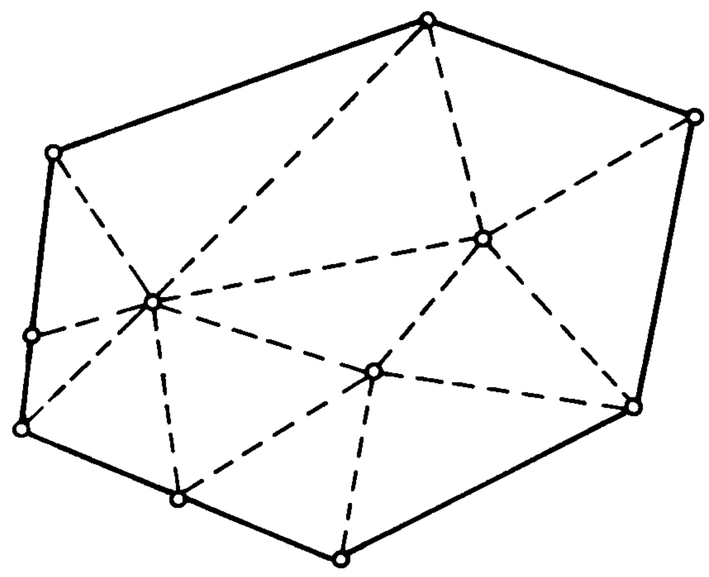

Figure 4.2.9 Discretization of the domain Ω into triangular cells.

When u_o and v_o are linearly interpolated inside each cell the following expression can be written

$$u_o = u_{oi}\mu_i \qquad (i=1,2,3) \qquad (4.2.30)$$

$$v_o = v_{oi}\mu_i$$

where u_{oi} and v_{oi} are respectively initial displacement and initial velocity at a node i of the cell O_1. $\frac{\partial u_o}{\partial r}$ is also required and can be calculated from expression (4.2.30), giving

$$\frac{\partial u_o}{\partial r} = u_{oi}\frac{\partial \mu_i}{\partial r} \quad . \qquad (4.2.31)$$

Triangular coordinates can be related to rectangular coordinates in the following way

$$\mu_\alpha = \frac{A^0_\alpha}{A} + \frac{1}{2A}(b_\alpha x_1 + a_\alpha x_2) \qquad (4.2.32)$$

where

$$\begin{aligned} a_\alpha &= x_1^\gamma - x_1^\beta \\ b_\alpha &= x_2^\beta - x_2^\gamma \\ 2A^0_\alpha &= x_1^\beta x_2^\gamma - x_1^\gamma x_2^\beta \\ A &= \frac{1}{2}(b_1 a_2 - b_2 a_1) \quad . \end{aligned} \qquad (4.2.33)$$

In expression (4.2.33) $\alpha = 1,2,3$ for $\beta = 2,3,1$ and $\gamma = 3,1,2$.

Considering a system of polar coordinates (r,θ) with origin at the source point S_i as depicted in figure 4.2.11, expression (4.2.32) becomes {36}

$$\mu_\alpha = C_\alpha + D_\alpha(\theta)r \qquad (4.2.34)$$

where

$$C_\alpha = A^0_\alpha / A$$

$$D_\alpha = \frac{1}{2A}(b_\alpha \cos\theta + a_\alpha \sin\theta) \quad . \tag{4.2.35}$$

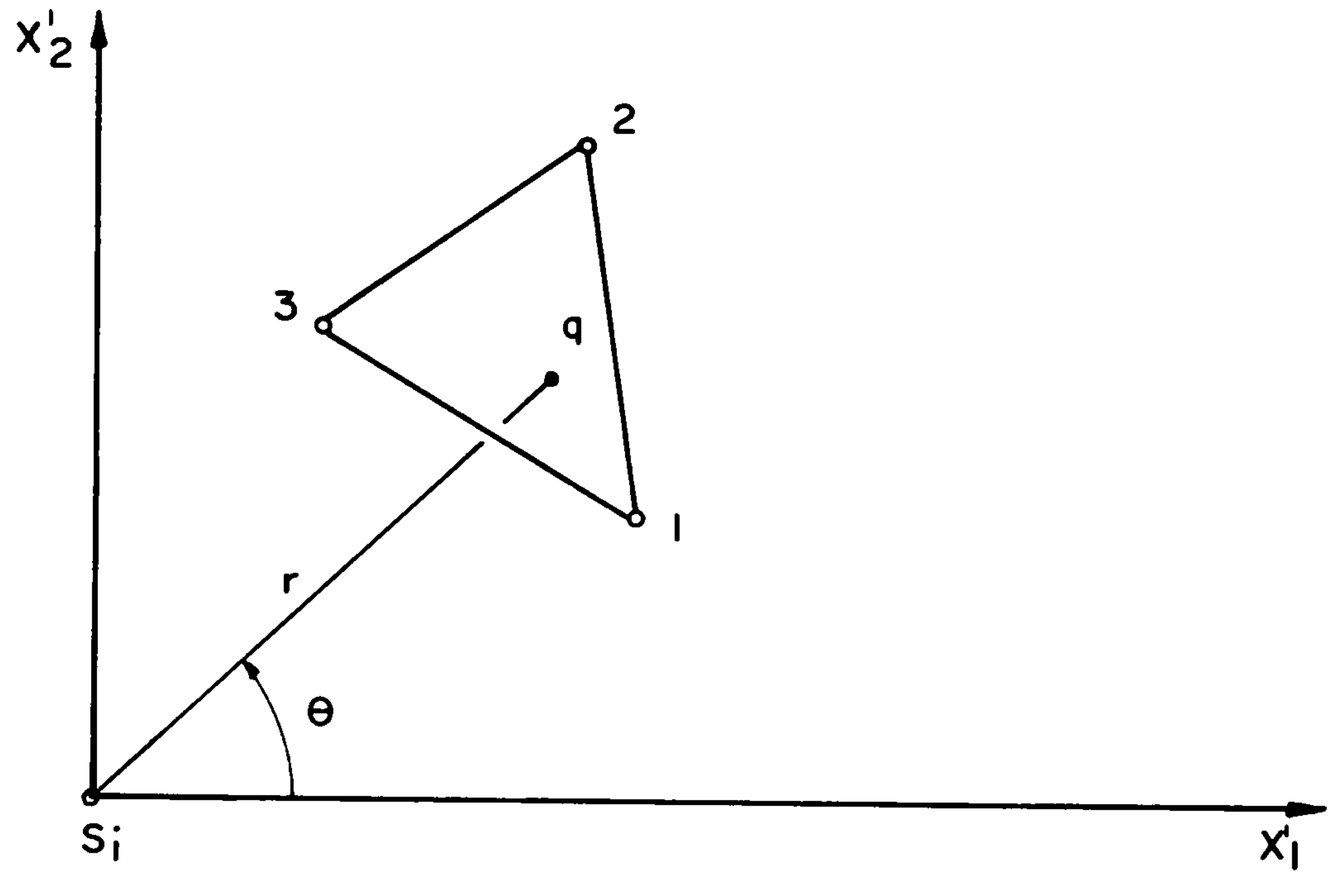

Figure 4.2.11 Polar coordinates based at the source point S_i.

Taking formulas (4.2.30), (4.2.31) and (4.2.34) into consideration, u_o, v_o and $\partial u_o/\partial r$ can be expressed as

$$\begin{aligned} u_o &= u_{o\alpha}\left[C_\alpha + D_\alpha(\theta) r\right] \\ v_o &= v_{o\alpha}\left[C_\alpha + D_\alpha(\theta) r\right] \end{aligned} \qquad (\alpha=1,2,3) \tag{4.2.36}$$

$$\frac{\partial u_o}{\partial r} = u_{o\alpha} D_\alpha(\theta) \quad .$$

Integration over a cell can now be performed using polar coordinates. In this work such integrals are obtained as a sum of three integrals over the domains E_1, E_2 and E_3 depicted in figure 4.2.12. Therefore, when formula (4.2.36) is substituted into expression (4.2.28)

the latter becomes

$$F_i^n = \sum_{l=1}^{L} \left(R_{li}^{\alpha n} \, v_{o\alpha} + T_{li}^{\alpha n} \, u_{o\alpha} \right) \qquad (\alpha=1,2,3) \qquad (4.2.37)$$

where $v_{o\alpha}$ and $u_{o\alpha}$ represent respectively the values of v_o and u_o at a node α of the cell O_1, and

$$R_{li}^{\alpha n} = \frac{1}{c^2} \sum_{t=1}^{3} \int_{\theta_u}^{\theta_v} \int_{0}^{g_t^i(\theta)} u_{oi}^{*n} \left[\bar{C}_\alpha + D_\alpha(\theta) r \right]_l r \, dr \, d\theta \qquad (4.2.38)$$

$$T_{li}^{\alpha n} = \sum_{t=1}^{3} \int_{\theta_u}^{\theta_v} \int_{0}^{g_t^i(\theta)} \left(\frac{1}{c} \, u_{oi}^{*n} \, D_\alpha(\theta) r + t_n B_{oi}^{*n} \left[\bar{C}_\alpha + D_\alpha(\theta) r \right] \right)_l dr \, d\theta \, .$$

In expression (4.2.38), t = 1,2,3 for u = 2,3,1 and v = 1,3,2,

$$g_t^i(\theta) = \begin{cases} r_t^i(\theta) & \text{when} \quad r_t^i(\theta) < ct_n \\ \\ ct_n & \text{when} \quad r_t^i(\theta) > ct_n \end{cases} \qquad (4.2.39)$$

and $r_t^i(\theta)$, θ_t, θ_u and θ_v are shown in figure 4.2.13.

Expression (4.2.38) can now be integrated analytically with respect to r, giving

$$R_{li}^{\alpha n} = \frac{1}{c} \sum_{t=1}^{3} \int_{\theta_u}^{\theta_v} \Big(2c_\alpha (ct_n - V_1 V_2)$$

$$+ D_\alpha(\theta) \left[-g_t^i(\theta) V_1 V_2 + c^2 t_n^2 V_3 \right] \Big)_l d\theta$$

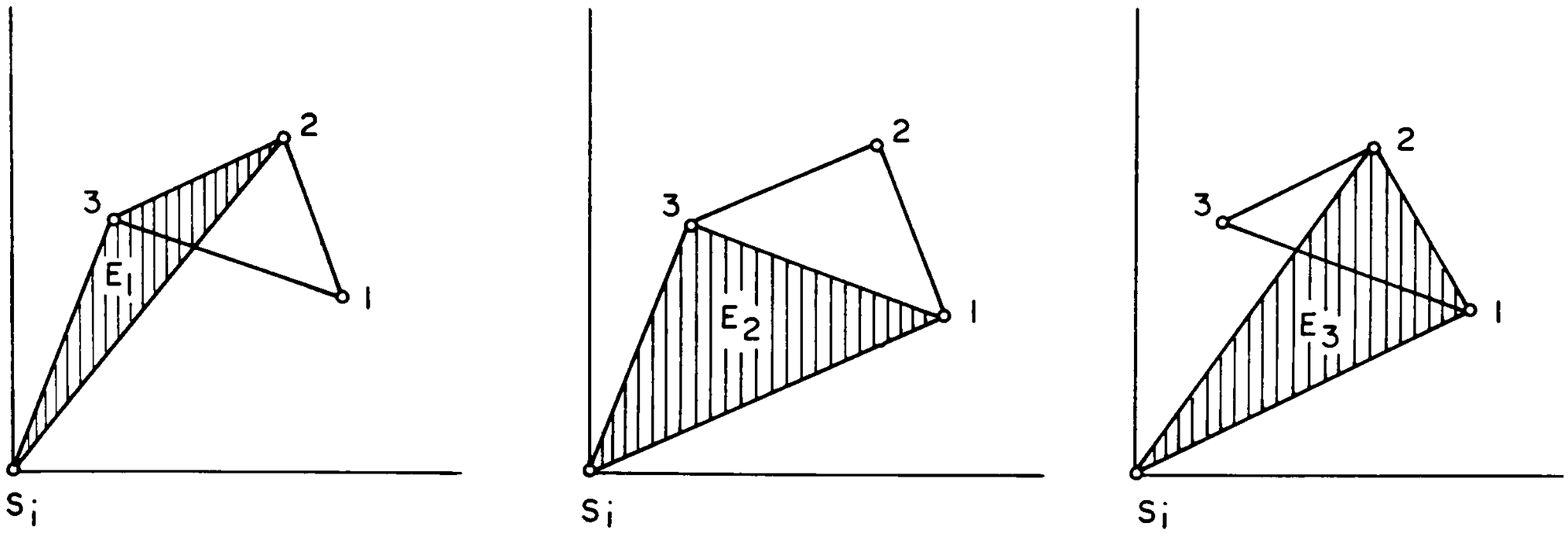

Figure 4.2.12 Domains used to integrate over a cell.

$$r_t^i(\theta) = \frac{-2A_\alpha^\circ}{b_t \cos\theta + a_t \sin\theta}$$

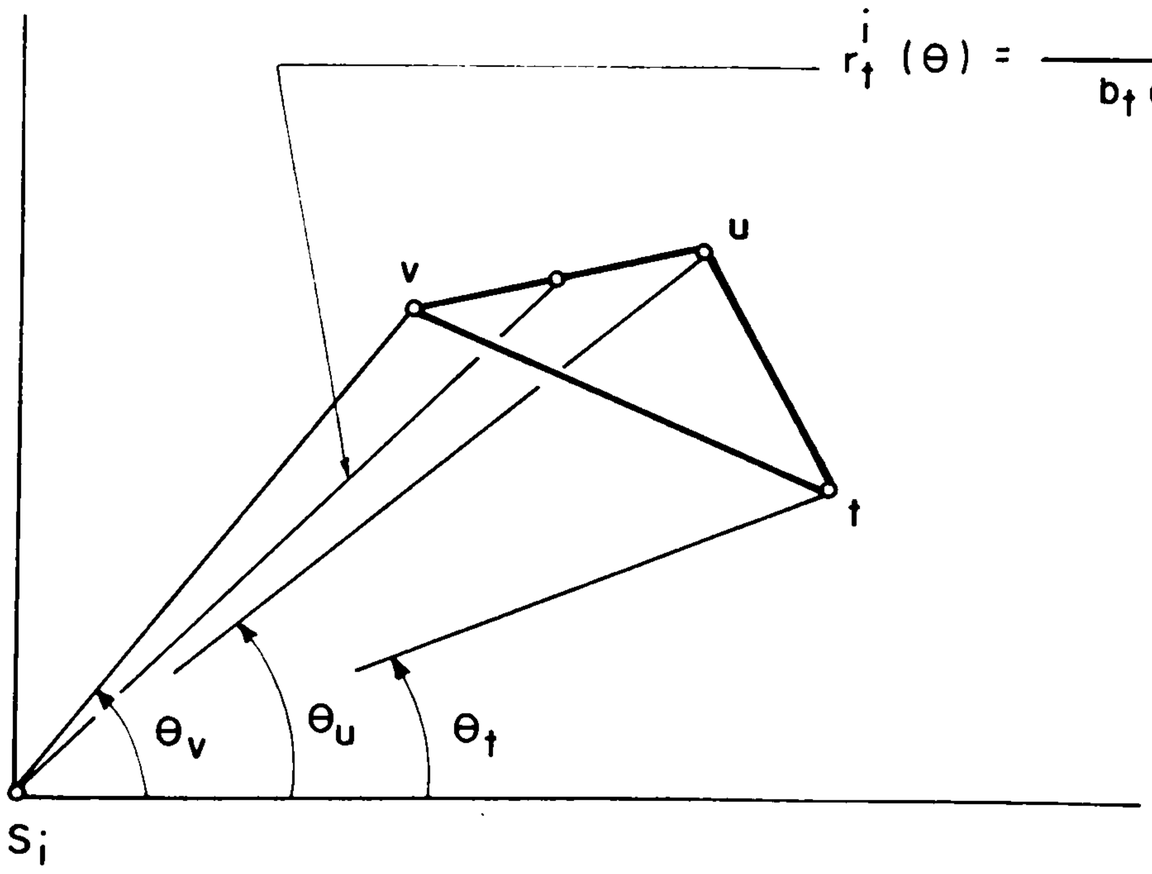

Figure 4.2.13 Definitions with cell integration purpose.

$$T_{li}^{\alpha n} = 2 \sum_{t=1}^{3} \int_{\theta_u}^{\theta_v} \left(c_\alpha \left(1 - \frac{V_1}{V_2} \right) \right.$$

$$\left. + D_\alpha(\theta) \left[ct_n \left(V_3 + \frac{V_1}{V_2} \right) - V_1 V_2 \right] \right]_1 d\theta \qquad (4.2.40)$$

where

$$V_1 = \sqrt{ct_n - g_t^i(\theta)}$$

$$V_2 = \sqrt{ct_n + g_t^i(\theta)} \qquad (4.2.41)$$

$$V_3 = \arcsin \frac{g_t^i(\theta)}{ct_n} \quad .$$

Integration with respect to θ can be carried out using one dimensional Gaussian quadrature. This can be done by simply interchanging the variable θ as follows

$$\theta = \frac{\xi}{2}(\theta_v - \theta_u) + \frac{1}{2}(\theta_v + \theta_u) \qquad (4.2.42)$$

where ξ is defined on the interval $[-1,1]$.

If the spatial distribution of source density can be represented by a Dirac delta function, i.e.

$$\gamma(q,\tau) = f(\tau)\ \delta(q - q_c) \quad . \qquad (4.2.43)$$

the integration over Ω shown in expression (4.2.8) can be carried out analytically giving

$$S_i^n = \int_0^{t_n} f(\tau)\ u^*(q_c, t_n; S_i, \tau) d\tau \quad . \qquad (4.2.44)$$

When $f(\tau)$ is linearly interpolated over the time the following expression can be written

$$f(\tau) = \sum_{m=1}^{N} \theta^m(\tau) f^m \qquad (4.2.45)$$

where $\theta^m(\tau)$ is given by expression (4.2.12) and $f^m = f(t_m)$.

Then, expression (4.2.44) can be written as

$$S_i^n = \sum_{m=1}^{N} w_i^{nm} f^m \qquad (4.2.46)$$

where

$$w_i^{nm} = \frac{1}{\Delta t}\left(\int_{t_{m-1}}^{t_m} (\tau - t_m)(u_i^{*n})_c \, d\tau + \int_{t_m}^{t_{m+1}} (t_{m+1} - \tau)(u_i^{*n})_c \, d\tau \right) \qquad (4.2.47)$$

and

$$(u_i^{*n})_c = u(q_c, t_n; S_i, \tau) \quad . \qquad (4.2.48)$$

Analytical integration of expression (4.2.47) gives

$$w_i^{nm} = \frac{2}{c\Delta t}\left((E_i^{nm})_I^c + (E_i^{nm})_F^c \right) \qquad (4.2.49)$$

where $(E_i^{nm})_I^c$ and $(E_i^{nm})_F^c$ can be computed from the expressions given in appendix E to calculate $(E_i^{nm})_I$ and $(E_i^{nm})_F$ by making $r = r_c$; r_c is given by

$$r_c = |q - q_c| \quad . \qquad (4.2.50)$$

When the source density is distributed over Ω, volume and time integrations can easily be carried out using time and domain interpolation functions respectively which appear in expressions (4.2.12) and (4.2.30). This case will not be discussed here.

4.2.3 Double Nodes - A very common situation in wave propagation problems concerns p being discontinuous on the boundary. A convenient way of analysing these sorts of problems is that in which two distinct values of tractions, p^r and p^l, and two values of displacements u^r and u^l are considered on the neighbourhood of each point where a discontinuity can occur (see figure 4.2.14). So, for each of these points two extra boundary unknowns are introduced in the analysis. When, p^r and p^l, or $u^r(u^l)$ and $p^l(p^r)$ are prescribed the continuity condition for displacements, namely

$$u^r = u^l \tag{4.2.51}$$

gives the extra equation required. When constant elements are used, this problem is naturally considered by the discontinuous nature of these elements. However, when linear or higher order elements are used special considerations are required. The system of equations given by expression (4.2.4) can still be used and the condition (4.2.51) can be introduced using "double nodes", i.e. two different nodes being placed at points where p can be discontinuous. An extensive study on this subject can be found in the references {99-101}.

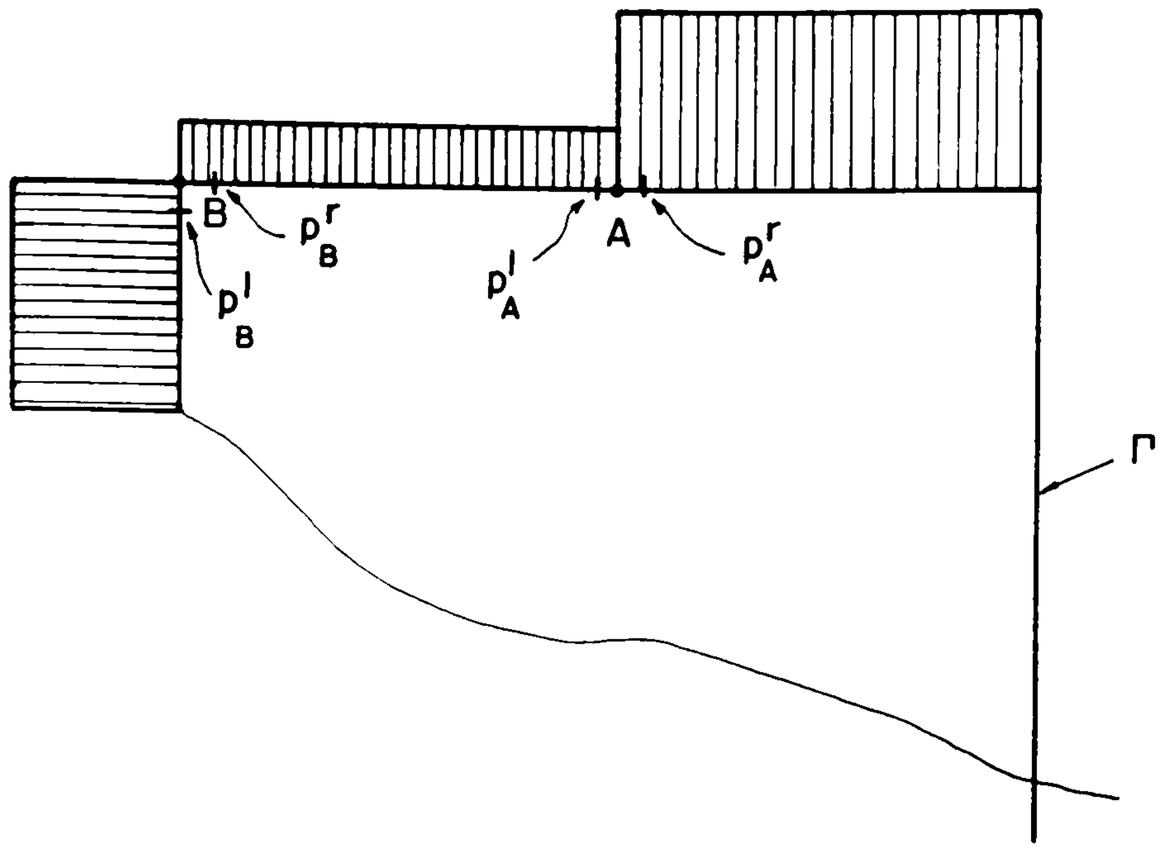

Figure 4.2.14 Discontinuous p on the Γ boundary.

A more involved situation is that in which p^l and p^r are different from each other in the neighbourhood of a point where the potential is prescribed. The approach to be followed in this case can be found in references {37 and 100}.

In quite a number of situations it is not possible to determine a priori when and where tractions are discontinuous. In this case the mean value of the unknowns is to be expected from the numerical analysis.

Another method of dealing with discontinuities is by using discontinuous elements {102 and 103}. The discontinuity is then avoided because as shown in figure 4.2.15 the nodes of the discontinuous elements are placed inside them, rather than on their extremities. It should be recognized that this procedure can also be used when time discontinuities occur in a problem.

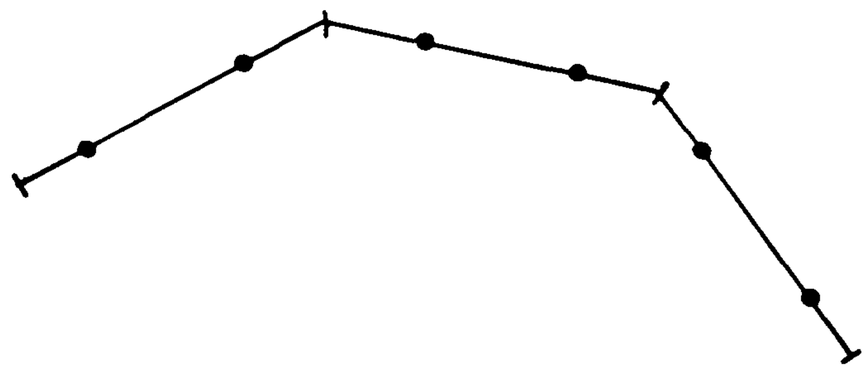

Figure 4.2.15 Discontinuous linear elements.

4.3 Examples - Scalar Wave Equation

If it is desired to find boundary unknowns at a time t_n, it is convenient to write equation (4.2.4) in the following way (summation convention does not apply)

$$C(S_i)u_i^n + \frac{1}{4\pi}\sum_{j=1}^{J} H_{ij}^{nn}\, u_j^n = \frac{1}{4\pi}\left(\sum_{j=1}^{J} G_{ij}^{nn}\, p_j^n - \sum_{m=1}^{n-1}\sum_{j=1}^{J} H_{ij}^{nm}\, u_j^m + \sum_{m=1}^{n-1}\sum_{j=1}^{J} G_{ij}^{nm}\, p_j^m + F_i^n + S_i^n\right) . \tag{4.3.1}$$

Equation (4.3.1) can also be written as

$$\underline{H}\ \underline{u} = \underline{G}\ \underline{p} + \underline{B} \tag{4.3.2}$$

where $\underline{H}$ and $\underline{G}$ are square matrices of order (J×J) and $\underline{u}$, $\underline{p}$ and $\underline{B}$ are vectors.

If the boundary conditions at the time t_n are considered and the system of equations that arises is reordered expression (4.3.2) can be written as

$$\underline{A}\ \underline{y} = \underline{C} \tag{4.3.3}$$

where the vector $\underline{y}$ is formed by unknowns u_j^n and p_j^n at boundary nodes.

Within the examples analysed in this chapter the boundary conditions at boundary nodes are always of the same type, i.e. a node at which u (or p) is initially prescribed will only have prescribed u (or p) until the end of the transient analysis. Consequently, due to the time translation property (see expression (4.2.11)), $\underline{A}$ requires to be inverted only once. Gauss elimination is used in this work to obtain the inverse of $\underline{A}$.

In the examples discussed here the numerical integrations mentioned previously in section 4.2 were carried out using a maximum of ten Gauss points.

The choice of cell discretization to be used when solving a problem is fairly simple because u_o, v_o and j are known functions. However boundary discretization and time division depend on what the problem under consideration is like. For this reason, in many problems, more than one numerical analysis has to be carried out in which the boundary discretization and the time division are successively refined. The quantity of work required is considerably reduced as experience is gained in the method adopted. The observation of certain physical characteristics of the problem can also be of great help. For instance when studying wave propagation care should be taken on the choice of time intervals and boundary discretization in order to avoid contradicting the causality property too far, that is, in a time interval, waves should not be allowed to travel

between nodes far from each other. There are also certain precautions which must be taken when choosing the parameter β given by

$$\beta = \frac{c\Delta t}{l_j} \quad . \tag{4.3.4}$$

It is quite commonly regarded that there exist strict rules concerning the choice of a similar parameter in finite differences and finite elements; which if not followed can result in a completely invalid analysis. In boundary elements conclusive analytical studies regarding the choice of β have not yet been completed, consequently the discussion based on numerical experiments presented in the examples can be very helpful.

The numerical procedure discussed previously in this chapter was converted into FORTRAN and implemented on an ICL2970 computer. The computer code was used to analyse a number of examples which will be presented next.

4.3.1 <u>One-Dimensional Rod Under a Heaviside Type Forcing Function</u> - The results obtained from using the two-dimensional boundary element computer code were compared with the analytical results for a one-dimensional rod under a Heaviside type forcing function. The boundary element solution considered a rectangular domain with sides of length a and b (b = a/2) as depicted in figure 4.3.1. The u displacements were assumed to be zero at x_1=a and their normal derivative p were also taken as null at x_2=0 and x_2=b for any time 't'. At x_1=0 and t=0 a load Ep was suddenly applied and kept constant until the end of the analysis (E is the Young's modulus). Due to the topology and boundary conditions the

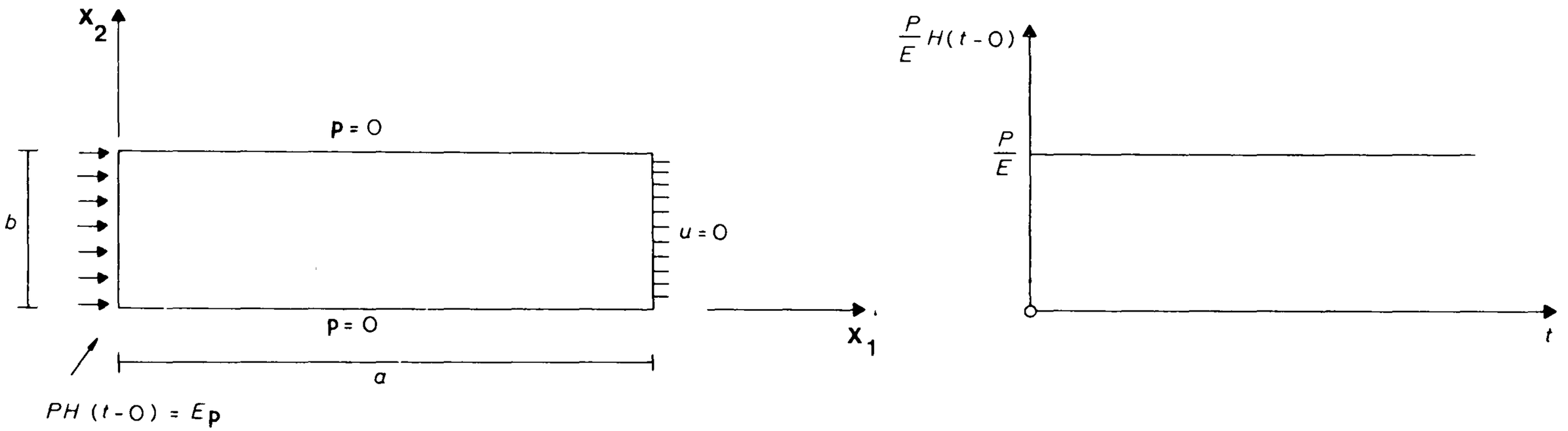

Figure 4.3.1 Boundary conditions and geometry definitions for one-dimensional rod under a Heaviside type forcing function.

problem is actually one-dimensional and its analytical solution can be found elsewhere {104}.

Three different combinations of interpolation functions were used in the analysis as given in table 4.3.1.

The boundary was discretized into twenty four constant and linear elements as shown in figure 4.3.2, double nodes were used at the corners for the latter model.

Combination 1 was tried with $\beta = .6$ and gave good results for the displacements u (the degree of accuracy was the same as combination 2). The numerical values of p, however, oscillated around the analytical solution, displaying the onset of instability. This unstable behaviour of p can be avoided in this particular analysis by replacing the jump of the forcing function PH(t-0) by a steep slope. Because of the oscillations that can occur on the numerical values of p, it was decided not to use combination 1 until further studies have been accomplished.

Combinations 2 and 3 were then compared and it was found that for the same number of boundary elements and the same time division, better results were obtained for linear $\eta_j(Q)$ and $\nu_j(Q)$ (combination 2) than for constant $\eta_j(Q)$ and $\nu_j(Q)$ (combination 3). As the computing time is much the same for both cases it was concluded that combination two is more efficient than combination three. Therefore, unless otherwise stated, all the boundary element method (B.E.M.) results presented from now on are based on combination 2.

Combination	Interpolation function		
	$\eta_j(\mathbf{Q})$ and $\nu_j(\mathbf{Q})$	$\phi^m(t)$	$\theta^m(t)$
1	Linear	Linear	Linear
2	Linear	Linear	Constant
3	Constant	Linear	Constant

Table 4.3.1 Combination of interpolation functions.

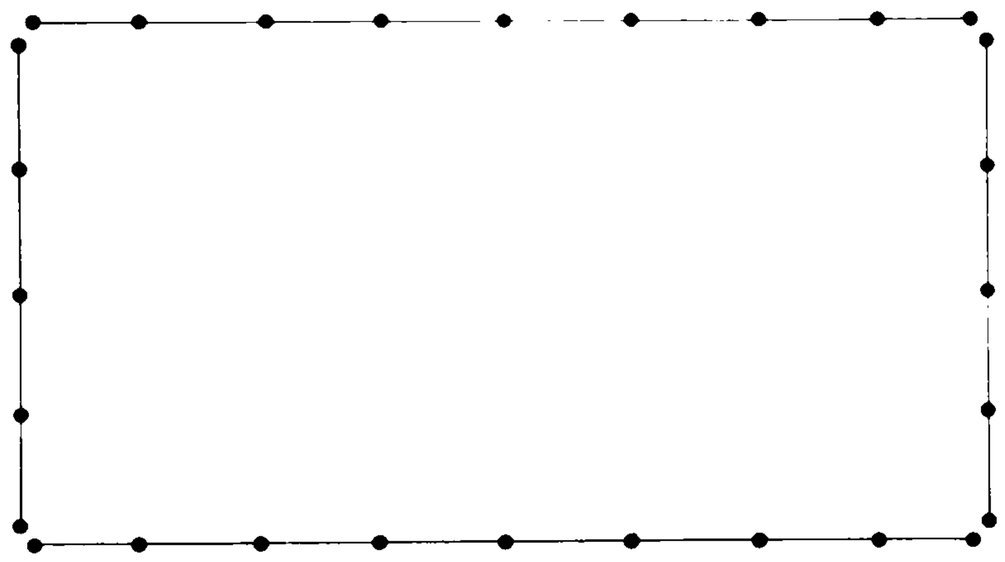

Figure 4.3.2 Boundary discretization for one-dimensional rod.

Figures 4.3.3 - 4.3.5 show B.E.M. and analytical displacement results at internal and boundary points. The degree of accuracy of B.E.M. results is quite good. In figure 4.3.6 the normal derivative of the u displacement at point (a,b/2) versus ct is presented. Except for the presence of a comparatively small amount of noise, boundary elements and analytical solutions are in good agreement.

Considerable care must be taken with the choice of β in order to avoid noise, which although usually not critical for displacements, can often be excessive for tractions. In order to study the effect of varying the parameter β on the level of noise four other values of β were investigated; 0.4, 0.5, 0.8 and 1.0 in addition to $\beta = 0.6$. The results for p at point (a,b/2) are plotted in figures 4.3.7 - 4.3.10. It is apparent that excessive noise occurred for $\beta<0.6$. The value $\beta = 0.6$ was considered the optimum for this problem.

4.3.2 <u>One-Dimensional Rod Under Prescribed Initial Velocity and Displacement</u> - For this problem the geometry and boundary conditions were identical to the previous case and, in addition, over the domain Ω_o depicted in figure 4.3.11, the following initial conditions were prescribed

$$u_o(x_1,x_2) = \frac{P}{E}\left(\frac{a}{4} - x_1\right) \tag{4.3.5}$$

$$v_o(x_1,x_2) = \frac{Pc}{E} \quad .$$

The analytical solution for this problem is the same as for the previous one but with the time t dephased by a/4c, i.e.

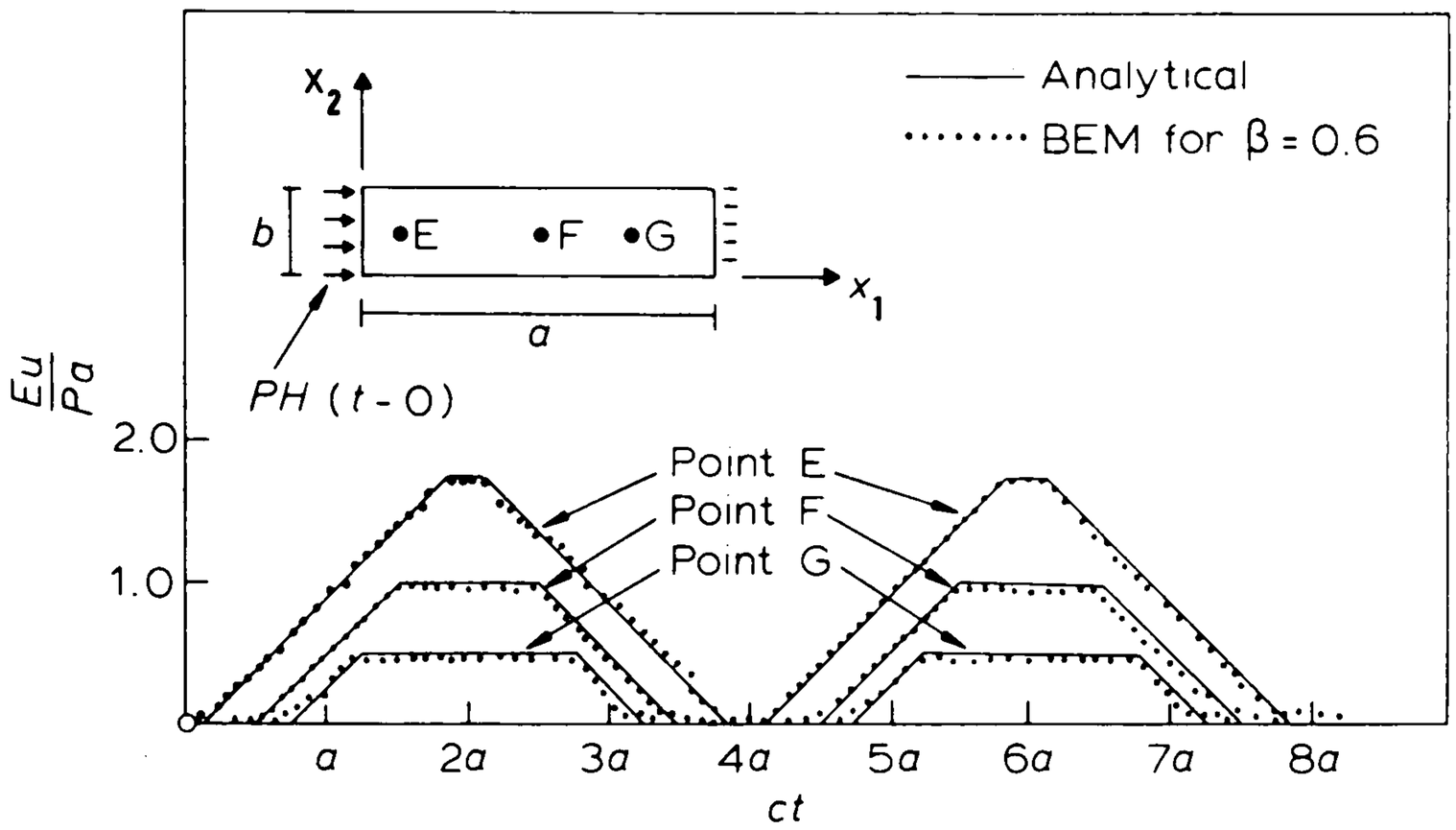

Figure **4.3.3** Displacements at internal points E($a/8, b/2$), F($a/2, b/2$) and G($3a/4, b/2$) for one-dimensional rod under a Heaviside type forcing function, $\eta_j(Q)$, $\nu_j(Q)$, $\phi^m(t)$ are linear and $\theta^m(t)$ is constant.

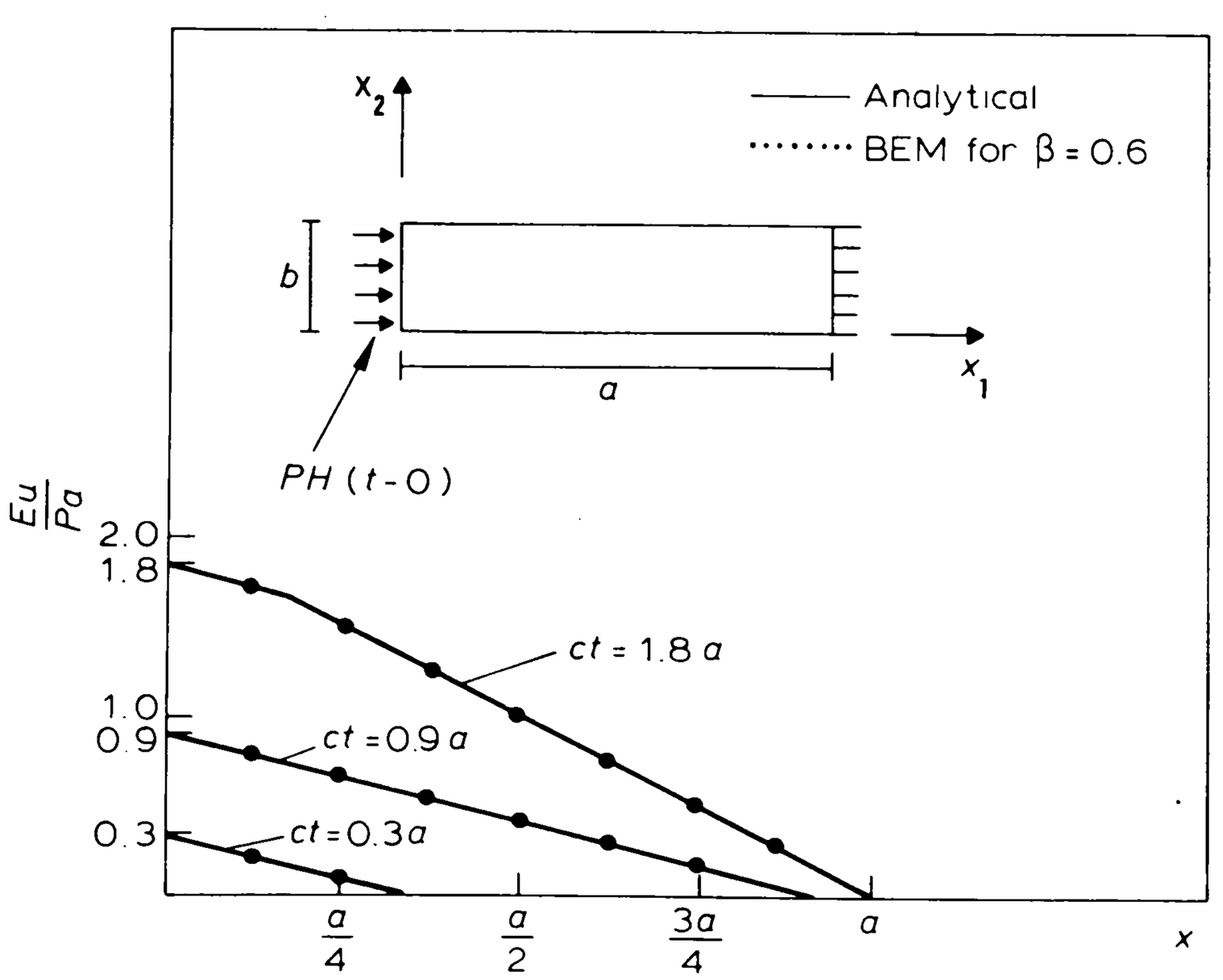

Figure **4.3.4** Displacements along boundary $y = 0$ at times $t = 0.3a/c$, $t = 0.9a/c$, $t = 1.8a/c$ for one-dimensional rod under a Heaviside type forcing function. $\eta_j(Q)$, $\nu_j(Q)$, $\phi^m(t)$ are linear, and $\theta^m(t)$ is constant.

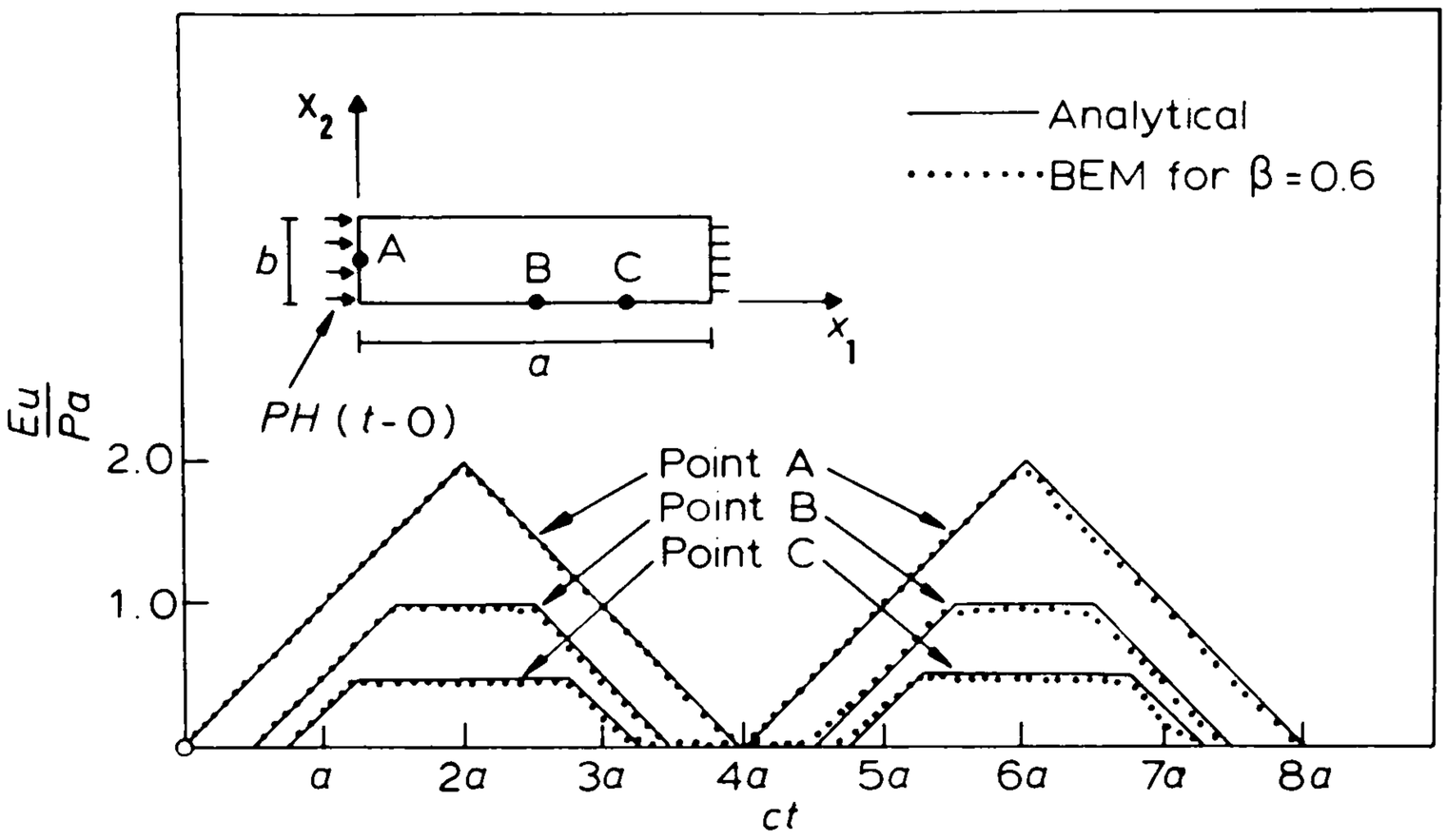

Figure **4.3.5** Displacements at boundary points A(0, $b/2$), B($a/2$, 0) and C($3a/4$, 0) for one-dimensional rod under a Heaviside type forcing function. $\eta_j(Q)$, $\nu_j(Q)$, $\phi^m(t)$ are linear and $\theta^m(t)$ is constant .

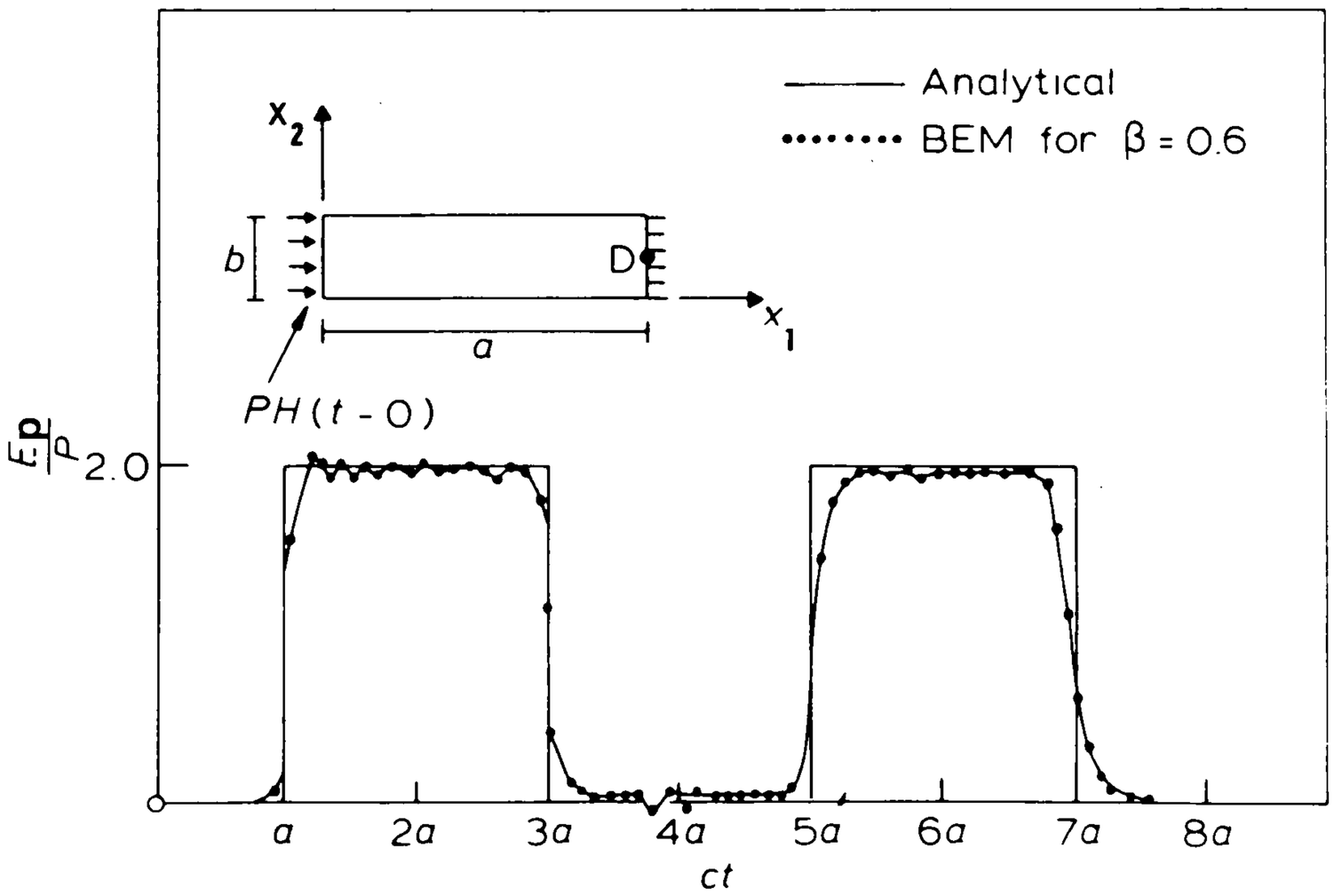

Figure **4.3.6** Normal derivative of displacement at point D(a, $b/2$) for one-dimensional rod under a Heaviside type forcing function. $\eta_j(Q)$, $\nu_j(Q)$, $\phi^m(t)$ are linear and $\theta^m(t)$ is constant .

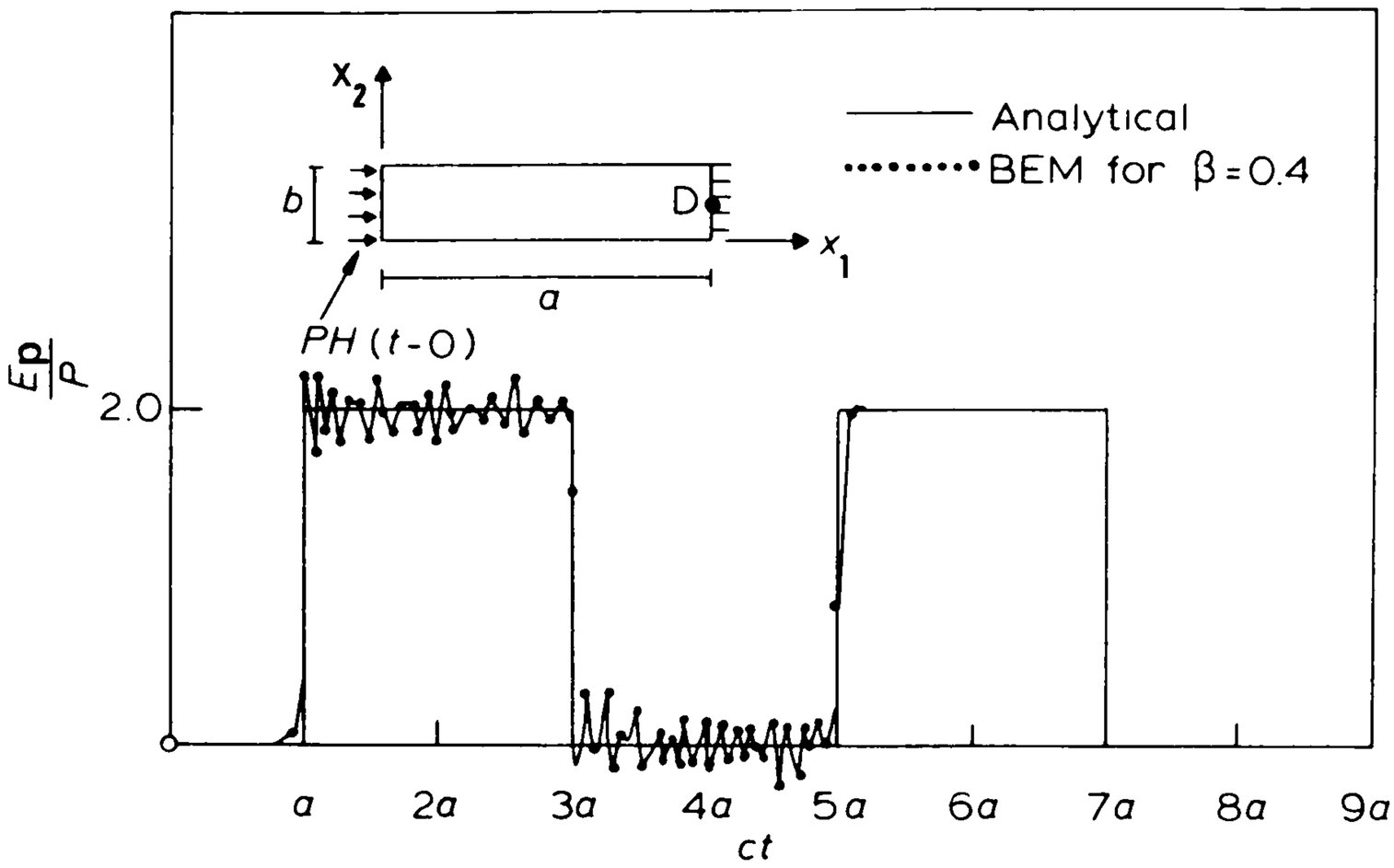

Figure **4.3.7** Normal derivative of displacement at point D(a, $b/2$) for one-dimensional rod under a Heaviside type forcing function. $\eta_j(Q)$, $\nu_j(Q)$, $\phi^m(t)$ are linear and $\theta^m(t)$ is constant .

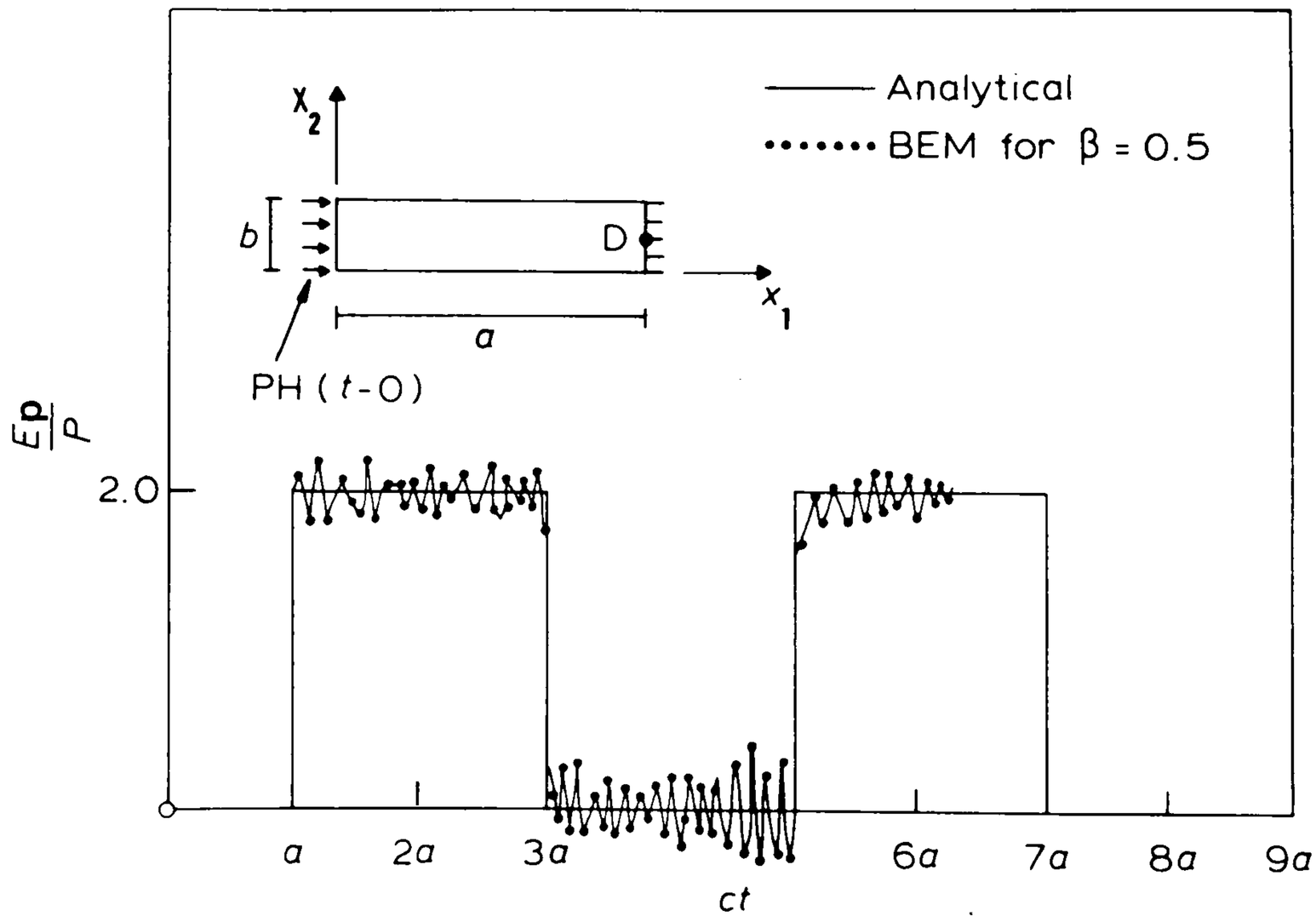

Figure **4.3.8** Normal derivative of displacement at point D(a, $b/2$), for one-dimensional rod under a Heaviside type forcing function. $\eta_j(Q)$, $\nu_j(Q)$, $\phi^m(t)$ are linear and $\theta^m(t)$ is constant .

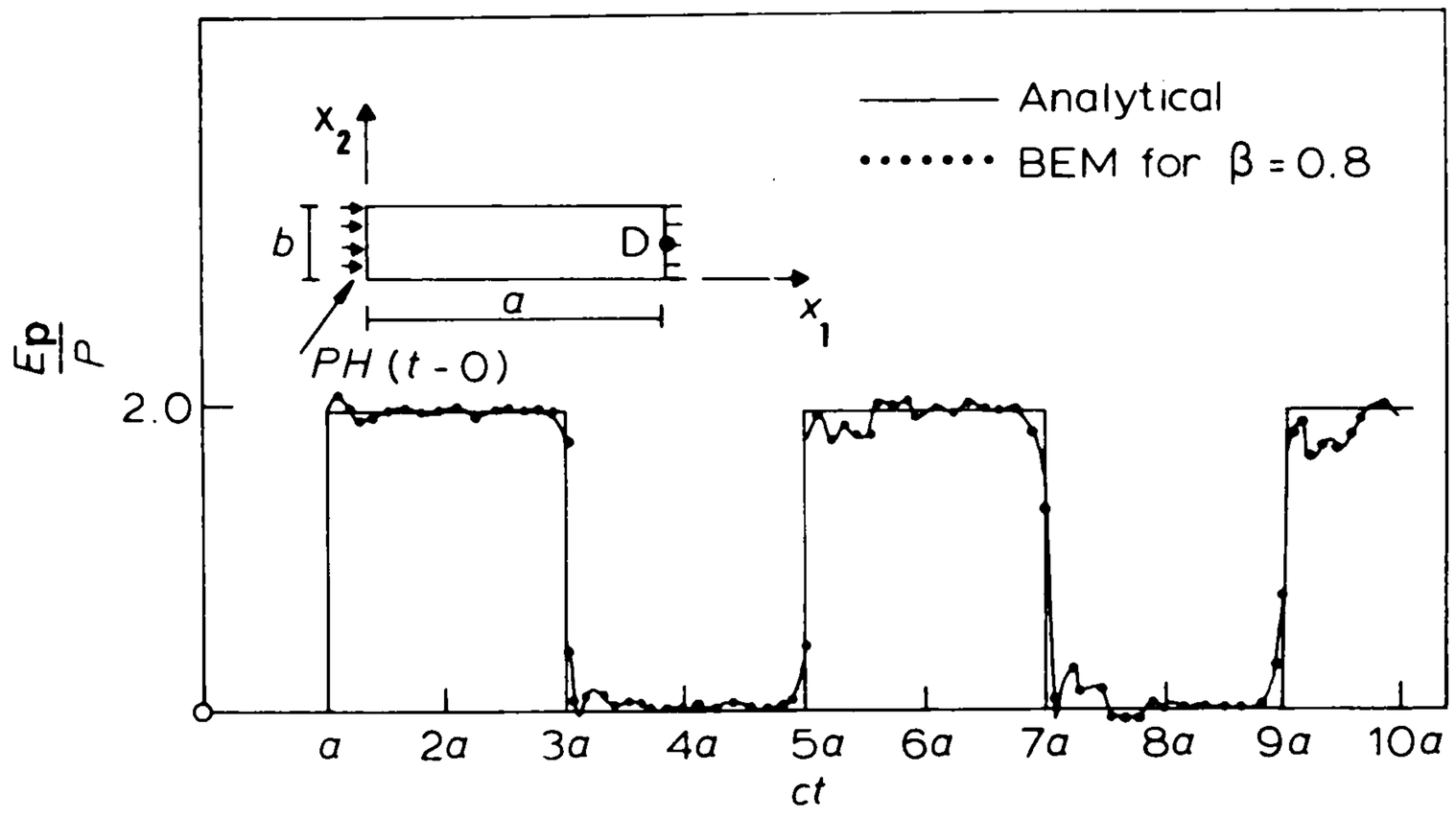

Figure **4.3.9** Normal derivative of displacement at point D(a, $b/2$), for one-dimensional rod under a Heaviside type forcing function. $\eta_j(Q)$, $\nu_j(Q)$, $\phi^m(t)$ are linear and $\theta^m(t)$ is constant .

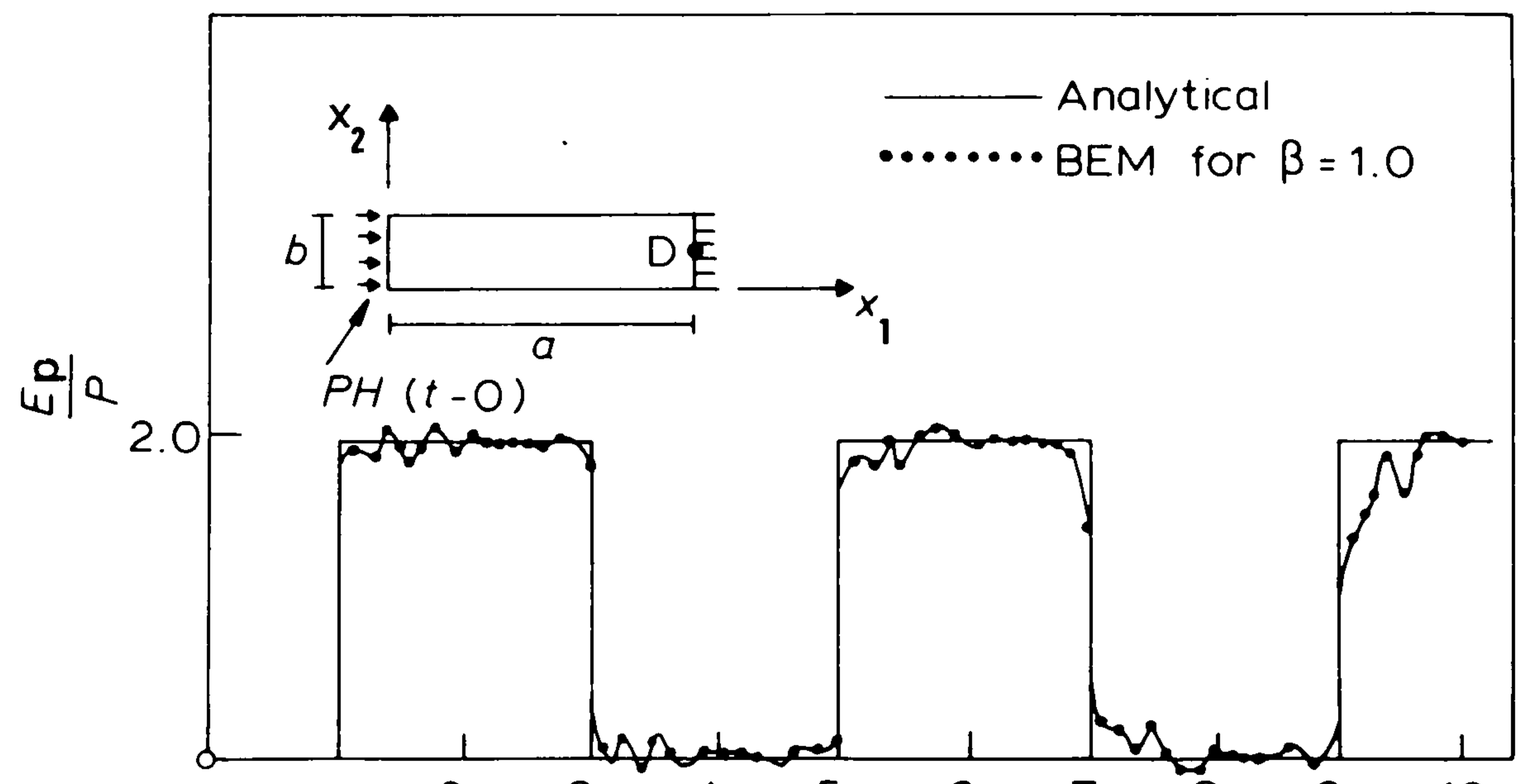

Figure **4.3.10** Normal derivative of displacement at point D(a, $b/2$) for one-dimensional rod under a Heaviside type forcing function. $\eta_j(Q)$, $\nu_j(Q)$, $\phi^m(t)$ are linear and $\theta^m(t)$ is constant .

$$u'(q,t) = u(q,\ t - \frac{a}{4c}) \tag{4.3.6}$$

$$p'(q,t) = p(q,\ t - \frac{a}{4c})$$

where u' and p' refer to the problem studied in section 4.3.1.

Twenty four linear elements were used to discretize the boundary and Ω_o was subdivided into four triangular cells as depicted in figure 4.3.12. The time steps were such that $\beta = 0.6$.

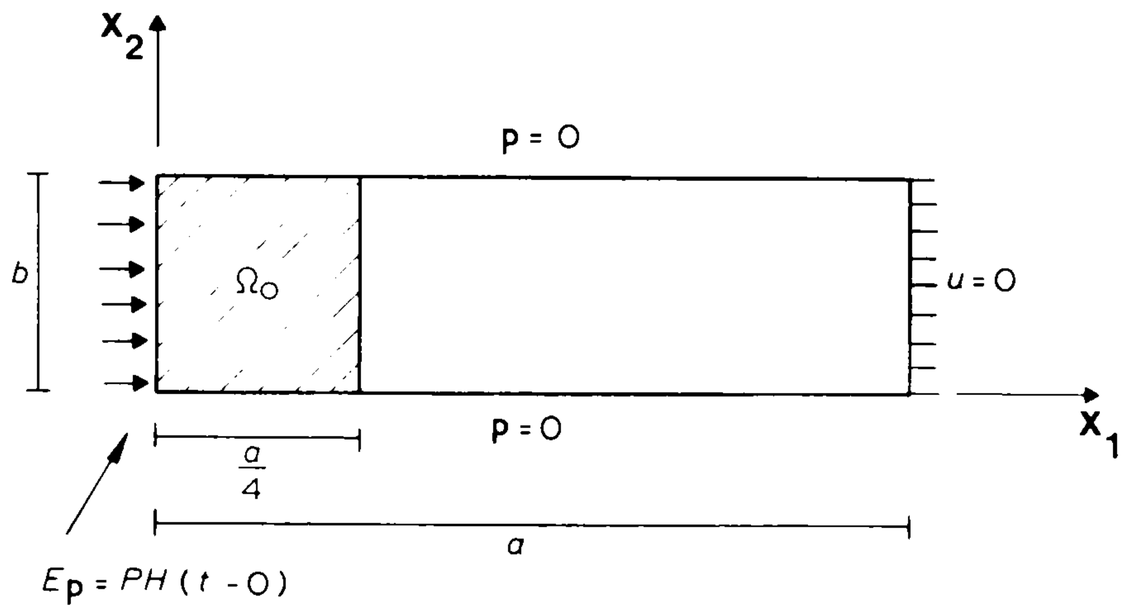

Figure 4.3.11 Geometry definitions, boundary and initial conditions for one-dimensional rod.

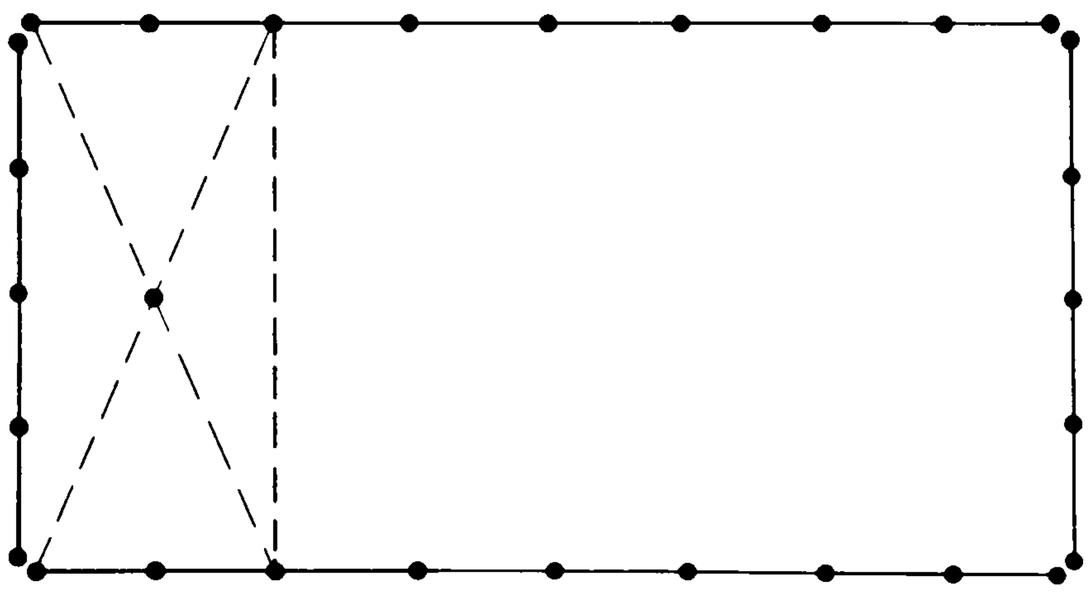

Figure 4.3.12 Domain and boundary discretization for one-dimensional rod under prescribed initial conditions.

Displacements at points (0,b/2),(3a/16,b/2), (3a/4,b/2) and traction at point (a,b/2) are presented in figures 4.3.13 and 4.3.14 respectively. The accuracy of the results is similar to that obtained in the previous problem.

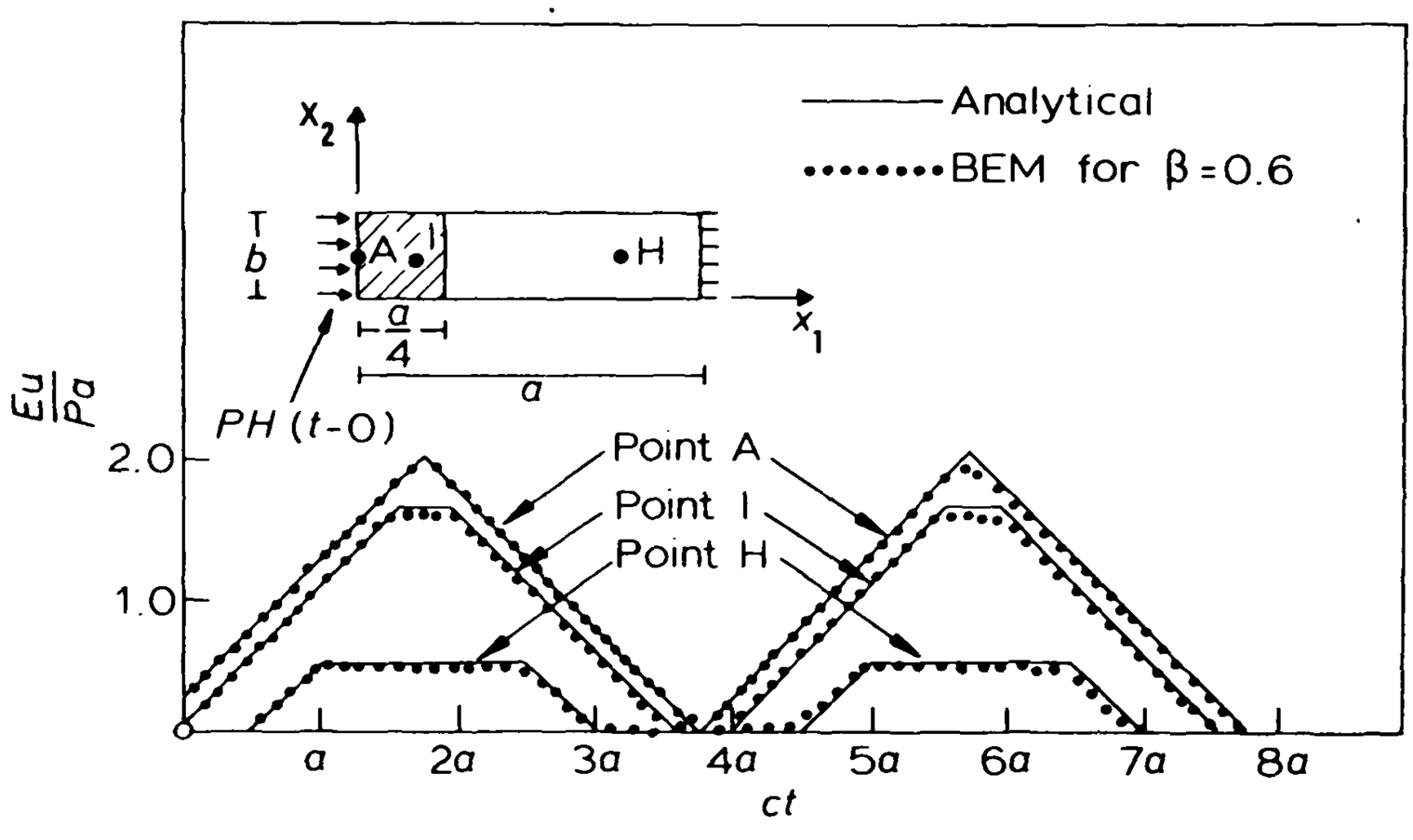

Figure 4.3.13 Displacements at boundary point A(0, $b/2$) and internal points I($3a/16$, $b/2$), H($3a/4$, $b/2$) for one-dimensional rod under prescribed initial conditions. $\eta_j(Q)$, $\nu_j(Q)$, $\phi^m(t)$ are linear and $\theta^m(t)$ is constant .

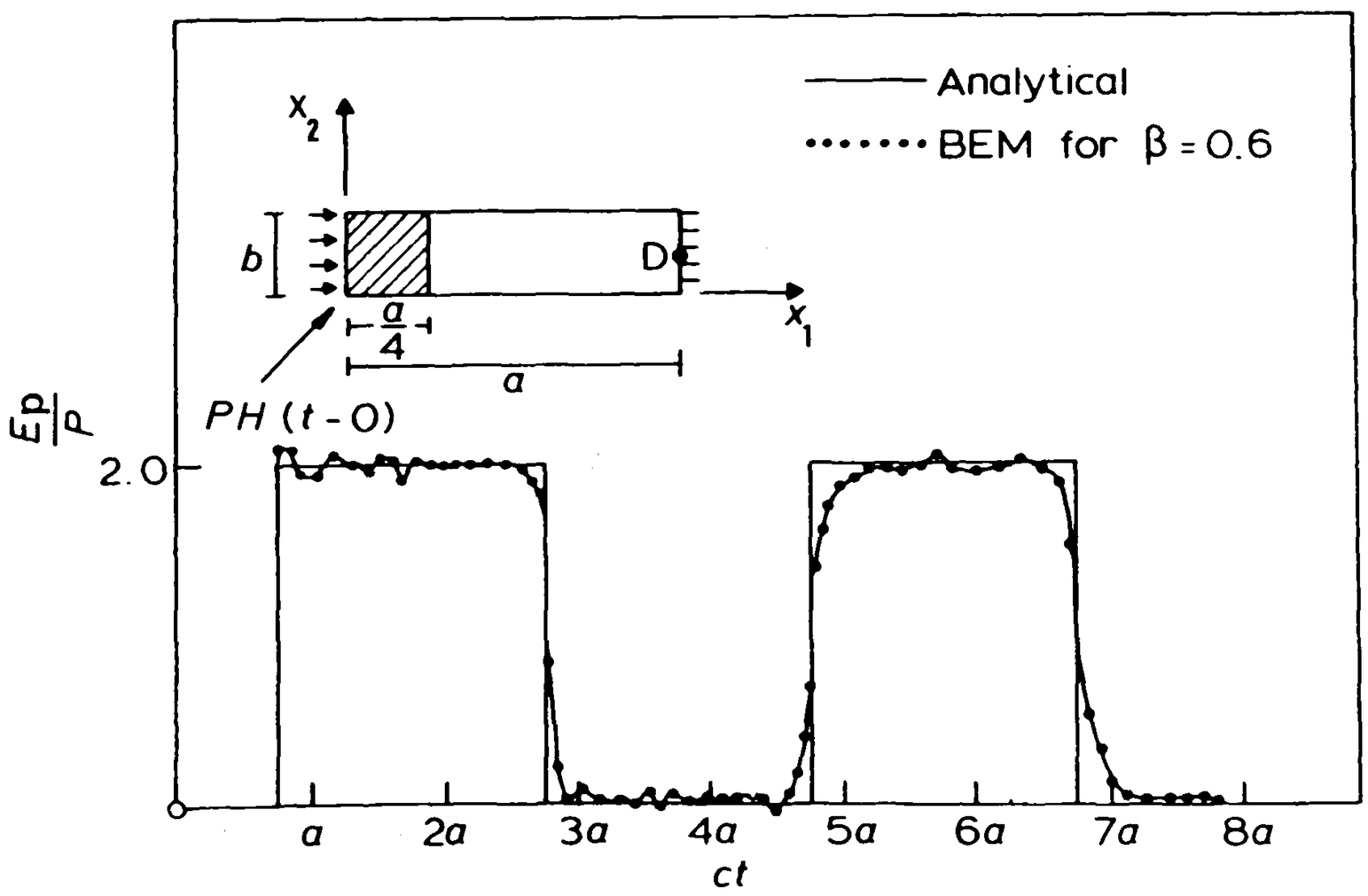

Figure 4.3.14 Normal derivative of displacement at point D(a, $b/2$) for one-dimensional rod under prescribed initial conditions. $\eta_j(Q)$, $\nu_j(Q)$, $\phi^m(t)$ are linear and $\theta^m(t)$ is constant .

4.3.3 Square Membrane Under Prescribed Initial Velocity - The subject of this investigation is the transverse motion of a square membrane with initial velocity $v_o = c$ prescribed over the domain Ω_o depicted in figure 4.3.15 and zero displacements prescribed over all the boundary.

The boundary was discretized into thirty two elements and Ω_o was divided into four cells as shown in figure 4.3.16. Analytical (see appendix G) and boundary element method results for displacements at point (a/2,a/2) and the normal derivative of displacements at point (a,a/2) were compared.

The values of u and p for $\beta = 0.6$ are plotted in figures 4.3.17 and 4.3.18 respectively. Although the agreement for displacements is reasonable, it was found that a more refined time division was needed to represent p more accurately. Another boundary element analysis was then carried out, with $\beta = 0.2$ and the results obtained for p, plotted in figure 4.3.19, show a better agreement. A final analysis was performed, in which the boundary was discretized into sixty four rather than thirty two elements, and the value of β was taken as 0.6. The results (see figure 4.3.20) were only slightly better than those for the previous case, apparently because unlike the rod analysis, $\beta<0.6$ did not introduce any great amount of noise into the numerical results.

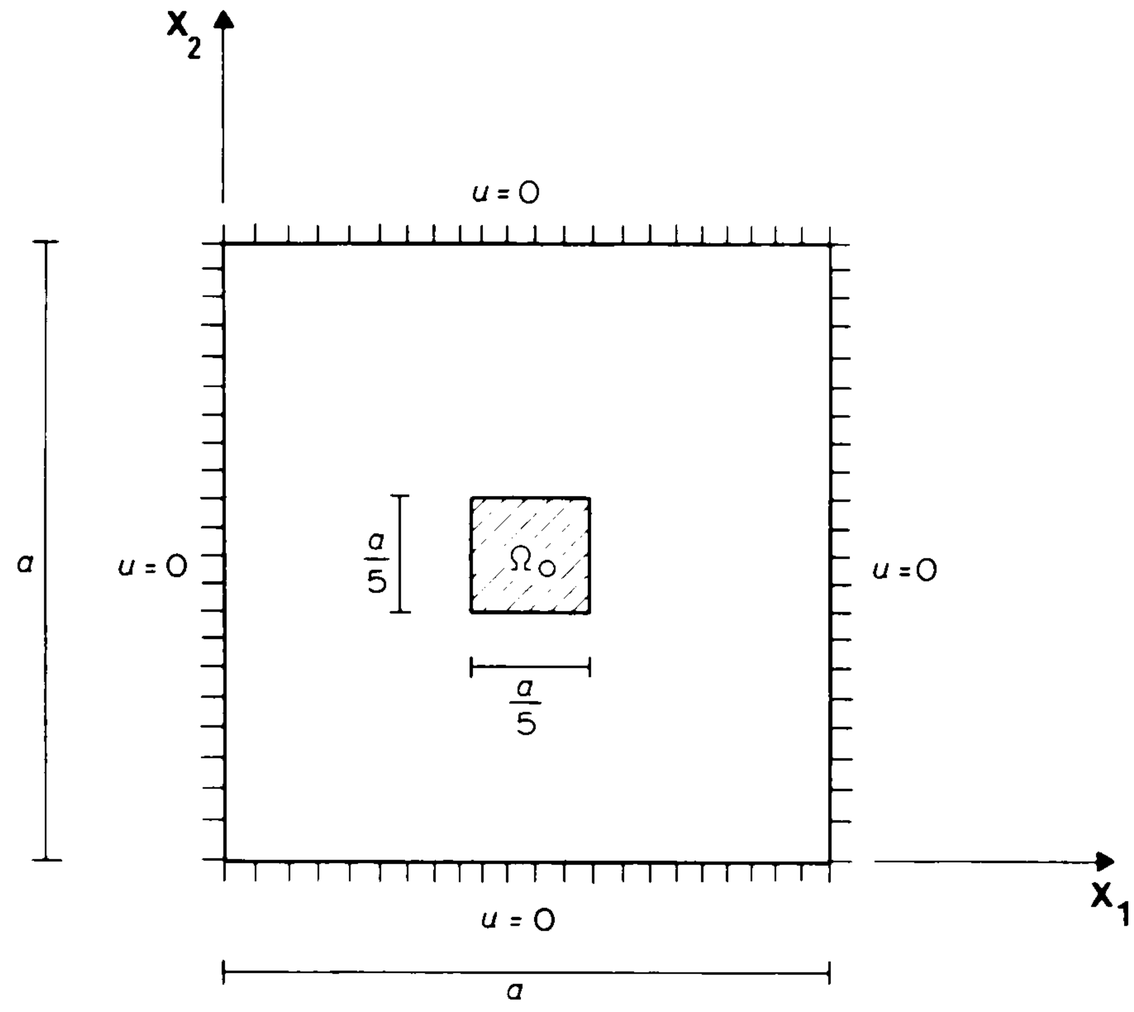

Figure 4.3.15 Geometry definition, boundary and initial conditions for membrane analysis.

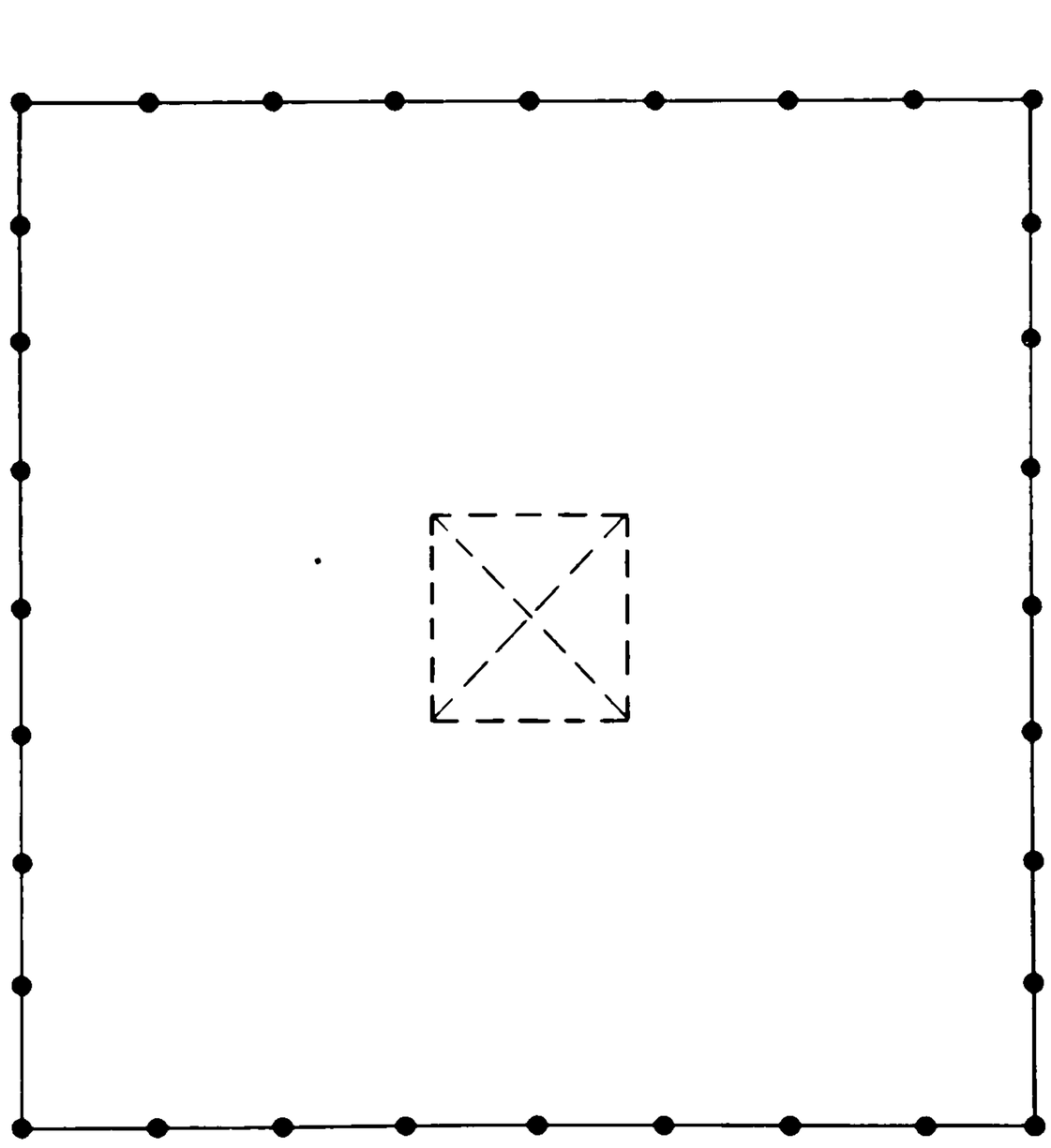

Figure 4.3.16 Membrane discretized into 32 elements and four cells.

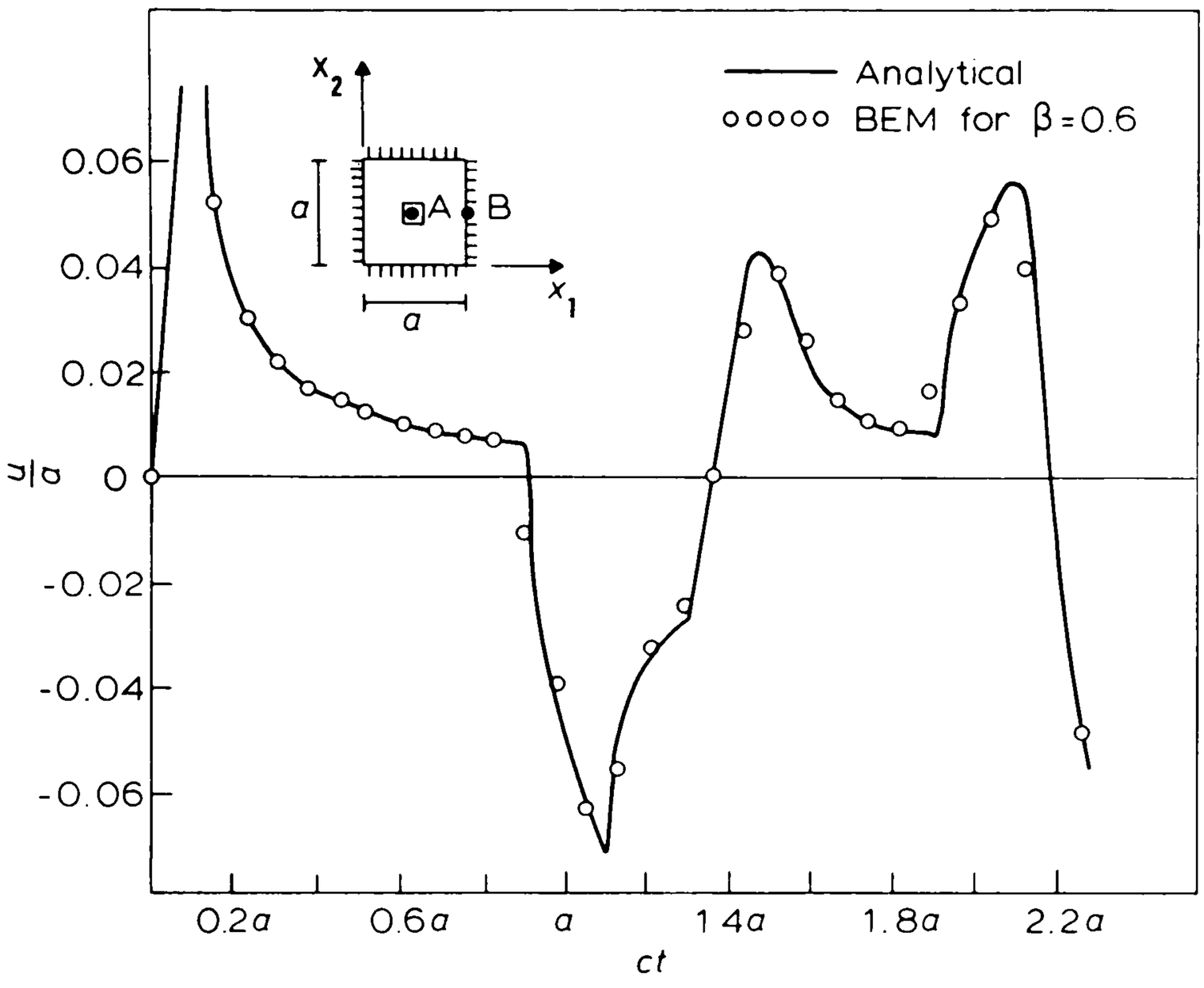

Figure **4.3.17** Displacement at point A($a/2$, $a/2$). 32 boundary elements.

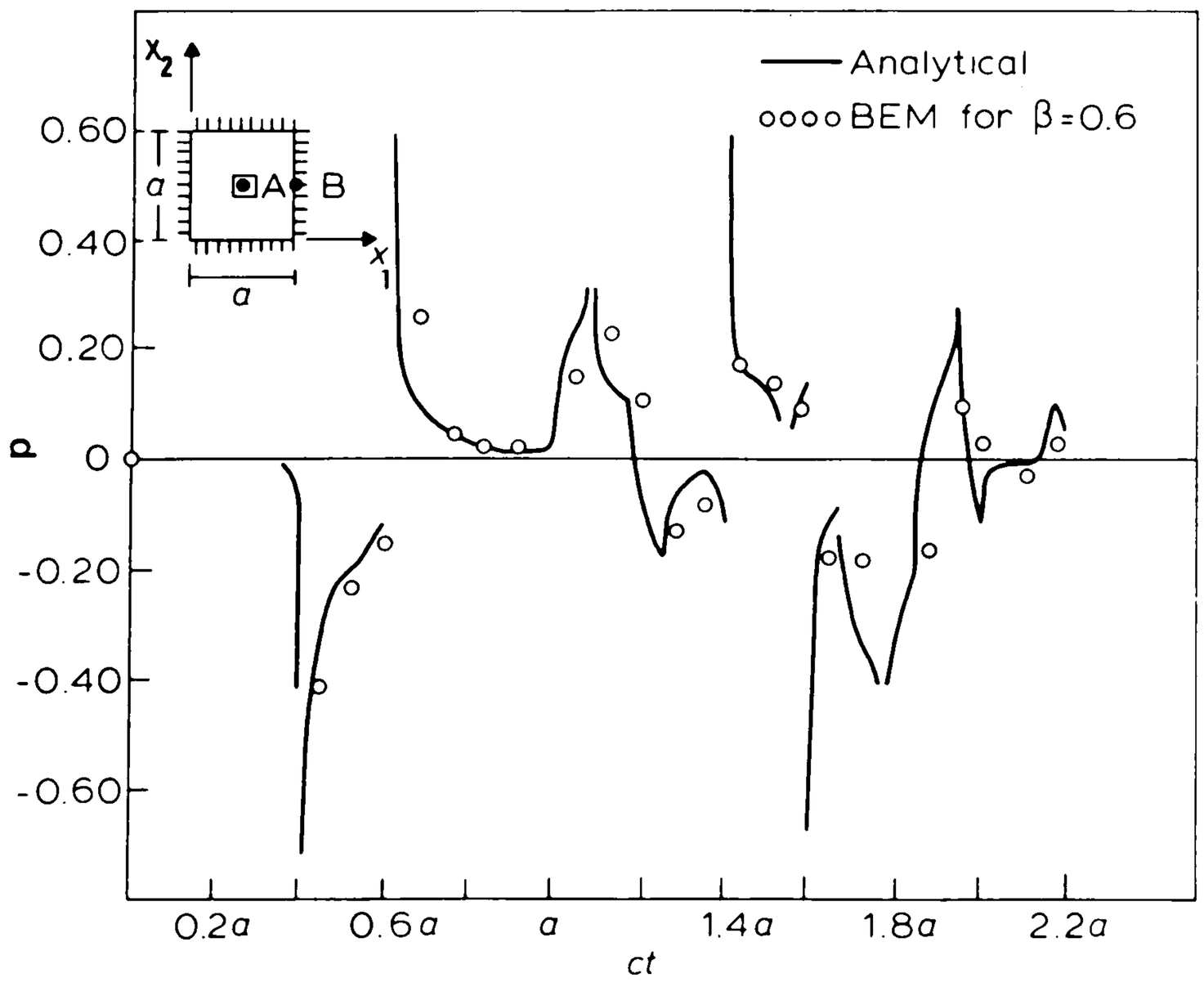

Figure **4.3.18** Normal derivative of displacement at point B(a, $a/2$). 32 boundary elements.

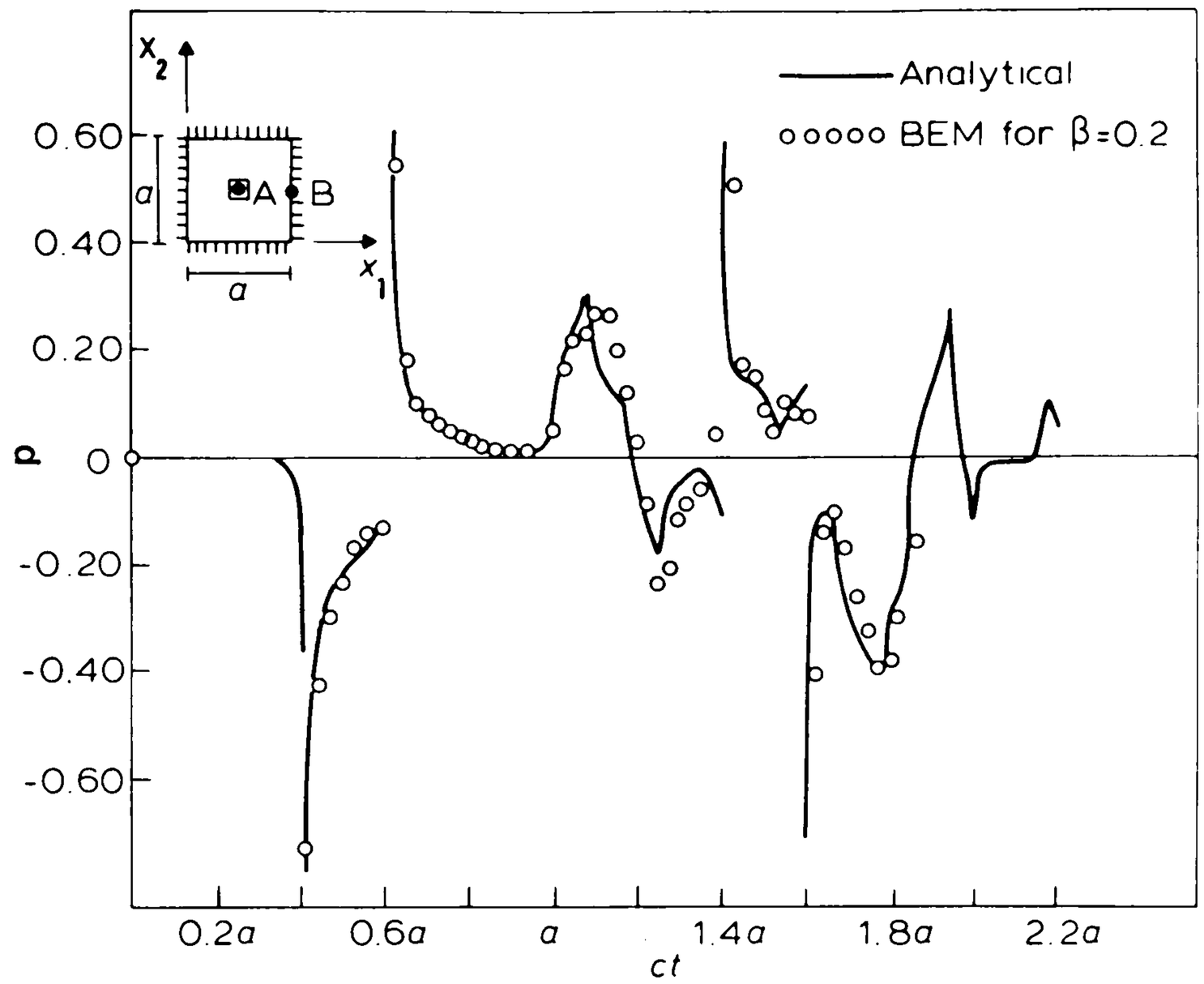

Figure **4.3.19** Normal derivative of displacement at point B(a, $a/2$). 32 boundary elements.

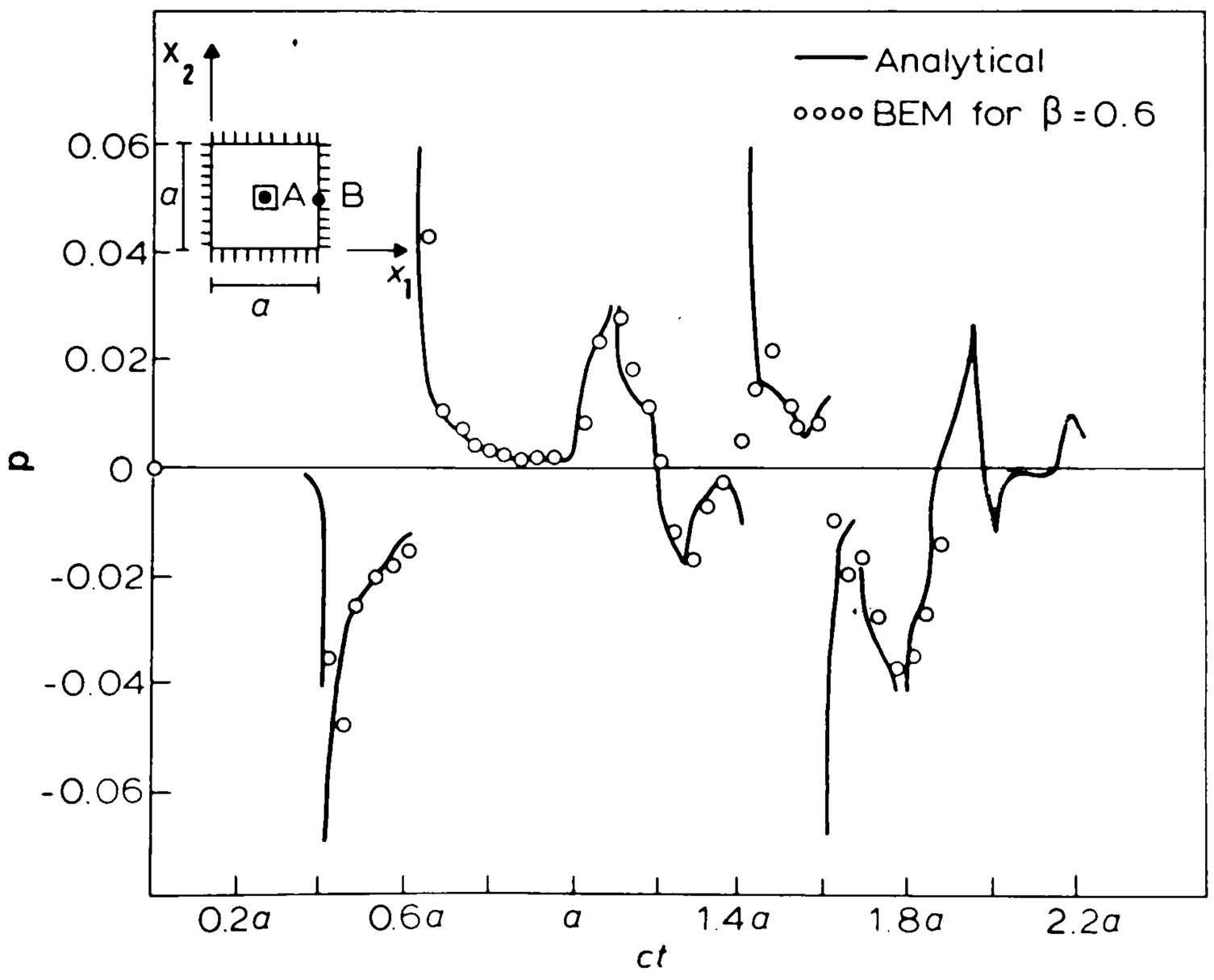

Figure **4.3.20** Normal derivative of displacement at point B(a, $a/2$). 64 boundary elements.

CHAPTER 5

BOUNDARY INTEGRAL EQUATIONS FOR TRANSIENT ELASTODYNAMICS

5.1 Introduction

In this chapter the discussion presented in chapter three concerning the scalar wave equation will be extended to elastodynamics.

Linear homogeneous isotropic elastodynamics is governed by Navier's equations (see expression (2.2.18)) which are frequently presented in the literature in the following alternative form

$$(c_d^2-c_s^2)u_{k,kj} + c_s^2 u_{j,kk} + f_j = \ddot{u}_j \qquad (5.1.1)$$

where c_d and c_s are respectively the speed of propagation of dilatational and equivoluminal body waves and

$$f_j = \frac{b_j}{\rho} \quad . \qquad (5.1.2)$$

As discussed in section 2.2 initial conditions u_{ok} and v_{ok} (k=1,2,3) are specified at all points inside the domain of the problem. In addition u_k and p_k must satisfy prescribed boundary conditions $u_k = \bar{u}_k$ on Γ_1, and $p_k = \bar{p}_k$ on Γ_2 ($\Gamma=\Gamma_1+\Gamma_2$).

Equivoluminal and dilatational wave propagation speeds can also be used to express stresses in terms of displacements. In this case equation (2.2.21) reads

$$\sigma_{ij} = \rho(c_d^2-2c_s^2)u_{m,m}\delta_{ij} + \rho c_s^2(u_{i,j}+u_{j,i}) \quad . \qquad (5.1.3)$$

An integral representation for elastodynamics can be obtained following a procedure similar to that described in section 3.5 for the scalar wave equation, however, Graffi's elastodynamic reciprocal theorem will be employed rather than weighted residues. From this, a very useful theorem which has commonly been used in elastodynamics will also be illustrated.

5.2 Elastodynamic Fundamental Solutions

The fundamental singular solution of elastodynamics which is used in this work is the function u^*_{ik} which satisfies the following equations

$$\sigma^*_{ijk,j} - \rho\ddot{u}^*_{ik} = -\delta_{ik}\delta(q-s)\delta(t-\tau) \qquad (5.2.1)$$

in an unbounded domain Ω^*, which is free from any imposed initial condition. The body forces in equations (5.2.1) correspond to a concentrated force in the x_i-direction which is an impulse at $t=\tau$ located at $q=s$.

In three dimensions, the solution of equations (5.2.1) can be written as follows {9}

$$u^*_{ik}(q,t;s,\tau) = \frac{t'}{4\pi\rho r^2}\left(\left(\frac{3r_ir_k}{r^3} - \frac{\delta_{ik}}{r}\right)\left[H\left(t' - \frac{r}{c_d}\right) - H\left(t' - \frac{r}{c_s}\right)\right]\right.$$

$$+ \frac{r_ir_k}{r^2}\left[\frac{1}{c_d}\delta\left(t' - \frac{r}{c_d}\right) - \frac{1}{c_s}\delta\left(t' - \frac{r}{c_s}\right)\right] \qquad (5.2.2)$$

$$\left. + \frac{\delta_{ik}}{c_s}\delta\left(t' - \frac{r}{c_s}\right)\right)$$

where

$$t' = t-\tau$$

$$r = |\underline{q}-\underline{s}| = (r_ir_i)^{1/2} \qquad (5.2.3)$$

$$r_i = x_i(q) - x_i(s) \quad .$$

It should be recognized that equivalent forms for u^*_{ik} other than that described by expression (5.2.2) are frequently to be found in the literature {9,80,81,84}.

Equations (2.2.4), (5.1.3) and (5.2.2) can be used to obtain the fundamental traction given by {9}

$$p^*_{ik} = \sigma^*_{ijk}n_j = \sigma^*_{ikj}n_j = \rho\left[(c_d^2-2c_s^2)u^*_{im,m}\delta_{jk}+c_s^2(u^*_{ik,j}+u^*_{ij,k})\right]n_j \tag{5.2.4}$$

where

$$\sigma^*_{ijk}(q,t;s,\tau) = \frac{1}{4\pi}\Bigg(-6\,\frac{c_s^2 t'}{r^2}\left[5\,\frac{r_i r_j r_k}{r^5} - \frac{\delta_{ij}r_k+\delta_{ik}r_j+\delta_{jk}r_i}{r^3}\right]$$

$$\cdot\left[H\left(t'-\frac{r}{c_d}\right) - H\left(t'-\frac{r}{c_s}\right)\right]$$

$$+2\left[6\,\frac{r_i r_j r_k}{r^5} - \frac{\delta_{ij}r_k+\delta_{ik}r_j+\delta_{jk}r_i}{r^3}\right]$$

$$\cdot\left[\delta\left(t'-\frac{r}{c_s}\right) - \frac{c_s^2}{c_d^2}\delta\left(t'-\frac{r}{c_d}\right)\right] \tag{5.2.5}$$

$$+2\,\frac{r_i r_j r_k}{r^4 c_s}\left[\dot{\delta}\left(t'-\frac{r}{c_s}\right) - \frac{c_s^3}{c_d^3}\dot{\delta}\left(t'-\frac{r}{c_d}\right)\right]$$

$$-\frac{r_i\delta_{jk}}{r^3}\left(1-2\,\frac{c_s^2}{c_d^2}\right)\left[\delta\left(t'-\frac{r}{c_d}\right)+\frac{r}{c_d}\dot{\delta}\left(t'-\frac{r}{c_d}\right)\right]$$

$$-\frac{\delta_{ik}r_j+\delta_{ij}r_k}{r^3}\left[\delta\left(t'-\frac{r}{c_s}\right)+\frac{r}{c_s}\dot{\delta}\left(t'-\frac{r}{c_s}\right)\right]\Bigg) \quad .$$

The two-dimensional fundamental solution of elastodynamics can be obtained by following a procedure similar to that given in section 3.6 for the scalar wave equation. In this case, descending from three dimensions gives (for details see reference {9})

$$u^*_{ik}(q,t;s,\tau) = \frac{1}{2\pi\rho c_s}\left(\left[\frac{\delta_{ik}}{\sqrt{c_s^2(t')^2-r^2}} + \frac{\delta_{ik}}{r^2}\sqrt{c_s^2(t')^2-r^2}\right.\right.$$

$$\left.\left. - \frac{r_{,i}r_{,k}}{r^2}\,\frac{2c_s^2(t')^2-r^2}{\sqrt{c_s^2(t')^2-r^2}}\right]H(c_s t'-r)\right. \qquad (5.2.6)$$

$$\left. - \frac{c_s}{c_d}\left[\frac{\delta_{ik}}{r^2}\sqrt{c_d^2(t')^2-r^2} - \frac{r_{,i}r_{,k}}{r^2}\,\frac{2c_d^2(t')^2-r^2}{\sqrt{c_d^2(t')^2-r^2}}\right]H(c_d t'-r)\right)$$

where

$$r_{,i} = \frac{\partial r}{\partial x_i(q)} = -\frac{\partial r}{\partial x_i(s)} = \frac{r_i}{r} \quad . \qquad (5.2.7)$$

Equations (5.2.4) and (5.2.6) can be applied to derive an expression for the two-dimensional fundamental traction, which is given by (see appendix F)

$$p^*_{ik}(q,t;s,\tau) = \frac{1}{2\pi\rho c_s}\left(A_{ik}\left[\frac{r}{\sqrt{\left[c_s^2(t')^2-r^2\right]^3}}\,H(c_s t'-r)\right.\right.$$

$$\left.\left. + \frac{1}{\sqrt{c_s^2(t')^2-r^2}}\,\frac{\partial}{\partial(c_s\tau)}\,H(c_s t'-r)\right]\right.$$

$$+\left[B_{ik}\,\frac{2c_s^2(t')^2-r^2}{\sqrt{c_s^2(t')^2-r^2}} + D_{ik}\,\frac{r^3}{\sqrt{\left[c_s^2(t')^2-r^2\right]^3}}\right]$$

$$\left. \cdot\, H(c_s t'-r) + D_{ik}\,\frac{2c_s^2(t')^2-r^2}{\sqrt{c_s^2(t')^2-r^2}}\,\frac{\partial}{\partial(c_s\tau)}\,H(c_s t'-r)\right)$$

$$- \frac{c_s}{c_d} \left(\left[B_{ik} \frac{2c_d^2(t')^2-r^2}{\sqrt{c_d^2(t')^2-r^2}} + D_{ik} \frac{r^3}{\sqrt{\left[c_d^2(t')^2-r^2\right]^3}} \right] \right.$$

$$\left. \cdot H(c_d t'-r) + D_{ik} \frac{2c_d^2(t')^2-r^2}{\sqrt{c_d^2(t')^2-r^2}} \frac{\partial}{\partial(c_d\tau)} H(c_d t'-r) \right) \Bigg] \qquad (5.2.8)$$

where

$$A_{ik} = G(2\theta n_k r_{,i} + \delta_{ik} \frac{\partial r}{\partial n} + n_i r_{,k})$$

$$B_{ik} = - \frac{2G}{r^3}(\delta_{ik} \frac{\partial r}{\partial n} + n_i r_{,k} + n_k r_{,i} - 4 \frac{\partial r}{\partial n} r_{,i} r_{,k}) \qquad (5.2.9)$$

$$D_{ik} = - \frac{2G}{r^2}(\theta n_k r_{,i} + \frac{\partial r}{\partial n} r_{,i} r_{,k})$$

$$\theta = \lambda/2G = (c_d^2-2c_s^2)/2c_s^2 \quad .$$

The fundamental solutions studied in this section have the following properties {9}

(i) causality

$$u^*_{ik}(q,t;s,\tau) = 0 \quad \text{whenever } c_s(t-\tau) < |\underline{q}-\underline{s}| \qquad (5.2.10)$$

(ii) reciprocity

$$u^*_{ik}(q,t;s,\tau) = u^*_{ik}(s,-\tau;q,-t) \qquad (5.2.11)$$

(iii) time translation

$$u^*_{ik}(q,t+t_1;s,\tau+t_1) = u^*_{ik}(q,t;s,\tau) \quad . \qquad (5.2.12)$$

It should be noted that the properties described in (i), (ii) and (iii) above are similar to the ones studied previously in section 3.4 for the scalar wave equation.

The symmetry of the tensors given by equations (5.2.2) and (5.2.6) implies that {9} the k-component of the displacement

at q due to the i-component of the concentrated force at s is equal to the i component of the displacement at q due to the k-component of the concentrated force at s, i.e.

$$u^*_{ik}(q,t;s,\tau) = u^*_{ki}(q,t;s,\tau) \quad . \tag{5.2.13}$$

5.3 Time Domain Elastodynamic Boundary Integral Representation

The reciprocal theorem for elastodynamics, to be derived in this section, effectively relates two elastodynamic states whose displacement fields will be denoted by u_k and u^*_k. These are defined over regions $\Omega+\Gamma$ and $\Omega^*+\Gamma^*$ respectively so that Ω^* contains $\Omega+\Gamma$ as depicted in figure 3.5.2. The bodies enclosed by Γ and Γ^* have the same physical properties, and u_k and u^*_k satisfy the elastodynamic equilibrium equations, i.e.

$$\sigma_{kj,j} + \beta_k = 0 \quad \text{in } \Omega$$

$$\sigma^*_{kj,j} + \beta^*_k = 0 \quad \text{in } \Omega^* \tag{5.3.1}$$

where

$$\beta_k = b_k - \rho \frac{\partial^2 u_k}{\partial \tau^2}$$

$$\beta^*_k = b^*_k - \rho \frac{\partial^2 u^*_k}{\partial \tau^2} \quad . \tag{5.3.2}$$

Using Hooke's law the following integral statement can easily be inferred

$$\int_\Omega \sigma^*_{ij}\varepsilon_{ij}\,d\Omega = \int_\Omega \sigma_{ij}\varepsilon^*_{ij}\,d\Omega \quad . \tag{5.3.3}$$

If the divergence theorem (see equation (A.2)) is applied to both sides of equation (5.3.3) and equations (2.2.8) and (5.3.1) are used, the following statement is inferred

$$\int_{\Omega} \beta_k^* u_k d\Omega + \int_{\Gamma} p_k^* u_k d\Gamma = \int_{\Omega} \beta_k u_k^* d\Omega + \int_{\Gamma} p_k u_k^* d\Gamma \quad . \tag{5.3.4}$$

Equation (5.3.4) corresponds to Betti's second reciprocal work theorem for two distinct elastostatic states with body forces β and β^*.

When equation (5.3.4) is integrated from 0 to t, and expression (5.3.2) is taken into consideration, the following equation is obtained

$$\int_0^t \int_{\Omega} b_k^* u_k d\Omega d\tau - \rho \int_0^t \int_{\Omega} \frac{\partial^2 u_k^*}{\partial \tau^2} u_k \, d\Omega d\tau + \int_0^t \int_{\Gamma} p_k^* u_k \, d\Gamma d\tau$$

$$= \int_0^t \int_{\Omega} b_k u_k^* \, d\Omega d\tau - \rho \int_0^t \int_{\Omega} \frac{\partial^2 u_k}{\partial \tau^2} u_k^* \, d\Omega d\tau + \int_0^t \int_{\Gamma} p_k u_k^* \, d\Gamma d\tau \quad . \tag{5.3.5}$$

When expression (A.1) is considered it is then possible to write

$$\int_0^t \frac{\partial^2 u_k}{\partial \tau^2} u_k^* d\tau = v_k(q,t) u_k^*(q,t) - v_{ok} u_{ok}^* - \int_0^t v_k(q,\tau) v_k^*(q,\tau) d\tau$$

$$\int_0^t \frac{\partial^2 u_k^*}{\partial \tau^2} u_k d\tau = v_k^*(q,t) u_k(q,t) - v_{ok}^* u_{ok} - \int_0^t v_k^*(q,\tau) v_k(q,\tau) d\tau \tag{5.3.6}$$

where

$$v_k(q,t) = \left|\frac{\partial u_k}{\partial \tau}\right|_{\tau=t} \tag{5.3.7}$$

and

$$v_{ok}(q) = v_k(q,0) \quad . \tag{5.3.8}$$

When expression (5.3.6) is substituted into equation (5.3.5), the reciprocal theorem of elastodynamics is obtained, i.e.

$$\int_0^t\int_\Omega b_k^* u_k d\Omega d\tau - \rho\int_\Omega v_k^* u_k d\Omega + \rho\int_\Omega v_{ok}^* u_{ok} d\Omega$$

$$+ \int_0^t\int_\Gamma p_k^* u_k d\Gamma d\tau = \int_0^t\int_\Omega b_k u_k^* d\Omega d\tau - \rho\int_\Omega v_k u_k^* d\Omega \tag{5.3.9}$$

$$+ \rho\int_\Omega v_{ok} u_{ok}^* d\Omega + \int_0^t\int_\Gamma p_k u_k^* d\Gamma d\tau \quad .$$

If one of the elastodynamic states is taken at a time $t'=t-\tau$ the reciprocal theorem given by equation (5.3.9) can be cast into Graffi's theorem, in the form in which it is presented in references {9 and 10}.

In order to obtain a boundary integral equation for the problem being studied, one of the elastodynamic states in expression (5.3.9) will be considered to be that governed by equation (5.2.1). In this case, due to the reciprocity property

$$\frac{\partial^2 u^*_{ik}}{\partial t^2} = \frac{\partial^2 u^*_{ik}}{\partial \tau^2} \quad , \tag{5.3.10}$$

and as a result of the causality property

$$\int_\Omega v^*_{ik}(q,t;s,t^+)u_k d\Omega = \int_\Omega v_k u^*_{ik}(q,t;s,t^+)d\Omega = 0 \quad . \tag{5.3.11}$$

Then, if the time integration limits indicated in equation (5.3.9) are taken to be zero and t^+ ($t^+ = t+\varepsilon$, $\varepsilon \to 0$) the following equation is obtained

$$\int_0^{t^+}\int_\Omega u_k \delta_{ik}\delta(q-s)\delta(t-\tau)d\Omega d\tau + \int_0^{t^+}\int_\Gamma p^*_{ik}u_k d\Gamma d\tau$$

$$= \int_0^{t^+}\int_\Gamma p_k u^*_{ik} d\Gamma d\tau + \rho\int_\Omega v_{ok}u^*_{oik}d\Omega - \rho\int_\Omega v^*_{oik}u_{ok}d\Omega \tag{5.3.12}$$

$$+ \int_0^{t^+}\int_\Omega b_k u^*_{ik} d\Omega d\tau \quad .$$

Taking account of the Dirac delta properties

$$\int_0^{t^+}\int_\Omega u_k \delta_{ik}\delta(q-s)\delta(t-\tau)d\Omega(q)d\tau = u_i(s,t) \tag{5.3.13}$$

the following integral statement is then obtained

$$u_i(s,t) = \int_0^{t^+}\int_\Gamma u^*_{ik}(Q,t;s,\tau)p_k(Q,\tau)d\Gamma(Q)d\tau$$

$$- \int_0^{t^+}\int_\Gamma p^*_{ik}(Q,t;s,\tau)u_k(Q,\tau)d\Gamma(Q)d\tau$$

$$+ \rho \int_{\Omega} u^*_{oik}(q,t;s)v_{ok}(q)d\Omega(q)$$

$$- \rho \int_{\Omega} v^*_{oik}(q,t;s)u_{ok}(q)d\Omega(q)$$

$$+ \int_0^{t^+}\int_{\Omega} u^*_{ik}(q,t;s,\tau)b_k(q,\tau)d\Omega(q)d\tau \quad . \qquad (5.3.14)$$

Equation (5.3.14) gives the u_i-component of the displacement, at an internal point s, as a function of boundary tractions and displacements, initial conditions and body forces. When s→S a procedure similar to that discussed in chapter 3, for the scalar wave equation, can be followed giving

$$c_{ik}(S)u_k(S,t) = \int_0^{t^+}\int_{\Gamma} u^*_{ik}(Q,t;S,\tau)p_k(Q,\tau)d\Gamma(Q)d\tau$$

$$- \int_0^{t^+}\int_{\Gamma} p^*_{ik}(Q,t;S,\tau)u_k(Q,\tau)d\Gamma(Q)d\tau$$

$$+ \rho \int_{\Omega} u^*_{oik}(q,t;S)v_{ok}(q)d\Omega(q) \qquad (5.3.15)$$

$$- \rho \int_{\Omega} v^*_{oik}(q,t;S)u_{ok}(q)d\Omega(q)$$

$$+ \int_0^{t^+}\int_{\Omega} u^*_{ik}(q,t;S,\tau)b_k(q,\tau)d\Omega(q)d\tau$$

where

$$c_{ij}(S) = \frac{1}{2}\delta_{ij} \qquad (5.3.16)$$

whenever the Γ boundary is smooth. It should be recognized that the integrals indicated in equation (5.3.15) are to be calculated in the Cauchy principal value sense.

Equation (5.3.15) can also be used when the source point is outside $\Omega+\Gamma$. In this case c_{ij} must be regarded as being equal to zero.

Additional information on how equation (5.3.15) can be obtained from equation (5.3.14), for both, three and two dimensions, can be found in {9,80,81,84}. In these references, discussions concerning expression (5.3.16) are also considered.

In order to implement a numerical time-stepping algorithm to solve the three-dimensional boundary integral equation analytical integrations must be performed first, to eliminate the Dirac-delta functions and its derivatives that appear in equations (5.2.2) and (5.2.5). This matter is discussed in references {80 and 81} where two-dimensional elastodynamic problems are analysed using three-dimensional fundamental solutions. In these papers the two-dimensional problem is considered to be a cylinder, whose axis has infinite length and is parallel to the x_3-direction, as explained in section 3.6. As this approach is essentially three-dimensional, an extra integration with respect to the coordinate x_3 is required.

In the present investigation, two-dimensional elastodynamic problems are analysed using a two-dimensional

boundary integral equation, i.e., the fundamental solution considred is that given by equation (5.2.6). In order to implement a general two-dimensional numerical time-stepping algorithm, some additional transformations must first be carried out in order to eliminate the derivatives of Heaviside functions that appear in equation (5.2.8). This is discussed in the next section.

5.4 Additional Transformations to the Two-Dimensional Boundary Integral Equation of Elastodynamics

In the numerical analysis concerning two-dimensional elastodynamics, initial conditions and body forces will not be considered. Consequently when u^*_{ik} and p^*_{ik} given by expressions (5.2.6) and (5.2.8) respectively, are substituted into equation (5.3.15) and manipulations similar to those described in section 3.7 are carried out the following expression is obtained

$$c_{ik}(S)u_k(S,t) = \frac{1}{2\pi\rho c_s}\left\{\int_0^{t^+}\int_\Gamma (A_{ik}L_2^3M_2 - B_{ik}L_2N_2 + D_{ik}L_2^3O_2)u_k H\left[c_s t' - r\right]d\Gamma d\tau\right.$$

$$- \frac{c_s}{c_d}\int_0^{t^+}\int_\Gamma (-B_{ik}L_1N_1 + D_{ik}L_1^3O_1)u_k H\left[c_d t' - r\right]d\Gamma d\tau$$

$$\left. + \frac{1}{c_s}\int_0^{t^+}\int_\Gamma (A_{ik}L_2 + D_{ik}L_2N_2)v_k H\left[c_s t' - r\right]d\Gamma d\tau\right.$$

$$- \frac{c_s}{c_d^2} \int_0^{t^+} \int_\Gamma D_{ik} L_1 N_1 v_k H\left[c_d t' - r\right] d\Gamma d\tau$$

$$+ \int_0^{t^+} \int_\Gamma (\delta_{ik} L_2 + F_{ik} L_2^{-1} + J_{ik} L_2 N_2) p_k H\left[c_s t' - r\right] d\Gamma d\tau$$

$$\left. - \frac{c_s}{c_d} \int_0^{t^+} \int_\Gamma (F_{ik} L_1^{-1} + J_{ik} L_1 N_1) p_k H\left[c_d t' - r\right] d\Gamma d\tau \right) \qquad (5.4.1)$$

where A_{ik}, B_{ik} and D_{ik} are given by expression (5.2.9),

$$F_{ik} = \frac{\delta_{ik}}{r^2}, \qquad (5.4.2)$$

$$J_{ik} = - \frac{r_{,i} r_{,k}}{r^2}$$

and

$$L_1 = L_1(Q,t;S,\tau) = \left[c_d^2 (t')^2 - r^2\right]^{-1/2}$$

$$M_1 = M_1(Q,t;S,\tau) = c_d t' - r \qquad (5.4.3)$$

$$N_1 = N_1(Q,t;S,\tau) = 2c_d^2 (t')^2 - r^2$$

$$O_1 = O_1(Q,t;S,\tau) = 3c_d t' r^2 - 2c_d^3 (t')^3 - r^3 \quad .$$

L_2, M_2, N_2 and O_2 can be respectively obtained from L_1, M_1, N_1 and O_1 replacing c_d by c_s in expression (5.4.3).

In items (i) and (ii) described below details are given of the modifications required to obtain equation (5.4.1) from expression (5.3.15).

(i) Applying the same procedure used in item (i) of section 3.7 it is possible to write

$$\int_0^{t^+}\int_\Gamma A_{ik}u_k L_2 \frac{\partial}{\partial(c_s\tau)} H\left[c_s t'-r\right]d\Gamma d\tau$$

$$= -\frac{1}{c_s}\int_\Gamma A_{ik}u_{ok}L_{o2}H\left[c_s t -r\right]d\Gamma \qquad (5.4.4)$$

$$-\frac{1}{c_s}\int_0^{t^+}\int_\Gamma A_{ik}v_k L_2 H\left[c_s t'-r\right]d\Gamma d\tau$$

$$-\int_0^{t^+}\int_\Gamma A_{ik}u_k c_s t' L_2^3 H\left[c t'-r\right]d\Gamma d\tau$$

where

$$L_{o2} = L_2(Q,t;S,0) \quad . \qquad (5.4.5)$$

The first term on the right-hand side of expression (5.4.4) was regarded as being equal to null because non zero initial conditions have not been considered in the elastodynamic formulation.

(ii) The remaining term in equation (5.3.15) that requires to be further manipulated is given by

$$I = \int_0^{t^+}\int_\Gamma D_{ik}u_k L_2 N_2 \frac{\partial}{\partial(c_s\tau)} H\left[c_s t'-r\right]d\Gamma d\tau \qquad (5.4.6)$$

$$= \frac{1}{c_s}\int_\Gamma D_{ik}\int_0^{t^+} u_k L_2 N_2 \frac{\partial}{\partial\tau} H\left[c_s t'-r\right]d\tau d\Gamma \quad .$$

If expression (A.1) is used, integration by parts with respect to time gives

$$\int_0^{t^+} u_k L_2 N_2 \frac{\partial}{\partial \tau} H\left[c_s t'-r\right] d\tau$$

$$= \left| u_k L_2 N_2 H\left[c_s t'-r\right] \right|_0^{t^+} - \int_0^{t^+} v_k L_2 N_2 H\left[c_s t'-r\right] d\tau \qquad (5.4.7)$$

$$- \int_0^{t^+} u_k \frac{\partial}{\partial \tau} (L_2 N_2) H\left[c_s t'-r\right] d\tau \quad .$$

In view of the causality property and the fact that

$$\frac{\partial}{\partial \tau}(L_2 N_2) = \left(-2c_s^4 (t')^3 + 3c_s^2 t' r^2\right) L_2^3 \qquad (5.4.8)$$

the following expression results

$$I = - \frac{1}{c_s} \int_\Gamma D_{ik} u_{ok} N_{o2} L_{o2} H\left[c_s t - r\right] d\Gamma$$

$$- \frac{1}{c_s} \int_0^{t^+} \int_\Gamma D_{ik} v_k N_2 L_2 H\left[c_s t'-r\right] d\Gamma d\tau \qquad (5.4.9)$$

$$+ \int_0^{t^+} \int_\Gamma D_{ik} u_k \left[2c_s^3 (t')^3 - 3c_s t' r^2\right] L_2^3 H\left[c_s t'-r\right] d\Gamma d\tau$$

where

$$N_{o2} = N_2(Q,t;S,0). \qquad (5.4.10)$$

The first term on the right-hand side of expression (5.4.9) was not included in equation (5.4.1) because u_{ok} was taken as being equal to zero.

The operations carried out in sub-sections (i) and (ii) above refer to terms in equation (5.4.1) that account

for waves which propagate with speed c_s. The term in expression (5.3.15) given by

$$\int_0^{t^+} \int_\Gamma D_{ik} u_k L_1 N_1 \frac{\partial}{\partial (c_d \tau)} H\left[c_s t' - r\right] d\Gamma d\tau \qquad (5.4.11)$$

which refers to dilatational waves also has to undergo additional transformations. The final expression for this case can easily be obtained if c_s is replaced by c_d in equation (5.4.9).

A close examination of equation (5.4.1) reveals that some integrands in that expression are singular at the wave fronts of both equivoluminal ($r = c_s t'$) and dilatational ($r = c_d t'$) waves, represented by the Green's function. These singularities are of the same type previously discussed in section 3.7 for the scalar wave equation, i.e., the functions being integrated behave like

$$\frac{1}{\sqrt{c^2 (t-\tau)^2 - r^2}} \quad . \qquad (5.4.12)$$

An additional difficulty in the two-dimensional elastodynamic boundary element formulation is discussed in reference {81}and refers to the singularities that appear when $r \to 0$ and

$$c_s (t-\tau) \neq 0 \qquad (5.4.13)$$

$$c_d (t-\tau) \neq 0 \quad .$$

These singularities, however, are only apparent ones and disappear if contributions from similar terms referring to equivoluminal and dilational waves are calculated together

in expression (5.4.1). The type of manipulations required will now be discussed by considering the integrals that involve B_{ik} in expression (5.4.1).

When considered alone $B_{ik}L_2N_2$ and $B_{ik}L_1N_1$ behave like $1/r^3$ when $r \to 0$. However these singularities can easily be eliminated from the integral equation if it is realized that

$$B_{ik}\left[-L_2N_2 + \frac{c_s}{c_d} L_1N_1\right] \tag{5.4.14}$$

$$= -B_{ik}r^4 \frac{\left[(c_d^4-c_s^4)(t')^2-(c_d^2-c_s^2)r^2\right]L_1L_2}{c_d(c_dN_2L_1^{-1}+c_sN_1L_2^{-1})} \quad .$$

Therefore, the only singularities present in the numerical analysis are those that occur when r and t' go to zero simultaneously.

CHAPTER 6

BOUNDARY ELEMENT METHOD FOR TWO-DIMENSIONAL TRANSIENT ELASTODYNAMICS

6.1 Introduction

A time-stepping scheme to solve equation (5.4.1) will be discussed in this chapter. The procedure employed for two-dimensional transient elastodynamics is similar to that already discussed in chapter 4 concerning the scalar wave equation.

After the boundary unknowns $u_i(S,t)$ and $p_i(S,t)$ have been obtained, internal displacements $u_i(s,t)$ can be calculated by applying the integral equation that results from equation (5.4.1) when S is replaced by s and $c_{ik}(s)$ is made to equal to δ_{ij}. In elasticity problems it is important to compute stresses as well. The scheme implemented in section 6.2 to calculate internal stresses is similar to the simplest one used in finite elements. Triangular cells are employed and stresses at their centroids are obtained by carrying out derivatives of displacements, which are linearly interpolated inside each cell as a function of the displacements at the cell nodes. Following this procedure one avoids performing analytical derivatives of the integral equation for internal displacements is avoided. This alternative procedure however, should be attempted in future research because it almost certainly yields more accurate results.

Interpolation functions of the type given by equation (4.2.1) are also used to approximate u_k and p_k in

equation (5.4.1). Analytical time integration can also be carried out, resulting in expressions which are considerably longer than those previously derived when investigating the scalar wave equation (see chapter 4). A certain degree of care must be taken when integrating analytically with respect to time. If conveniently manipulated, the final expressions obtained will have no singularity at the fronts of the equivoluminal and dilatational waves represented by the Green's function. Convenient operations like those described by expression (5.4.14) must also be carried out in order to remove apparent singularities that occur when $r \to 0$. Consequently the only singularities which remain occur on the first time step, when $r \to 0$, and are of the same type as those for two-dimensional elastostatics, i.e., the integrands behave like $1/r$ and $\ln r$ on the boundary integrals involving u_k and p_k respectively.

6.2 Numerical Implementation

As in section 4.2, the implementation of a numerical scheme to solve equation (5.4.1) requires the consideration of a set of discrete points Q_j, $j=1,\ldots J$, on the Γ boundary and a set of values of time t_n, $n=1,\ldots,N$. $u_k(Q,t)$, $v_k(Q,t)$ and $p_k(Q,t)$ can be approximated using the same set of interpolation functions shown in section 4.2.1, i.e.,

$$u_k(Q,t) = \sum_{j=1}^{J} \sum_{m=1}^{N} \phi^m(t)\, \eta_j(Q)\, \bar{u}^m_{kj}$$

$$v_k(Q,t) = \sum_{j=1}^{J} \sum_{m=1}^{N} \frac{d\phi^m(t)}{dt}\, \eta_j(Q)\, \bar{u}^m_{kj}$$

$$p_k(Q,t) = \sum_{j=1}^{J} \sum_{m=1}^{N} \theta^m(t)\nu_j(Q)\bar{p}^m_{kj} \qquad (6.2.1)$$

where m and j refer to time and space respectively, k=1,2 relates to the x_k-direction and

$$\bar{u}^m_{kj} = u_k(Q_j,t_m) \qquad (6.2.2)$$

$$\bar{p}^m_{kj} = p_k(Q_j,t_m) \quad .$$

When equation (5.4.1) is written for every node l and also for all values of time t_n, and u_k, v_k and p_k are replaced by their approximations as given by expression (6.2.1), the following system of algebraic equations is then obtained

$$\sum_{k=1}^{2} c_{ik}(S_l)\bar{u}^n_{kl} + \frac{1}{2\pi\rho c_s} \sum_{k=1}^{2} \sum_{m=1}^{N} \sum_{j=1}^{J} \bar{H}^{nm}_{iljk}\bar{u}^m_{kj} \qquad (6.2.3)$$

$$= \frac{1}{2\pi\rho c_s} \sum_{k=1}^{2} \sum_{m=1}^{N} \sum_{l=1}^{J} \bar{G}^{nm}_{iljk}\bar{p}^m_{kj}$$

where

$$\bar{H}^{nm}_{iljk} = -\int_0^{t_n}\int_\Gamma \Big[\big(A_{ik}\bar{L}^3_2\bar{M}_2 - B_{ik}\bar{L}_2\bar{N}_2 + \bar{D}_{ik}\bar{L}^3_2\bar{O}_2\big) - \frac{c_s}{c_d}\big(-B_{ik}\bar{L}_1\bar{N}_1 + D_{ik}\bar{L}^3_1\bar{O}_1\big)\Big]\phi^m(\tau)\eta_j(Q) \qquad (6.2.4)$$

$$+\Big[\frac{1}{c_s}\big(A_{ik}\bar{L}_2 + D_{ik}\bar{L}_2\bar{N}_2\big) - \frac{c_s}{c_d^2} D_{ik}\bar{L}_1\bar{N}_1\Big]\frac{d\phi^m(\tau)}{d\tau}\eta_j(Q)\Big) d\Gamma d\tau \quad ,$$

$$\bar{G}^{nm}_{iljk} = \int_0^{t_n}\int_\Gamma \Big((\delta_{ik}\bar{L}_2 + F_{ik}\bar{L}_2^{-1} + J_{ik}\bar{L}_2\bar{N}_2) - \frac{c_s}{c_d}(F_{ik}\bar{L}_1^{-1} + J_{ik}\bar{L}_1\bar{N}_1)\theta^m(\tau)\nu_j(Q)\Big) d\Gamma d\tau \qquad (6.2.5)$$

and

$$\begin{aligned}
\bar{L}_1^\alpha &= L_1^\alpha(Q,t_n;S_1,\tau)H\left[\bar{c}_d t'-r\right] \\
\bar{M}_1^\alpha &= M_1^\alpha(Q,t_n;S_1,\tau)H\left[\bar{c}_d t'-r\right] \qquad (6.2.6)\\
\bar{N}_1^\alpha &= N_1^\alpha(Q,t_n;S_1,\tau)H\left[\bar{c}_d t'-r\right] \\
\bar{O}_1^\alpha &= O_1^\alpha(Q,t_n;S_1,\tau)H\left[\bar{c}_d t'-r\right] \quad .
\end{aligned}$$

$\bar{L}_2^\alpha$, $\bar{M}_2^\alpha$, $\bar{N}_2^\alpha$ and $\bar{O}_2^\alpha$ can be obtained from $\bar{L}_1^\alpha$, $\bar{M}_1^\alpha$, $\bar{N}_1^\alpha$ and $\bar{O}_1^\alpha$ respectively, replacing c_d by c_s in expression (6.2.6). It should be realised that α in expression (6.2.6) is an exponent, not an index.

Only constant time steps, t_m, will be considered in the two-dimensional transient elastodynamic numerical analysis. In this case causality and time translation properties can be assigned to $\bar{H}^{nm}_{iljk}$ and $\bar{G}^{nm}_{iljk}$ and the discussion conducted in section 4.2.1 concerning the scalar wave equation can be extended to elastodynamics (see figure 4.2.1 and expression (4.2.11)).

In the numerical analysis undertaken in this chapter $\phi^m(\tau)$ is linear, $\theta^m(\tau)$ is constant, $\eta_1(Q)$ and $\nu_1(Q)$ are constant, and linear discretization is used to approximate the Γ boundary. The time interpolation functions $\phi^m(\tau)$ and $\theta^m(\tau)$ given by expressions (4.2.12) and (4.2.18) respectively can then be substituted into equations (6.2.4) and (6.2.5) and the resulting expressions can then be

[illegible] with respect to time.

The integrations over the Γ boundary are carried out numerically, using Gauss quadrature formulae for all time steps, but the first. When n=m=1 and when it is necessary to integrate over the element in which the source point is (j=1), the integrand of $\bar{G}^{11}_{iljk}$ has a singularity of the type $\ln r$ when $r \to 0$. In this case it is advisable to carry out analytical integrations via the procedure outlined in appendix F. When j=1 the integrand of $\bar{H}^{11}_{iljk}$ behaves like $1/r$ when $r \to 0$. This singularity is of the same type as the one which occurs when studying elastostatics. As constant elements were used the principal value of integrals that appear when computing $\bar{H}^{11}_{iljk}$ (j=1) are equal to zero. However this is not the case when higher order elements are used to approximate displacements. In this situation, principal values that are not zero can be calculated analytically.

It is now convenient to initial each node j, with numbers 2j-1 and 2j referring, respectively to directions 1 and 2 of that node, as shown in figure 6.2.1.

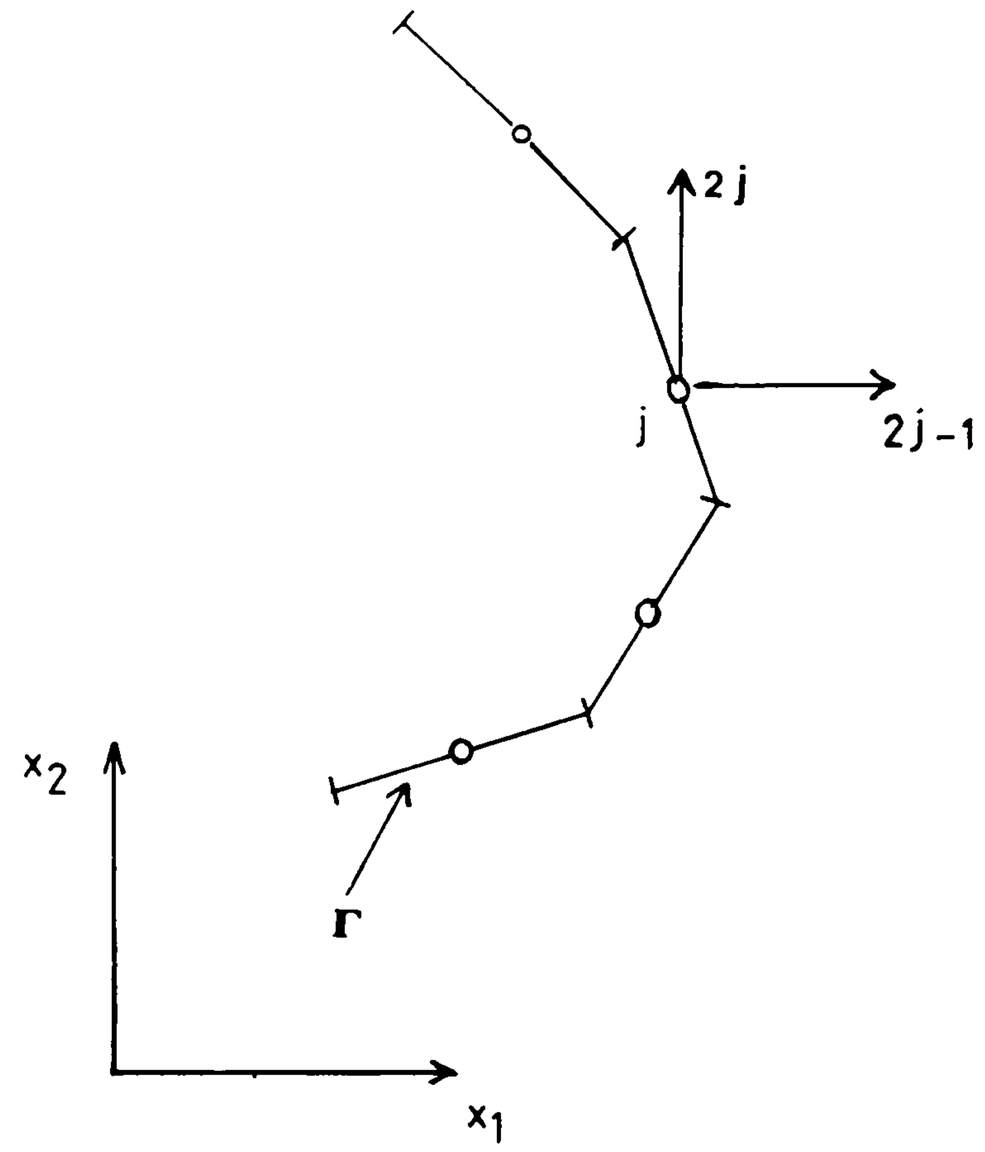

Figure 6.2.1 Global numeration.

Consequently, the following relationships can be written

$$\begin{aligned} \bar{u}^{m}_{kj} &= u^{nm}_{2j+k-2} \\ \bar{p}^{m}_{kj} &= p^{nm}_{2j+k-2} \\ \bar{H}^{nm}_{iljk} &= H^{nm}_{(2l+i-2)(2j+k-2)} \\ \bar{G}^{nm}_{iljk} &= G^{nm}_{(2l+i-2)(2j+k-2)} \end{aligned} \qquad (6.2.7)$$

Therefore, when constant elements are used,

$$c_{ik}(S_l)\bar{u}^{n}_{kl} = .5\delta_{ik}\bar{u}^{n}_{kl} = .5\bar{u}^{n}_{il} = .5u^{n}_{2l+i-2} \; . \qquad (6.2.8)$$

Taking full account of expressions (6.2.7) and (6.2.8), equation (6.2.3) can be written as

$$\begin{aligned} .5u^{n}_{i} + \frac{1}{2\pi\rho c_s}\sum_{j=1}^{2J} H^{nn}_{ij}\, u^{n}_{j} = \frac{1}{2\pi\rho c_s}\Bigg[& \sum_{j=1}^{2J} G^{nn}_{ij}\, p^{n}_{j} \\ & - \sum_{m=1}^{n-1}\sum_{j=1}^{2J} H^{nm}_{ij}\, u^{m}_{j} + \sum_{m=1}^{n-1}\sum_{j=1}^{2J} G^{nm}_{ij}\, p^{m}_{j}\Bigg] \; . \end{aligned} \qquad (6.2.9)$$

Equation (6.2.9) can also be cast into

$$\underline{H}\ \underline{u} = \underline{G}\ \underline{p} + \underline{B} \qquad (6.2.10)$$

where $\underline{H}$ and $\underline{G}$ are square matrices of order $(2J \times 2J)$ and $\underline{u}$, $\underline{p}$ and $\underline{B}$ are vectors.

When boundary conditions at a time t_n are considered and equation (6.2.10) is conveniently reordered equation (6.2.10) becomes

$$\underline{A}\ \underline{y} = \underline{c} \qquad (6.2.11)$$

where, in similarity to equation (4.3.3), the vector $\underline{y}$ is formed by unknowns u_j and p_j at boundary nodes.

After equation (6.2.11) has been solved displacements at internal points can be computed using the boundary equation for such points.

In order to use expression (2.4.4) to calculate internal stresses it is first necessary to calculate the derivatives of the displacement components with regard to the rectangular coordinates x_j. In this thesis this is accomplished numerically using triangular cells. Linear interpolation functions are used to approximate components of displacements u_k $(k=1,2)$ inside each cell, i.e.,

$$u_1 = \mu_1 U_1 + \mu_2 U_2 + \mu_3 U_3$$

$$u_2 = \mu_1 U_4 + \mu_2 U_5 + \mu_3 U_6 \qquad (6.2.12)$$

where μ_α is given by expression (4.2.32) and U_j $(j=1,6)$ are the components of the displacements at the cell nodes as shown in figure (6.2.2).

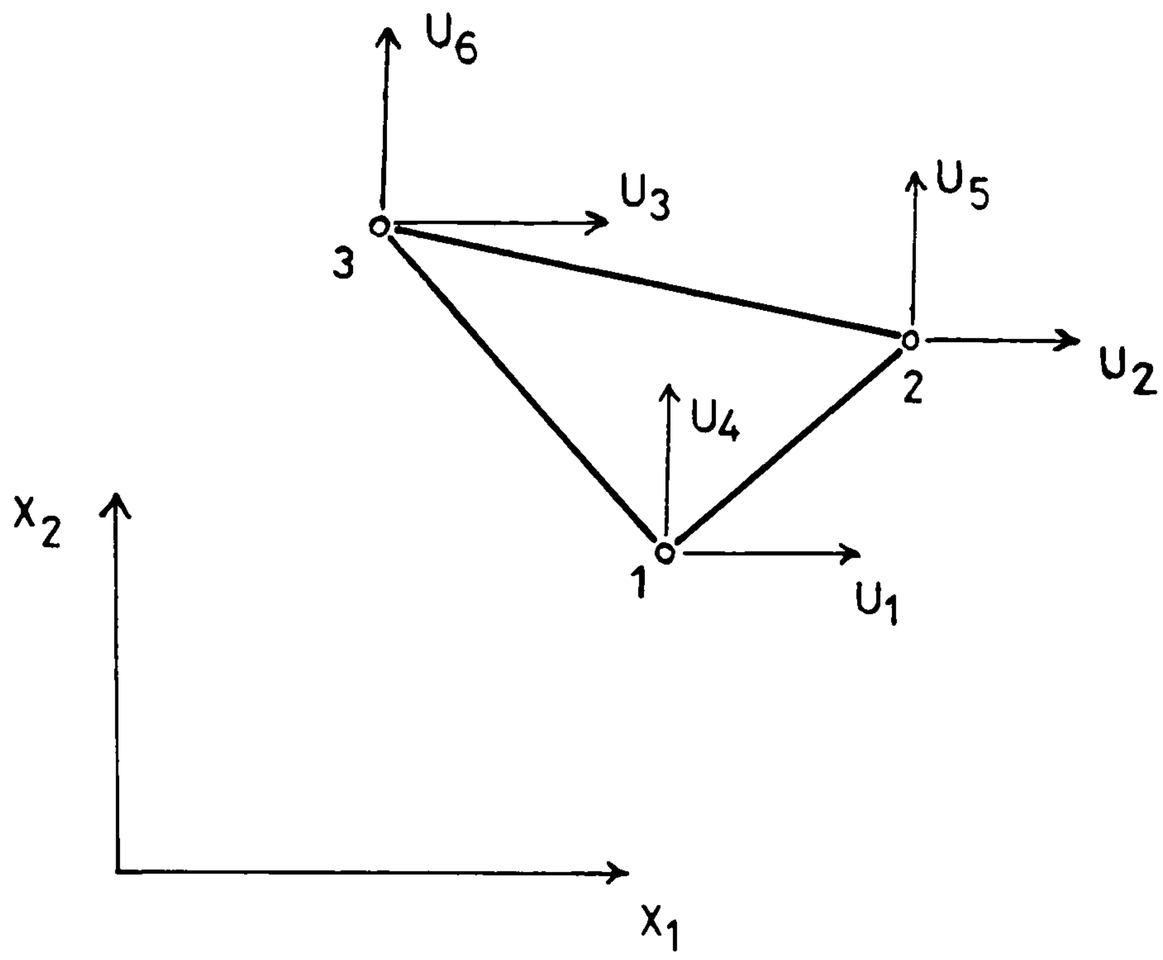

Figure 6.2.2 Triangular cell used to calculate stresses.

When expressions (2.4.4) and (6.2.12) are used the following equation is obtained

$$\underline{\sigma} = \underline{D} \quad \underline{\mu}' \underline{U} \tag{6.2.13}$$

where

$$\underline{\sigma} = \begin{pmatrix} \sigma_{11} \\ \sigma_{12} \\ \sigma_{22} \end{pmatrix} ,$$

$$\underline{D} = \begin{bmatrix} \lambda+2G & 0 & \lambda \\ 0 & 2G & 0 \\ \lambda & 0 & \lambda+2G \end{bmatrix} , \tag{6.2.14}$$

$$\underline{\mu}' = \begin{bmatrix} \mu_{1,1} & \mu_{2,1} & \mu_{3,1} & 0 & 0 & 0 \\ \mu_{1,2}/2 & \mu_{2,2}/2 & \mu_{3,2}/2 & \mu_{1,1}/2 & \mu_{2,1}/2 & \mu_{3,1}/2 \\ 0 & 0 & 0 & \mu_{1,2} & \mu_{2,2} & \mu_{3,2} \end{bmatrix}$$

and

$$\mu_{i,j} = \frac{\partial \mu_i}{\partial x_j} \quad . \tag{6.2.15}$$

6.3 Examples - Two-Dimensional Elastodynamics

In this section the numerical procedure previously discussed in section 6.2 is illustrated by a series of examples comparing boundary elements with other numerical methods.

In all of the problems examined, the boundary integrations shown in equations (6.2.4) and (6.2.5) were performed using a maximum of twenty Gauss points.

Further on in this section reference will be made to the parameter β given by equation (4.3.4). It is important to realize that in elastodynamics c_d is used to compute such a parameter, i.e.,

$$\beta = \frac{c_d \Delta t}{l_j} \quad . \tag{6.3.1}$$

6.3.1 Half-Plane Under Discontinuous Prescribed Stress Distribution

- Cruse {61-63} used the Laplace transform to solve transient elastodynamic problems. In this approach the boundary element method is used to find solutions in the transformed domain. The problem is solved for various distinct values of the Laplace parameter and then a numerical algorithm of inversion due to Papoulis {64} is employed to find time domain solutions.

In his investigation, Cruse studied the problem of a half-plane (see figure 6.3.1) initially at rest, with uniform compressive tractions p_i applied as a step function

in time, as given by

$$p_i(x_1,0,t) = -P_o(x_1,0)\delta_{i2}H(t-0) \tag{6.3.2}$$

where

$$P_o = \begin{cases} p_o H\left[x_1-(-b)\right]\left[1-H(x_1-b)\right] & \text{whenever } x_2 = 0 \\ 0 & \text{whenever } x_2 \neq 0 \end{cases} . \tag{6.3.3}$$

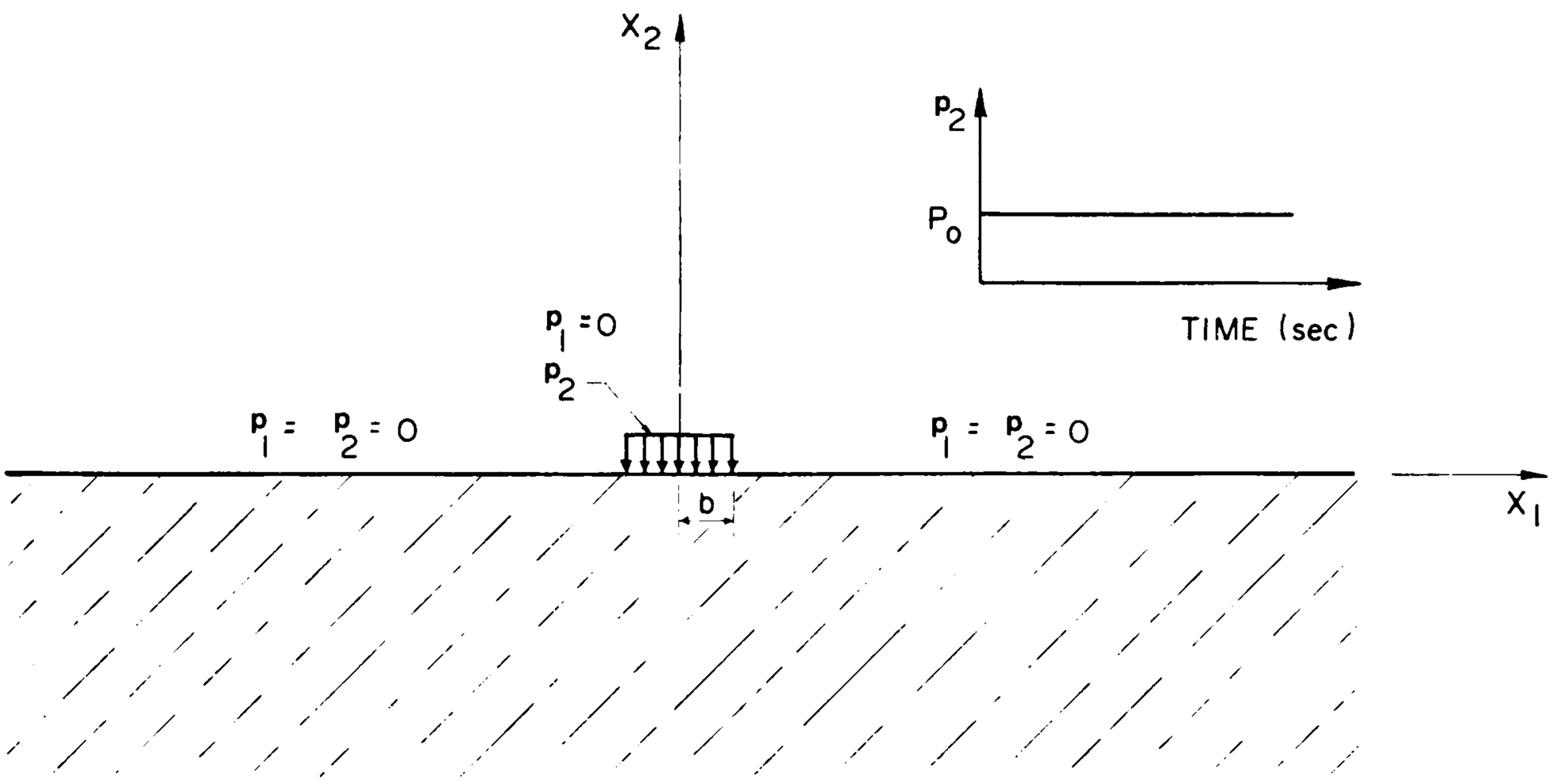

Figure 6.3.1 Half-plane under discontinuous boundary stress distribution.

The first example was taken to compare with Cruse's results, and the following numerical values were adopted for the constants of the problem

$$\lambda = G = 10^6 \text{ psi}$$

$$c_d = 3.27\times10^4 \text{ ips}, \quad c_s = 1.86\times10^4 \text{ ips}$$

$$b = 3000 \text{ inches}, \quad p_o = 10^4 \text{ psi} \quad .$$

Cruse compared his results with the ones presented by Craggs {106}, who solved the problem of an uniform compressive stress applied over half the surface of the half-plane, as a step function in time. Craggs results are also presented here, but complete correspondence with none of the boundary element analyses is to be expected, because Craggs' load is different from the one shown in figure 6.3.1 and Rayleigh waves are included in his solution.

Here and in Cruse's work, the surface of the half-plane was discretized into twenty equal boundary elements, each of them having a length of 6000 inches (see figure 6.3.2).

When evaluating stresses it must be recognized that the bigger the cell the less representative the stresses will be. Conversely, very small cells must also be avoided because when the differences between cell node displacements are too small contribution to stresses due to numerical errors can become excessively large. It is also important to notice that boundary element results for internal points close to the Γ boundary are not good, and therefore cell nodes close to Γ should be avoided.

Consequently, in view of the three restrictions just mentioned, the best cell that can be used to calculate stresses at point D(0,-b) is the one illustrated by figure 6.3.2.

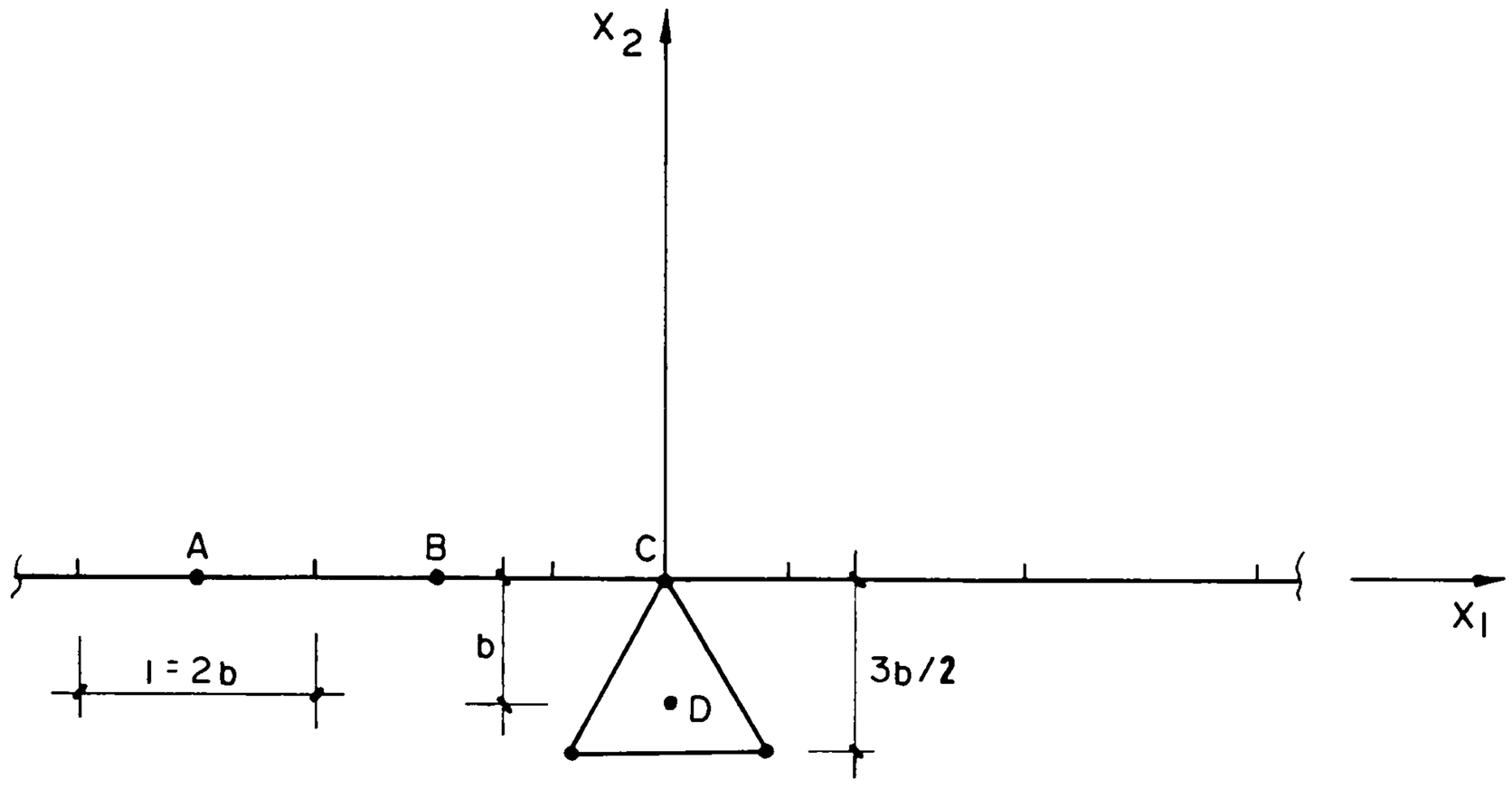

Figure 6.3.2 Boundary discretization and internal cell for the half-plane under discontinuous boundary stress distribution.

Not only the boundary discretization but also the parameter β must be chosen properly. If β is too large, errors due to contradicting the causality property and errors as a result of bad time interpolation will contribute to reduce the degree of accuracy of the results. Four values of β were tried; .13, .25, .50 and 1.; the solutions for the two larger values of β being unacceptable. The numerical results, for β being equal to .13 and .25 were similar, consequently β = .25 was chosen to be the best of the four values considered.

In figure 6.3.3, vertical displacements at boundary points A(-4b,0), B(-2b,0) and C(0,0) are plotted. It should be recognized that P, S and R in figure 6.3.3 stand for the

period of time that a dilatational, an equivoluminal and a Rayleigh wave respectively take to travel from the edge of a disturbance to a point.

The agreement with Cruse's results is good for points B and C, but no comparison could be considered for point A because Cruse terminated his analysis at t = .5s.

The time-stepping results also agree well with Craggs' solution for the point C until t = R, where R is the time the Rayleigh wave takes to propagate from the edge of the disturbance to the point C.

In figure 6.3.4 the vertical displacement at the internal point D(0,-b) is plotted. The applicable range of Craggs' solution was taken by Cruse to be $t<P_2$, where P_2 is the time it takes the primary wave to propagate from the edge of the disturbance to the point D.

Figure 6.3.5 displays the stress σ_{22} at the internal point D. The accuracy is lower than for displacements because stresses are obtained from numerically computed derivatives of displacements. For this cell in particular, there are two other factors that contributes to reduce the stress accuracy; firstly the cell is too large and secondly it has two nodes which are close to the boundary.

The jump condition given by equation (2.2.25) must be satisfied at the wave front. Therefore at t=0 it is possible to write that at the boundary point C

$$\begin{aligned} \dot{u}_1 &= 0 \\ \dot{u}_2 &= \frac{1}{\rho c_d} p_o \quad . \end{aligned} \tag{6.3.4}$$

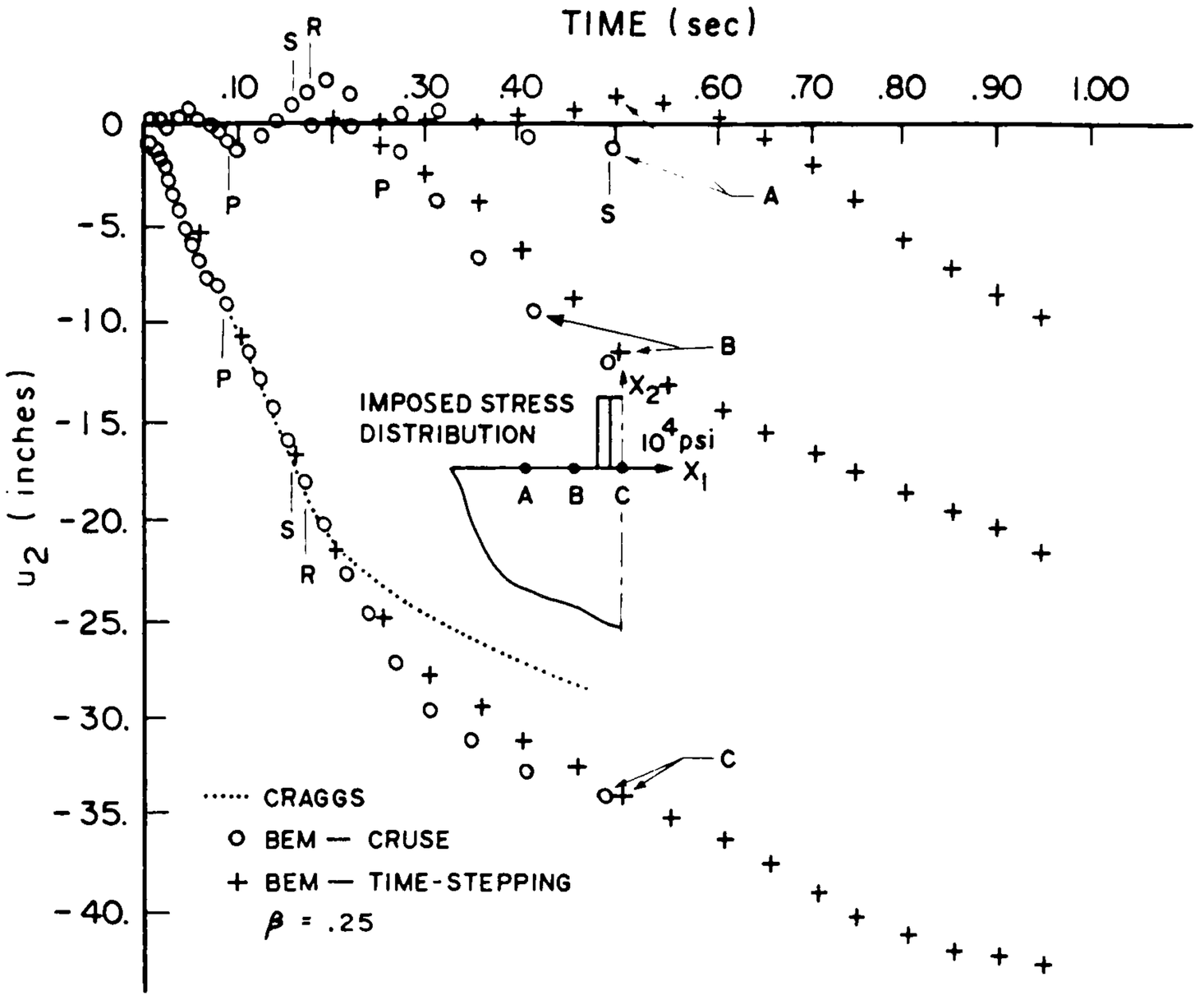

Figure 6.3.3 Half-plane under discontinuous boundary stress distribution. Vertical displacements at the boundary points A(-4b,0), B(-2b,0) and C(0,0).

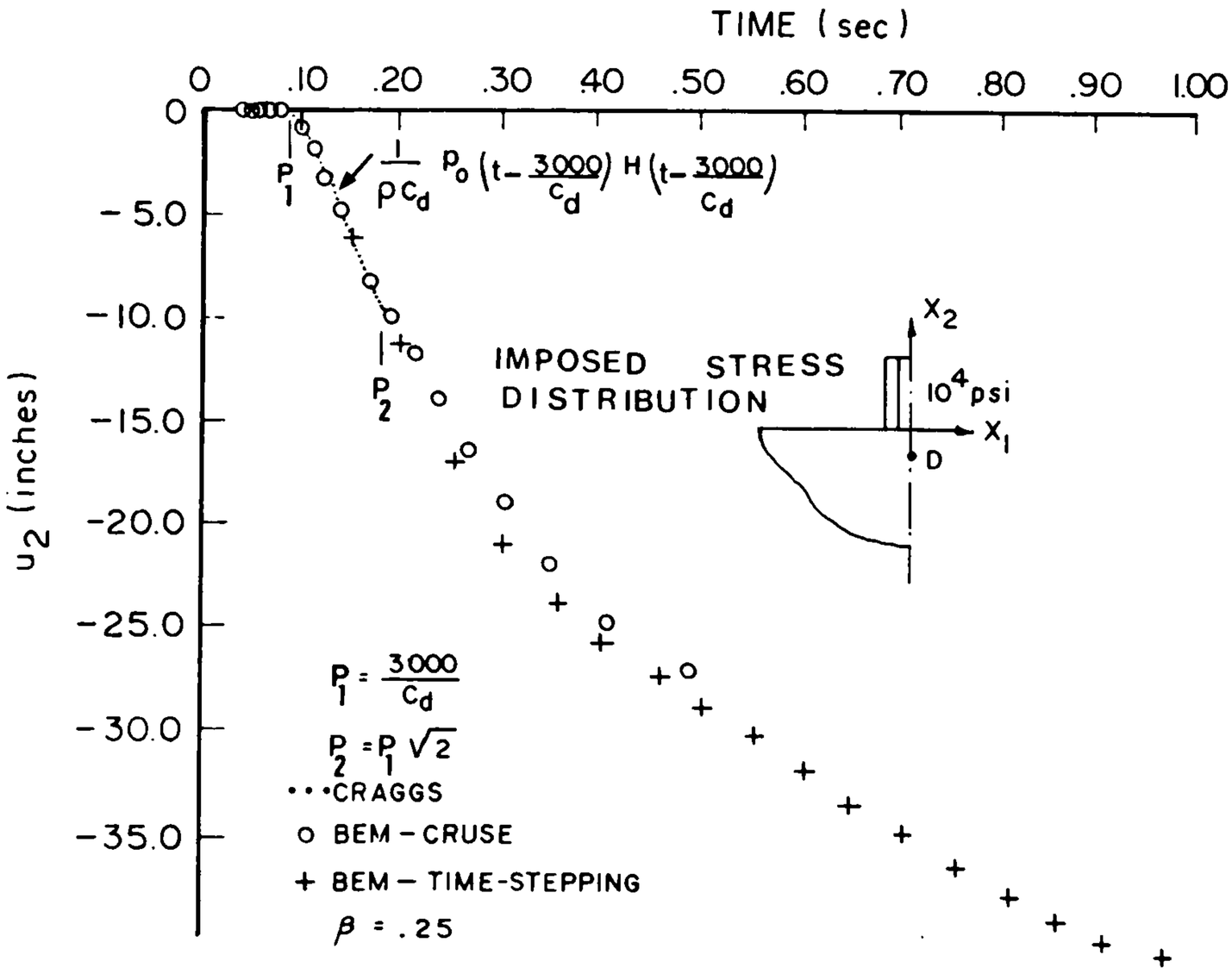

Figure 6.3.4 Half-plane under discontinuous boundary stress distribution. Vertical displacement at the internal point D(0,-b).

Figure 6.3.3 demonstrates that the results of the numerical analyses obey equation (6.3.4).

Craggs' solution also predicts that when the wave front reaches the point D the stress σ_{22} jumps from zero to $-p_o$. This can easily be verified by the inspection of figure 6.3.5.

As the value of the jump in the stress σ_{22} is known, it is not difficult to conclude that when the wave front reaches the point D, $\dot{u}_2$ jumps from zero to the value given by expression (6.3.4). Inspection of figure 6.3.4 demonstrates that this jump is well represented by the numerical solutions under consideration.

Finally for this example it can be concluded that

(a) The displacements obtained using the time-stepping technique were close to the displacements obtained by Cruse.

(b) Despite the large cell used, the time-stepping technique gave results for stresses which were acceptable.

(c) Both the Laplace transform and the time-stepping technique gave results that followed very closely the predicted physical behaviour of the problem analysed.

6.3.2 Half-Plane Under Imposed Boundary Velocity - In this application, the half-plane is initially at rest and part of its surface is forced to move with constant velocity in the vertical direction. The prescribed boundary conditions for this problem are shown in figure 6.3.6 and are given by

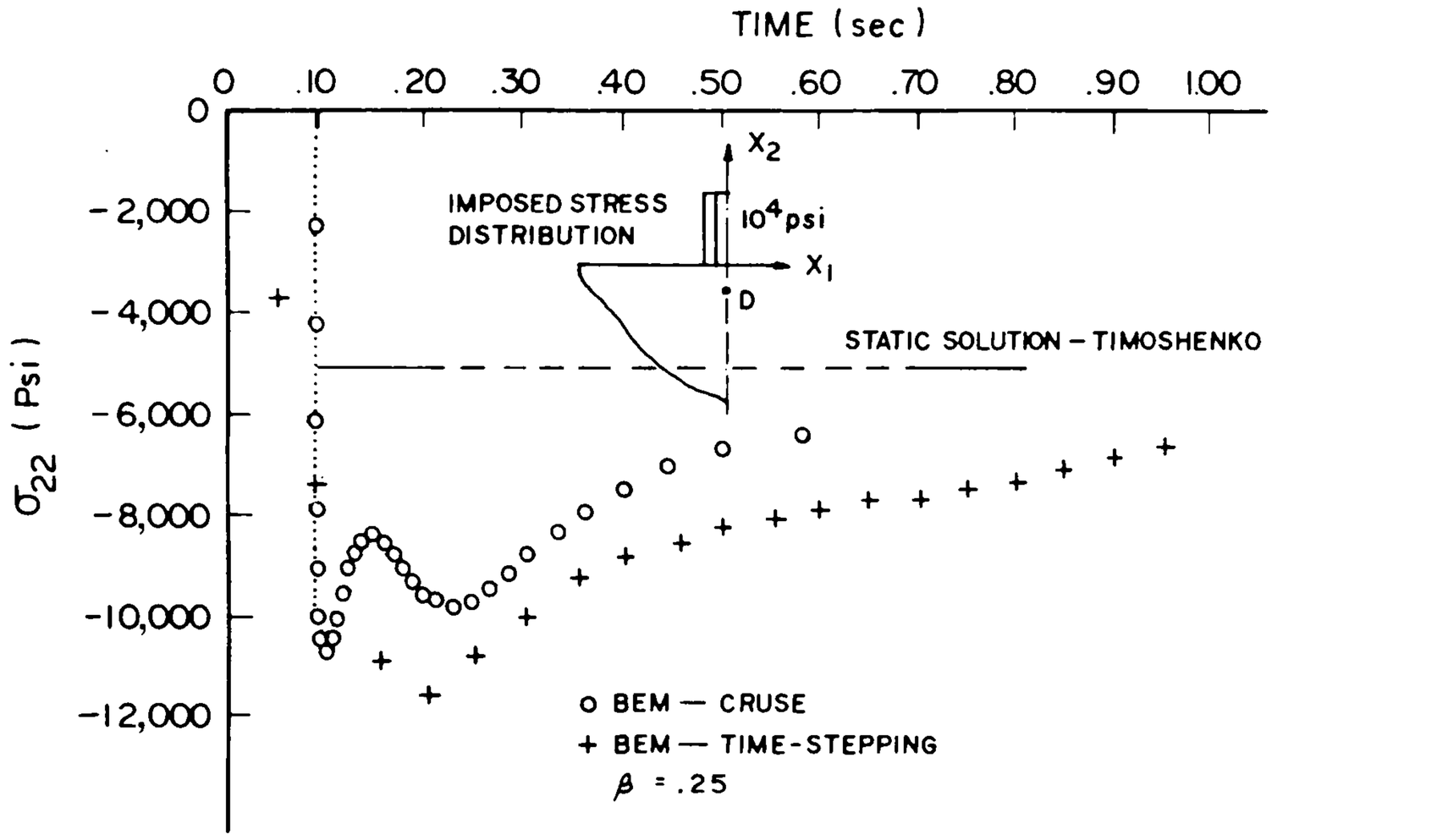

Figure 6.3.5 Half-plane under discontinuous boundary stress distribution. Stress σ_{22} at the internal point D(0,-b).

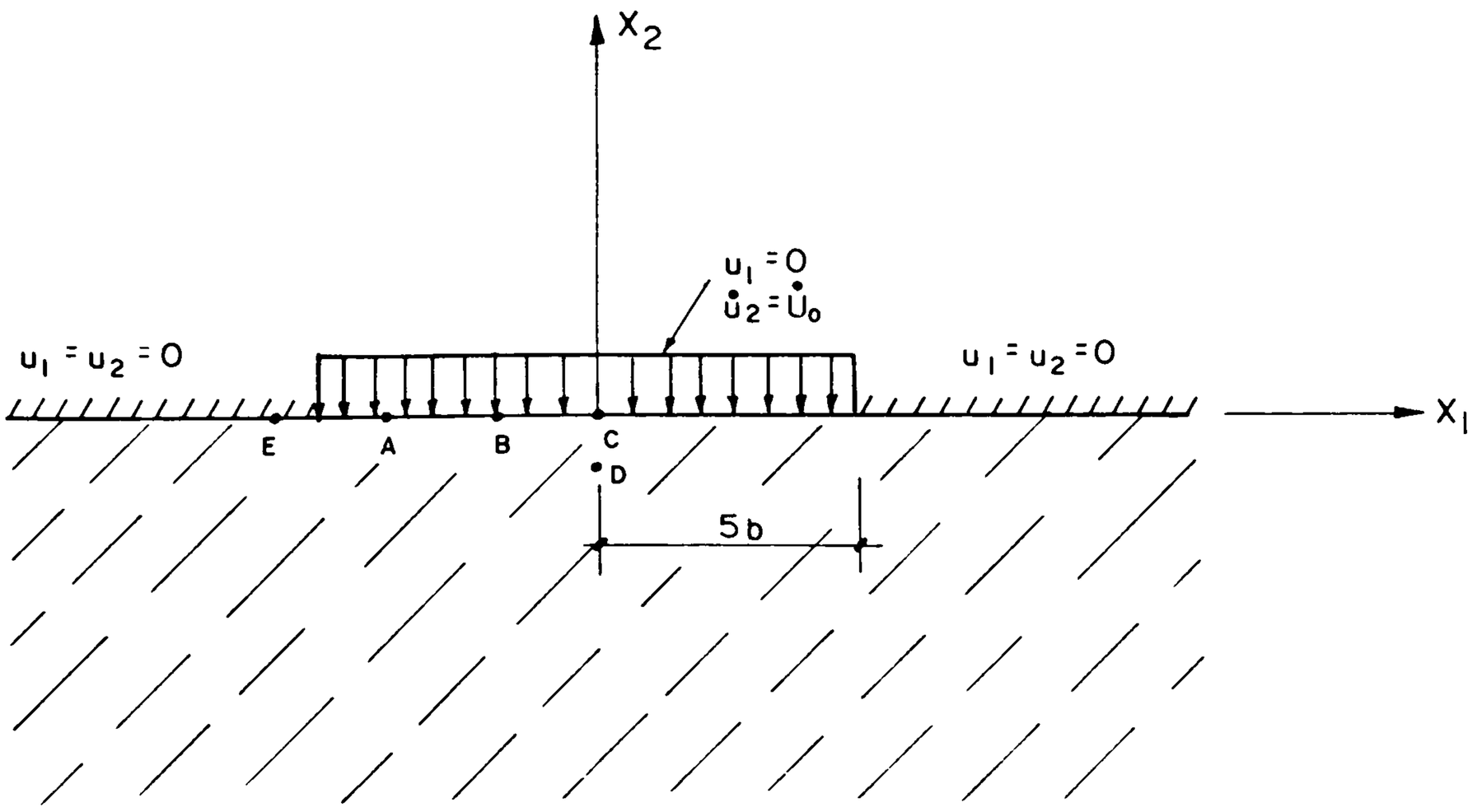

Figure 6.3.6 Boundary conditions for the half-plane under imposed boundary velocity.

$$u_i = -\delta_{i2}\dot{U}_o(x_1,0)\ t\ H(t-0) \qquad (6.3.5)$$

where

$$\dot{U}_o(x_1,0) = \begin{cases} \dot{u}_o H\left[x_1-(-5b)\right]\left[1-H(x_1-5b)\right] & \text{whenever } x_2 = 0 \\ 0 & \text{whenever } x_2 \neq 0 \ . \end{cases} \qquad (6.3.6)$$

The traction at a boundary point which has not yet been reached by the wave generated at the points of the surface where the velocity is discontinuous is given by

$$p_i = -\rho c_d \delta_{i2}\dot{U}_o(x_1,0)H(t-0) \ . \qquad (6.3.7)$$

Expression (6.3.7) can be obtained from the uniqueness of Craggs' solution and from the causality property.

The boundary discretization and cell, first used in this analysis are shown in figure 6.3.2. Four values of β; .13, .25, .50 and 1. were again considered and β = .25 was chosen to be the best for this analysis.

The vertical displacement and the stress σ_{22} at the internal point D are plotted in figures 6.3.7 and 6.3.8 respectively. Inspection of these two figures shows that the numerical results obey equation (2.2.25). At $t = b/c_d$ the stress σ_{22} jumps from zero to $-\rho c_d \dot{u}_o$ as predicted by Craggs' solution, and as expected, the agreement with Cruse's solution is better for displacements than for stresses.

In figures 6.3.9, 6.3.10 and 6.3.11 tractions at the boundary points E(-6b,0), A(-4b,0), B(-2b,0) and C(0,0) are plotted. Tractions at points E and A obtained with both boundary element techniques were not as close to each other

as the displacements in the previous analysis. At points C and D both numerical techniques gave the results predicted by expression (6.3.7). The time-stepping scheme results oscillated slightly around the analytical solution. This fact had already been noticed in chapter four when investigating problems governed by the scalar wave equation. Apparently oscillation can occur whenever boundary displacements are prescribed and β is too small.

Another analysis in which β was regarded as being equal to .75 and the size of the elements taken to be equal to 2000 inches was also undertaken.

Displacements and stresses at D were similar to the ones obtained with the first discretization, however tractions varied. A comparison of figures 6.3.9 and 6.3.12 demonstrates that the boundary discretization depicted in figure 6.3.2 is too coarse, resulting in bad numerical results for tractions at the boundary points A and E.

In figures 6.3.13 and 6.3.14 tractions at points B and C are plotted respectively. These figures show that by using $\beta = .75$ the oscillation of the numerical results was practically eliminated.

Finally as far as this problem is concerned it can be concluded that

(a) The displacements obtained using the time-stepping technique agreed with the results obtained by Cruse.

(b) Excessively small values of β should be avoided in problems in which displacements are prescribed over portions of the boundary.

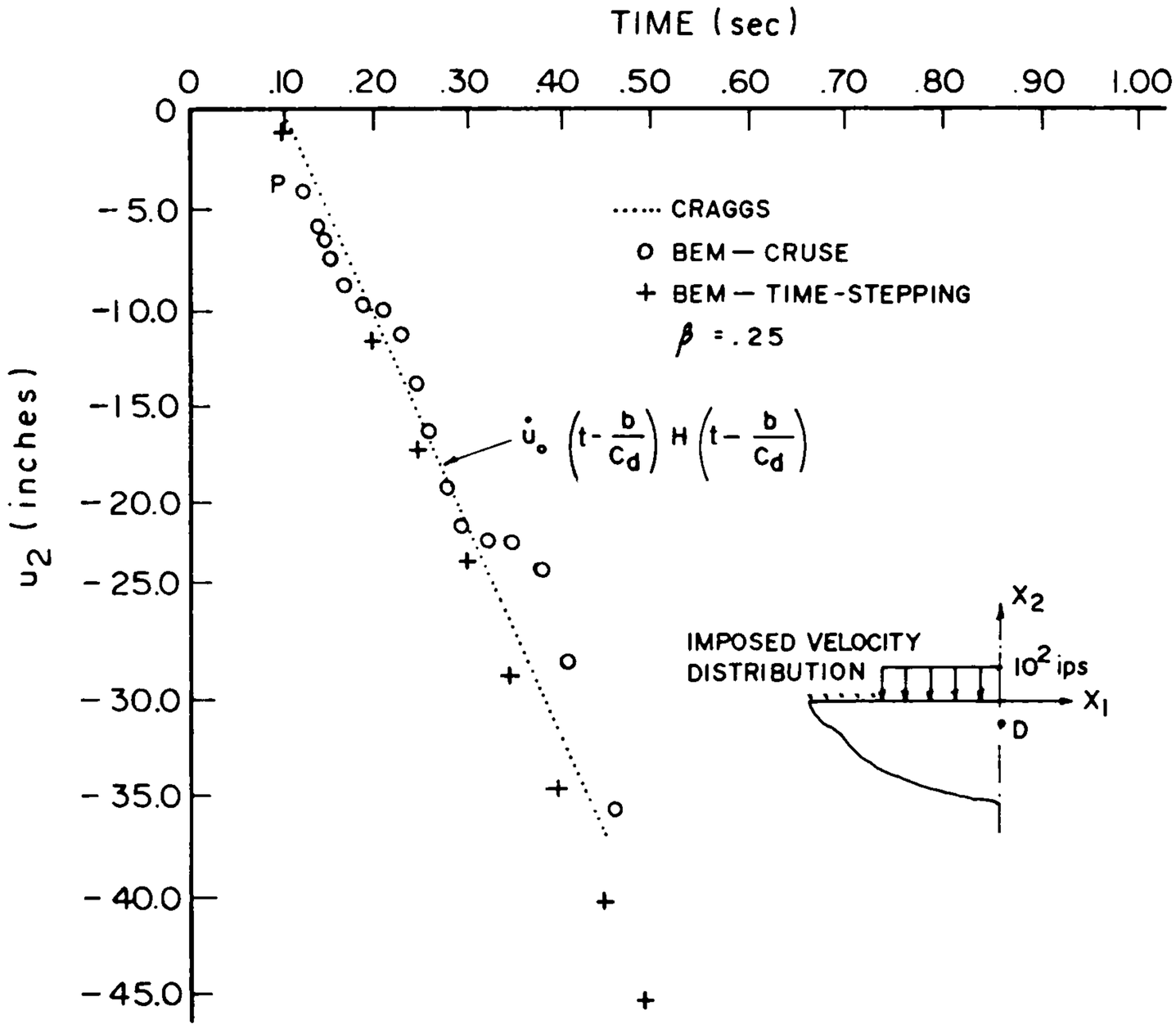

Figure 6.3.7 Half-plane under imposed boundary velocity. Vertical displacement at the internal point D(0,-b).

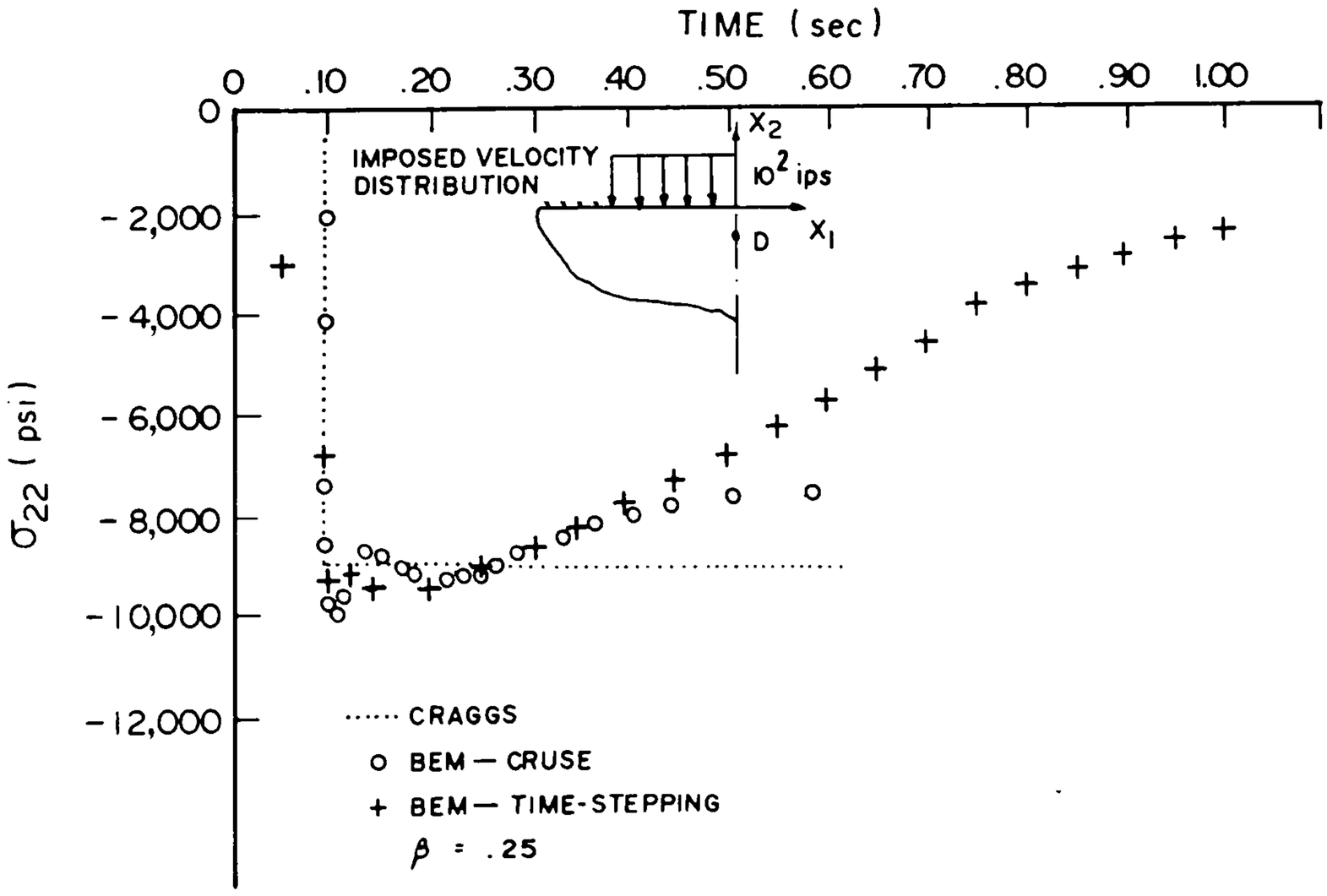

Figure 6.3.8 Half-plane under imposed boundary velocity. Stress σ_{22} at the internal point D(0,-b).

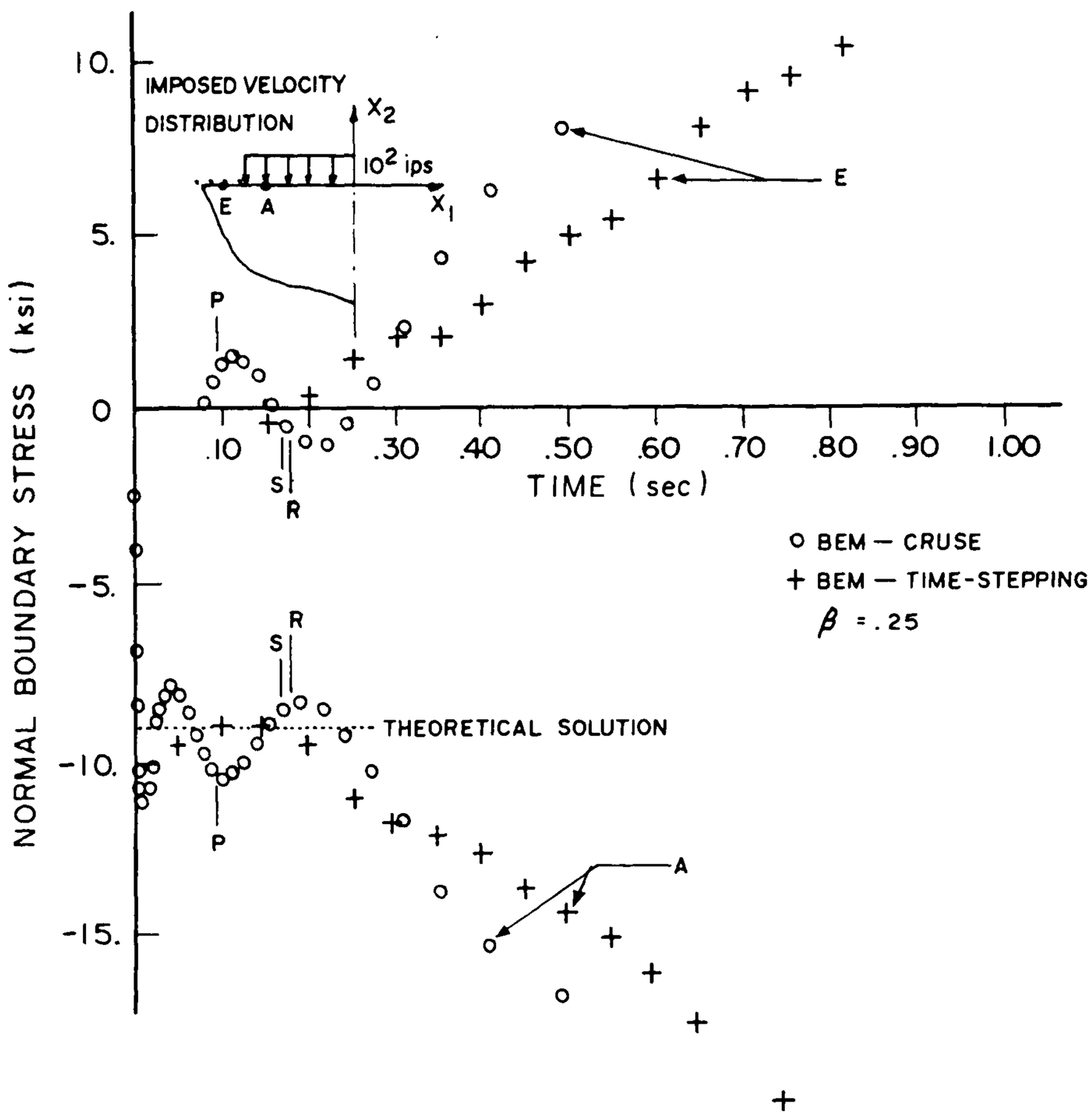

Figure 6.3.9 Half-plane under imposed boundary velocity. Normal boundary stress at the points E(-6b,0) and A(-4b,0).

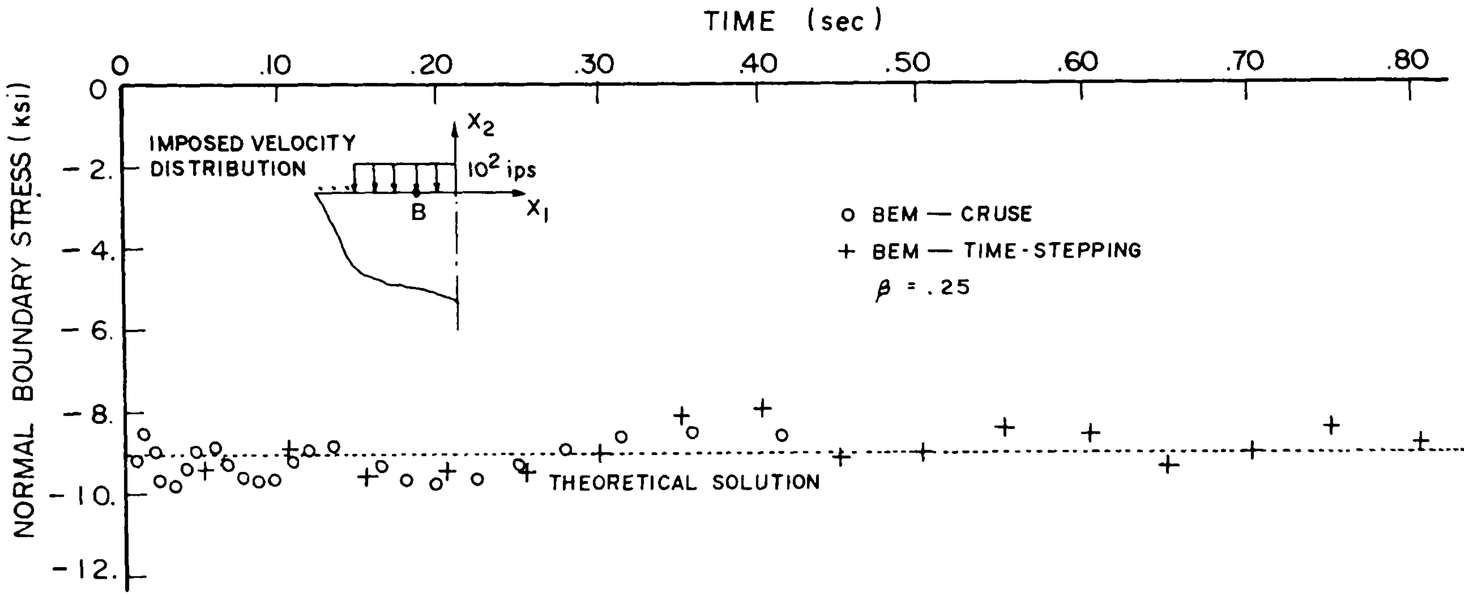

Figure 6.3.10 Half-plane under imposed boundary velocity. Normal boundary stress at the point B(-2b,0).

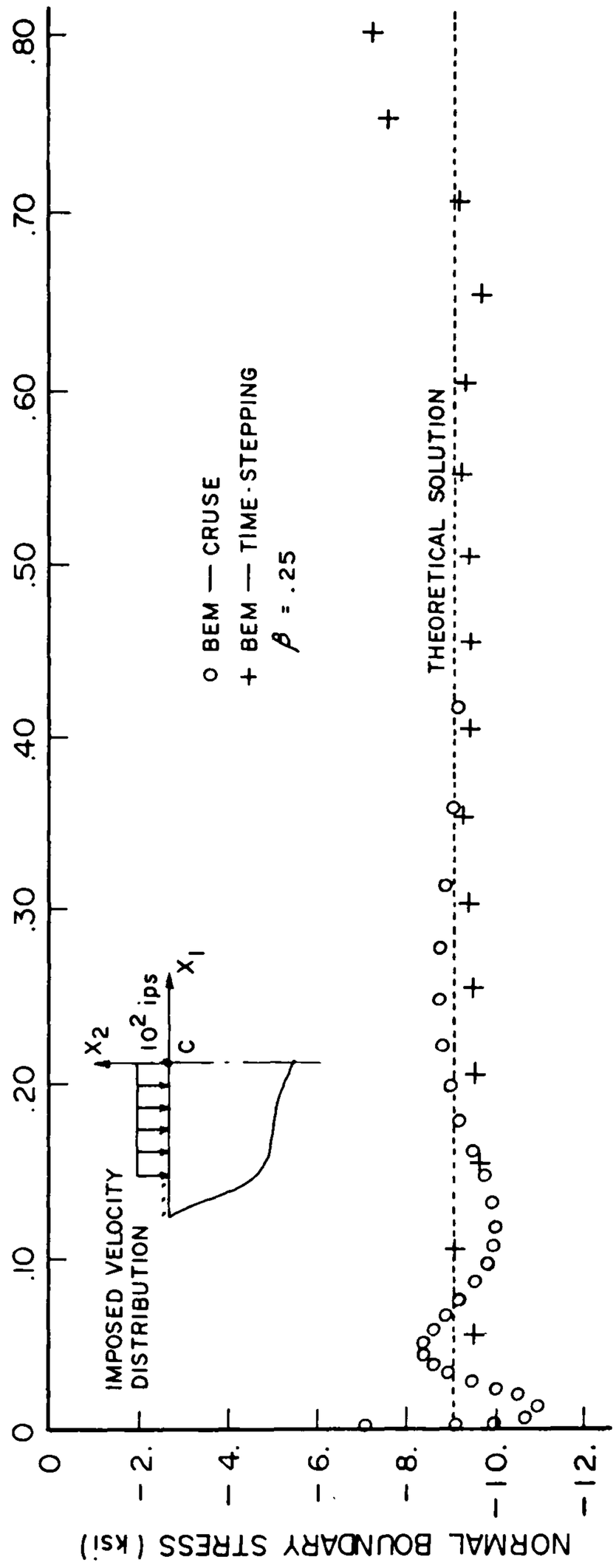

Figure 6.3.11 Half-plane under imposed boundary velocity. Normal boundary stress at the point C(0,0).

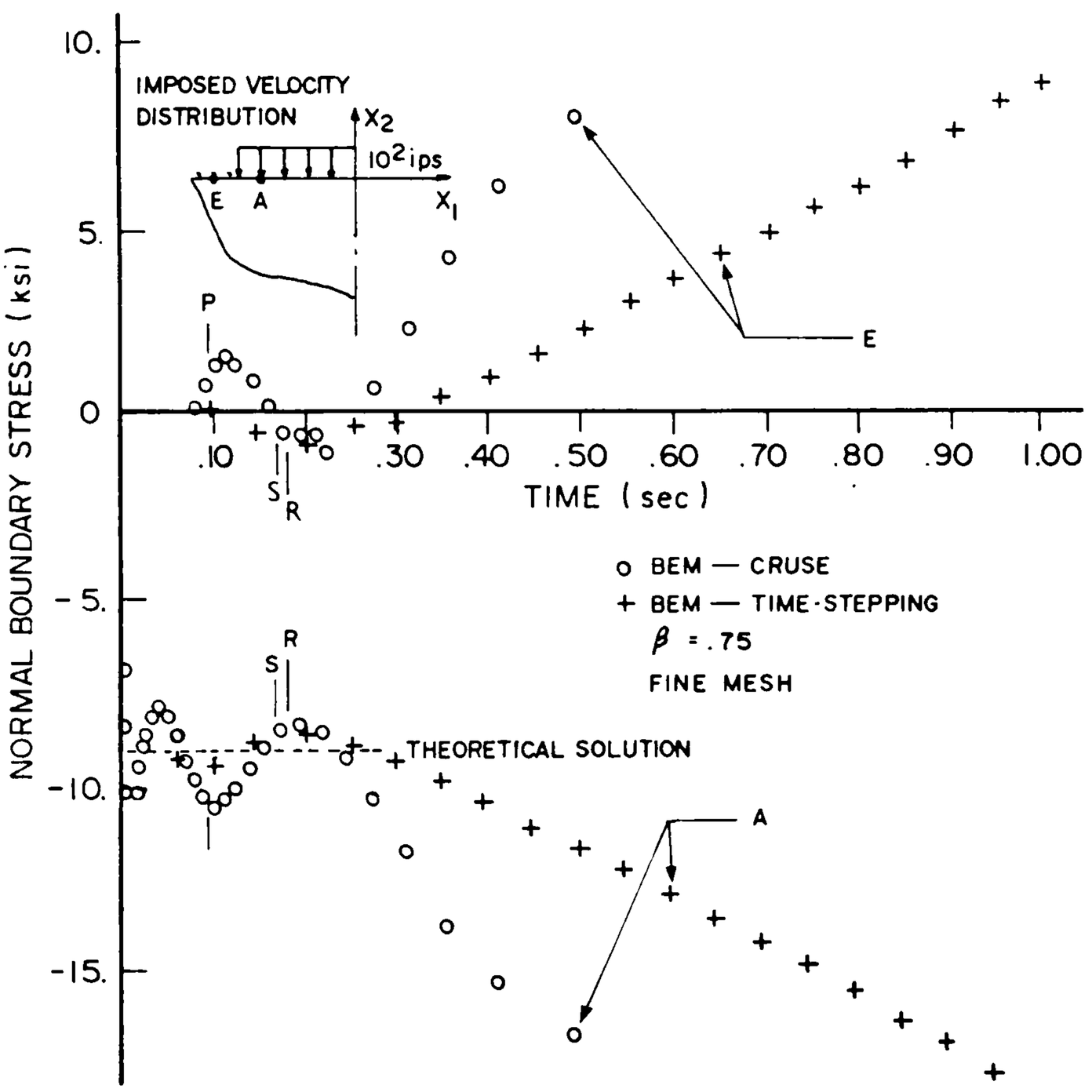

Figure 6.3.12 Half-plane under imposed boundary velocity. Normal boundary stress at the points E(-6b,0) and A(-4b,0).

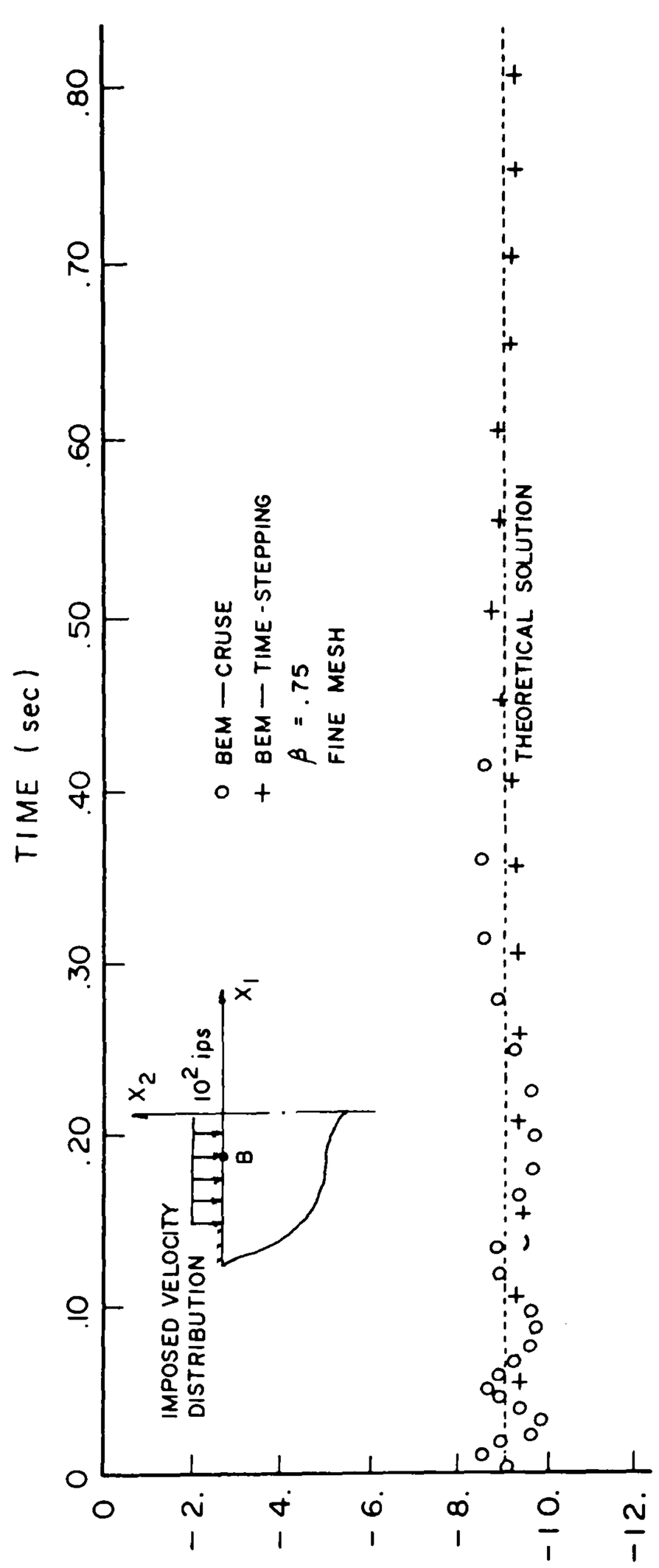

Figure 6.3.13 Half-plane under imposed boundary velocity. Normal boundary stress at the point B(-2b,0).

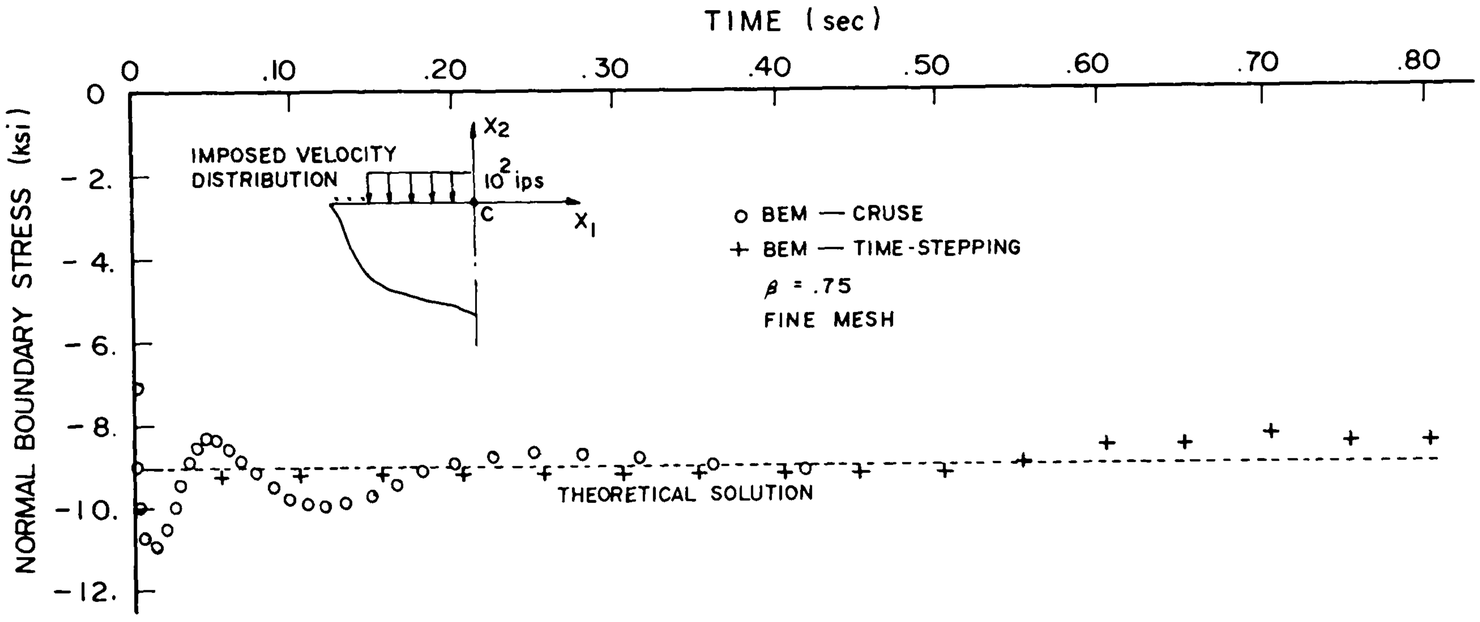

Figure 6.3.14 Half-plane under imposed boundary velocity. Normal boundary stress at the point C(0,0).

(c) Both, the time-stepping and the Laplace transform techniques, yielded results which very closely followed the predicted physical behaviour of the problem analysed.

6.3.3 Half-Plane Under Continuous Prescribed Stress Distribution - In this application the time-stepping technique discussed in this work is compared with the finite-difference model implemented by Tseng et al. {11}. In that report a transmitting boundary was developed and used together with the generalized lumped parameter model presented in references {107-109}.

The problem to be analysed is depicted in figure 6.3.15. The half-plane is initially at rest and its surface is disturbed by a vertical traction which is continuous in both time and space.

The following numerical values were adopted for the constants of the problem

$$E = 200 \text{ ksi}, \quad \nu = .15$$

$$c_d = 3.288\times10^4 \text{ ips}, \quad c_s = 2.112\times10^4 \text{ ips} \quad .$$

The criterion given by Tseng {11} to choose the finite difference mesh requires that

$$t_r > 2\,\frac{\Delta x}{c_d} \tag{6.3.8}$$

where t_r is rise or decay time of the applied pressure and Δx gives the mesh refinement. When t_r = 20 msec, $\Delta x \leq 27.4$ ft is obtained. Tseng chose Δx = 10 ft and the discretization as depicted in figure 6.3.16, where the position selected for the cylindrical wave transmitting boundaries can also be seen.

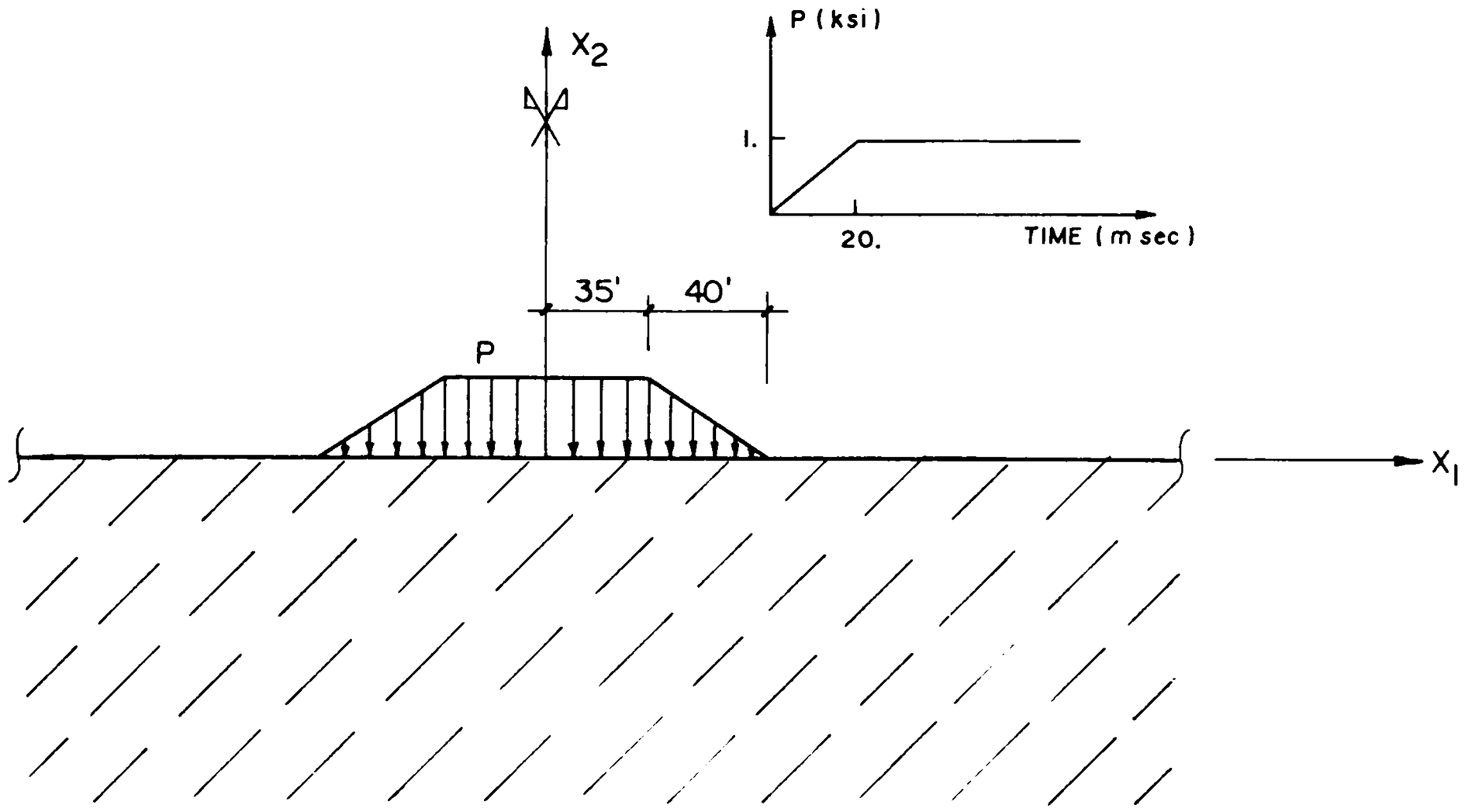

Figure 6.3.15 Load for the half-plane under continuous prescribed stress distribution.

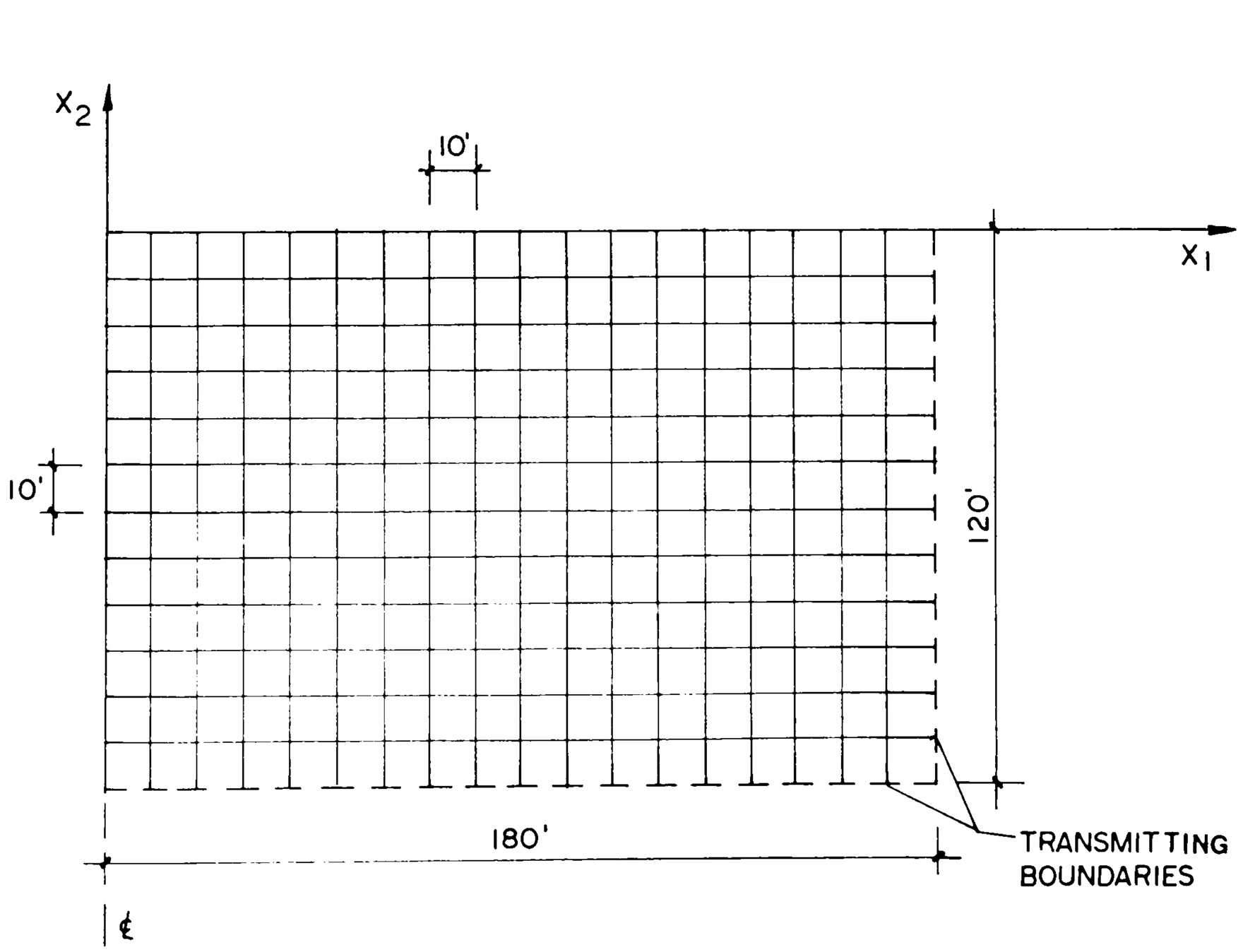

Figure 6.3.16 Finite-difference mesh for the half-plane under continuous prescribed stress distribution.

The boundary element discretization and cells used in the analysis are shown in figure 6.3.17.

According to reference {11} the time increment Δt, used in this finite-difference analysis, must obey equation (6.3.9) and Δt = 1. msec was adopted.

$$\Delta t \leq .433 \frac{\Delta x}{c_d} \qquad (6.3.9)$$

For the boundary element analysis, β was taken to be equal to .5, which gives

$$\Delta t = 3.65 \text{ msec} \quad .$$

The time history of the vertical displacements plotted in figures 6.3.18, 6.3.19 and 6.3.20 shows an acceptable agreement for the time interval considered.

In his research Tseng carried out another analysis using a pair of transmitting boundaries which enclosed a smaller rectangular region whose side lengths were equal to 90 ft and 150 ft. The two finite-difference analyses showed that the larger the region enclosed by the transmitting boundaries, the closer finite difference and boundary elements results were. Therefore it is quite justified to suppose that the major proportion of the difference between the displacements obtained with the two numerical methods under consideration is caused by errors generated at the transmitting boundaries.

Tseng also presented the time history of the vertical displacements for the point G(150',10') obtained with the 90'×150' rectangular region. As G is located exactly on the transmitting boundary it can be expected that

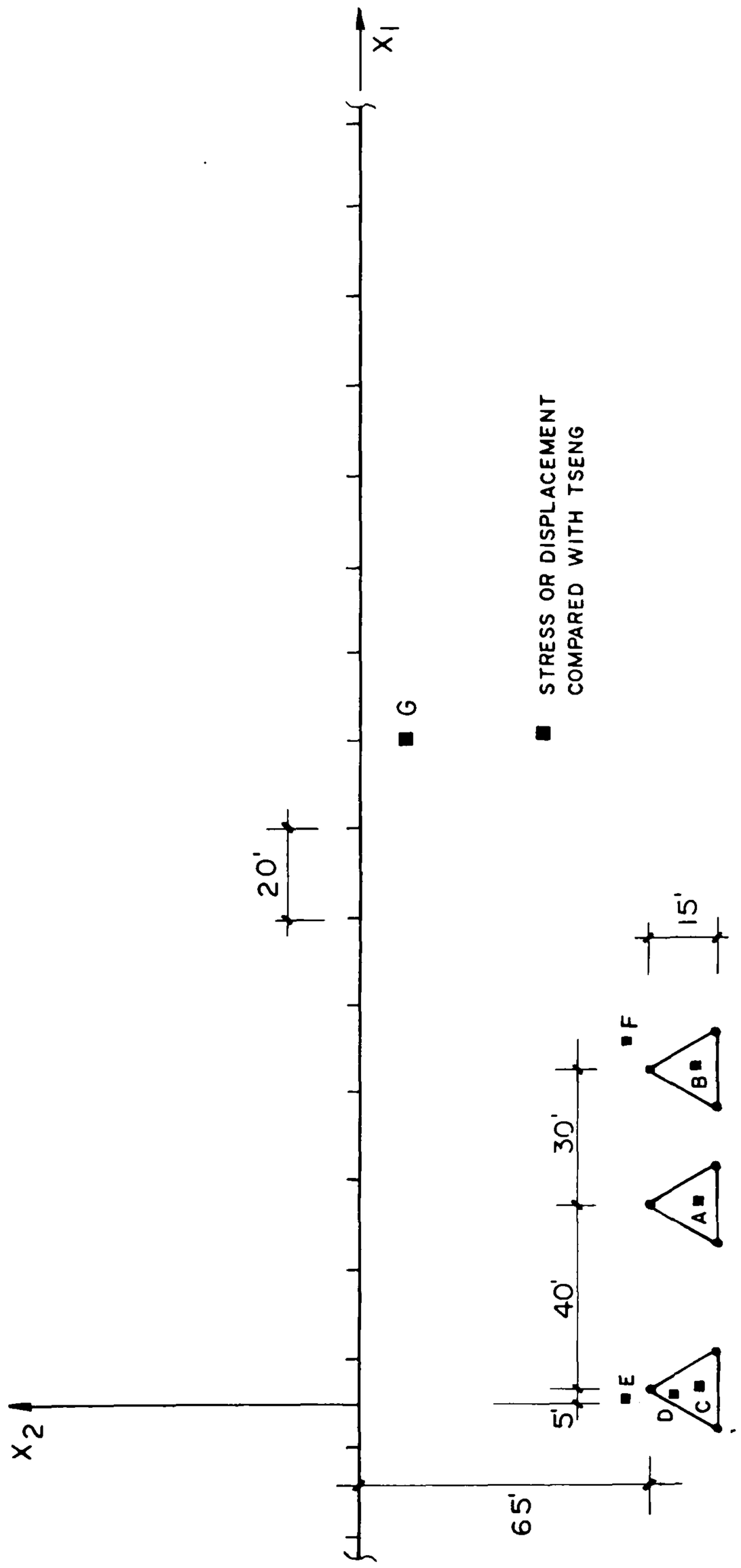

Figure 6.3.17 Boundary element discretization for the half-plane under continuous prescribed stress distribution.

finite-difference displacements at this point will have a low accuracy. The point G is also a critical one in the boundary element analysis because it is too close to the boundary of the half-plane. Results obtained with the two methods are shown in figure 6.3.21. As it was expected the agreement is not as close as recorded previously.

Figures 6.3.22 to 6.3.24 describe the time history of stresses at points A(45',75'), B(75',75') and C(5',75').

When the load is applied as a step function in time, finite-differences can not be used because of the restrictions imposed by equation (6.3.8). A possible way of overcoming this difficulty is by replacing the jump by a slope. In order to check the errors introduced by such a procedure the problem displayed in figure 6.3.15 was re-investigated using boundary elements, but this time the load was abruptly applied at t = 0 (see figure 6.3.25). The time history of stress plotted in figure 6.2.4 shows that a complete agreement occurs with the previous analysis during late times, but during early times the results are different.

Finally, for this example it can be concluded that

(a) The solutions using both the finite difference and boundary element methods are in good agreement.

(b) The time increment required by boundary elements was bigger than that necessary for finite differences.

(c) When the time variation of the load includes jumps, boundary elements are more suitable than finite differences.

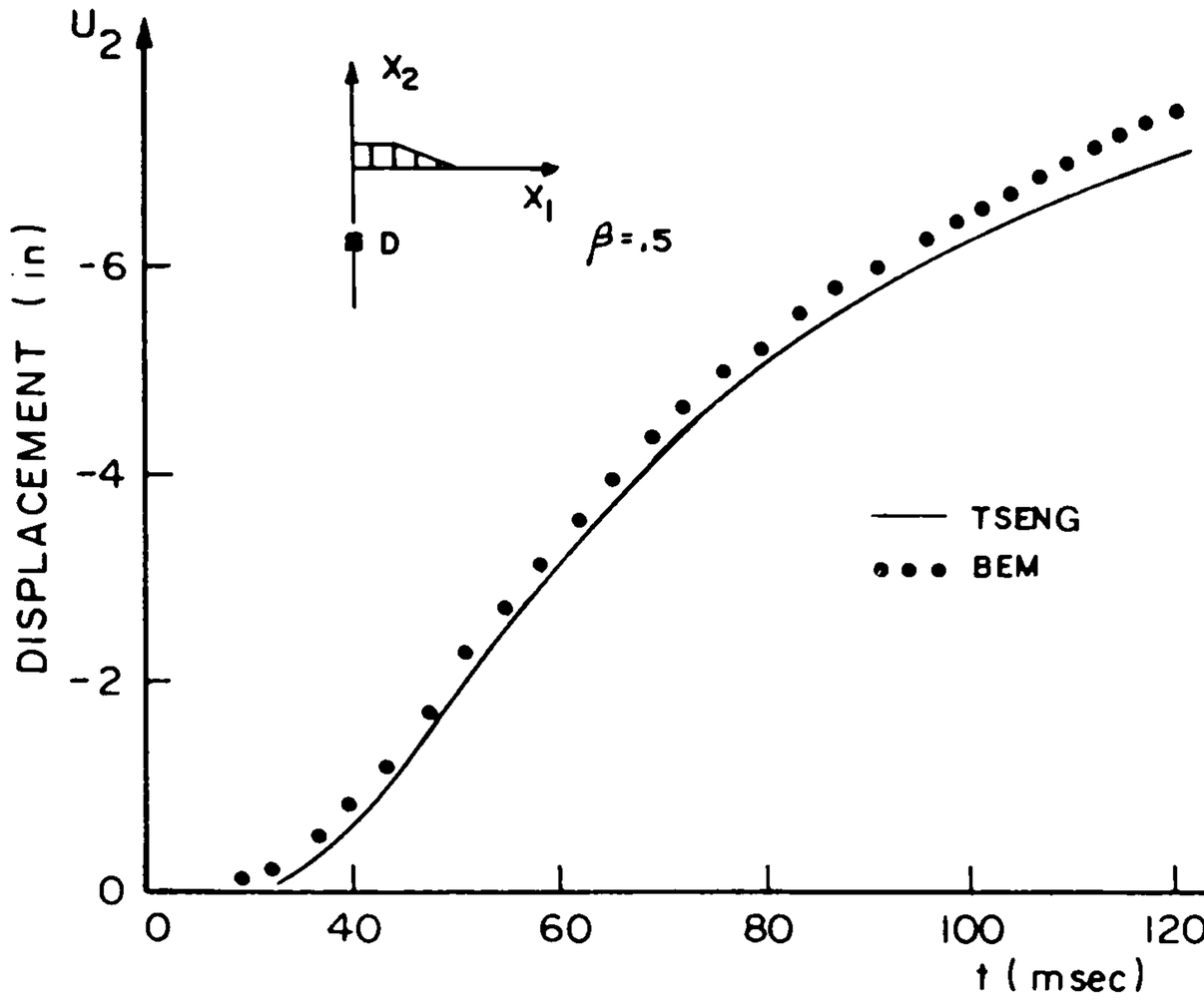

Figure 6.3.18 Half-plane under continuous prescribed stress distribution. Displacement u_2 at the internal point D(0',70').

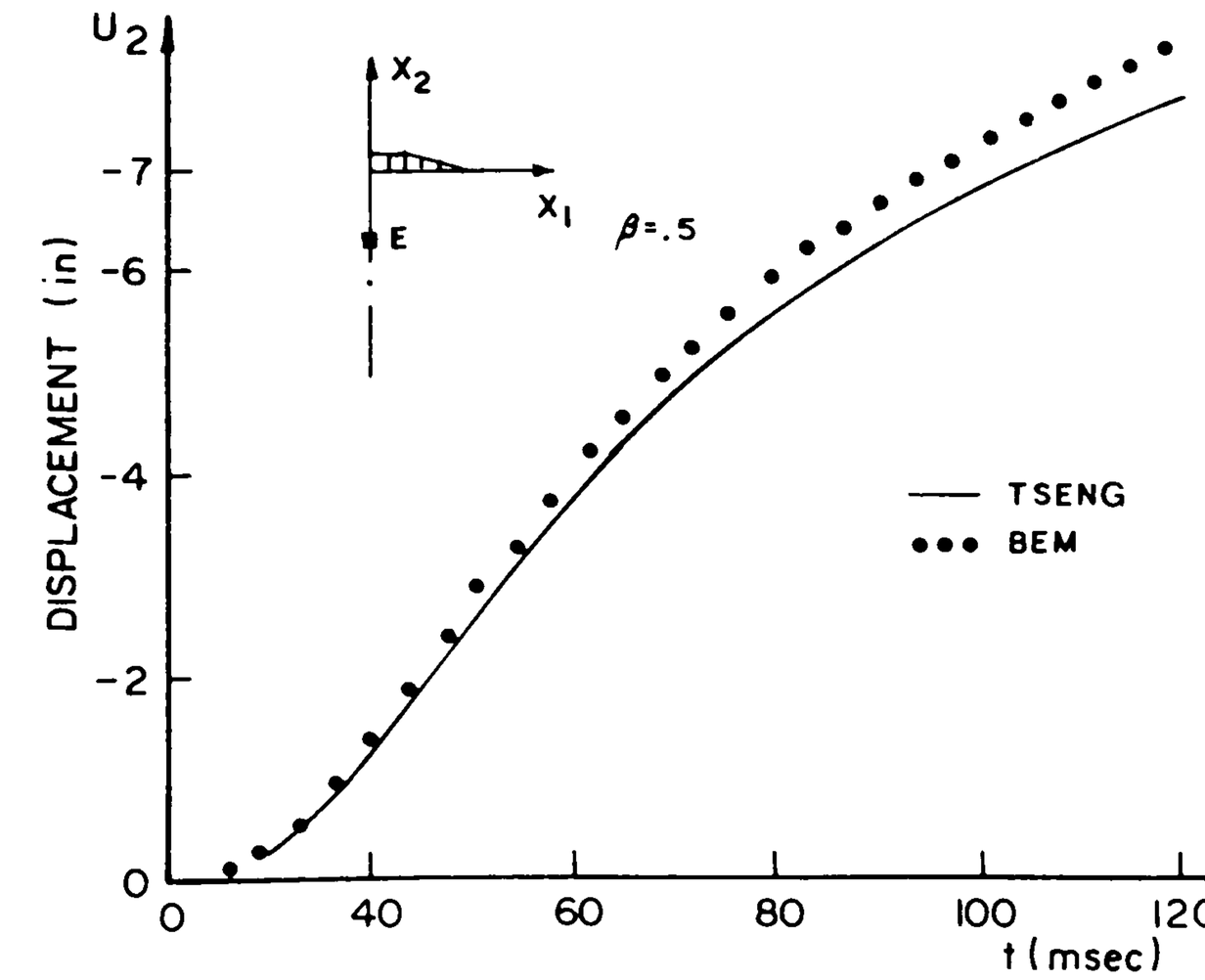

Figure 6.3.19 Half-plane under continuous prescribed stress distribution. Displacement u_2 at the internal point E(0',60').

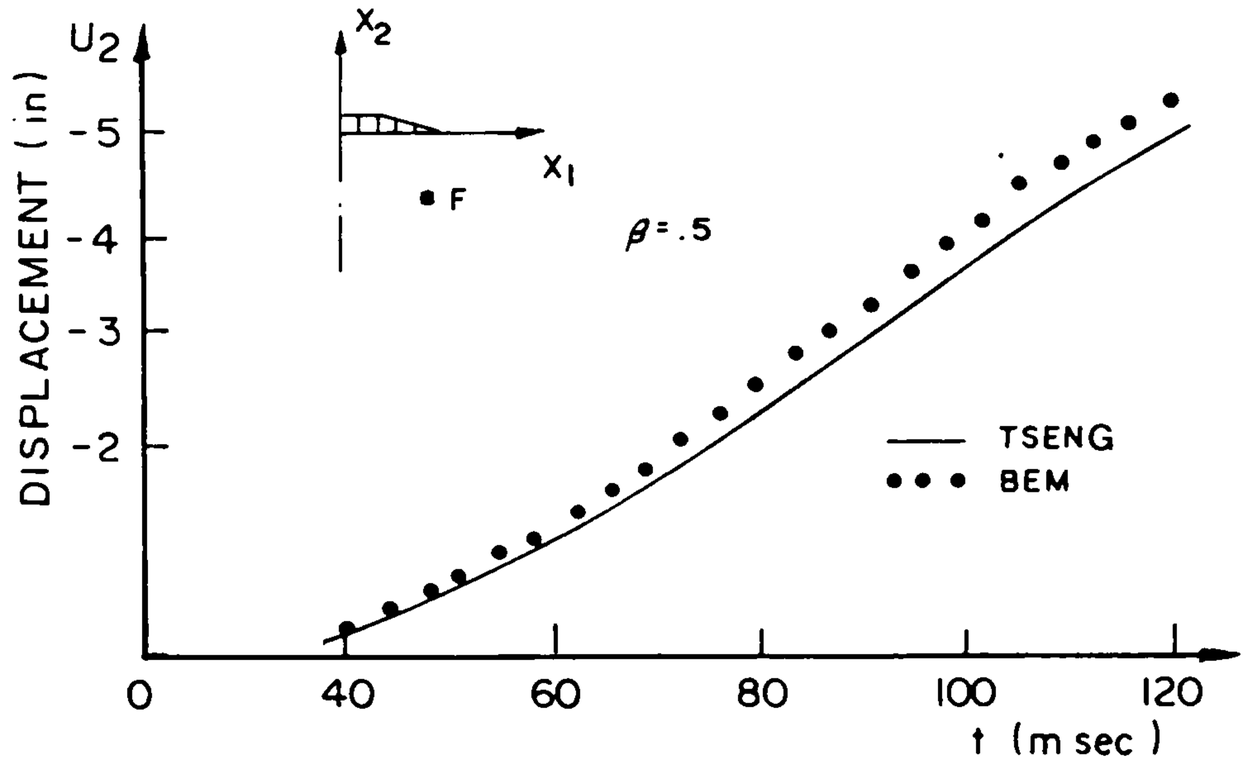

Figure 6.3.20 Half-plane under continuous prescribed stress distribution. Displacement u_2 at the internal point F(80',60').

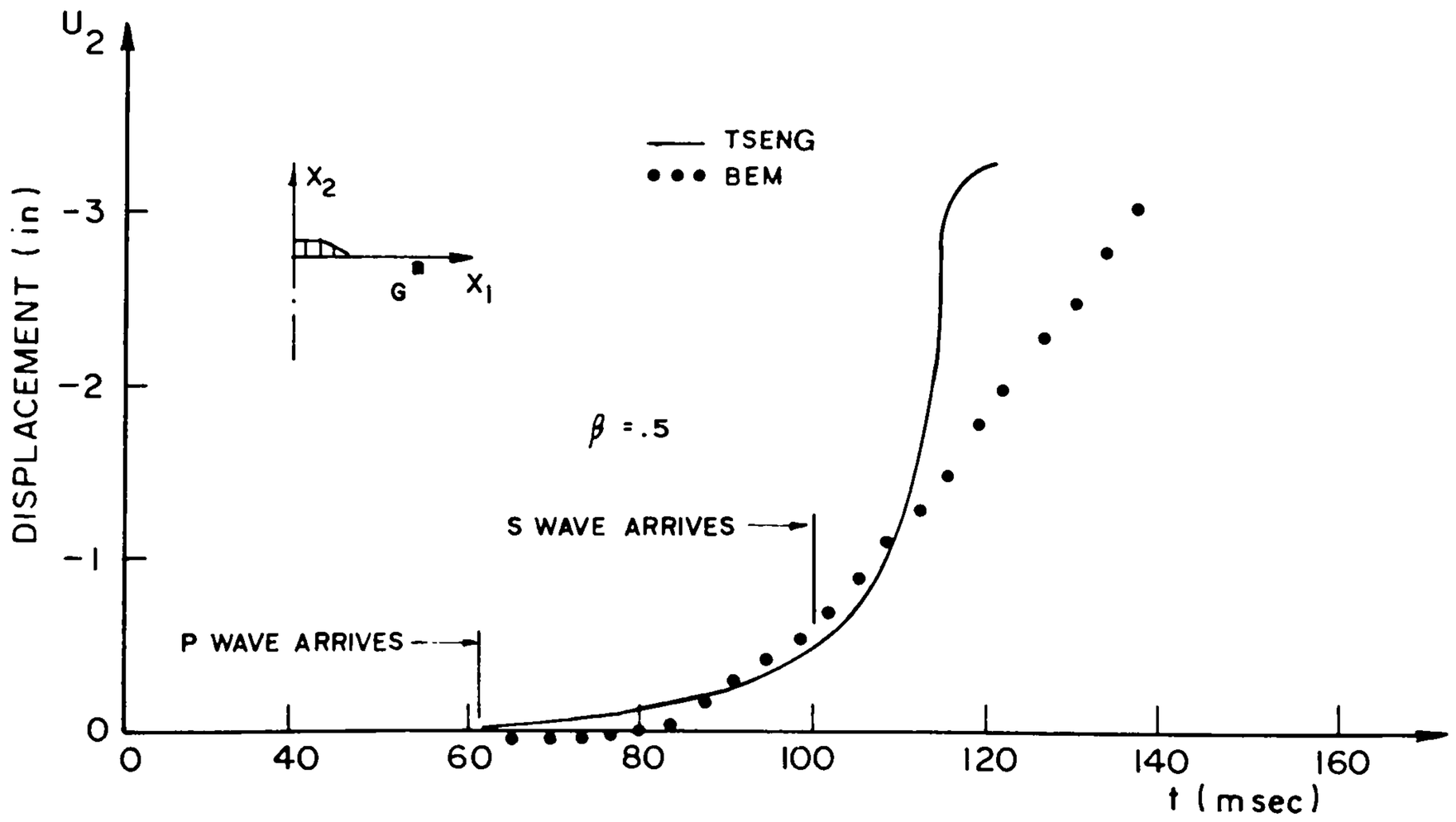

Figure 6.3.21 Half-plane under continuous prescribed stress distribution. Displacement u_2 at the internal point G(150',10').

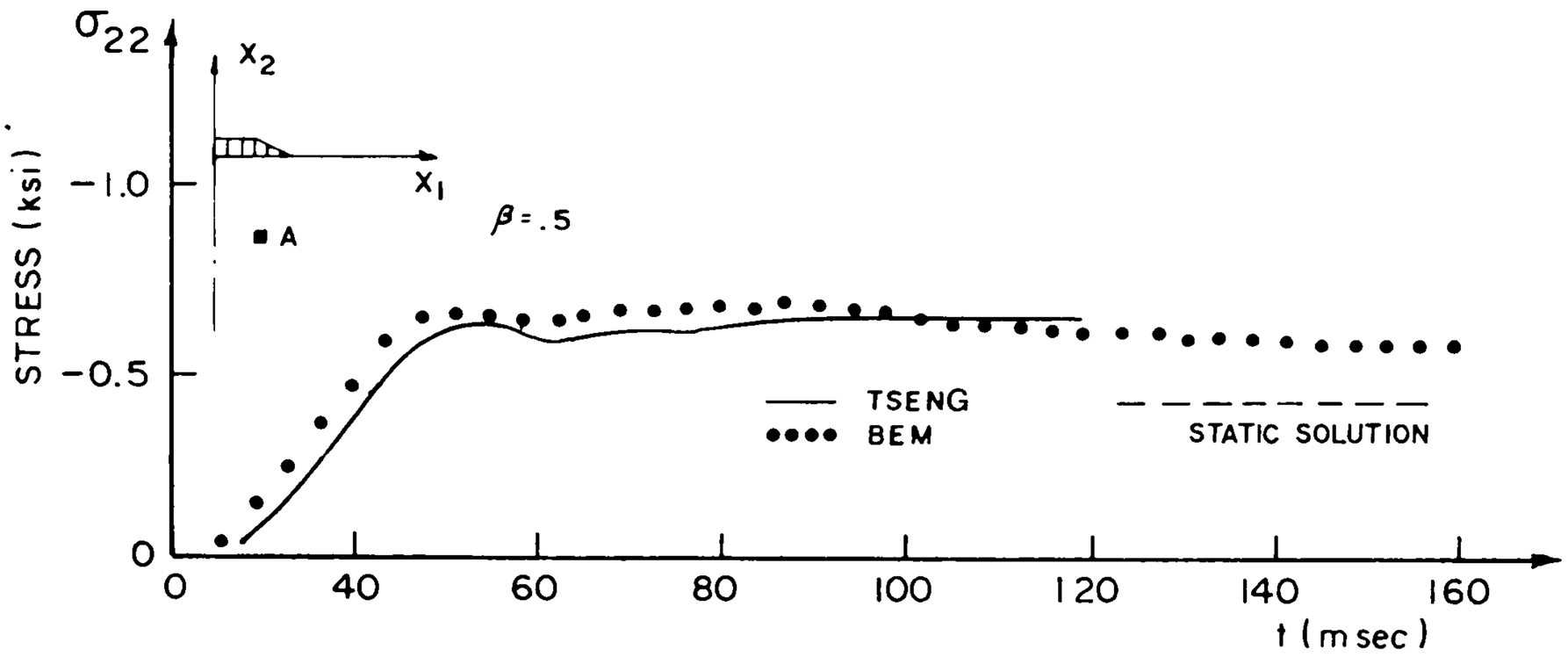

Figure 6.3.22 Half-plane under continuous prescribed stress distribution. Stress σ_{22} at the internal point A(45',75').

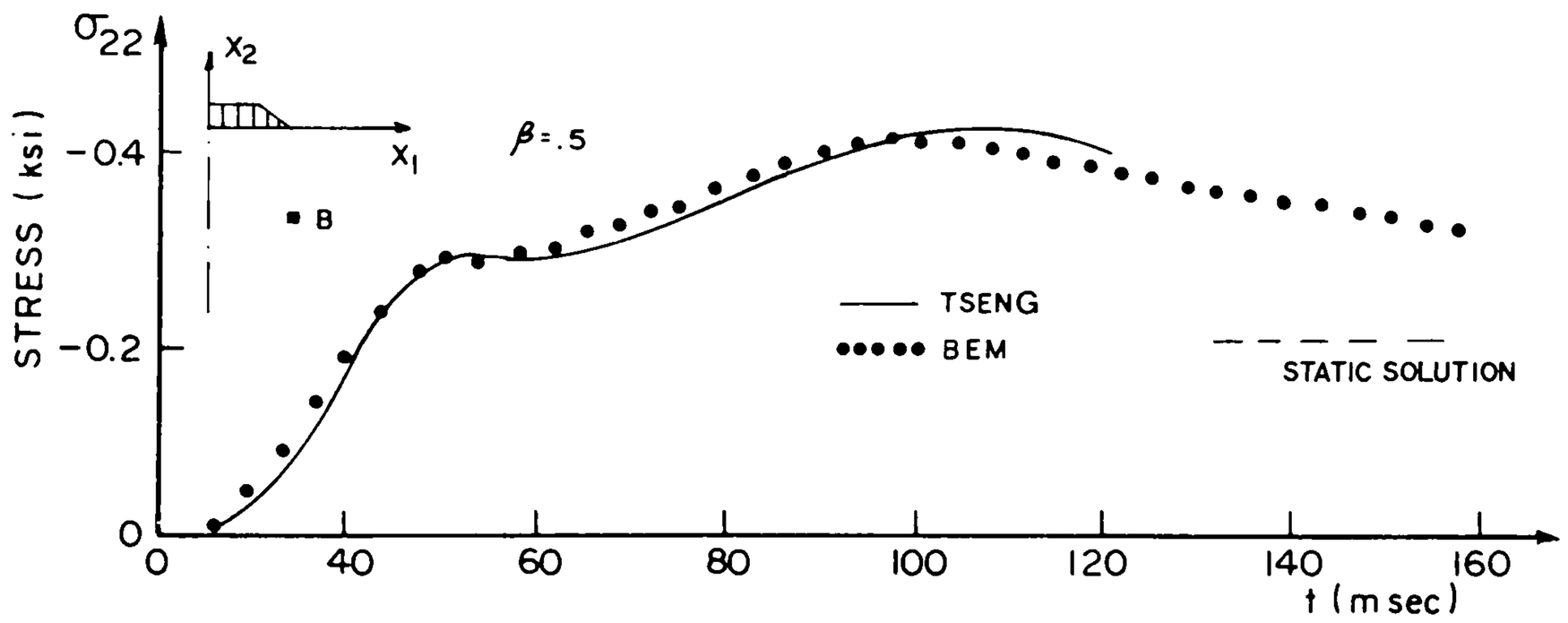

Figure 6.3.23 Half-plane under continuous prescribed stress distribution. Stress σ_{22} at the internal point B(75',75').

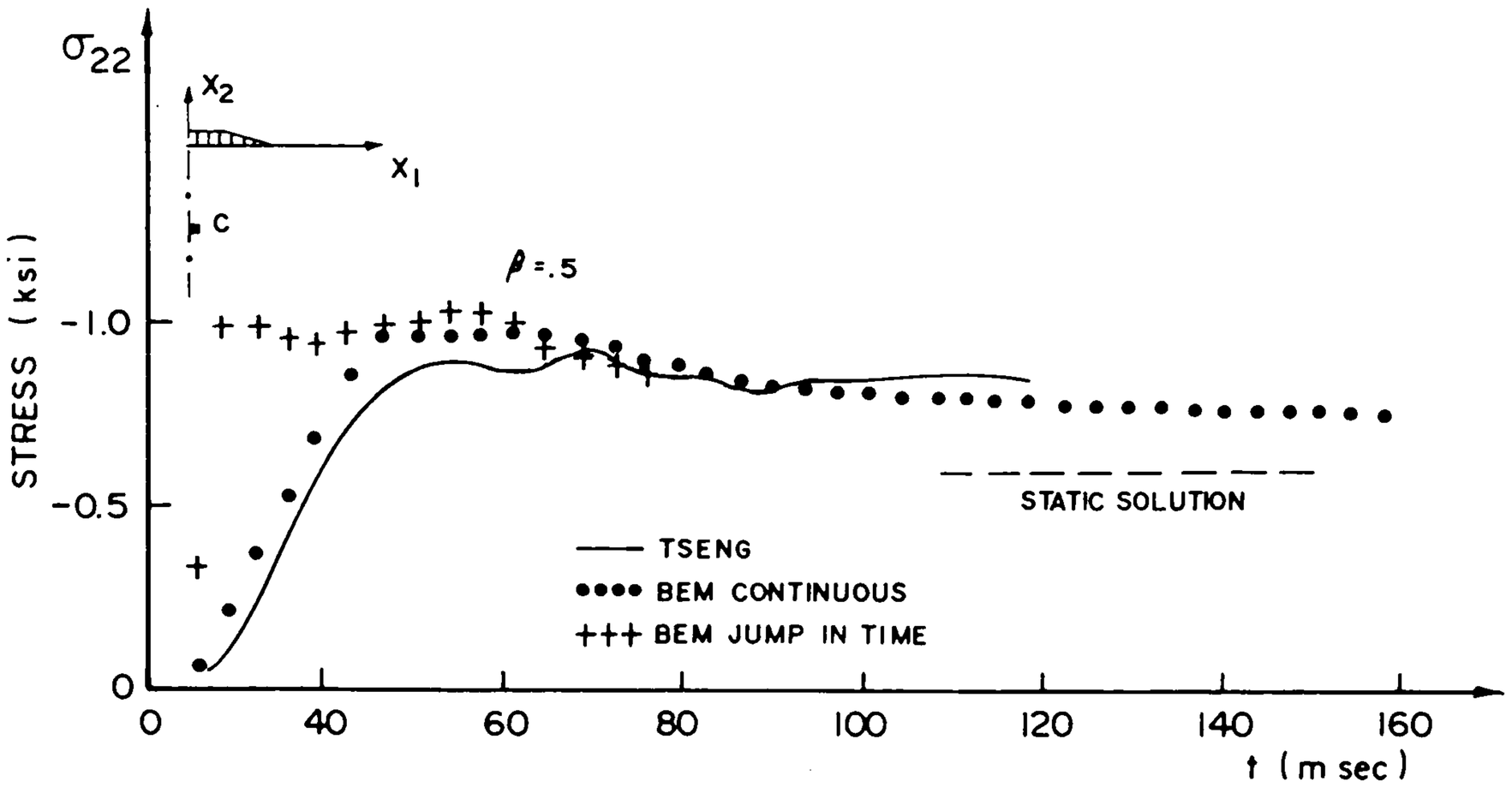

Figure 6.3.24 Half-plane under continuous prescribed stress distribution. Stress σ_{22} at the internal point C(5',75').

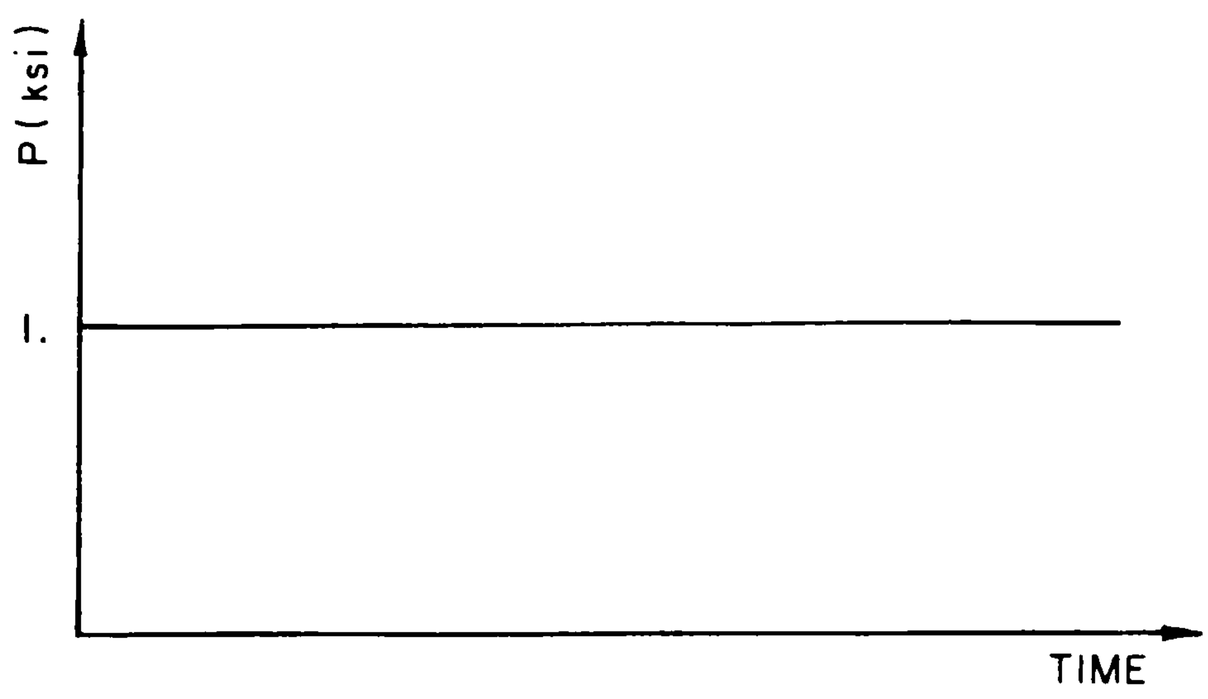

Figure 6.3.25 Load applied as a Heaviside function in time for the half-plane under continuous prescribed stress distribution.

6.3.4 Semi-Infinite Beam - This application consists of a semi-infinite beam simply supported along its edge (see figure 6.3.26) and subjected to a suddenly applied bending moment

$$M_o = M\ H(t-0) \quad . \tag{6.3.10}$$

The Poisson ratio for this plane stress problem was taken to be 1/3.

The boundary element mesh consisted of thirty six equal elements as depicted in figure 6.3.27 and β was taken as equal to .5.

A finite element analysis of this problem was carried out by Fu {110} who used the mesh depicted in figure 6.3.28 in his numerical solution. Transverse displacements along the axes of the beam obtained with both numerical techniques are shown in figure 6.3.29. Within this same figure results obtained from the beam theory by Boley {111} are also plotted. The displacements depicted in figure 6.3.29 refer to

$$t = \frac{5r}{c_o} \tag{6.3.11}$$

where r is the radius of gyration of the beam cross section and c_o is the one-dimensional wave propagation speed {111}.

As it was expected none of the two-dimensional numerical analyses agreed completely with the analytical solution obtained from the beam theory. However the boundary element results show that the two-dimensional solution appears to be closer to the beam theory than initially indicated by the finite element method.

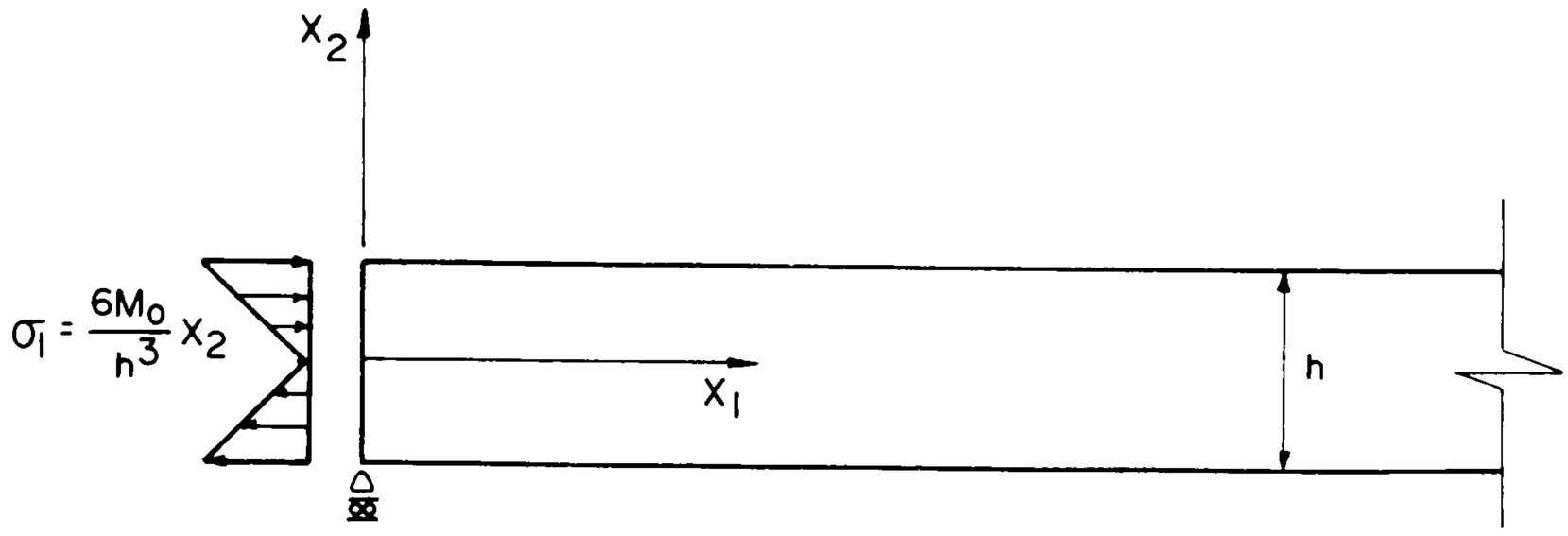

Figure 6.3.26 Geometry and loading of the semi-infinite beam.

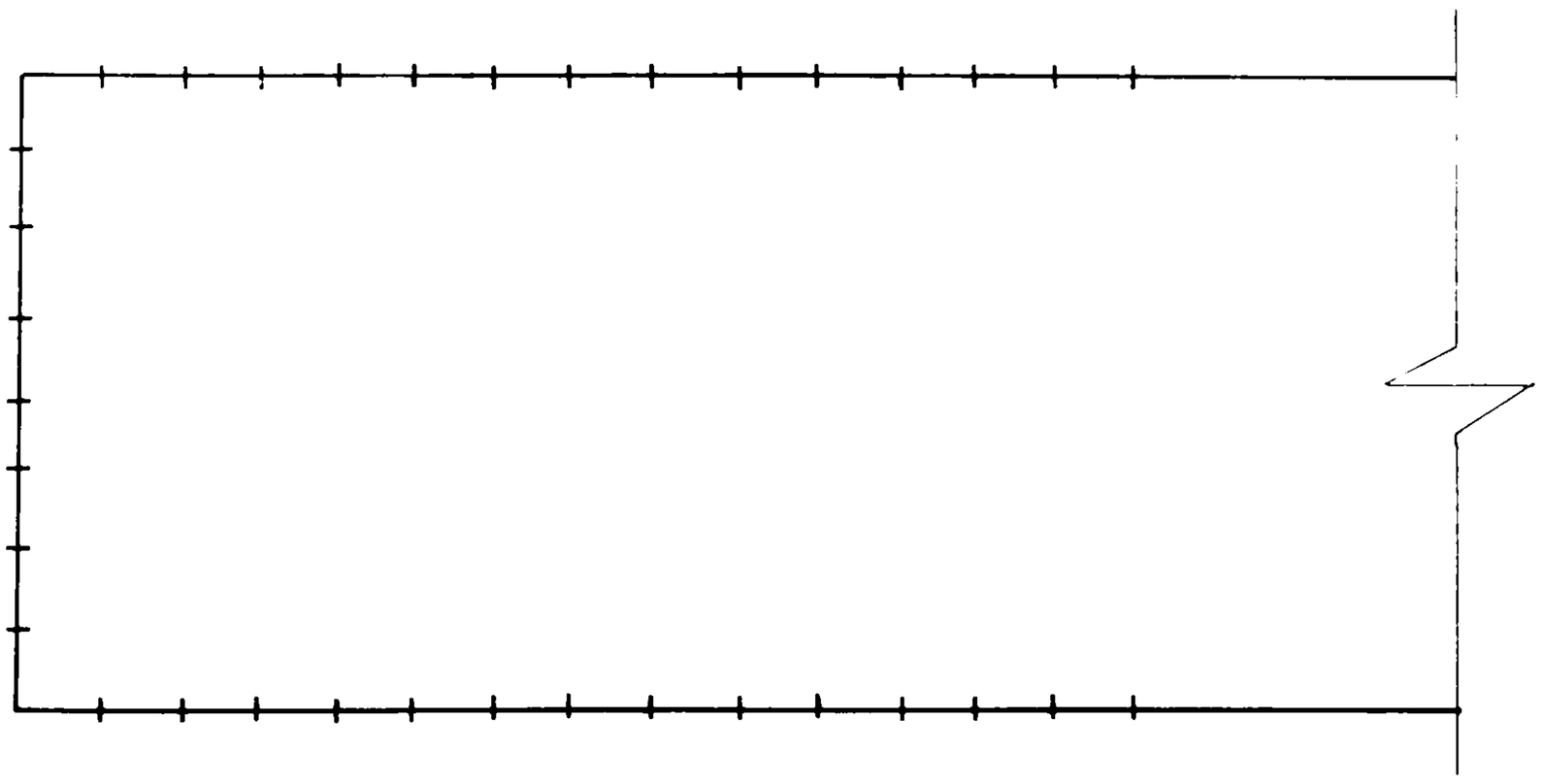

Figure 6.3.27 Boundary element mesh for the semi-infinite beam.

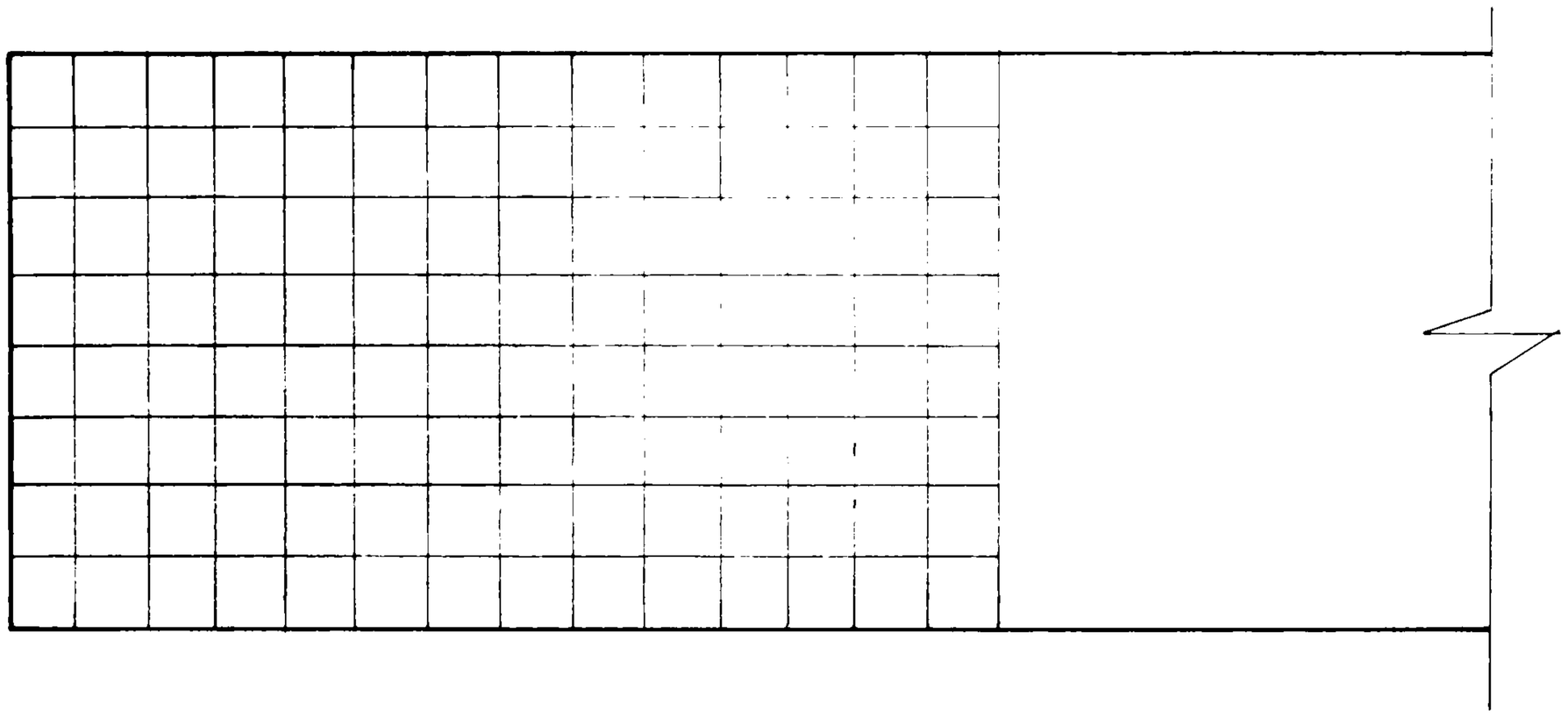

Figure 6.3.28 Finite element mesh for the semi-infinite beam.

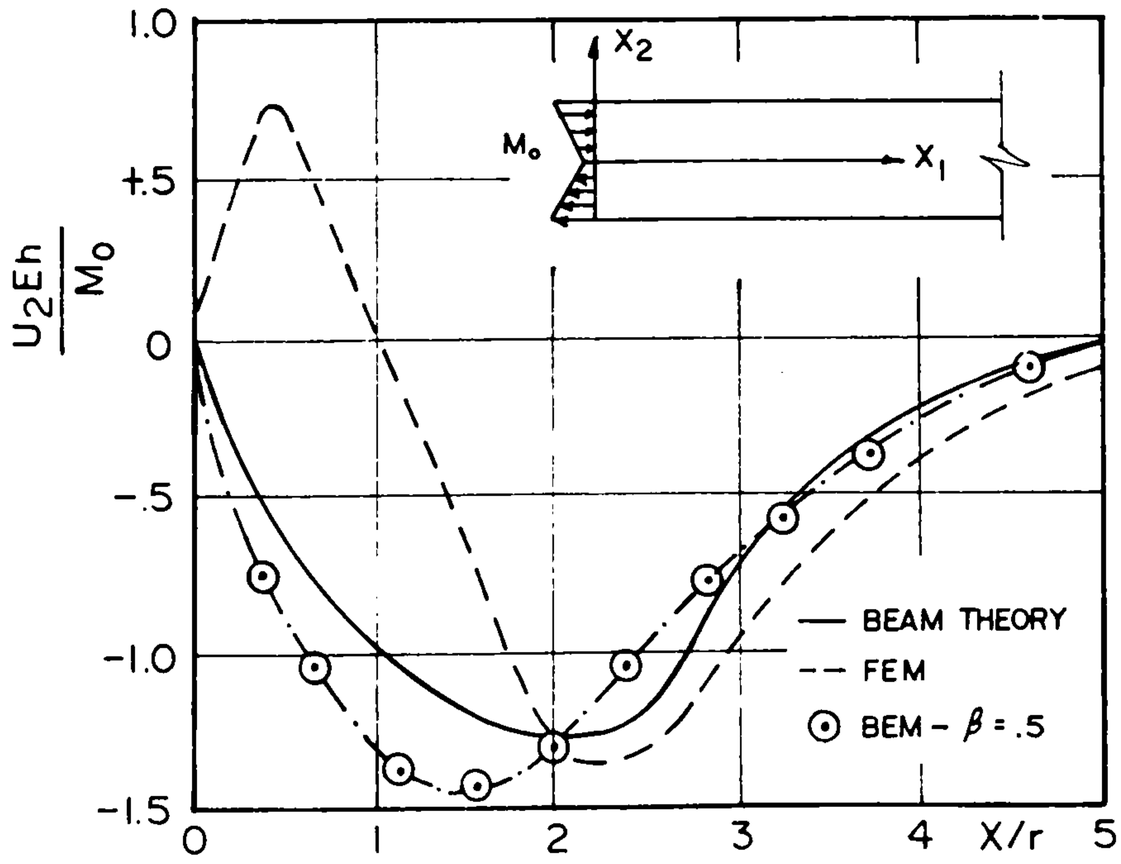

Figure 6.3.29 Transverse displacement along the semi-infinite beam at the time $t = 5r/c_o$.

6.3.5 Hole in an Infinite Plate - In addition to the beam analysed in the last section, Fu {110} also studied another problem which consisted of a hole in an infinite plate and compared results with those obtained by Chow and Koenig {112} using the method of characteristics.

The load in this example consists of a constant internal pressure suddenly applied on the hole surface as depicted in figure 6.3.30. The applied pressure is independent of θ, therefore the stresses and the displacements calculated with respect to the system of polar coordinates shown in figure 6.3.30 are also independent of θ.

The Poisson ratio for this plane stress analysis was taken as being equal to 1/3.

The boundary element discretization and cells used in this analysis are depicted in figure 6.3.31. The parameter β was taken to be equal to 0.5.

The finite element discretization used in this analysis is not presented in reference {110}, however an idea of the number of finite elements and time increments required in this sort of problem is provided by reference {65}.

Figure 6.3.32 depicts the time history of radial and circumferential stresses at points A, B and C displayed in figure 6.3.31. The agreement is acceptable for the internal points, but the boundary element results do not represent well the hoop stress at the boundary point A. Another analysis was then carried out with β = .2, and the stress at the point A, displayed in figure 6.3.32,

improved considerably. Further reduction of the time increments would certainly improve the boundary element results, however this was not done due to limitations on computer time available.

Finally it should be recognized that the stress $\sigma_{\theta\theta}$ at the boundary point A was calculated as described in appendix I.

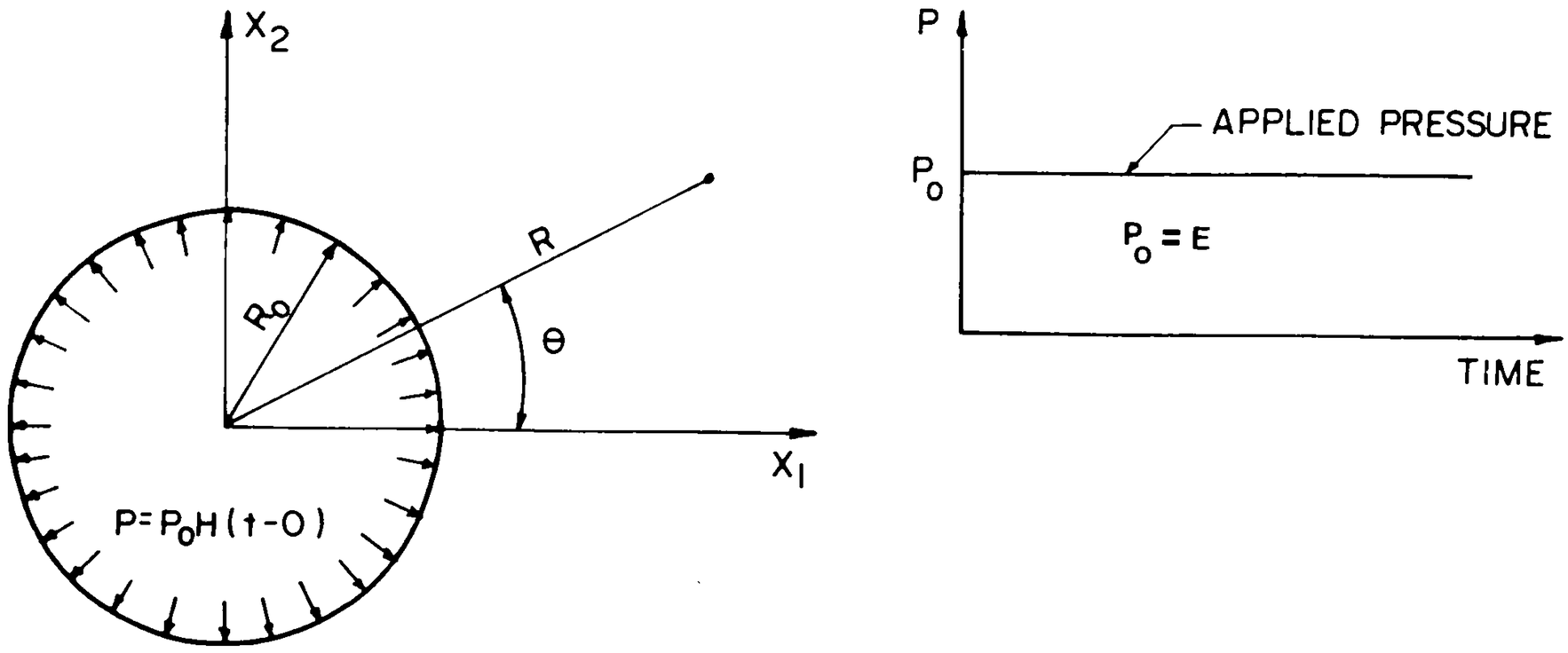

Figure 6.3.30 Loading of the hole in an infinite plate.

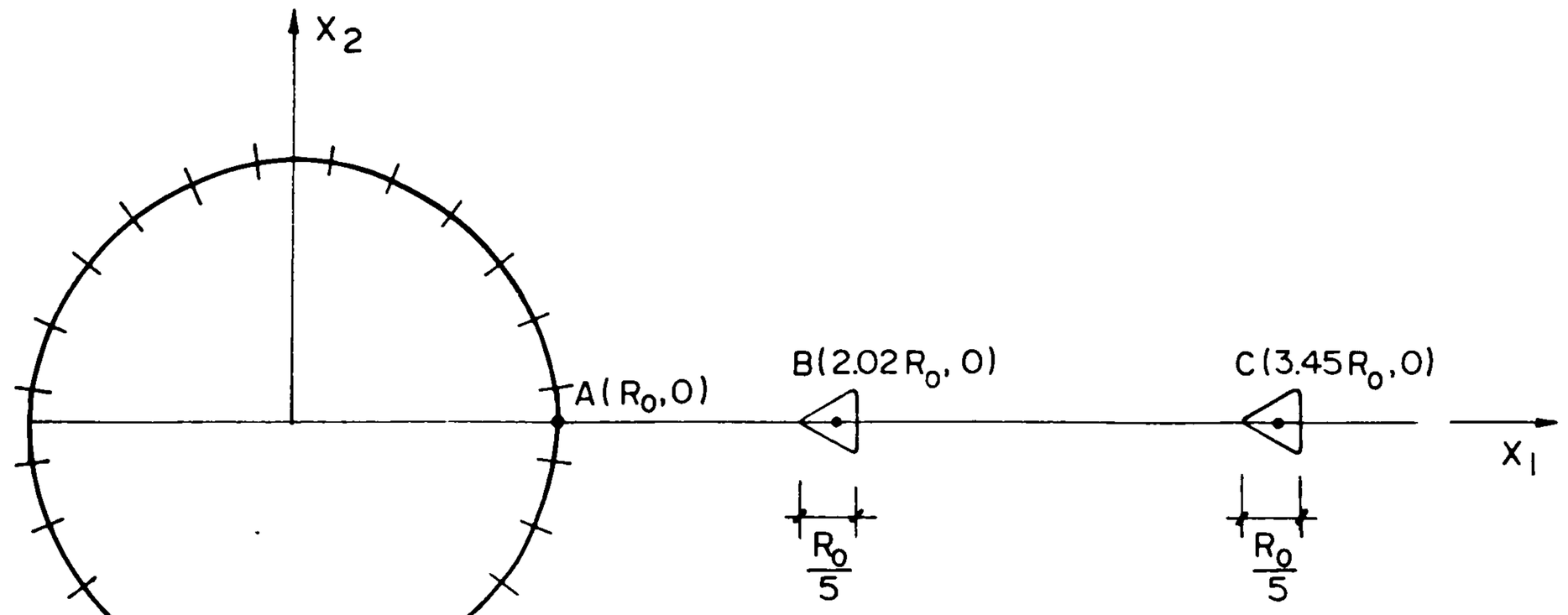

Figure 6.3.31 Boundary discretization and cells for the hole in an infinite plate.

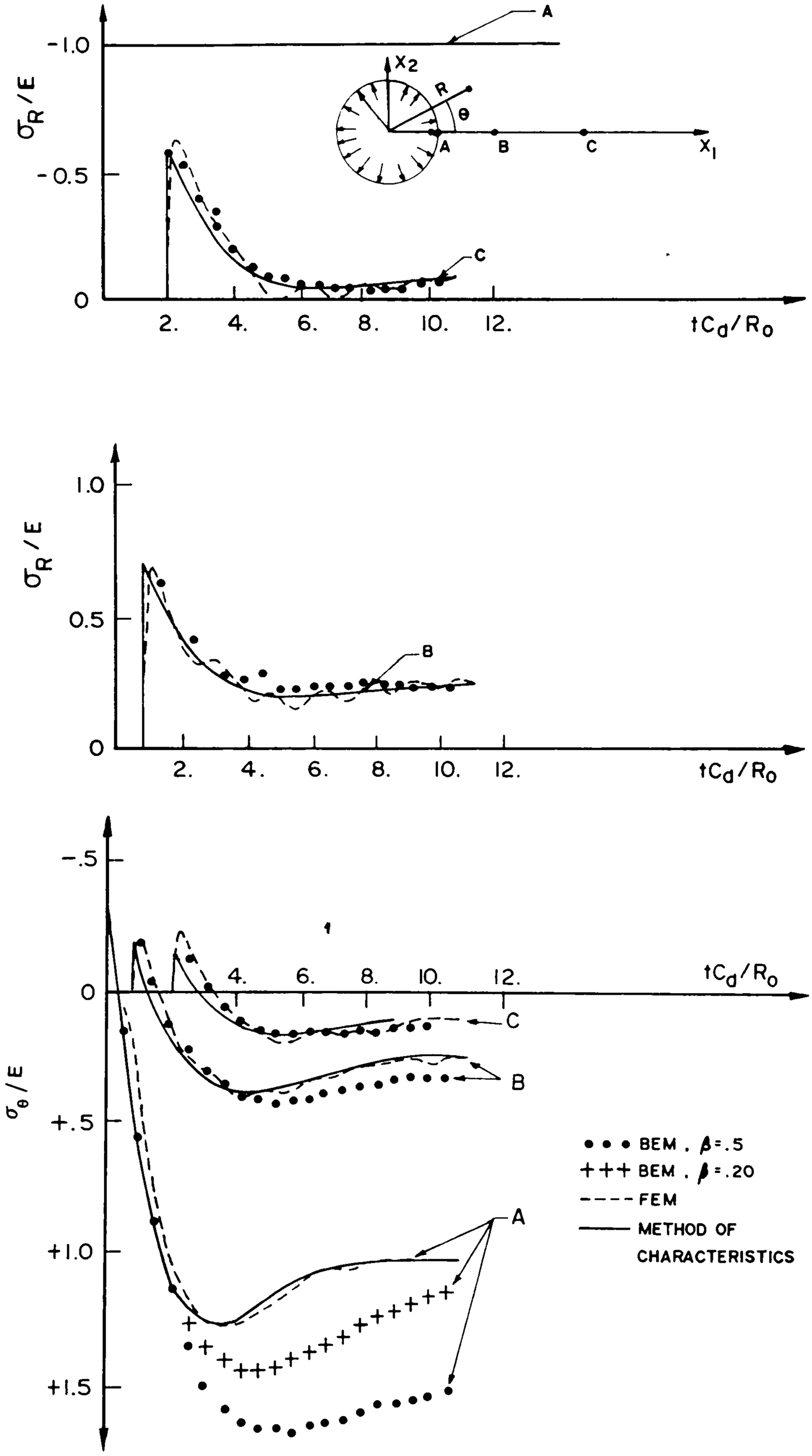

Figure 6.3.32 Radial and circunferential stresses at points $A(R_o,0)$, $B(2.02R_o,0)$ and $C(3.45R_o,0)$ for the hole in an infinite plate.

CHAPTER 7

GENERAL DISCUSSION AND CONCLUSIONS

At present there exist a number of papers (see Chapter 1) which formulate the boundary element method for solving transient wave propagation problems using three-dimensional time domain boundary integral equations. However the only general approaches that use two-dimensional fundamental solutions are those discussed in Chapter 1, which employ either Laplace or Fourier transforms to eliminate the time dependence of the problem. So far the only general numerical procedure that has been developed to analyse transient wave propagation problems in two dimensions, using time dependent fundamental solutions, considers the two-dimensional case as being a particular three-dimensional problem. Using this approach it is possible to benefit from the existing knowledge regarding the three-dimensional case.

In this research, two-dimensional time dependent Green's functions were used to deduce integral equations, amenable to numerical solutions of two-dimensional transient wave propagation problems. A boundary element scheme was applied to solve numerical problems governed by the scalar wave and Navier's equations. Therefore the proposed method can be used to analyse plane-stress, plane strain and antiplane motions.

In chapter 2, a revision of the linear elastodynamics was provided, with the purpose of briefly investigating the basic theory and also simultaneously introducing notation

and terminology that would be employed later.

Although this research was primarily concerned with two-dimensional applications, the three-dimensional problem was also discussed. In this way some important discrepancies of the behaviour of two- and three-dimensional waves could be shown. The three-dimensional formulation was also required to obtain two-dimensional boundary integral equations, because in the procedure applied the method of descent was employed.

One of this thesis' objectives was to derive the boundary integral equation (3.7.18) which constituted the basis for developing a time-stepping scheme to solve numerically transient two-dimensional problems governed by the scalar wave equation.

Usual time marching schemes treat each time step as a new problem, and consequently at the end of each time interval, values of displacements and velocities are calculated for a number of internal points, in order to use them as pseudo-initial conditions for the next step, i.e. the integral equation (3.7.18) is applied from 0 to Δt; Δt to $2\Delta t$ etc. In this thesis however, the time integration process is always considered to start at the time '0' and so values of displacements and velocities do not need to be calculated at intermediate steps. With this procedure, the domain discretization is restricted to regions where source density and initial conditions do not disappear. The domain integrations at a time step 'j' are consequently avoided at the expense of having to calculate time integrations for all time steps previous to 'j'. Two square

matrices of order (J×J) must be stored for each time step; J being the number of boundaries nodes. Therefore when results for very late times are required a computer with a large storage area is needed. The first time marching scheme discussed previously is useful for bounded domains in which late time solutions are sought, in all other cases the second scheme is more suitable.

Linear discretization was used to approximate the geometry of the Γ boundary. However it should be recognized that it could be an advantage to use higher order discretizations when analysing problems with more complicated geometries than those considered in section 4.3.

Of the three distinct combinations of interpolation functions used to approximate u and p on the boundary, combination 2 was considered the most suitable one (see table 4.3.1 reproduced below).

Combination	Interpolation function		
	$\eta_j(\mathbf{Q})$ and $\nu_j(\mathbf{Q})$	$\phi^m(t)$	$\theta^m(t)$
1	Linear	Linear	Linear
2	Linear	Linear	Constant
3	Constant	Linear	Constant

Table 4.3.1 Combination of interpolation functions.

In a considerable number of wave propagation problems, p can be discontinuous and the use of continuous $\theta^m(t)$, introduces excessive oscillations in the numerical results. For this reason a discontinuous time interpolation

function, $\theta^m(\tau)$ = constant, was used to approximate p. However higher order discontinuous $\theta^m(t)$ should also be considered in future research primarily to improve the efficiency of the numerical analysis.

In the numerical applications carried out in section 4.3, p is also discontinuous in space. Despite this fact, continuous linear elements yielded good numerical results for all of the three problems studied.

The time integrations indicated in expressions (4.2.5) and (4.2.6) were performed analytically. The integrands of the boundary integrals obtained with this procedure (see expression 4.2.17) have singularities which are of the same order as those which appear when considering steady state potential problems. Consequently Gauss quadrature could be applied to integrate numerically over all of the elements except those with singularities. Singular boundary integrals were carried out analytically.

Linear triangular cells were used to calculate contributions due to initial conditions. In the semi-analytical scheme discussed in section (4.2.2) a system of polar coordinates (r,θ) was employed and integrations with respect to r were performed analytically. The expressions obtained were then integrated numerically with respect to θ using one-dimensional Gauss quadrature. This method of computing initial conditions contributions, that appear in expression (3.7.18), was tested in the examples discussed in sections 4.3.2 and 4.3.3 and proved to be very efficient.

A maximum of ten Gauss points was used to perform both, cell and boundary integrations. The number of Gauss points was gradually reduced as the time-stepping scheme advanced in time, but no general rule was derived; consequently further investigations on this subject are required.

Three examples concerning two-dimensional problems governed by the scalar wave equation were considered in section 4.3. The first example (see section 4.3.1) tested the performance of the proposed time-stepping scheme on a problem in which p was discontinuous in both time and space. The second example was studied in section 4.3.2 and was concerned with checking the numerical performance of the time-stepping technique described in this thesis when the prescribed initial conditions were not null. A further illustration of the numerical technique under consideration can be found in section 4.3.3. In the example analysed there, the time was divided into intervals that were shorter than in the two previous examples. This was because of the rather complicated time and space behaviour of p. In all of these three applications the accuracy of the numerical solutions was considered to be very good.

From the problems analysed in section 4.3 it can also be concluded that very small values of the parameter β, can in certain situations introduce an excessive level of noise into the numerical results. Another important conclusion that can be inferred from the applications is that great care should be taken when choosing the time intervals and boundary discretization, in order to avoid

contradicting the causality property too far, that is, in each time step waves should not be allowed to travel between nodes far from each other.

A discussion concerning two- and three-dimensional time-domain integral equations for transient elastodynamics was the object of chapter 5. The primary intention was to describe the mathematical manipulations required to obtain equation (5.4.1) (see section 5.4), which can be used on the two-dimensional numerical analysis. Initial conditions were not considered in equation (5.4.1), however they can be included by following a procedure similar to that presented in section 3.7.

Linear discretization was used to approximate the geometry of the Γ boundary and combination 3 displayed in table 4.3.1 was adopted to interpolate boundary displacements and tractions.

As in the case of the scalar wave equation, both time integrations and space integrations of singular expressions were performed analytically. Non-singular boundary integrals were computed numerically employing a maximum of twenty Gauss points.

The scheme implemented to compute internal stresses was similar to the simplest procedure used in finite elements. Triangular cells were used and stresses at their centroids were calculated from displacements which were linearly interpolated inside each cell as a function of the displacements at the cell nodes.

Five numerical applications were considered in section 6.3, where discussions concerning the choice of boundary element meshes and time intervals were presented. Results obtained with the time-domain boundary element formulation were compared with those obtained using boundary elements in conjunction with Laplace transform, finite-differences and finite elements.

The agreement of the results was acceptable for displacements and tractions. The accuracy of the stress numerical results was however dependent on a good selection of cells. Large cells can lead to incorrect results mainly on regions of stress concentration. Conversely excessively small cells should also be avoided because the displacements of these cell nodes can often be too close to each other which may result in a large contribution to stresses due to numerical errors. A more appropriate scheme in which constant stress cells can still be employed is that in which stresses, at any internal point, are obtained as the average value of stresses computed at various cells having such a point as a common node. Higher order cells should also be tested in future, however the most suitable alternative method to improve stress accuracy is to calculate them using a proper integral equation.

In a brief review it should be recognized that the boundary integral technique presented in this report showed to be very promising. Despite the poor interpolation functions used in the numerical analyses encouraging results were obtained.

In order to improve the numerical technique discussed here higher order time and space interpolation functions together with a more accurate scheme to compute stresses are recommended to be implemented in future research.

With reference to extending the present research to a more diverse range of problems, initial conditions and body forces can easily be introduced into the two-dimensional elastodynamic formulation. Sub-regions must also be implemented to introduce the possibility of analysing non-homogeneous bodies. A vastly more efficient solution of half-plane problems can be obtained using fundamental solutions specifically derived for that case. Implementation of such solutions must also be the object of future research efforts.

The recommendations for future research mentioned above only consider a few topics which can have immediate applications to a diverse range of practical engineering problems. However, there are many other possible extensions which can be derived from this report and the case which requires to be analysed first is a matter to be decided according to the specific problem which needs to be solved.

REFERENCES

1. POISSON, S.D. (1829). Mémoire sur l'Équilibre et le Mouvement des Corps Élastiques. Mém. Acad. Sci. Paris, t.8, 357-570.

2. LORD RAYLEIGH (1885). On Waves Propagated Along the Plane Surface of an Elastic Solid. Proc. London Math. Soc., 17, 4-11.

3. LAMB, H. (1904). On the Propagation of Tremors Over the Surface of an Elastic Solid. Philos. Trans. Royal Soc. London, Ser. A, 203, 1-42.

4. LOVE, A.E.H. (1911). Some Problems of Geodynamics. Cambridge Univ. Press, Cambridge, 165-178.

5. LOVE, A.E.H. (1944). A Treatise on the Mathematical Theory of Elasticity. Dover, New York.

6. MORSE, P.M. and FESHBACH, H. (1953). Methods of Theoretical Physics. McGraw-Hill, New York, Toronto and London.

7. PAO, Y.H. and MOW, C.C. (1973). Diffraction of Elastic Waves and Dynamic Stress Concentrations. Crane Russak, New York.

8. ACHENBACH, J.D. (1973). Wave Propagation in Elastic Solids. North-Holland Publishing Company, Amsterdam and London.

9. ERINGEN, A.C. and SUHUBI, E.S. (1975). Elastodynamics. Vols I and II, Academic Press, New York, San Francisco and London.

10. MIKLOWITZ, J. (1980). Elastic Waves and Waveguides. North-Holland Publishing Company, Amsterdam, New York and Oxford.

11. TSENG, M.N. and ROBINSON, A.R. (1975). A Transmitting Boundary for Finite-Difference Analysis of Wave Propagation in Solids. Project No NR 064-183, University of Illinois, Urbana, Illinois.

12. BATHE, K.J. and WILSON, E.L. (1976). Numerical Methods in Finite Element Analysis. Prentice-Hall, Inc., Englewood Cliffs, New Jersey.

13. BREBBIA, C.A. and CONNOR, J.J. (1973). Fundamentals of Finite Elements Techniques for Structural Engineers. Butterworths, London.

14. ZIENKIEWICZ, O.C. (1977). The Finite Element Method. 3rd ed., McGraw-Hill, London.

15. COOK, R.D. (1974). Concepts and Applications of Finite Element Analysis, Wiley, New York.

16. DESAI, C.S. and ABEL, J.F. (1972). Introduction to the Finite Element Method. Van Nostrand Reinhold Company, New York.

17. BATHE, K.J., WILSON, E.L. and PETERSON, F.E. (1973). SAP IV, A Structural Analysis Program for Static and Dynamic Response of Linear Systems. Report No. EERC 73-11, University of California, Berkeley.

18. KEY, S.M. (1975). HONDO - A Finite Element Computer Program for the Large Deformation Dynamic Response of Axisymmetric Solids. Sandia Laboratories, Albuquerque, New Mexico.

19. MacNEAL, R.H. and McCORMICK, C.W. (1971). The Nastran Computer Program for Structural Analysis. Computer & Structures, 1, 389-412.

20. BREBBIA, C.A. (1978). The Boundary Element Method for Engineers. Pentech Press, London.

21. BREBBIA, C.A. and WALKER, S. (1980). The Boundary Element Techniques in Engineering. Newes-Butterworths, London.

22. BREBBIA, C.A., TELLES, J.C. and WROBEL, L.C. (1983). Boundary Element Techniques - Theory and Application in Engineering. Springer-Verlag, Berlin and New York.

23. FREDHOLM, I. (1905). Solution d'un Probleme Fondamental de la Theorie de l'Elasticite. Arkiv fön Matematik, Astronomi och Fysik, 11, 28.

24. KUPRADZE, V.D. (1963). Dynamical Problems in Elasticity. Progress in Solid Mechanics, Volume III, (I.N. Snedon and R. Hill eds.), Interscience Publishers, New York.

25. BANAUGH, R.P. and GOLDSMITH, W. (1963). Diffraction of Steady Acoustical Waves by Surface of Arbitrary Shape. J. Acoustical Soc. Amer., 35, 1590-1601.

26. CRUSE, T.A. (1977). Mathematical Foundations of the Boundary Integral Equation Method in Solid Mechanics. Report No AFOSR-TR-77-1002, Pratt and Whitney Aircraft Group.

27. JASON, M.A. and SYMN, G.T. (1977). Integral Equation Methods in Potential Theory and Elastostatics. Academic Press, London.

28. RIZZO, F.J. (1967). An Integral Equation Approach to Boundary Value Problems of Classical Elastostatics. Q. Appl. Math., 25, 83-95.

29. CRUSE, T.A. (1969). Numerical Solutions in Three-Dimensional Elastostatics. Int. J. Solids Structures, 5, 1259-1274.

30. CRUSE, T.A. (1972). Application of the Boundary Integral Equation Solution Method in Solid Mechanics. In Variational Methods in Engineering, (BREBBIA and TOTTENHAM eds.), Southampton University Press, 2, 9/1-9/29.

31. CRUSE, T.A. (1974). An Improved Boundary Integral Equation Method for three Dimensional Elastic Stress Analysis. Computer & Structures, 4, 741-754.

32. LACHAT, J.C. (1975). A Further Development of the Boundary Integral Technique for Elastostatics. Ph.D. Thesis, University of Southampton.

33. LACHAT, J.C. and WATSON, J.O. (1977). Progress in the Use of Boundary Integral Equations Illustrated by Examples. Computer Meth. Appl. Mech. Engng., 10, 273-289.

34. NAKAGUMA, R.K. (1979). Three Dimensional Elastostatics Using The Boundary Element Method. Ph.D. Thesis, University of Southampton.

35. WROBEL, L.C. (1981). Potential and Viscous Flow Problems Using the Boundary Element Method. Ph.D. Thesis, University of Southampton.

36. TELLES, J.C.F. (1981). On the Application of the Boundary Element Method to Inelastic Problems. Ph.D. Thesis, University of Southampton.

37. VENTURINI, W.S. (1982). Application of the Boundary Element Formulation to Solve Geomechanical Problems. Ph.D. Thesis, University of Southampton.

38. BUTTERFIELD, R. and BANERJEE, P.K. (1971). The Problem of Pile Cap-Pile Group Interaction. Géotechnique, 21, 135-142.

39. WATSON, J.O. (1972). The analysis of Thick Shells with Holes by Integral Representation of Displacement. Ph.D. Thesis, University of Southampton.

40. CRUSE, T.A. and RIZZO, F.J. (eds.) (1975). Boundary Integral Equation Method: Computational Applications in Applied Mechanics. ASME, AMD - Vol. 11, New York.

41. CRUSE, T.A., LACHAT, J.C., RIZZO, F.J. and SHAW, R.P. (eds.) (1977). First Int. Symp. on Innovative Numerical Analysis in Applied Engineering Science. CETIM, Versailles.

42. BREBBIA, C.A. (ed.) (1978). Recent Advances in Boundary Element Methods. Pentech Press, London.

43. BANERJEE, P.K. and BUTTERFIELD, R. (eds.) (1979). Developments in Boundary Element Methods, Vol. 1. Applied Science Publishers, London.

44. BREBBIA, C.A. (ed.) (1983). New Developments in Boundary Element Methods. Second edition, CML Publications, Southampton.

45. SHAW, R.P. et al. (eds.) (1980). Innovative Numerical Analysis for the Engineering Sciences. University Press of Virginia, Charlottesville.

46. BREBBIA, C.A. (ed.) (1981). Progress in Boundary Element Methods, Vol. 1. Pentech Press, London and Halstead Press, New York.

47. BREBBIA, C.A. (ed.) (1983). Progress in Boundary Element Methods, Vol. 2. Pentech Press, London and Springer Verlag, New York.

48. BREBBIA, C.A. (ed.) (1981). Boundary Element Methods. Springer Verlag, Berlin and New York.

49. BREBBIA, C.A. (ed.) (1982). Boundary Elements in Engineering. Springer Verlag, Berlin, Heidelberg and New York.

50. BREBBIA, C.A. (ed.) (1983). Boundary Element Methods. Proceedings of the Fifth Conference on Boundary Element Methods, Hiroshima.

51. BETTI, E. (1872). Teoria dell'Elasticita. Il Nuovo Ciemento, t.7-10.

52. THOMPSON, Sir W. (Lord Kelvin) (1848). Cambridge and Dublin Mathematical Journal.

53. SOMIGLIANA, C. (1886). Sopra l'Equilibrio di un Corpo Elastico Isotropo. Il Nuovo Ciemento, t. 17-19.

54. CRUSE, T.A. (1978). Two Dimensional BIE Fracture Mechanics Analysis. Appl. Math. Modelling, 2, 287-293.

55. de HOOP, A.T. (1958). Representation Theorems for the Displacement in an Elastic Solid and their Application in Elastodynamic Diffraction Theory. Doctoral Dissertation, Technische Hogeschool Delft, Delft, the Netherlands.

56. DIRAC, P.A.M. (1935). The Principles of Quantum Mechanics. Second edition, Clarendon, Oxford.

57. KIRCHHOFF, G. (1883). Zur Theorie der Lichstrahlen. Ann. Physik., 18, 663-695.

58. FRIEDMAN, M.B. and SHAW, R. (1962). Diffraction of Pulses by Cylindrical Obstacles of Arbitrary Cross Section. Trans. ASME, J. Appl. Mech., series E, 29, 40-46.

59. MITZNER, R.M. (1967). Numerical Solution for Transient Scattering from a Hard Surface of Arbitrary Shape - Retarded Potential Technique. J. Acoust. Soc. Amer., 42, 391-397.

60. GROENENBOON, P.H.L. (1981). The Application of Boundary Elements to Steady and Unsteady Potential Flow Problems in Two and Three-Dimensional Problems. In Boundary Element Methods (ed. C.A. Brebbia), Springer Verlag, Berlin.

61. CRUSE, T.A. (1967). The Transient Problem in Classical Elastodynamics Solved by Integral Equations. Ph.D. Thesis,University of Washington.

62. CRUSE, T.A. and RIZZO, F.J. (1968). A Direct Formulation and Numerical Solution of the General Transient Elastodynamic Problem I. J. Math. Anal. Appl., 22, 244-259.

63. CRUSE, T.A. (1968). A Direct Formulation and Numerical Solution of the General Transient Elastodynamic Problem II. J. Math. Anal. Appl., 22, 341-355.

64. PAPOULIS, A. (1957). A New Method of Inversion of the Laplace Transform. Q. Appl. Math., 14(4), 405-414.

65. MANOLIS, G.D. (1980). Dynamic Response of Underground Structures. Ph.D. Thesis, University of Minnesota.

66. MANOLIS, G.D. and BESKOS, D.E. (1981). Dynamic Stress Concentration Studies by Boundary Integrals and Laplace Transform. Int. J. Num. Meth. Engng.,17, 573-599.

67. DURBIN, F. (1974). Numerical Inversion of Laplace Transforms: an Efficient Improvement to Dubner and Abate's Method. Computer J., 17, 371-376.

68. ALARCON, E. and DOMINGUEZ, J. (1981). Elastodynamics. Chapter 7 in {46}.

69. SHAW, R.P. (1967). Diffraction of Acoustic Pulses by Obstacles of Arbitrary Shape with a Robin Boundary Condition. Part A, J.A.S.A., 41, 855-859.

70. SHAW, R.P. (1967). Scattering of Plane Acoustic Pulses by an Infinite Plane with a General First Order Boundary Condition. J. Appl. Mech., 34, 770-772.

71. SHAW, R.P. (1968). Retarded Potential Approach to the Scattering of Elastic Pulses by Rigid Obstacles of Arbitrary Shape. J.A.S.A., 44, 745-748.

72. SHAW, R.P. (1968). Diffraction of Pulses by Obstacles of Arbitrary Shape with an Impedance Boundary Condition. J.A.S.A., 44, 1962-1968.

73. SHAW, R.P. (1971). Singularities in Acoustic Pulse Scattering by Free Surface Obstacles with Sharp Corners. J. Appl. Mech., 38, 526-528.

74. SHAW, R.P. & ENGLISH, J.A. (1972). Transient Acoustic Scattering by a Free Sphere. J. Sound Vibration, 20, 321-331.

75. SHAW, R.P. (1975). Transient Scattering by a Circular Cylinder. J. Sound Vibration, 42, 295-304.

76. SHAW, R.P. (1975). An Outer Boundary Integral Equation Applied to Transient Wave Scattering in an Inhomogeneous Medium. J. Appl. Mech., 42, 147-152.

77. KELLOG, O.D. (1929). Foundations of Potential Theory. Springer, Berlin.

78. NEILSON, H.C., LIU, Y.P. and WANG, Y.F. (1978). Transient Scattering by Arbitrary Axisymmetric Surfaces. J. Acoust. Soc. Am., 63(6), 1719-1726.

79. HERMAN, G.C. (1981). Scattering of Transient Acoustic Waves in Fluids and Solids. Thesis, DELFT University of Technology.

80. NIWA, Y., FUKUI, T., KATO, S. and FUJIKI, K. (1980). An application of the Integral Equation Method to Two-Dimensional Elastodynamics. Theor. Appl. Mech., University of Tokyo Press, 28, 281-290.

81. MANOLIS, G.D. (1983). A Comparative Study on Three Boundary Element Method Approaches to Problems in Elastodynamics. Int. J. Num. Meth. Engng., 19, 73-91.

82. DAS, S. (1976). A Numerical Study of Rupture Propagation and Earthquake Source Mechanism. Thesis, Massachusetts Institute of Technology, Massachusetts.

83. DAS, S. and K. AKI (1977). A Numerical Study of Two-Dimensional Spontaneous Rupture Propagation. Geophys. J., 50, 643-648.

84. COLE, D.M., KOSLOFF, D.D. and MINSTER, J.B. (1978). A Numerical Boundary Integral Equation Method for Elastodynamics I. Bull. Seis. Soc. America, 68(5), 1331-1357.

85. MANSUR, W.J. and BREBBIA, C.A. (1982). Formulation of the Boundary Element Method for Transient Problems Governed by the Scalar Wave Equation. Appl. Math. Modelling, 6, 307-311.

86. MANSUR, W.J. and BREBBIA, C.A. (1982). Numerical Implementation of the Boundary Element Method for Two-Dimensional Transient Scalar Wave Propagation Problems. Appl. Math. Modelling, 6, 299-306.

87. FUNG, Y.C. (1965). Foundations of Solid Mechanics. Prentice-Hall, Inc., New Jersey.

88. NEUMANN, F. (1885). Vorlesungen Über die Theorie der Elasticität der Festen Körper und des Lichtäthers. B.G. Teubner, Leipzig.

89. WHEELER, L.T. and STERNBERG, E. (1968). Some Theorems in Classical Elastodynamics. Arch. Rational Mech. Anal., 31, 51-90.

90. KNOPS, R.J. and PAYNE, L.E. (1968). Uniqueness in Classical Elastodynamics. Arch. Rational Mech. Anal., 27, 349-355.

91. BROCKWAY, G.S. (1972). On the Uniqueness of Singular Solutions to Boundary-Initial Value Problems in Linear Elastodynamics. Arch. Rational Mech. Anal. 48, 213-244.

92. FICHERA, G. (1972). Existence Theorems in Elasticity, in "Handbuch der Physik" (C. Truesdell, ed.), VIa/2, pp. 347-389. Springer-Verlag, Berlin and New York.

93. LAMB, H. (1902). On Wave Propagation in Two-Dimensions. Proc. London Math. Soc. {1}, 35, 141-161.

94. VOLTERRA, V. (1894). Sur les Vibrations des Corps Elastiques Isotropes. Acta Math., 18, 161-332.

95. JONES, D.S. (1966). Generalised Functions. McGraw-Hill, London.

96. LIGHTHILL, M.J. (1958). Fourier Analysis and Generalised Functions. Cambridge University Press.

97. BAKER, B.B. and COPSON, E.T. (1939). The Mathematical Theory of Huygens' Principle. Oxford Univ. Press, London, 1939.

98. ROOS, B.W. (1969). Analytic Functions and Distributions in Physics and Engineering. Wiley, New York.

99. HALBRITTER, A.L., TELLES, J.C.F. and MANSUR, W.J. (1978). Application of the Boundary Element Method to Field Problems. Proceedings of the Conference, on Structural Analysis, Design & Construction in Nuclear Power Plants (in Portuguese), paper N. 39, pp. 707-724, Porto Alegre, Brasil.

100. CHAUDONNERET, M. (1978). On the Discontinuity of the Stress Vector in the Boundary Integral Equation Method for Elastic Analysis. Proceedings of the First International Seminar on Recent Advances in Boundary Element Methods, (C.A. Brebbia, ed.), Southampton, pp. 185-194.

101. MANSUR, W.J., HALBRITTER, A.L. and TELLES, J.C.F. (1979). Boundary Element Method - Formulation for Two-Dimensional Elasticity. Commemorative Annals of the 15th Anniversary of COPPE-UFRJ, (COPPE-UFRJ ed. in Portuguese), pp. 1-22, Rio de Janeiro, Brasil.

102. PATTERSON, C. and SHEIKH, M.A. (1981). Non-Conforming Boundary Elements for Stress Analysis. Proceedings of the Second International Conference on Boundary Element Methods (C.A. Brebbia ed.) Springer Verlag, Berlin, Heidelberg and New York.

103. PATTERSON, C. and ELSEBAI, N.A.S. (1982). A Regular Boundary Method Using Non-Conforming Elements for Potential Problems in Three Dimensions. Proceedings of the Fourth International Seminar on Boundary Element Methods in Engineering (C.A. Brebbia ed.), Springer Verlag, Berlin, Heidelberg and New York.

104. MILES, J.W. (1961). Modern Mathematics for the Engineer (Beckenbach, E.F. ed.), pp. 82-84, McGraw-Hill, London.

105. MORSE, P.M. and INGARD, K.V. (1968). Theoretical Acoustics, McGraw-Hill, London.

106. CRAGGS, J.W. (1960). On Two-Dimensional Waves in an Elastic Half-Space. Proceedings of the Cambridge Philosophical Society, 56, 269-285.

107. ANG, A.H.-S, and NEWMARK, N.M. (1971). Development of a Transmitting Boundary for Numerical Wave Motion Calculations. Report to Defense Atomic Support Agency, DASA 2631.

108. GALLOWAY, J.C. and ANG, A.H.-S. (1968). A Generalized Lumped-Parameter Model for Plane Problem of Solid Media. Civil Engineering Studies, Structural Research Series, No. 341, University of Illinois, Urbana, Illinois.

109. SAMEH, A.H.M., and ANG, A.H.-S. (1968). Numerical Analysis of Axisymmetric Wave Propagation in Elastic-Plastic Layered Media. Civil Engineering Studies, Structural Research Series No. 335, University of Illinois, Urbana, Illinois.

110. FU, C.C. (1970). A Method for the Numerical Integration of the Equations of Motion Arising from a Finite-Element Analysis. Trans. ASME, J. Appl. Mech., series E, 37, 599-605.

111. BOLEY, B.A. (1955). An Approximate Theory of Lateral Impact on Beams. Trans. ASME, J. Appl. Mech., Series E, 22, 69-76.

112. CHOW, P.C. and KOENIG, H.A. (1966). An Unified Approach to Cylindrical and Spherical Elastic Waves by Method of Characteristics. Trans. ASME, J. Appl. Mech., Series E, 33, 159-167.

113. RIZZO, F.J. and SHIPPY, D.J. (1970). A Formulation and Solution Procedure for the General Non-Homogeneous Elastic Inclusion Problem. Int. J. Solids Struct., 4, 1161-1179.

APPENDIX A

DIVERGENCE THEOREM AND INTEGRATION BY PARTS

In this appendix the operations required to obtain equation (3.5.4) from equation (3.5.3) are outlined. The two simple mathematical formulas given in (a) and (b) below, will be required.

(a) Integration by parts

$$\int_a^b f\, dg\, dx = \Big[fg\Big]_a^b - \int_a^b g\, df\, dx \quad . \tag{A.1}$$

(b) Divergence theorem

$$\int_\Omega f_{,j}\, d\Omega = \int_\Gamma f_j\, n_j\, d\Gamma \quad . \tag{A.2}$$

Initially it is important to recognize that

$$\int_\Omega \nabla^2 u\; u^*\, d\Omega = \int_\Omega (u_{,j}\; u^*)_{,j}\, d\Omega - \int_\Omega (uu^*_{,j})_{,j}\, d\Omega$$

$$+ \int_\Omega uu^*_{,jj}\, d\Omega \quad . \tag{A.3}$$

When the divergence theorem is applied to the first two terms on the right-hand side of equation (A.3), the following relationship can be written

$$\int_{\Omega} \nabla^2 uu^* \, d\Omega = \int_{\Omega} uu^*_{,jj} \, d\Omega + \int_{\Gamma} u^* u_{,j} \, n_j \, d\Gamma - \int_{\Gamma} uu^*_{,j} \, n_j \, d\Gamma$$

$$= \int_{\Omega} u \nabla^2 u^* \, d\Omega + \int_{\Gamma} pu^* \, d\Gamma - \int_{\Gamma} up^* \, d\Gamma \quad . \tag{A.4}$$

The application of expression (A.1) to integrate by parts with respect to time gives

$$\int_0^{t^+} \frac{\partial^2 u}{\partial \tau^2} \, u^* d\tau = \left[\frac{\partial u}{\partial \tau} \, u^* \right]_0^{t^+} - \int_0^{t^+} \frac{\partial u}{\partial \tau} \, \frac{\partial u^*}{\partial \tau} \, d\tau \quad . \tag{A.5}$$

When expression (A.1) is applied again to the second term on the right-hand side of expression (A.5), the following expression results

$$\int_0^{t^+} \frac{\partial^2 u}{\partial \tau^2} \, u^* d\tau = \left[\frac{\partial u}{\partial \tau} \, u^* - \frac{\partial u^*}{\partial \tau} \, u \right]_0^{t^+} + \int_0^{t^+} u \, \frac{\partial^2 u^*}{\partial \tau^2} \, d\tau \quad . \tag{A.6}$$

Substitution of expressions (A.4) and (A.6) into equation (3.5.3) results in equation (3.5.4).

A final consideration concerning a change in tractions and displacements notation must be discussed. This notation is shown in equation (A.7) for the normal derivative of u, and a similar procedure was adopted for the potentials.

$$\int_{\Gamma} u^*p \, d\Gamma - \int_{\Gamma_2} pu^* \, d\Gamma + \int_{\Gamma_2} \bar{p}u^* \, d\Gamma = \int_{\Gamma_1} pu^* \, d\Gamma + \int_{\Gamma_2} \bar{p}u^* \, d\Gamma$$

$$= \int_{\Gamma} pu^* \, d\Gamma \quad . \tag{A.7}$$

Therefore, in order to simplify the notation, $\bar{p}$ was replaced by p over Γ_2. It is important to realize however, that integrations over the Γ_2 part of the boundary refers to prescribed normal derivatives of the potential.

APPENDIX B

EVALUATION OF CONTRIBUTIONS DUE TO SINGULAR BOUNDARY INTEGRALS

This appendix is concerned with the evaluation of the following limits (see expressions (3.5.18), (3.5.19) and (3.5.20))

$$S_p = \lim_{\varepsilon\to 0} \int_{\Gamma_\varepsilon} \frac{1}{r}\, p(Q,t_r)\, d\Gamma_\varepsilon \tag{B.1}$$

$$S_u = \lim_{\varepsilon\to 0} \int_{\Gamma_\varepsilon} \frac{\partial r}{\partial n(Q)}\, \frac{1}{r^2}\, u(Q,t_r)\, d\Gamma_\varepsilon \tag{B.2}$$

$$S_v = \lim_{\varepsilon\to 0} \int_{\Gamma_\varepsilon} \frac{\partial r}{\partial n(Q)}\, \frac{1}{cr} \left[\frac{\partial u(Q,\tau)}{\partial \tau}\right]_{\tau=t_r} d\Gamma_\varepsilon \tag{B.3}$$

where Γ_ε is the surface of the hemisphere shown in figure 3.5.3, $r = |\underline{S}-\underline{Q}|$ and $d\Gamma_\varepsilon = d\Gamma_\varepsilon(Q)$.

Expression (B.2), considered first, can be written as

$$S_u = \lim_{\varepsilon\to 0} \int_{\Gamma_\varepsilon} \frac{\partial r}{\partial n(Q)}\, \frac{1}{r^2} \left[u(Q,t_r) - u(S,t)\right] d\Gamma_\varepsilon$$

$$+ u(S,t) \lim_{\varepsilon\to 0} \int_{\Gamma_\varepsilon} \frac{\partial r}{\partial n(Q)}\, \frac{1}{r^2}\, d\Gamma_\varepsilon \quad . \tag{B.4}$$

It will be assumed that the potential satisfies a Hölder condition as a function of space about (S,t), i.e.

$$|u(Q,t) - u(S,t)| \leq Ar^{\alpha} \quad , A>0,\ 0<\alpha\leq 1 \tag{B.5}$$

and a Hölder condition as a function of time, i.e.

$$|u(Q,t-r/c) - u(Q,t)| \leq Br^{\beta} \quad , B>0,\ 0<\beta\leq 1. \tag{B.6}$$

Conditions (B.5) and (B.6) are stronger than continuity, but

weaker than differentiability {27}.

In view of expressions (B.5) and (B.6) it is possible to have an expansion of u about (S,t) which takes the form {84}

$$u(Q,t-r/c) = u(S,t) + \mathbf{o}(r^{\alpha}) + \mathbf{o}(r^{\beta}). \qquad (B.7)$$

Consequently expression (B.4) can be written as

$$S_u = \lim_{\varepsilon\to 0} \int_{\Gamma_\varepsilon} \frac{\partial r}{\partial n(Q)} \frac{1}{r^2}\left[\mathbf{o}(r^{\alpha}) + \mathbf{o}(r^{\beta})\right] d\Gamma_\varepsilon$$

$$+ u(S,t) \lim_{\varepsilon\to 0} \int_{\Gamma_\varepsilon} \frac{\partial r}{\partial n(Q)} \frac{1}{r^2}\, d\Gamma_\varepsilon \quad . \qquad (B.8)$$

Then, evaluation of the limits shown in expression (B.8) reduces to considering

$$L = \lim_{\varepsilon\to 0} \int_{\Gamma_\varepsilon} \frac{\partial r}{\partial n(Q)} \frac{1}{r^{2-\xi}}\, d\Gamma_\varepsilon \quad , \quad \xi > 0 \quad . \qquad (B.9)$$

By employing the spherical coordinates $(\varepsilon,\theta,\psi)$ depicted in figure (B.1), and recognizing that $\partial r/\partial n(Q) = 1$, expression (B.9) reduces to

$$L = \lim_{\varepsilon\to 0} \int_0^{\pi/2}\int_0^{2\pi} \frac{1}{\varepsilon^{2-\xi}}\, \varepsilon^2 \cos\psi \; d\theta \; d\psi$$

$$= \lim_{\varepsilon\to 0} (2\pi\varepsilon^{\xi}) = \begin{cases} 0 & \xi > 0 \\ 2\pi & \xi = 0 \end{cases} \quad . \qquad (B.10)$$

Therefore

$$S_u = 2\pi u(S,t) \quad . \qquad (B.11)$$

If p and $\frac{\partial u}{\partial \tau}$ satisfy Holder conditions (or continuity) in space and time, a procedure similar to the one just described can be employed to demonstrate that

$$S_v = S_p = 0 \quad . \tag{B.12}$$

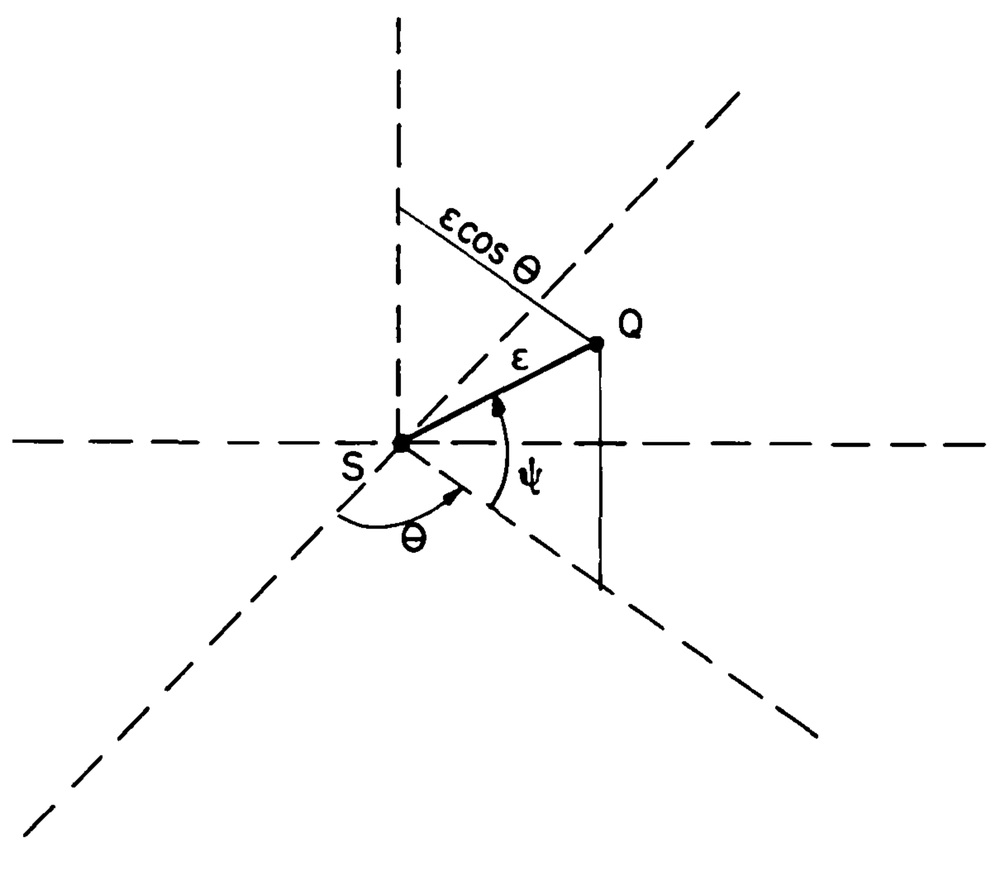

Figure B.1 Spherical coordinates.

The method just outlined to isolate singular contributions of boundary integrals is used in references {20-22,36}. However another interesting procedure to study the same problem has also been used {26,35,84} and will be described next.

Let $c(S,\varepsilon)$ be a circular cylinder of radius ε whose axis contains a boundary point S and with a generator parallel to the normal to Γ at S (see figure B.2). When the Γ boundary satisfies the Liapunov {27} smoothness condition at S, and ε is sufficiently small, the intersection of $c(S,\varepsilon)$ with Γ, denoted Γ_ε, can be considered to be a small

disc of radius ε, centred at S and tangent to Γ (see figure B.2). In addition, a point s inside the domain Ω, located at a distance δ from S, such that $\delta << \varepsilon$, should be considered. Consequently, when neither source density nor initial conditions are considered, equation (3.5.16) can be written as

$$u(s,t) = \frac{1}{4\pi} \int_{\Gamma-\Gamma_\varepsilon} \frac{1}{r}\, p(Q,t_r)\, d\Gamma$$

$$+ \frac{1}{4\pi} \int_{\Gamma-\Gamma_\varepsilon} \frac{\partial r}{\partial n(Q)} \left(\frac{1}{r^2}\, u(Q,t_r) + \frac{1}{cr} \left[\frac{\partial u(Q,\tau)}{\partial \tau} \right]_{\tau=t_r} \right) d\Gamma$$

$$+ \frac{1}{4\pi} \, (S_p + S_u + S_v) \qquad \text{(B.13)}$$

where $r = |\underline{s}-\underline{Q}|$ and S_p, S_u and S_v can be obtained from expressions (3.5.18), (3.5.19) and (3.5.20), changing S by s.

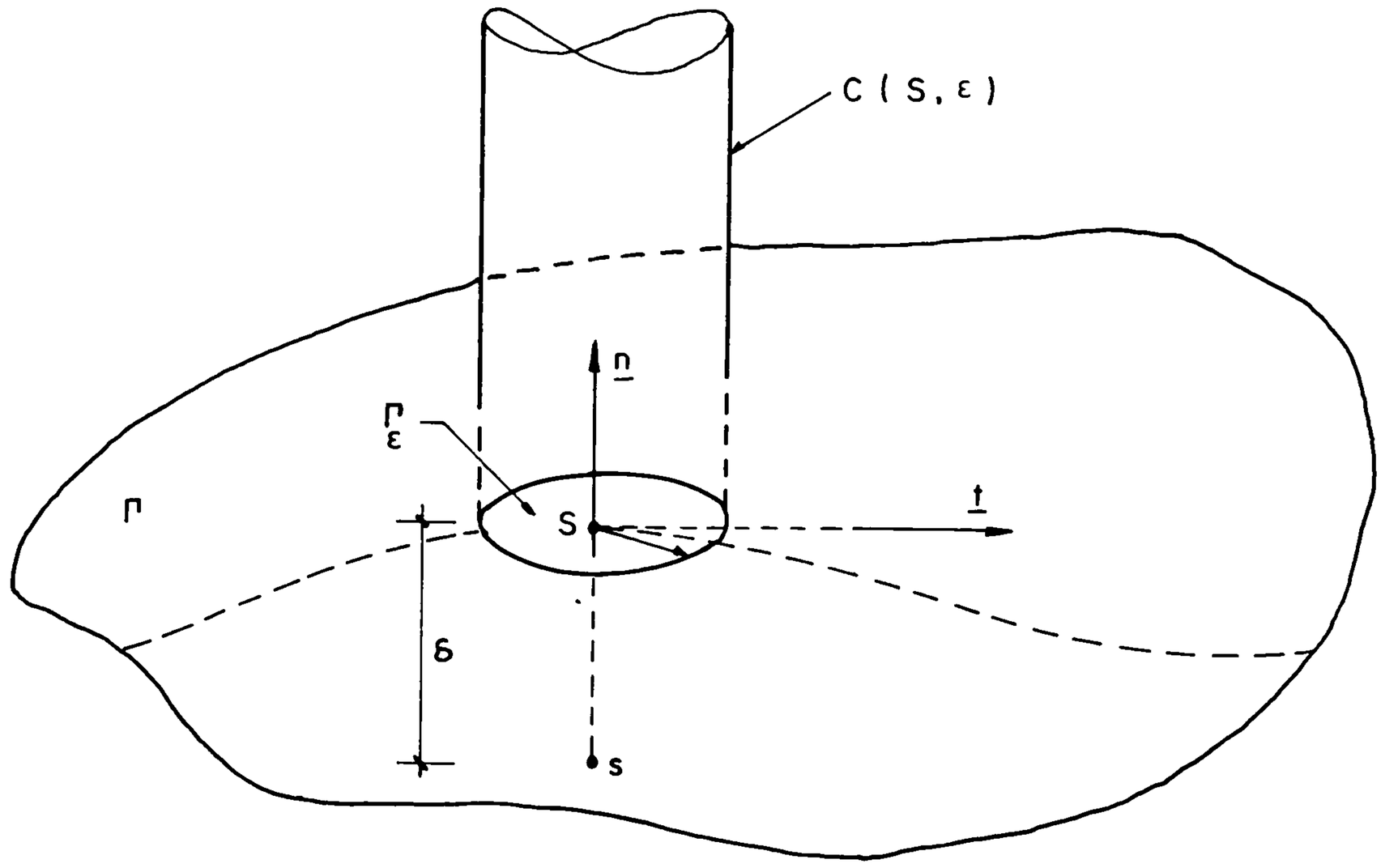

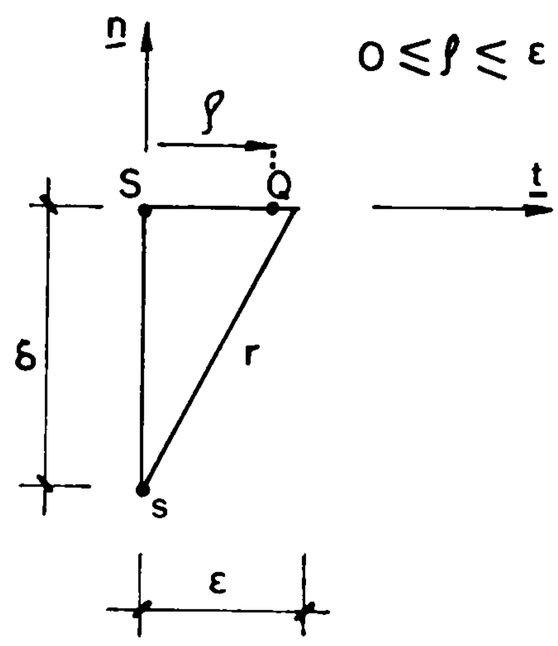

Figure B.2 Disc Γ_ε around the boundary point S.

When $\varepsilon \to 0$; $\Gamma - \Gamma_\varepsilon \to \Gamma$, $s \to S$ and

$$S_u = \lim_{\varepsilon \to 0} \int_{\Gamma_\varepsilon} \frac{\partial r}{\partial n(Q)} \frac{1}{r^2} u(Q,t_r) d\Gamma_\varepsilon \quad . \tag{B.14}$$

If expression (B.7) is taken into account it is possible to write,

$$S_u = \lim_{\varepsilon \to 0} \int_0^\varepsilon \frac{\delta}{r^3} \left[o(r^\alpha) + o(r^\beta) \right] 2\pi\rho d\rho$$

$$+ u(S,t) \lim_{\varepsilon \to 0} \int_0^\varepsilon \frac{\delta}{r^3} 2\pi\rho d\rho \quad . \tag{B.15}$$

Evaluation of the limits shown in expression (B.15) then reduces to evaluating

$$L = \lim_{\varepsilon \to 0} \int_0^{\varepsilon} \frac{\delta}{r^{3-\xi}} \rho d\rho \quad , \qquad \xi \geq 0 \quad . \tag{B.16}$$

Since $\rho d\rho = r dr$ for a given $\delta << \varepsilon$; it is possible to write

$$L = \lim_{\varepsilon \to 0} \int_{\delta}^{\varepsilon} \frac{\delta}{r^{2-\xi}} dr = - \frac{1}{1-\xi} \lim_{\varepsilon \to 0} \left| \frac{\delta}{r^{1-\xi}} \right|_{\delta}^{\varepsilon}$$

$$= \lim_{\delta \to 0} \frac{1}{1-\xi} \frac{\delta}{\delta^{1-\xi}} = \begin{cases} 0 & \text{when} \quad \xi > 0 \\ \\ 1 & \text{when} \quad \xi = 0 \end{cases} , \tag{B.17}$$

and so,

$$S_u = 2\pi u(S,t) \tag{B.18}$$

as before.

Although either of the two alternatives described can be used, the first one is preferred in this work because it can easily be employed for boundaries of the Kellog type as will be illustrated in the following paragraphs.

The next situation to be considered is that where the domain Ω is cylindrical as shown in figure B.3 and the boundary point S is located on a edge, that is, the Liapunov smoothness condition is not valid locally. The body must then be considered as being augmented by a volume about S whose boundary is formed by the intersection of a spherical surface Γ_ε with two planes as shown in figure B.3. The limit indicated in equation (B.9) can conveniently be written as

$$L = L' + L'' \tag{B.19}$$

with

$$L' = \lim_{\varepsilon \to 0} \int_{\Gamma'_\varepsilon} \frac{\partial r}{\partial n} \frac{1}{r^{2-\xi}} \, d\Gamma'_\varepsilon \tag{B.20}$$

$$L'' = \lim_{\varepsilon \to 0} \int_{\Gamma''_\varepsilon} \frac{\partial r}{\partial n} \frac{1}{R^{2-\xi}} \, d\Gamma''_\varepsilon \tag{B.21}$$

where Γ'_ε and Γ''_ε are depicted in figure (B.4).

It has already been shown that

$$L' = \begin{cases} 0 & \xi > 0 \\ \\ 2\pi & \xi = 0 \end{cases} . \tag{B.22}$$

L" can be obtained as outlined by the following operations (see figure B.4)

$$L'' = \lim_{\varepsilon \to 0} \int_0^{\pi} \frac{1}{\varepsilon^{2-\xi}} \beta \varepsilon^2 \sin\theta d\theta$$

$$= \lim_{\varepsilon \to 0} (2\varepsilon^{\xi}\beta) = \begin{cases} 0 & \xi > 0 \\ \\ 2\beta & \xi = 0 \end{cases} \tag{B.23}$$

where β is the angle indicated in figure B.3. Consequently

$$S_u = 2(\pi+\beta)u(S,t) \tag{B.24}$$

and

$$u(S,t) - \frac{1}{4\pi} S_u = \frac{\pi-\beta}{2\pi} u(S,t) = \frac{\alpha}{2\pi} u(S,t) = c(S)u(S,t) \tag{B.25}$$

where α is the internal angle depicted in figure B.3.

Finally it should be recognized that expression (B.25) can be extended for the situation in which the three

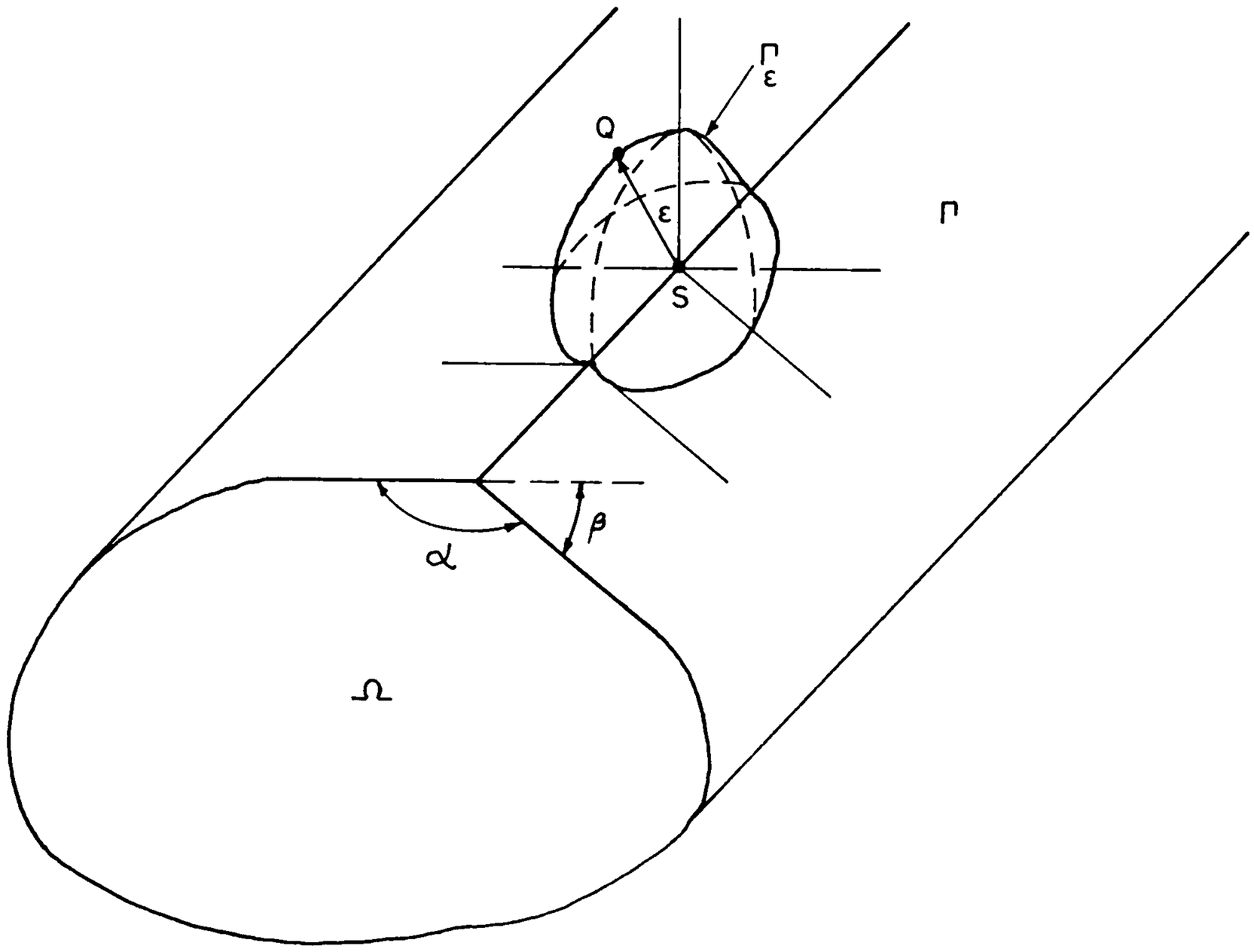

Figure B.3 Domain with a Kellog type boundary augmented by a sphere.

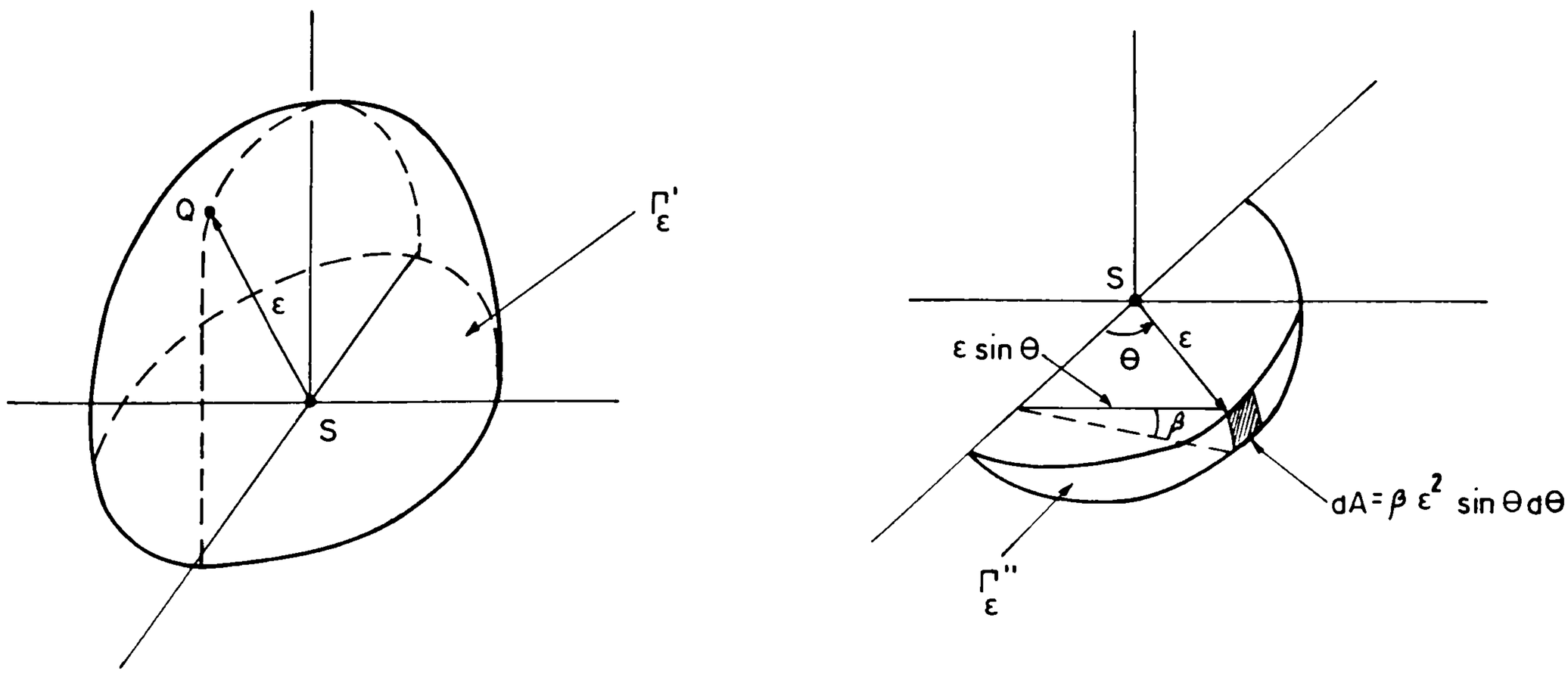

Figure B.4 Surfaces Γ'_ε and Γ''_ε.

dimensional domain is not cylindrical, therefore c(S) can be derived for points located on corners following a procedure similar to the one described in this appendix.

APPENDIX C

TWO-DIMENSIONAL FUNDAMENTAL SOLUTION TO THE SCALAR WAVE EQUATION

It was shown in section 3.6 that the fundamental solution to the two-dimensional scalar wave equation can be obtained from

$$u^*_{2D} = \int_{-\infty}^{+\infty} u^*_{3D}(q,t;s,\tau)\,dx_3(q) \qquad (C.1)$$

or, in view of expression (3.4.6)

$$u^*_{2D} = c\int_{-\infty}^{+\infty} \frac{\delta\left[r-c(t-\tau)\right]}{r}\,dx_3(q) \quad . \qquad (C.2)$$

According to figure C.1 the following relationship can be written

$$r^2 = R^2 + x_3{}^2 \qquad (C.3)$$

where

$$R^2 = (R_i R_i) \qquad (C.4)$$

and

$$R_i = x_i(q) - x_i(s) \quad , \quad (i=1,2) \quad . \qquad (C.5)$$

It should be recognized that s in this case is a point belonging to the (x_1,x_2) plane.

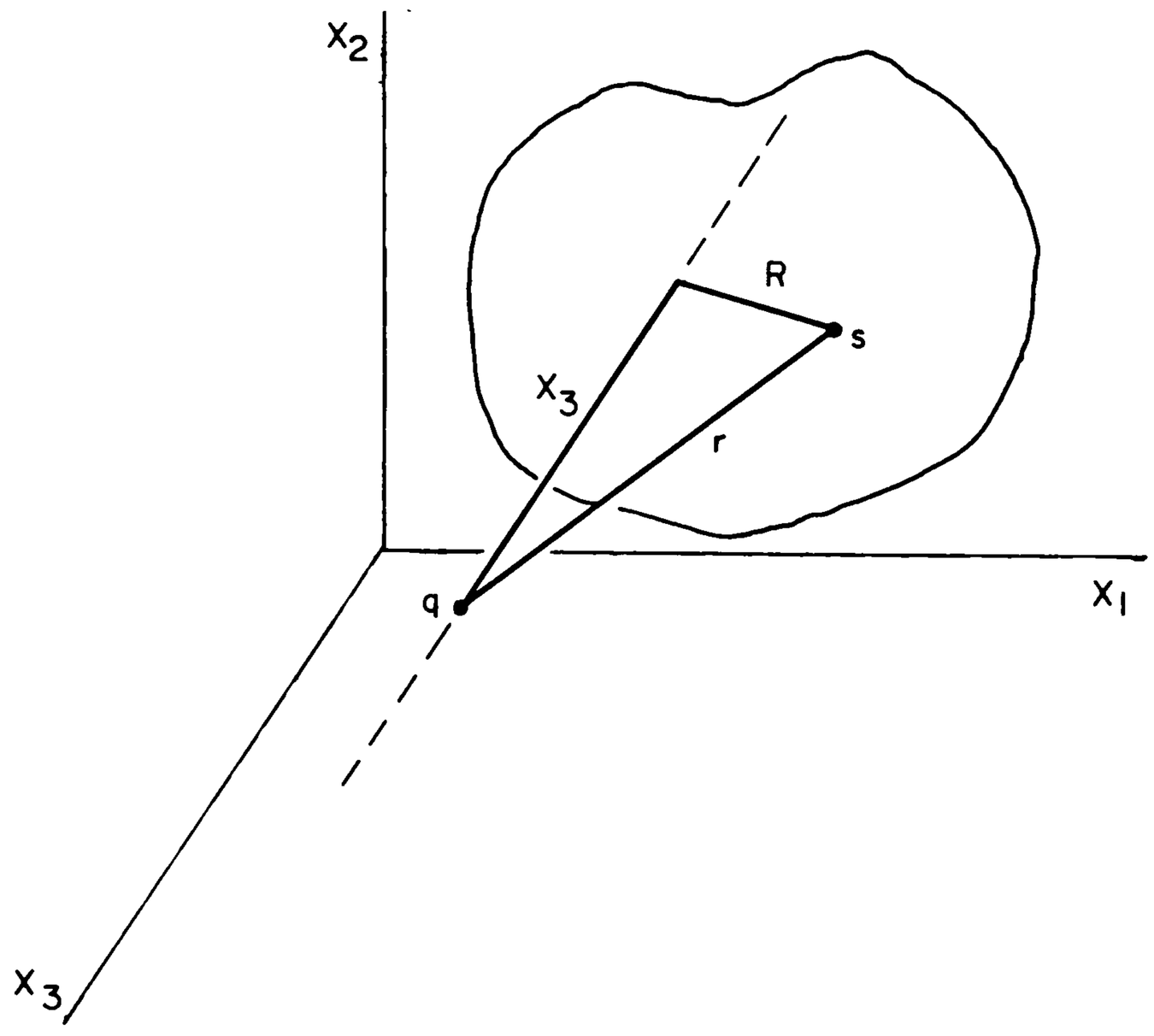

Figure C.1 Illustration of the relationship given by expression (C.3).

In view of expression (C.3), expression (C.2) can be written as {9}

$$u^*_{2D} = c\int_{-\infty}^{+\infty} \frac{\delta\left[(R^2+x_3^2)^{1/2} - c(t-\tau)\right]}{(R^2+x_3^2)^{1/2}}\, dx_3 \quad . \qquad (C.6)$$

To perform the integration indicated in expression (C.6) the following property of the Dirac delta function {98} is required

$$\delta\left[f(x)\right] = \sum_{i=1}^{n} \frac{\delta(x-x_i)}{|f'(x_i)|} \qquad (C.7)$$

which can be used whenever $f'(x) = \frac{df(x)}{dx}$ does not vanish at the roots x_i (i=1,2...n) of f(x). The two roots of the argument of the Dirac delta in expression (C.6) are $\pm\left[c^2(t-\tau)^2-R^2\right]^{1/2}$. Thus

$$\frac{1}{|f'(x_1)|} = \frac{1}{|f'(x_2)|} = c(t-\tau)\left[c^2(t-\tau)^2-R^2\right]^{-1/2} . \qquad (C.8)$$

Therefore

$$\delta\left[(R^2+x_3^2)^{1/2} - c(t-\tau)\right] =$$

$$= c(t-\tau)\left[c^2(t-\tau)^2-R^2\right]^{-1/2}\left(\delta\left(x_3-\left[c^2(t-\tau)^2-R^2\right]^{1/2}\right)\right.$$

$$\left. + \delta\left(x_3+\left[c_2^2(t-\tau)^2-R^2\right]^{1/2}\right)\right) \qquad . \qquad (C.9)$$

In view of expression (C.9) the integration indicated in expression (C.6) can now be carried out, resulting in {6,9}

$$u^*_{2D} = \frac{2c}{\sqrt{c^2(t-\tau)^2-R^2}} H\left[c(t-\tau)-R\right] \qquad . \qquad (C.10)$$

It should be noted that when R is replaced by r, expression (C.10) becomes expression (3.6.9).

APPENDIX D

LINE INTEGRATIONS OVER THE CURVE DEFINED BY THE Γ BOUNDARY

In this appendix the following relationship which was used previously in section 3.7

$$\int_{\theta_1}^{\theta_2} f\left[\underline{r}(\theta)\right] r(\theta)\, d\theta = \int_{\Gamma} f(r)\, \frac{\partial r(s,Q)}{\partial n(Q)}\, d\Gamma(Q) \qquad (D.1)$$

will be obtained. From a comparison of expressions (D.1) and (3.7.15) it is apparent that the notation has been changed, i.e. $r_{\Gamma}(\theta)$ has been replaced by $r(\theta)$. It is believed that this should not cause confusion, once it is understood that $r(\theta)$ is the distance between the origin of the polar coordinate system shown in figure D.1 and a point Q on the Γ boundary.

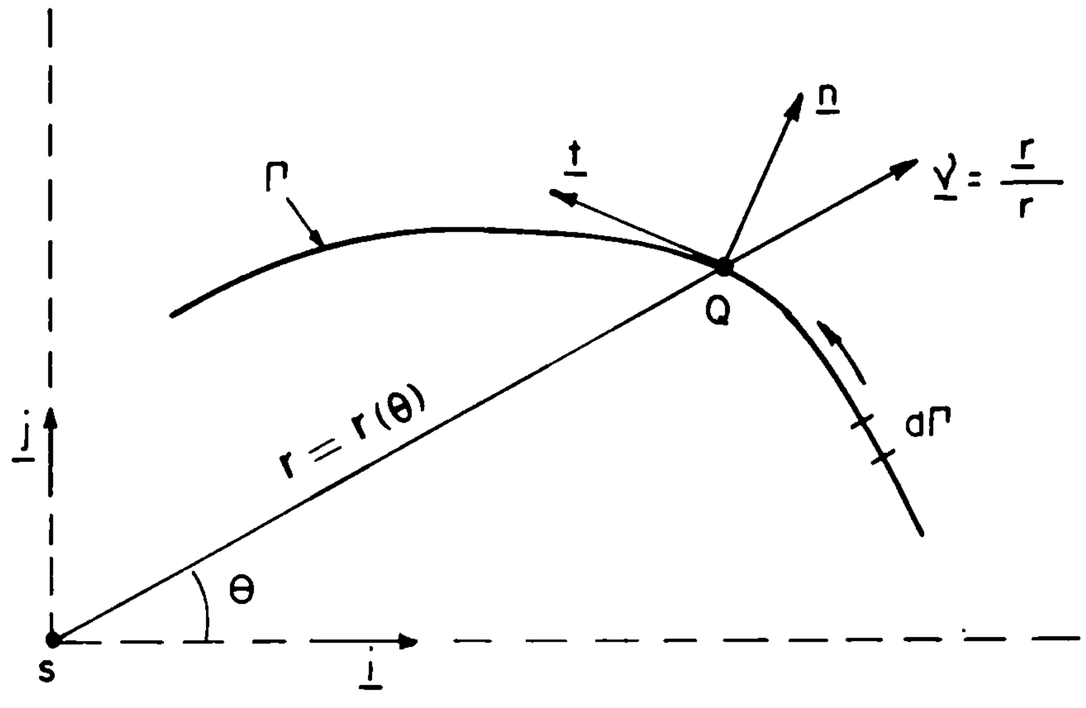

Figure D.1 Unit vectors, polar and line coordinates.

The following expressions can now be written

$$\int_{\theta_1}^{\theta_2} f\left[\underline{r}(\theta)\right] r(\theta)\, d\theta = \int_{\Gamma} f(r)\; r\; \frac{\partial \theta}{\partial \Gamma}\; d\Gamma \qquad (D.2)$$

$$\int_{\Gamma} f(r)\; \frac{\partial r}{\partial n}\; d\Gamma = \int_{\Gamma} f(r)\; (\underline{\nu}.\underline{n})\; d\Gamma \qquad (D.3)$$

where $\underline{\nu} = \dfrac{\underline{r}}{|r|}$ is the unit vector parallel to the line that joins the poins s and Q in figure D.1. In view of expressions (D.2) and (D.3), expression (D.1) is valid as long as it can be proved that

$$\underline{\nu} \cdot \underline{n} = r\; \frac{\partial \theta}{\partial \Gamma} \qquad (D.4)$$

With reference to figure D.1

$$\underline{r} = r(\cos\theta \underline{i} + \sin\theta \underline{j}) \quad , \qquad (D.5)$$

hence

$$d\underline{r} = \left[\left(\frac{dr}{d\theta}\cos\theta - r\sin\theta\right)\underline{i} + \left(\frac{dr}{d\theta}\sin\theta + r\cos\theta\right)\underline{j}\right] d\theta \qquad (D.6)$$

and

$$d\Gamma = \sqrt{d\underline{r}\cdot d\underline{r}} \quad = \sqrt{\left(\frac{dr}{d\theta}\right)^2 + r^2}\; d\theta \quad . \qquad (D.7)$$

Let t which is given as

$$\underline{t} = a\; \underline{i} + b\; \underline{j} \qquad (D.8)$$

be a tangent vector to Γ at Q, as shown in figure D.1.

Then the unit outward normal vector at Q can be written as

$$\underline{n} = (b\; \underline{i} - a\; \underline{j})/\sqrt{a^2+b^2} \quad . \qquad (D.9)$$

$\underline{t}$ is given by

$$\underline{t} = \frac{\partial \underline{r}}{\partial \theta} = \left(\frac{\partial r}{\partial \theta}\cos\theta - r\sin\theta\right)\underline{i} + \left(\frac{\partial r}{\partial \theta}\sin\theta + r\cos\theta\right)\underline{j} \quad , \qquad (D.10)$$

then the expression for $\underline{n}$ reads

$$\underline{n} = \left[\left(\frac{\partial r}{\partial \theta}\sin\theta + r\cos\theta\right)\underline{i} - \left(\frac{\partial r}{\partial \theta}\cos\theta - r\sin\theta\right)\underline{j}\right] \Big/ \sqrt{\left(\frac{\partial r}{\partial \theta}\right)^2 + r^2} \quad . \qquad (D.11)$$

Taking expressions (D.5) and (D.11) into consideration it is fairly simple to demonstrate that

$$\underline{\nu} \cdot \underline{n} = \frac{r}{\sqrt{\left(\frac{\partial r}{\partial \theta}\right)^2 + r^2}} \quad . \qquad (D.12)$$

A comparison of expressions (D.7) and (D.12) demonstrates that formula (D.4) is valid, consequently expression (D.1) is proved.

APPENDIX E

ANALYTICAL TIME INTEGRATION

This appendix presents expressions for $(D_i^{nm})_I$, $(D_i^{nm})_F$, $(E_i^{nm})_I$, $(E_i^{nm})_F$ and F_i^{nm} that appear in equations (4.2.17) and (4.2.20). Initially it is convenient to define the following constants

$$\begin{aligned} A_1 &= \sqrt{c(t_n - t_{m-1}) - r} \\ A_2 &= \sqrt{c(t_n - t_{m-1}) + r} \\ A_3 &= \sqrt{c(t_n - t_m) - r} \\ A_4 &= \sqrt{c(t_n - t_m) + r} \\ A_5 &= \sqrt{c(t_n - t_{m+1}) - r} \\ A_6 &= \sqrt{c(t_n - t_{m+1}) + r} \end{aligned} \qquad \text{(E.1)}$$

.

$(D_i^{nm})_I$, $(D_i^{nm})_F$, $(E_i^{nm})_I$ and $(E_i^{nm})_F$ which appear in equation (4.2.17) can be calculated from (I), (II), (III), (IV) and (V) which follow,

(I) $t_{m+1} < t_n - r/c$

$$(D_i^{nm})_I = -\left[\frac{A_1}{A_2} - \frac{A_3}{A_4} + \frac{2c^2\Delta t(t_n - t_{m-1})}{A_2A_4(A_1A_4 - A_2A_3)}\right]$$

$$(D_i^{nm})_F = \frac{A_3}{A_4} - \frac{A_5}{A_6} + \frac{2c^2\Delta t(t_n - t_{m+1})}{A_4A_6(A_3A_6 - A_4A_8)} \qquad \text{(E.2)}$$

$$(E_i^{nm})_I = A_3A_4 - A_1A_2 - c(t_n - t_{m-1}) \ln\left[\frac{A_3A_4 + c(t_n - t_m)}{A_1A_2 + c(t_n - t_{m-1})}\right]$$

$$(E_i^{nm})_F = -\left[A_5A_6 - A_3A_4 - c(t_n - t_{m+1}) \ln \frac{A_5A_6 + c(t_n - t_{m+1})}{A_3A_4 + c(t_n - t_m)}\right]$$

(II) $t_{m+1} > t_n - r/c$, $t_m < t_n - r/c$ and $t_{m+1} < t_n$ $(r \neq 0)$

$$(D_i^{nm})_I \rightarrow \text{Use expression given in (I)}$$

$$(D_i^{nm})_F = \frac{A_3 (A_6)^2}{A_4} \frac{1}{r} \qquad (E.3)$$

$$(E_i^{nm})_I \rightarrow \text{Use expression given in (I)}$$

$$(E_i^{nm})_F = A_3 A_4 + c(t_n - t_{m+1}) \ln \left[\frac{r}{A_3 A_4 + c(t_n - t_m)} \right]$$

(III) $t_m \bar{>} t_n - r/c$ and $t_{m-1} < t_n - r/c$ (r can be equal to zero)

$$(D_i^{nm})_I = -A_1 A_2 \frac{1}{r}$$

$$(D_i^{nm})_F = 0 \qquad (E.4)$$

$$(E_i^{nm})_I = -A_1 A_2 - c(t_n - t_{m-1}) \ln \left[\frac{r}{A_1 A_2 + c(t_n - t_{m-1})} \right]$$

$$(E_i^{nm})_F = 0$$

(IV) $t_{m+1} \bar{>} t_n - r/c$, and $t_{m+1} = t_n$

$$(D_i^{nm})_I \rightarrow \text{Use expression given in (I)}$$

$$(D_i^{nm})_F = \frac{A_3}{A_4} \qquad (E.5)$$

$$(E_i^{nm})_I \rightarrow \text{Use expression given in (I)}$$

$$(E_i^{nm})_F = A_3 A_4$$

(V) $t_{m-1} \geq t_n - r/c$

$$(D_i^{nm})_I = (D_i^{nm})_F = (E_i^{nm})_I = (E_i^{nm})_F = 0 \qquad (E.6)$$

F_i^{nm} can be computed from (VI), (VII) and (VIII) below.

(VI) $t_m < t_n - r/c$

$$F_i^{nm} = -c\Delta t \ \ln \left[\frac{A_3 A_4 + c(t_n - t_m)}{A_1 A_2 + c(t_n - t_{m-1})} \right] \qquad (E.7)$$

(VII) $t_m \geq t_n - r/c$, $t_{m-1} < t_n - r/c$

$$F_i^{nm} = -c\Delta t \ \ln \frac{r}{A_1 A_2 + c(t_n - t_{m-1})} \qquad (E.8)$$

(VIII) $t_{m-1} \geq t_n - r/c$

$$F_i^{nm} = 0 \qquad (E.9)$$

Each expression presented in this appendix must be multiplied by a Heaviside function whose argument is equal to the first argument of a square root to become negative in the expression under consideration.

APPENDIX F

INTRINSIC COORDINATES

Let $x_i(S)$ represent the coordinates of the source point S with regard to the system of Cartesian coordinates shown in figure F.1. The element e_k shown in this figure joints two nodes whose coordinates are given by

$$\begin{aligned} x_1(-1) &= \left[\bar{x}_1\right]_{\xi_k} = -1 \\ x_2(-1) &= \left[\bar{x}_2\right]_{\xi_k} = -1 \\ x_1(1) &= \left[\bar{x}_1\right]_{\xi_k} = 1 \\ x_2(1) &= \left[\bar{x}_2\right]_{\xi_k} = 1 \quad . \end{aligned} \tag{F.1}$$

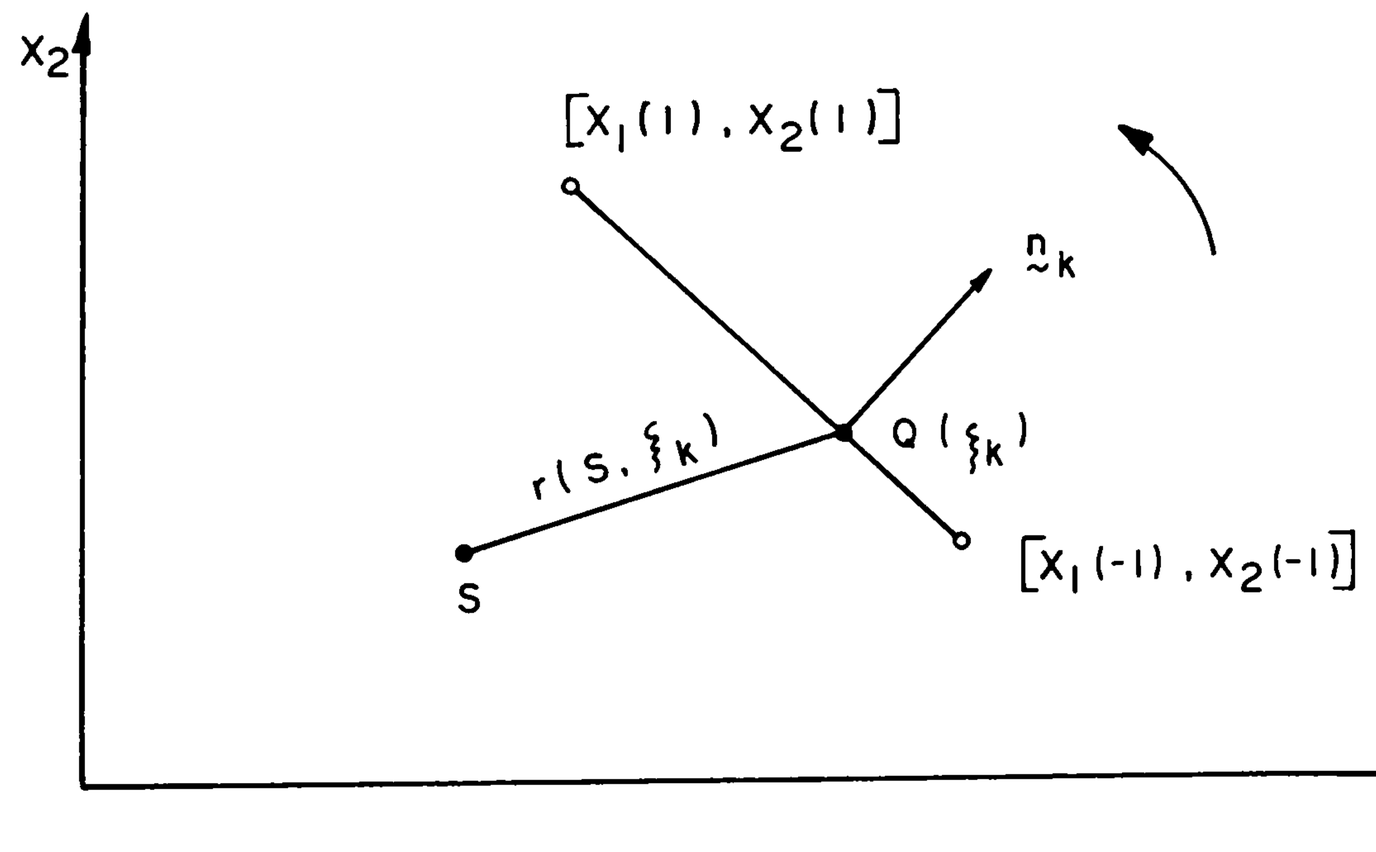

Figure F.1 Intrinsic and rectangular coordinates.

Considering that $r = r(S,\xi_k) = |\underline{S}-\underline{Q}(\xi_k)|$ and denoting the components of n_k by $(n_k)_i$, the following relationships can be written

$$r = (r_i r_i)^{1/2}$$

$$\frac{\partial r}{\partial n(Q)} = (n_k)_i \, r_{,i} \qquad \text{(F.2)}$$

$$d\Gamma_k = |J| \, d\xi_k = \frac{l_k}{2} \, d\xi_k$$ (Summation convention not to be used for the indice k).

In expression (F.2), J is the Jacobian of the coordinate transformation, l_k is the length of e_k and

$$r_i = x_i(Q)-x_i(S) = x_i(\xi_k)-x_i(S)$$

$$r_{,i} = \frac{\partial r}{\partial x_i(Q)} = \frac{r_{,i}}{r} \qquad \text{(F.3)}$$

$$x_i(\xi_k) = x(-1) + \frac{1}{2} (1+\xi_k)\left[x_i(1)-x_i(-1)\right] \quad .$$

In view of equations (F.2) and (F.3) the integrals in equations (4.2.22) and (4.2.23) can be easily calculated using intrinsic coordinates ξ_k. When linear interpolation functions in time and space are adopted, the following expressions can be written

$$(H_{ij}^{nm})_I = \frac{1}{2c\Delta t}\left(l_p\int_{-1}^{1}\frac{\partial r}{\partial n}(D_i^{nm})_I(\xi_p+1)d\xi_p - l_q\int_{-1}^{1}\frac{\partial r}{\partial n}(D_i^{nm})_I(\xi_q-1)d\xi_q\right)$$

$$(H_{ij}^{nm})_F = \frac{1}{2c\Delta t}\left(l_p\int_{-1}^{1}\frac{\partial r}{\partial n}(D_i^{nm})_F(\xi_p+1)d\xi_p - l_q\int_{-1}^{1}\frac{\partial r}{\partial n}(D_i^{nm})_F(\xi_q-1)d\xi_q\right)$$

$$(G_{ij}^{nm})_I = \frac{1}{2c\Delta t}\left[l_p \int_{-1}^{1} (E_i^{nm})_I (\xi_p+1) d\xi_p - l_q \int_{-1}^{1} (E_i^{nm})_I (\xi_q-1) d\xi_q \right]$$

$$(G_{ij}^{nm})_F = \frac{1}{2c\Delta t}\left[l_p \int_{-1}^{1} (E_i^{nm})_F (\xi_p+1) d\xi_p - l_q \int_{-1}^{1} (E_i^{nm})_F (\xi_q-1) d\xi_q \right] \qquad (F.4)$$

As previously stated in section 4.2, with the exception of $(G_{i,i-1}^{nn})_I$, $(G_{i,i}^{nn})_I$ and $(G_{i,i+1}^{nn})_I$, all others coefficients in expression (F.4) can be computed using one-dimensional Gauss quadrature. When n=m and i=j, $(E_i^{nn})_I$ is required to compute $(G_{ii}^{nn})_I$. In this situation, $(E_i^{nm})_I$ in expression (F.4) can be written as (see expression E.4)

$$(E_i^{nn})_I = \left[-A_1 A_2 + c(t_n - t_{n-1}) \ln \left[\overline{A_1 A_2 + c(t_n - t_{n-1})} \right] - c(t_n - t_{n-1}) \ln r \right] H\left[\overline{c(t_n - t_{n-1}) - r} \right] \quad . \qquad (F.5)$$

Analytical integration can now be carried out to calculate the contributions to $(G_{ii}^{nn})_I$, in expression (F.4), of the term that have a logarithm singularity. The manipulations required are described below.

$$\frac{1}{2c\Delta t}\, l_p \int_{-1}^{1} \ln(r)(\xi_p+1) H\left[\overline{c\Delta t - r} \right] d\xi_p =$$

$$= (1/2)\left[\ln(a_p) - 1 - \frac{a_p}{l_p}\left[\ln(a_p) - 1/2 \right] \right] \quad ,$$

$$\frac{1}{2c\Delta t}\, l_q \int_{-1}^{1} \ln(r)(\xi_q-1) H\left[\overline{c\Delta t - r} \right] d\xi_q = \qquad (F.6)$$

$$= (1/2)\left[\ln(a_q) - 1 - \frac{a_q}{l_q}\left[\ln(a_q) - 1/2 \right] \right]$$

where

$$a_p = \begin{cases} c\Delta t & \text{when } c\Delta t < l_p \\ \\ l_p & \text{otherwise} \end{cases} \qquad (F.7)$$

$$a_q = \begin{cases} c\Delta t & \text{when } c\Delta t < l_q \\ \\ l_q & \text{otherwise} \end{cases}$$

The procedure to be followed for the coefficients $(G^{nn}_{i,i-1})_I$ and $(G^{nn}_{i,i+1})_I$ is similar to the one just presented for $(G^{nn}_{i,i})_I$; consequently it will not be described here.

It is important to recognize that although the coefficients G^{mn}_{ij} for linear and constant θ^m are different from each other, their singular term is the same. Therefore results similar to those defined by expression (F.6) can be obtained in the case of constant time interpolation.

APPENDIX G

TRANSVERSE MOTION OF A RECTANGULAR MEMBRANE UNDER PRESCRIBED INITIAL VELOCITY

This appendix is concerned with obtaining expressions to represent the transverse motion of the rectangular membrane analysed in section 4.3.3. The displacements are null on the Γ boundary and an initial velocity v_o is prescribed over the rectangular area A_o shown in figure G.1. The analytical solution for this specific problem was derived using the general expressions given in reference {105}.

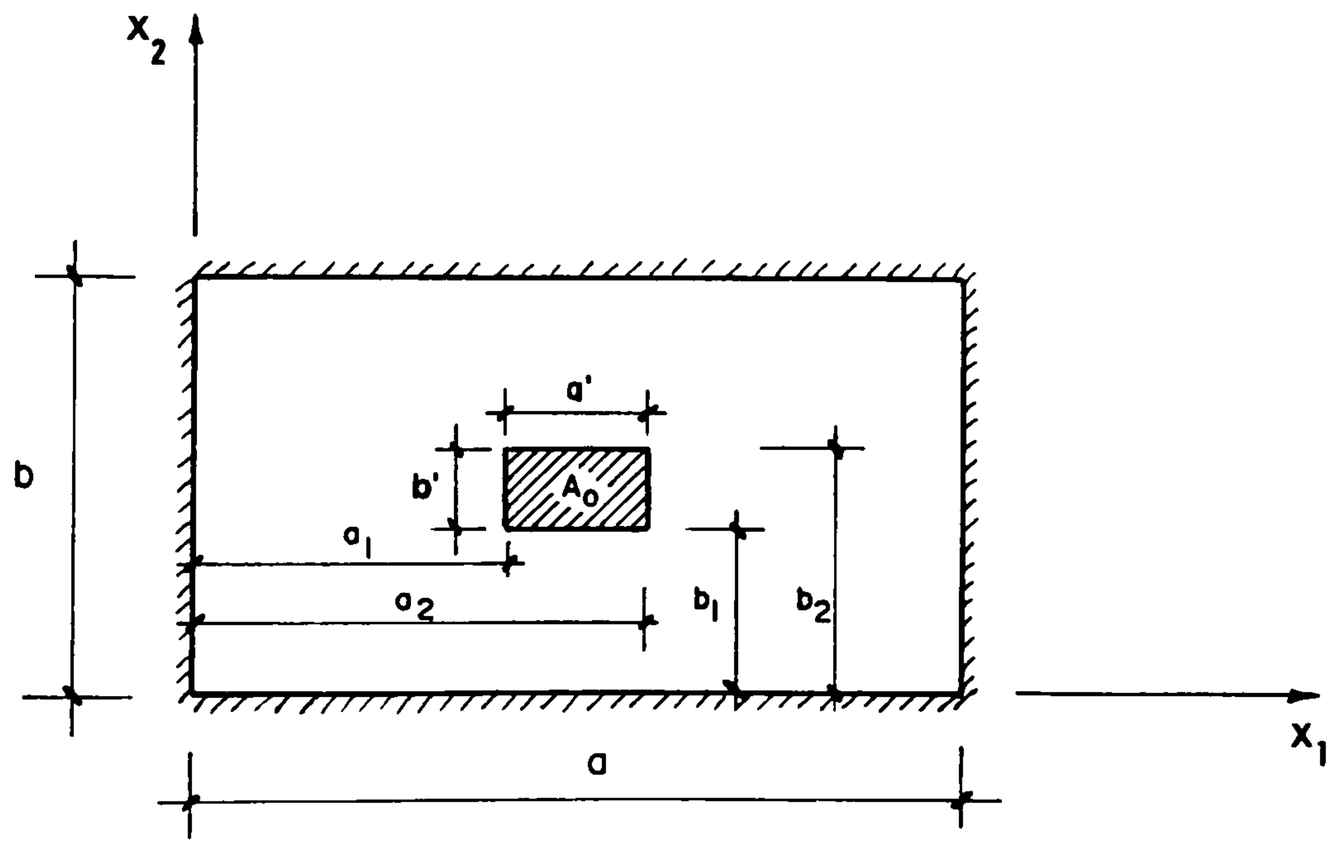

Figure G.1 Geometry, boundary and initial conditions for the membrane.

The transverse displacement $u(x_1,x_2,t)$ at any point inside the domain defined by the membrane and the tractions $p(a,x_2,t)$ at any point on the line $x_1=a$ can be

calculated from

$$u(x_1,x_2,t) = \frac{2v_o}{\pi^3} \sum_{m=1}^{\infty} \sum_{n=1}^{\infty} \frac{1}{mn\nu_{mn}} \sin\left(\frac{\pi m x_1}{a}\right) \sin\left(\frac{\pi n x_2}{b}\right) G_{mn} \qquad (G.1)$$

$$p(a,x_2,t) = \frac{2v_o}{a\pi^2} \sum_{m=1}^{\infty} \sum_{n=1}^{\infty} \frac{1}{n\nu_{mn}} \cos m\pi \sin \frac{n\pi x_2}{b} G_{mn} \qquad (G.2)$$

where

$$G_{mn} = \left(\cos \frac{n\pi b_2}{b} - \cos \frac{n\pi b_1}{b}\right)\left(\cos \frac{m\pi a_2}{a} - \cos \frac{m\pi a_1}{a}\right)$$

$$\cdot \sin(2\pi\nu_{mn} t) \qquad (G.3)$$

and the natural frequencies ν_{mn} are given by

$$\nu_{mn} = \frac{c}{2}\sqrt{\left(\frac{m}{a}\right)^2 + \left(\frac{n}{b}\right)^2} \quad . \qquad (G.4)$$

In the case of the membrane analysed in chapter 4, ($a=b$, $a'=b'=\frac{a}{5}$) the series of expressions (G.1) and (G.2) were computed with eighty and one hundred terms respectively.

APPENDIX H

FUNDAMENTAL TRACTION

The two-dimensional fundamental traction given by expression (5.2.4) can also be computed from

$$p^*_{ik} = 2G(\theta n_k \varepsilon^*_{imm} + n_j \varepsilon^*_{ijk}) \qquad (H.1)$$

where ε^*_{ijk} is the fundamental strain, i.e.

$$\varepsilon^*_{ijk} = \frac{1}{2}(u^*_{ik,j} + u^*_{ij,k}) \qquad (H.2)$$

and θ is the constant given by expression (5.2.9). In order to work out an expression for ε^*_{ijk}; $u^*_{ik,j}$ must be computed first, from u^*_{ik} outlined by equation (5.2.6). $u^*_{ik,j}$ can conveniently be written as

$$u^*_{ik,j} = \frac{1}{2\pi\rho c_s} \frac{\partial}{\partial x_j}\left(T_1 + T_2 - T_3 - \frac{c_s}{c_d}(T_4 - T_5)\right) \qquad (H.3)$$

where

$$T_1 = \delta_{ik} L_2 H\left[\overline{c}_s t' - r\right] \qquad (H.4)$$

$$T_2 = \frac{\delta_{ik}}{r^2} L_2^{-1} H\left[\overline{c}_s t' - r\right] \qquad (H.5)$$

$$T_3 = \frac{r_{,i} r_{,k}}{r^2} L_2 N_2 H\left[\overline{c}_s t' - r\right] \qquad (H.6)$$

$$T_4 = \frac{\delta_{ik}}{r^2} L_1^{-1} H\left[\overline{c}_d t' - r\right] \qquad (H.7)$$

$$T_5 = \frac{r_{,i} r_{,k}}{r^2} L_1 N_1 H\left[\overline{c}_d t' - r\right] \quad . \qquad (H.8)$$

L_1, N_1, L_2 and N_2 in expressions (H.4) to (H.8) are given by expression (5.4.3).

$u^*_{ik,j}$ can then easily be obtained once expressions for the derivatives of T_1, T_2, T_3, T_4 and T_5 with respect to x_j, have been calculated. The procedure to be followed

will now be described; the following relationships will be used

$$r_{,ij} = \frac{1}{r}(\delta_{ij} - r_{,i} r_{,j}) \tag{H.9}$$

$$r_{,m} r_{,m} = 1 \tag{H.10}$$

$$\frac{\partial r}{\partial n} = r_{,i} n_i \tag{H.11}$$

$$n_j \delta_{ij} = n_i \tag{H.12}$$

$$\frac{\partial}{\partial x_j} f(r,t') = r_{,j} \frac{\partial}{\partial r} f(r,t') \tag{H.13}$$

$$\frac{\partial}{\partial r} H\left[ct'-r\right] = \frac{\partial}{\partial (c\tau)} H\left[c(t-\tau)-r\right] = -\delta\left[c\tau-(ct-r)\right] \quad . \tag{H.14}$$

To begin with the operations required to obtain $\frac{\partial T_1}{\partial x_j}$, $\frac{\partial T_2}{\partial x_j}$ and $\frac{\partial T_3}{\partial x_j}$ will be described in (a), (b) and (c) below.

(a) When expression (H.13) is employed the following relationship can be written

$$\frac{\partial T_1}{\partial x_j} = r_{,j} \frac{\partial T_1}{\partial r} = r_{,j} \delta_{ik} \left(r\, L_2^3 H\left[c_s t'-r\right] + \right.$$

$$\left. + L_2 \frac{\partial}{\partial r} H\left[c_s t'-r\right] \right) \quad . \tag{H.15}$$

Taking account of expression (H.14) it is possible to write

$$\frac{\partial T_1}{\partial x_j} = r_{,j} \delta_{ik} \left(r\, L_2^3 H\left[c_s t'-r\right] + L_2 \frac{\partial}{\partial (c_s \tau)} H\left[c_s t'-r\right] \right) \quad . \tag{H.16}$$

(b) When expressions (H.13) and (H.14) are considered, the following formula can be derived

$$\frac{\partial T_2}{\partial x_j} = r_{,j}\delta_{ik}\left(-\left[\frac{2}{r^3}\,L_2^{-1} + \frac{1}{r}\,L_2\right]H\left[c_s t'-r\right] - \right. \qquad (H.17)$$

$$\left. - \frac{1}{r^2}\,L_2^{-1}\delta(-c_s t'-r)\right) \quad .$$

The third term on the right hand side of expression (H.17) is null, and consequently

$$\frac{\partial T_2}{\partial x_j} = -\frac{r_{,j}\delta_{ik}}{r^3}\,L_2 N_2 H\left[c_2 t'-r\right] \quad . \qquad (H.18)$$

(c) Considering expression (H.13), the following formula can be written

$$\frac{\partial T_3}{\partial x_j} = \left(\frac{\partial}{\partial x_j}\left(\frac{r_{,i}r_{,k}}{r^2}\right)L_2 N_2 + \frac{r_{,i}r_{,k}}{r^2}\,r_{,j}\,\frac{\partial}{\partial r}(L_2 N_2)\right)H\left[c_s t'-r\right] +$$

$$+ \frac{r_{,i}r_{,k}}{r^2}\,r_{,j}\,L_2\,N_2\,\frac{\partial}{\partial r}\,H\left[c_s t'-r\right] \quad . \qquad (H.19)$$

Using expression (H.9) the formula below can be derived

$$\frac{\partial}{\partial x_j}\left(\frac{r_{,i}r_{,k}}{r^2}\right) = \frac{1}{r^3}\left(\delta_{ij}r_{,k}+\delta_{kj}r_{,i}-4r_{,i}r_{,j}r_{,k}\right) \quad . \qquad (H.20)$$

The following expression can also be deduced

$$\frac{\partial}{\partial r}(L_2 N_2) = r^3 L_2^3 \quad . \qquad (H.21)$$

Substituting expressions (H.20) and (H.21) into (H.19) and using expression (H.14) then gives

$$\frac{\partial T_3}{\partial x_j} = \left[\frac{1}{r^3}(\delta_{ij}r,_k+\delta_{kj}r,_i - 4r,_ir,_jr,_k)L_2N_2 + \right.$$

$$\left. + r,_ir,_jr,_krL_2^3\right]H\left[c_st'-r\right] + \qquad (H.22)$$

$$+ \frac{1}{r^2} r,_ir,_jr,_kL_2N_2 \frac{\partial}{\partial(c_s\tau)} H\left[c_st'-r\right] \quad .$$

T_4 and T_5 can now be obtained replacing c_s by c_d in expressions (H.18) and (H.22). Then, $u^*_{ik,j}$ can be derived from expressions (H.3), (H.16), (H.18) and (H.22). $u^*_{ij,k}$ can easily be obtained by interchanging j and k by k and j respectively, in the expression that yields $u^*_{ik,j}$. Having obtained $u^*_{ik,j}$ and $u^*_{ij,k}$, expression (H.2) can then be employed to work out ε^*_{ijk}, resulting in

$$\varepsilon^*_{ijk} = \frac{1}{4\pi\rho c_s}\left(E_{ijk}\left(rL_2^3H\left[c_st'-r\right] + L_2\frac{\partial}{\partial(c_s\tau)}H\left[c_st'-r\right]\right) + \right.$$

$$+ \left[F_{ijk}L_2N_2 + G_{ijk}r^3L_2^3\right]H\left[c_st'-r\right] +$$

$$+ G_{ijk}L_2N_2\frac{\partial}{\partial(c_s\tau)}H\left[c_st'-r\right] - \qquad (H.23)$$

$$- \frac{c_s}{c_d}\left(\left[F_{ijk}L_1N_1 + G_{ijk}r^3L_1^3\right]H\left[c_dt'-r\right] + \right.$$

$$\left.\left. + G_{ijk}L_1N_1\frac{\partial}{\partial(c_d\tau)}H\left[c_dt'-r\right]\right)\right)$$

where

$$E_{ijk} = \delta_{ik}r,_j+\delta_{ij}r,_k$$

$$F_{ijk} = -\frac{2}{r^3}(\delta_{ik}r,_j+\delta_{ij}r,_k+\delta_{jk}r,_i-4r,_ir,_jr,_k) \qquad (H.24)$$

$$G_{ijk} = -\frac{2}{r^2} r,_ir,_jr,_k \quad .$$

The fundamental traction p^*_{ik}, as described by equation (5.28) can now be obtained by substituting expression (H.23) into (H.1).

APPENDIX I

STRESS AT BOUNDARY POINTS

No integral expression is derived in this thesis to compute stresses. At internal points, cells are used to obtain space derivatives of displacements which are subsequently used to compute stresses. However the same procedure cannot be employed for boundary points. In this instance the procedure outlined in this section must be applied.

From Hooke's law (equation (2.2.15)) the components of the stress tensor, which refer the directions s and n shown in figure I.1, are given by

$$\sigma_{ss} = (\lambda+2G)\varepsilon_{ss}+\lambda\varepsilon_{nn}$$

$$\sigma_{nn} = \lambda\varepsilon_{ss}+(\lambda+2G)\varepsilon_{nn} \qquad (I.1)$$

$$\sigma_{sn} = \sigma_{ns} = 2G\varepsilon_{sn} \quad .$$

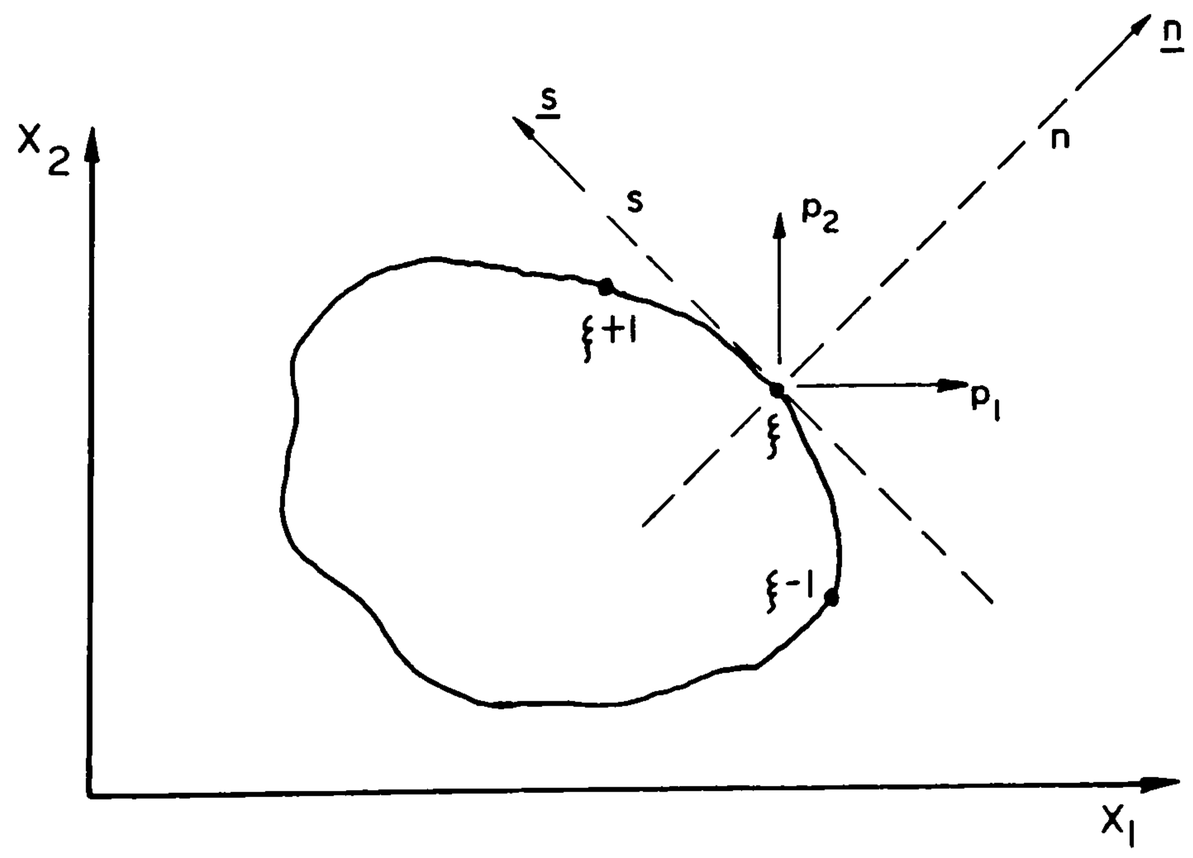

Figure I.1 System of coordinates and boundary points used to compute the stress σ_{ss}.

If the expression (I.1) is employed, σ_{ss} can be computed from

$$\sigma_{ss} = 4G \frac{\lambda+G}{\lambda+2G} \varepsilon_{ss} + \frac{\lambda}{\lambda+2G} \sigma_{nn} \quad . \tag{I.2}$$

Equilibrium conditions give

$$\sigma_{nn} = p_i n_i \quad , \tag{I.3}$$

and therefore when p_1 and p_2 are known only ε_{ss} remains to be determined, in order to compute σ_{ss} given by expression (I.2). The displacement component in a direction parallel to s is given by

$$u_s = -u_1 n_2 + u_2 n_1 \quad , \tag{I.4}$$

consequently ε_{ss} can be calculated from

$$\varepsilon_{ss} = -u_{1,s} n_2 + u_{2,s} n_1 \quad . \tag{I.5}$$

The following expression can now be used to obtain $u_{i,s}$ at a node ξ of the Γ boundary (see figure I.1)

$$u_{i,s}\Big/_{\xi} = \frac{u_i(\xi+1,t) - u_i(\xi-1,t)}{\left| Q(\xi+1) - Q(\xi-1) \right|} \quad . \tag{I.6}$$

Expression (I.6) has already been used in {36,37,65,113} and the accuracy for boundary stresses obtained in those references was considered satisfactory.